SANDIA REPORT

RECEIVED
SEP 15 1997
O S T I

Porosity, Single-Phase Permeability, and Capillary Pressure Data from Preliminary Laboratory Experiments on Selected Samples from Marker Bed 139 at the Waste Isolation Pilot Plant

Volume 2 of 3: Appendix B

MASTER

Susan M. Howarth, Tracy Christian-Frear

Sandia National Laboratories

Porosity, Single-Phase Permeability, and Capillary Pressure Data from Preliminary Laboratory Experiments on Selected Samples from Marker Bed 139 at the Waste Isolation Pilot Plant
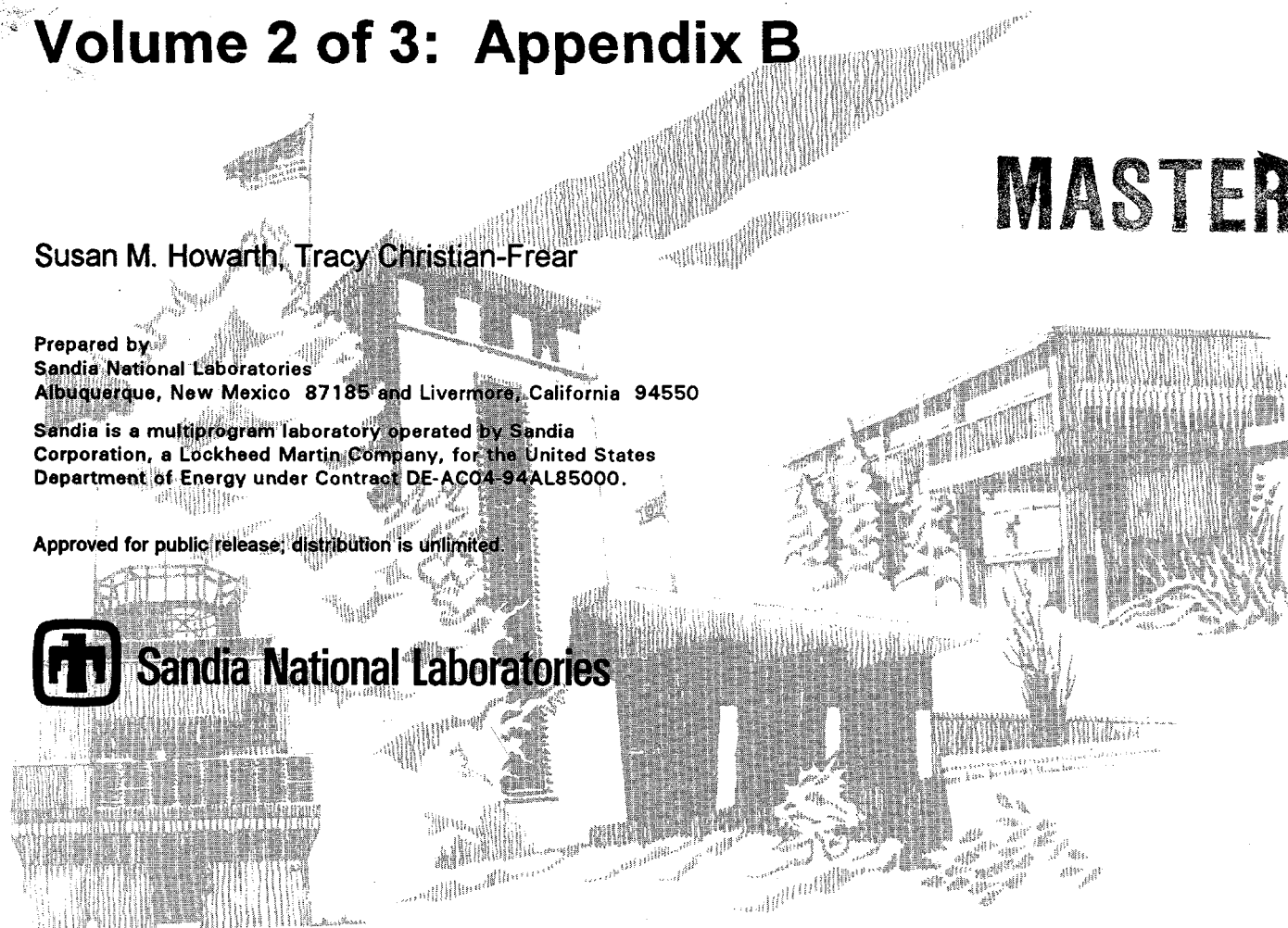
Volume 2 of 3: Appendix B

Susan M. Howarth
Tracy Christian-Frear

Geohydrology Department 6115
Sandia National Laboratories
Albuquerque, NM 87185

ABSTRACT

This volume contains the mineralogy, porosity, and permeability results from the Marker Bed 139 specimens evaluated by RE/SPEC, Inc.

DISCLAIMER

Portions of this document may be illegible
in electronic image products. Images are
produced from the best available original
document.

Appendix B.
Data Report: RE/SPEC Inc.

The following section includes Appendix B and Appendices B-A through B-J.

Appendix B

Laboratory Measurements of Fluid Transport Properties for Marker Bed 139 Anhydrite from the Waste Isolation Pilot Plant

Errata Sheet

The following data are not included in the data report because the data were not qualified by the time of report publication:

1. Total porosity data on all specimens.
2. Effective porosity data on all specimens.

The liquid permeability data are included in the data report as "scoping only" because the brine dissolved the specimens.

The liquid permeability results for specimen P3X10-6-SP2 are not included in the data report because the gas permeability measurements were unusable (negative slopes for the Klinkenberg correction were reported by RE/SPEC).

One entry in Table 4-8 is in error. The flow rate for the gas inlet pressure at 0.7 MPa and the first 10 MPa confining pressure should be 7.59, not 7.63 10^{-8} m^3 / s.

The following modifications should be made to the reference citations in Appendix B.

Page No.	Change
B-7	in the abstract: Davies et al., 1992 should read Davies et al., 1991
B-17	Brodsky (1990) should read Brodsky and Munson (1991)
B-39	Brodsky (1993) should read Brodsky (1994)
B-58	ANSI/ASME (1986) should read ANSI/ASME (1985)
B-102	Davies et al., 1992 should read Davies et al., 1991
B-103	change ANSI/ASME, 1986 to ANSI/ASME, 1985; copy on file in SWCF as WPO#44996
B-103	change ASTM, 1989 to ASTM, 1992; copy on file in SWCF as WPO#43089
B-103	change ASTM, 1989 to ASTM, 1990; copy on file in SWCF as WPO#43223
B-103	change Brodsky, N.S., 1993 to Brodsky, N.S. 1994; copy on file in SWCF as WPO#10087
B-103	change Brodsky, N.S., 1990 to Brodsky, N.S. and D.E. Munson, 1991; correct title is *The Effect of Brine on the Creep of WIPP Salt in Laboratory Tests*; copy on file in SWCF as WPO#26136
B-103	to citation for Chowdiah, 1988 add Vol. 3, no. 4
B-103	copy of Costin and Wawersik, 1980 on file in SWCF as WPO#26748
B-103	in citation for Gilpatrick et al., 1982 the second author is C.G. Baes Jr.; copy on file in SWCF as WPO#45931
B-103	in citation for Davies et al., 1991 the correct name for second author is L.H. Brush; copy on file in SWCF as WPO#25381

Page No.	Change
B-103	copy of Howarth, 1993 on file in SWCF as WPO#21611
B-104	copy of Holcomb and Shields, 1987 on file in SWCF as WPO#26778
B-104	complete author name is C.S. Hurlbut, Jr.; add 18th edition to book title
B-104	in citation for IT Corporation, 1987 add to publication facts: Battelle Memorial Institute; copy on file in SWCF as WPO#45954
B-104	copy of Klinkenberg, 1941 on file in SWCF as WPO#8556
B-104	Stone and Webster, 1983 is available from the NTIS as DE83018265 and on file in SWCF as WPO#46602
B-104	in Stormont and Daemen, 1992 the correct second author's name is J.K.K. Daemen; correct journal title is *International Journal of Rock Mechanics and Mining Sciences and Geomechanics Abstracts*; copy on file in SWCF as WPO#45950
B-104	in Sutherland and Cave, 1980 capitalize "Salt" in paper title; correct journal title is *International Journal of Rock Mechanics and Mining Sciences and Geomechanics Abstracts*; copy on file in SWCF as WPO#45951
B-104	in citation for Weast, 1974 add 55th edition
B-116	for Chung, 1974 the full journal title is *Journal of Applied Crystallography* Vol. 7, no. 6; copy on file in SWCF as WPO#45584
B-116	for Davis, 1981 the full journal title is *Atmospheric Environment* Vol. 15, no. 3; copy on file in SWCF as WPO#45585
B-116	for Davis, 1984 capitalize "Using" in title; full journal title is *Advances in X-ray Analysis, Proceedings of the Annual Conference on Applications of X-Ray Analysis*, Vol. 27
B-116	for Davis, 1986 the full journal title is *Powder Diffraction* Vol. 1, no. 3; copy on file in SWCF as WPO#45586
B-116	for Davis, 1988 the full journal title is *Advances in X-Ray Analysis, Proceedings of the Annual Conference*, Vol. 31
B-116	for Davis and Johnson, 1982 the full journal title is *Atmospheric Environment* Vol. 16, no 2; copy on file in SWCF as WPO#45587
B-116	for Davis and Johnson, 1987 the full journal title is *Advances in X-Ray Analysis, Proceedings of the Annual Conference*, Vol. 30
B-116	for Davis et al., 1984 the full journal title is *Atmospheric Environment* Vol. 18, no 4; copy on file in SWCF as WPO#45588
B-176	the existence of Lab Notebook No. WIPP 04 could not be verified
B-176	the existence of Lab Notebook No. WIPP 02 could not be verified
B-188	copy of ANSI/ASME, 1985 on file in SWCF as WPO#44996
B-196	Holcomb and Shields: no date given; assumed to be 1987; copy on file in SWCF as WPO#26778
B-198	copy of ANSI/ASME, 1985 on file in SWCF as WPO#44996
B-198	Stroup and Senseny, 1987: RSI-0309; copy on file in SWCF as WPO#45638
B-199	Stroup and Senseny, 1987: RSI-0309; copy on file in SWCF as WPO#45638

LABORATORY MEASUREMENTS OF FLUID TRANSPORT PROPERTIES FOR MARKER BED 139 ANHYDRITE FROM THE WASTE ISOLATION PILOT PLANT

Topical Report RSI-0491

by

Nancy S. Brodsky

RE/SPEC Inc.
P.O. Box 725
Rapid City, South Dakota 57709

prepared for

Sandia National Laboratories
P.O. Box 5800
Albuquerque, NM 87185

January 1994

Laboratory Measurements of Fluid Transport Properties for Marker Bed 139 Anhydrite From the Waste Isolation Pilot Plant

N.S. Brodsky
RE/SPEC Inc.
P. O. Box 725
Rapid City, SD 57709-0725

ABSTRACT

Fluid transport properties were measured in the laboratory for specimens of Marker Bed 139 anhydrite from the Waste Isolation Pilot Plant. Measurements included single-phase permeabilities to nitrogen and brine, porosities and mineralogies of materials immediately adjacent to each permeability specimen, and mineralogies of additional specimens taken from near each permeability specimen. An assessment of coring-induced damage was also conducted. The marker bed is non-homogeneous with respect to composition. Specimen mineralogy was characterized and correlations between fluid transport properties and compositional variations were investigated.

Two permeability specimens were taken from the upper and lower sections of borehole P3X11, and a third permeability specimen was taken from the upper/central region of adjacent borehole P3X10. Measurements of permeability to gas and brine were made on each specimen using steady-state flow techniques at confining pressures of 2 MPa, 6 MPa, and 10 MPa. For each value of confining pressure, permeability measurements were made at inlet pore pressures of 0.4 MPa, 0.7 MPa, and 1.0 MPa and at an outlet pore pressure of 0.1 MPa. Gas permeabilities ranged from approximately 1.8×10^{-19} m^2 to 2.5×10^{-17} m^2 and the Klinkenberg-corrected equivalent liquid permeabilities ranged from 1.4×10^{-18} m^2 to 1.6×10^{-17} m^2. Measured brine permeabilities ranged from 4.4×10^{-20} m^2 to 9.7×10^{-17} m^2. Brine permeabilities were higher than gas permeabilities, perhaps because some specimen dissolution occurred during saturation. The laboratory data include the range of permeability values indicated by field measurements, 8×10^{-20} m^2 to 5×10^{-17} m^2 (Davies et. al, 1992). The highest permeabilities were measured in the lowermost section of borehole P3X11, while the lowest permeabilities were measured for the central to upper region of adjacent borehole P3X10. Permeability values do not strongly correlate with any single material characteristic such as porosity, halite content, or anhydrite content; however, these material characteristics may contribute to spatial variations in permeability.

CONTENTS

CONTENTS (Continued)

CONTENTS (Continued)

Tables

Tables (Continued)

Figures

Figures (Continued)

Figures (Continued)

Figures (Continued)

1.0 INTRODUCTION

1.1 Background

The Department of Energy (DOE) has developed the Waste Isolation Pilot Plant (WIPP) as a research and development facility for the purpose of demonstrating safe management, storage, and disposal of radioactive transuranic (TRU) waste generated by defense programs of the U.S. Government. The WIPP is located in southeastern New Mexico. The underground workings are in the bedded salt of the Salado Formation at a depth of about 660 m. Interbeds of nonsalt materials, principally anhydrite, are also found at the WIPP. Concerns have been raised about the role of gas and brine flow at the WIPP. The Salado salt contains small quantities of brine (0.1 – 1.0 percent by volume) and the interbeds may contain similar amounts. Decomposition of organic wastes and corrosion of metallic wastes and waste canisters may eventually generate gases. The geologic formations of the WIPP will provide the final barrier to radionuclide migration and so the permeability and fluid transport properties of these interbed formations are of great importance in determining the performance of the site for radioactive waste disposal. Of particular concern is the permeability of Marker Bed 139 (MB 139), a 1-m-thick anhydrite layer that underlies the TRU storage rooms at the WIPP. In situ tests show that permeabilities in the anhydrite interbeds are one to two orders of magnitude greater than in the halite. This marker bed may therefore provide a pathway for gas and brine flow.

1.2 Scope

Sandia National Laboratories established the Salado Two-Phase Flow Laboratory Program to measure fluid transport properties for the WIPP and to provide site-specific data to support performance assessment modeling (Howarth, 1993). RE/SPEC Inc. performed scoping activities associated with this program, and this report presents the results of these activities. The scoping activities are divided into three tasks summarized below.

Task 1. Specimen Characterization.
MB 139 is known to have lateral and vertical compositional variations and these may in turn affect fluid transport properties. Detailed characterization of composition can provide correlations between fluid transport properties and composition. X-ray diffraction and petrographic analyses were conducted on three samples that were spaced apart vertically and horizontally within the marker bed. In addition, X-ray diffraction analyses were conducted on material taken from above

and below the axis of each permeability specimen. These data were used to correlate variations in permeability with inhomogeneities in specimen composition.

Task 2. Assessment of Coring-Induced Surface Damage.

One concern that has been raised about laboratory testing is that surface damage produced during coring and finishing will affect laboratory measurements of permeability (Stormont and Daemen, 1992). The extent of surface damage was assessed by impregnating cored specimens with epoxy dye-penetrants and measuring crack densities near the cored surfaces and in the center of the specimens.

Damage, whether it is introduced by coring in the laboratory, or in situ, by deviatoric stresses that form in response to excavation of rooms and shafts at the WIPP, is of concern because it will affect rock permeability. A search of the literature concerning the healing of damage was conducted which did not reveal any studies of fracture healing on anhydrite or within MB 139. The search did, however, reveal a number of studies focusing on fracture healing in salt. The marker bed contains a significant amount of halite, and several studies indicate that halite can fill and perhaps heal fractures in more brittle rocks such as anhydrite. Stone and Webster Engineering Corp (1983) report many observations of salt having filled and healed fractures in adjacent, more brittle rocks, such as fractures and gaps in anhydrite layers at the Cleveland Mine, and fractures in dolomite in the Cleveland and Cayuga Mines.

A laboratory demonstration of crack healing in halite was performed by Costin and Wawarsik (1980) who measured fracture toughness in short rod specimens of salt. Specimens were pieced back together and fracture toughness was remeasured after subjecting specimens to hydrostatic pressures for varied lengths of time at two temperatures. Confining pressure had a more pronounced effect than temperature. Typically, specimens subjected to 10 to 35 MPa regained 70 to 80 percent of their original fracture toughness.

Permeability tests have also been used to assess crack closure and healing. Gilpatrick et al. (1982) measured flow of brine between two optical-quality sodium chloride crystals subjected to 14 MPa confining pressure at temperatures up to 80°C. Permeability decreased as a function of time and this was attributed to deformation by pressure solution. Permeability tests on rock salt have shown that the permeability and porosity of as-received specimens decrease over time at hydrostatic load (Southerland and Cave, 1980, Stormont and Daemen, 1992), implying that damage is introduced during coring but heals at pressure. IT Corp (1987) conducted permeability tests on naturally and artificially fractured rock salt specimens by subjecting them to confining

pressures of 20.6 MPa for up to 8 days. In most cases, the permeabilities of the fractured specimens returned to the same order of magnitude as before fracturing.

The technique of using ultrasonic properties to assess crack closure and healing was applied to rock salt by Brodsky (1990). In that study, compressional wave ultrasonic data were used to assess the extent of crack closure during hydrostatic compression of damaged WIPP salt specimens at 20°C. It was determined that the recovery of ultrasonic velocities depended on pressure and damage level. As expected, the higher the pressure, the greater the velocity recovery during crack closure and healing. It was also found that recovery was more complete in specimens with the least damage and it was concluded that recovery is slower when damage is sufficient to cause changes in the geometry of the crack walls.

Task 3. Determination of Porosity, and Measurements of Gas and Liquid Single-Phase Permeabilities Under Varying Triaxial Stress Conditions.

Sections of MB 139 were taken from two boreholes that were spaced 0.61 m (2 feet) apart in the underground workings at the WIPP. Two boreholes were required to provide a sufficient amount of material. Three cylindrical test specimens with axes parallel to the bedding plane were manufactured from approximately the upper, middle, and lower sections of the marker bed and used for permeability measurements. Specimens from the upper and lower sections of the marker bed were taken from one borehole, while the middle section was taken from the other borehole. Specimens from the upper and middle sections were only 61 mm apart in depth of origin. Pieces of material were taken from directly above and below each specimen axis and used for porosity measurements and for compositional characterization by X-ray diffraction. All permeability and porosity specimens were dried at controlled temperature and relative humidity. Effective (interconnected) porosities were measured by Core Laboratories of Houston, Texas, using a small volume helium porosimeter and then total porosities were measured on the same specimens by RE/SPEC Inc. using gravimetric techniques. Three additional specimens were taken from different sections of the marker bed and characterized using petrographic analysis and X-ray diffraction. Two of these specimens were taken from the upper and lower sections of one borehole, and the third specimen was taken from the upper region of the second borehole.

Gas (nitrogen) and liquid (brine) permeability tests were conducted using the steady-state flow method under the conditions given in Tables 1-1 and 1-2, respectively. Gas permeability tests were conducted first, then the specimens were saturated so that brine permeability tests could be conducted on the same set of specimens. As shown in Tables 1-1 and 1-2, three replicate gas permeability tests and one liquid permeability test were conducted at each test condition for a total of 103 individual permeability determinations. Gas and liquid permeability

tests on each specimen were performed at confining pressures of 2 MPa, 6 MPa, and 10 MPa. At each confining pressure, tests were conducted at three different pore pressure gradients to establish that the relationship between flow rate and pore pressure gradient was linear and that measurements were made in the laminar flow regime. Changes in mean pore pressure can affect gas permeability measurements in a process referred to as "slippage" or the Klinkenberg effect. A Klinkenberg correction was performed for gas permeability tests on each specimen at each value of confining pressure to determine the equivalent liquid permeability.

Table 1-1. Test Matrix for Nitrogen Permeability Tests[a]

Confining Pressure (MPa)	Gas Inlet Pressure (MPa)	Gas Outlet Pressure (MPa)	Number of Tests		
			Specimen P3X11-5-2-SP1	Specimen P3X10-6-SP2	Specimen P3X11-5-3-SP3
2	1.0[b]	0.1	3	3	3
	0.7	0.1	3	3	3
	0.4	0.1	3	3	3
6	1.0	0.1	3	3	3
	0.7	0.1	3	3	3
	0.4	0.1	3	3	3
10	1.0	0.1	3	3	3
	0.7	0.1	3	3	3
	0.4	0.1	3	3	3

(a) All tests were conducted at 25°C.
(b) Gas inlet pressure = 1.1 MPa for first test on P3X10-6-SP2.

1.3 Report Organization

This report consists of seven chapters, including this introductory chapter, and ten appendices. Chapter 2.0 discusses specimen preparation and drying, the experimental methods are described in Chapter 3.0, and experimental results are given in Chapter 4.0. A discussion of results is given in Chapter 5.0 and the report summary and conclusions are in Chapter 6.0. Cited references are given in Chapter 7.0. Four appendices (B-A, B-B, B-C, B-E) contain procedures and reports for work performed by subcontractors, Appendix B-D contains the derivation of an

Table 1-2. Test Matrix for Brine Permeability Tests[a]

Confining Pressure (MPa)	Brine Inlet Pressure (MPa)	Brine Outlet Pressure (MPa)	Number of Tests		
			Specimen P3X11-5-2-SP1	Specimen P3X10-6-SP2	Specimen P3X11-5-3-SP3
2	1.0	0.1	2	1	1
	0.7	0.1	1	1	1
	0.4	0.1	1	1	1
6	1.0	0.1	Jacket Leak	1	1
	0.7	0.1		1	1
	0.4	0.1		1	1
10	1.0	0.1		1	1
	0.7	0.1		1	1
	0.4	0.1		1	1

(a) All tests were conducted at 25°C.

equation for determining porosity using gravimetric methods, Appendix B-F contains error analyses, and the remaining appendices (B-G, B-H, B-I, B-J) contain plotted data.

2.0 SPECIMENS

2.1 Sample Acquisition

Sections of MB 139 anhydrite core from two boreholes were shipped from New Mexico to the RE/SPEC Inc. Rapid City location during August of 1992. The first section was marked with identification numbers beginning with P3X11 and the second section with identification numbers beginning with P3X10. The boreholes were 0.61 m (2 feet) apart. The two sample sections are diagrammed in Figure 2-1. Samples P3X11-5 and P3X10-5 each broke into three pieces during shipping. Each of the broken pieces was assigned its original sample number plus a sequential number (i.e., P3X11-5-1, P3X11-5-2, etc.). The locations from which the permeability and porosity specimens were cored are labeled "SP1 4-in core hole," "SP2 4-in core hole," and "SP3 4-in core hole. Labels LC1, LC2, and LC3 designate material used for studies of laboratory coring-induced damage, and labels TS1, TS2, and TS3 designate material used for petrographic thin section and X-ray diffraction analyses.

After core sectioning and labeling of specimens were completed, RE/SPEC Inc. was notified that Sandia National Laboratories had generated a nonconformance report to document mislabeling of these cores. Instead of relabeling all pieces, which could later prove confusing, the matrix shown in Table 2-1 was used to correlate the original and corrected sample identification numbers.

Table 2-1. Correlation Between Sample Identification Numbers Used by Sandia National Laboratories and by RE/SPEC Inc.

Sandia Core Identification Number [a]	RE/SPEC Inc. Core Identification Number
P3X10-2	P3X10-5
P3X10-3-1	P3X10-6
P3X10-3-2	P3X10-7
P3X11-3	P3X11-5
P3X11-4	P3X11-6

(a) Corrected sample identification numbers furnished by Janis Trone on March 12, 1993
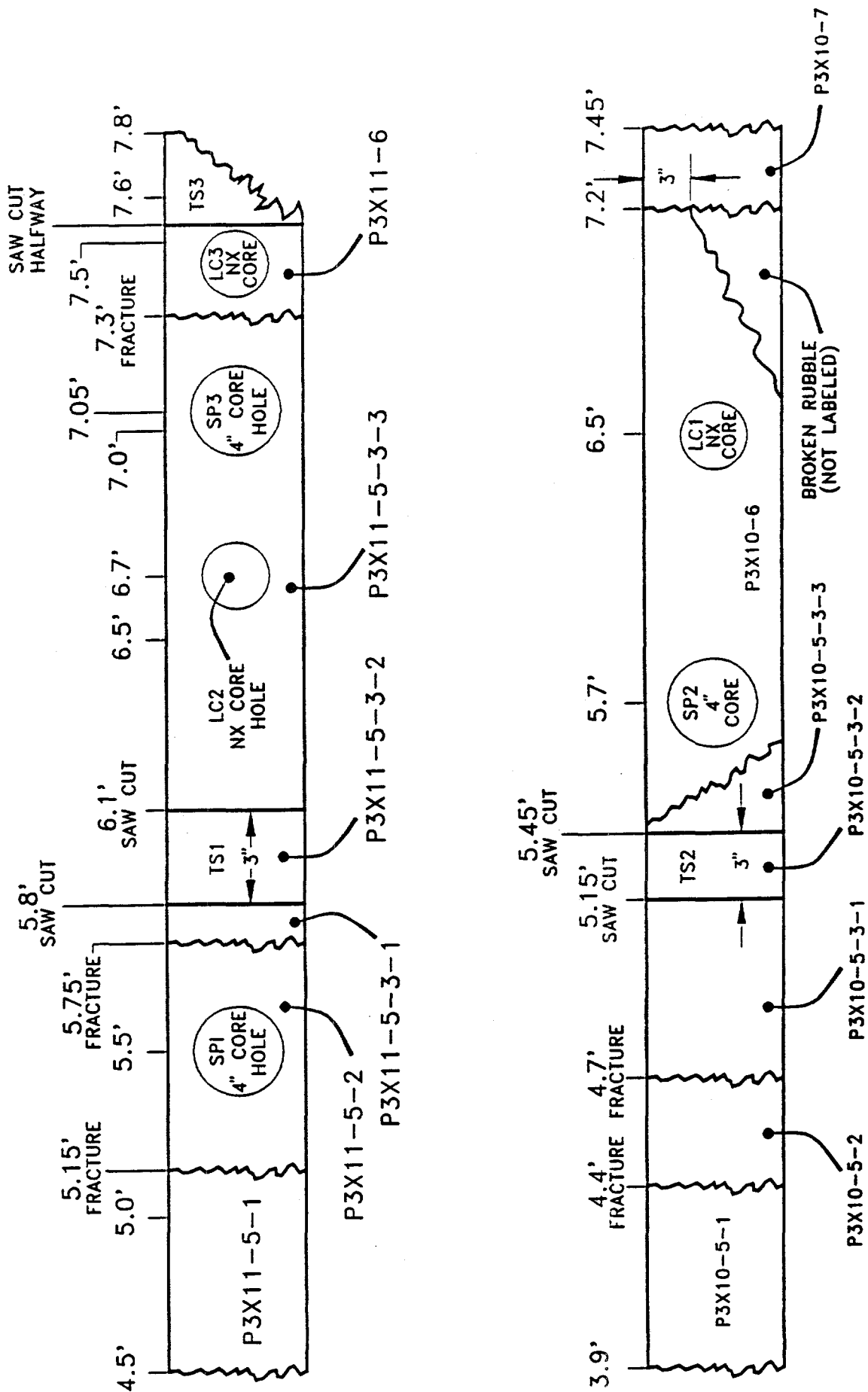
Figure 2-1. Map of WIPP MB 139 anhydrite cores.

Permeability Specimen SP1 had a planar zone of cracks oriented diagonal to the specimen axis. The specimen maintained cohesion across the zone, indicating that the cracks were discontinuous. The zone intersected the specimen surface at about specimen midheight and extended across diagonally, intersecting the other side of the specimen approximately 1 cm from the lower edge.

2.2 Coring and Finishing

Coring was performed according to standard RE/SPEC laboratory procedures. The core was cut dry at a core barrel rotation speed of 1,300 rpm and specimen ends were finished using a lathe. Permeability specimens were cored parallel to the bedding plane of MB 139. Pieces of material were taken from directly above and below each specimen axis and each piece was used for manufacture of a porosity specimen and an X-ray diffraction specimen. The porosity and X-ray diffraction specimens were therefore from the same stratigraphic layers as the permeability specimen. The specimen identification numbers and dimensions of all permeability and porosity test specimens are given in Table 2-2. The same specimens were used for both gas and liquid permeability tests. Specimens P3X11-5-2-SP1, P3X10-6-SP2, and P3X11-5-3-SP3 will be abbreviated in the text as Specimens SP1, SP2, and SP3, respectively. The letters "T" and "B" are appended to permeability specimen identification numbers to denote porosity specimens taken from above and below the permeability specimen axes, respectively.

Table 2-2. Specimen Dimensions

Specimen	Length (m)	Diameter (m)
Permeability Specimens		
P3X11-5-2-SP1	0.10187	0.10145
P3X10-6-SP2	0.10146	0.10147
P3X11-5-3-SP3	0.10141	0.10103
Porosity Specimens		
P3X11-5-2-SP1-T	0.01065	0.03885
P3X11-5-2-SP1-B	0.01178	0.03886
P3X10-6-SP2-T	0.01231	0.03885
P3X10-6-SP2-B	0.01113	0.03885
P3X11-5-3-SP3-T	0.01263	0.03885
P3X11-5-3-SP3-B	0.01508	0.03885

Blocks of material were taken from the locations marked TS1, TS2, and TS3 (see Figure 2-1). Three mutually perpendicular thin sections and an X-ray diffraction specimen were made from each block. The sectioning histories of blocks TS1, TS2, and TS3 are given in Figures 2-2, 2-3, and 2-4, respectively. Thin section specimens P3X11-5-3-2-TS1-1, P3X10-5-3-2-TS2-1, and P3X11-6-TS3-1 (these will be abbreviated in the text as TS1-1, TS2-1, and TS3-1, respectively), were oriented parallel to the bedding plane while the remaining thin sections were perpendicular to the bedding plane and to each other. Specimens TS1-4, TS2-4, and TS3-4 were used for X-ray analyses. These specimens were oriented perpendicular to the bedding plane so that representative samples would be obtained. Additional X-ray diffraction specimens were taken from material above and below the axes of Specimens SP1, SP2, and SP3.

2.3 Drying

All permeability and porosity specimens were dried at 60°C and 45 percent relative humidity to prevent dehydration of clays[1] (Chowdiah, 1988). The changes in mass are given as a function of time in Figures 2-5, 2-6, and 2-7 for Specimens SP1, SP2, and SP3, respectively. The Y-axis for each plot is current mass divided by initial mass. Each figure contains data for a permeability test specimen and for the two 38.9-mm diameter porosity specimens taken from above and below each permeability specimen. Upon initial exposure to humidity, several pieces exhibited an increase in mass. During the first day in the humidity chamber, beads of moisture were observed for a short time on some specimens and so the increase in mass was attributed to moisture absorption. A loss of mass was expected for the first day because a powder, assumed to be salt or rock dust, collected on the bottom of the humidity chamber. This rock dust probably collected on specimens during preparation and then came off in the humidity chamber. The precipitate was cleaned from the chamber and no further accumulations were observed. Specimens were dried until the masses of permeability specimens were constant to within 0.01 g over a one-week period. Each permeability specimen weighed approximately 2,200 g and so a 0.01 g change corresponded to a change in mass of 0.0005 percent.

During the setup of Specimen SP3 for permeability testing, the specimen jacket that protected the specimen from the confining fluid was breached, resulting in wetting of the upper specimen surface with silicone oil and a specimen mass gain of 0.3 g. After the specimen was wiped clean with a freon-dampened cloth, its mass returned to its previous value. This specimen was placed back in the humidity chamber to ensure that its mass was stable over a one-week period.

---

[1] ASTM Standard D4525, "Standard Test Method for Permeability of Rocks by Flowing Air" recommends conditions of 45 percent relative humidity and 63°C for drying specimens that may contain swelling clays.
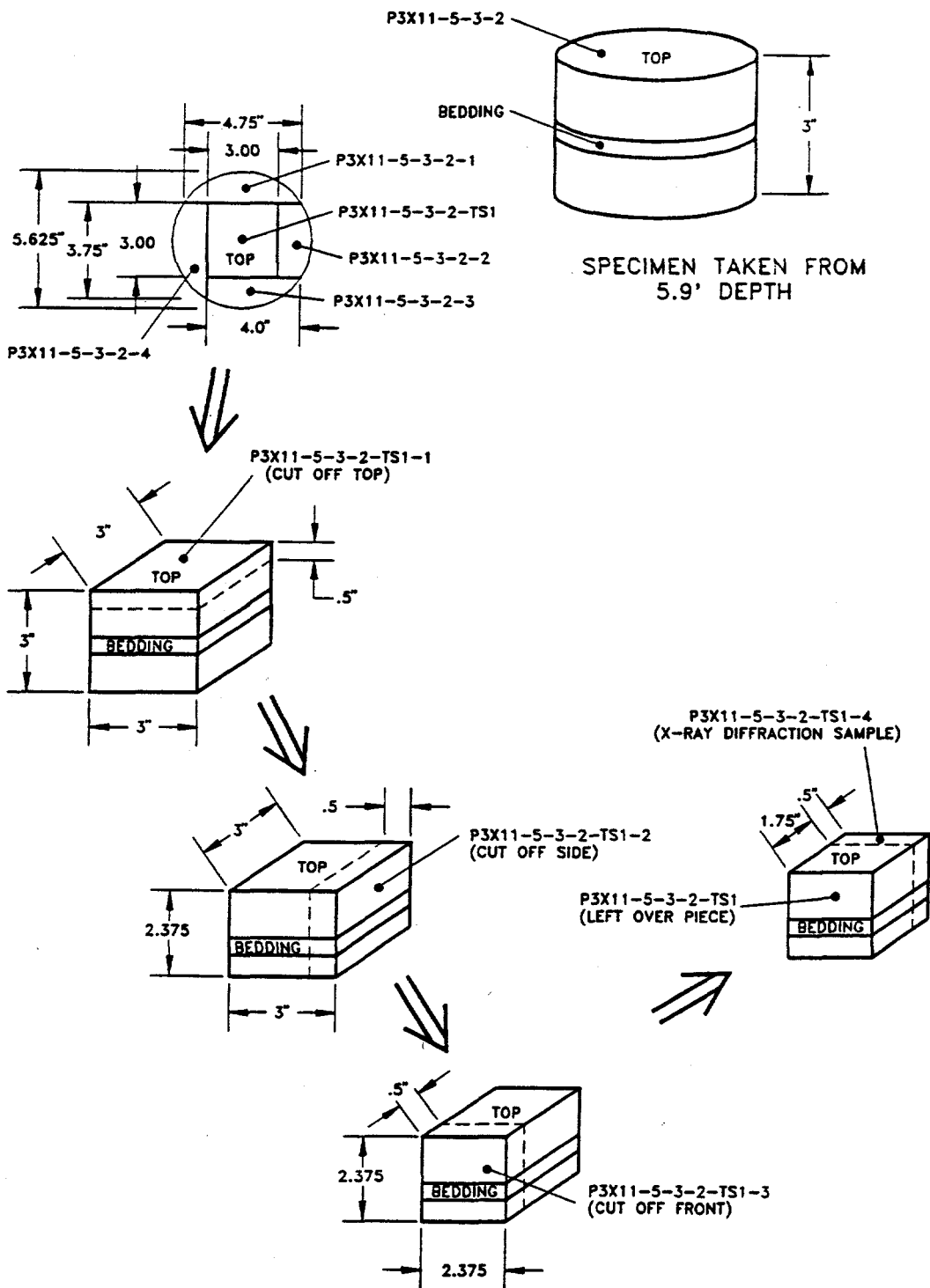
Figure 2-2. Expanded view of MB 139 anhydrite core showing locations of X-ray diffraction specimen and thin sections for TS1.
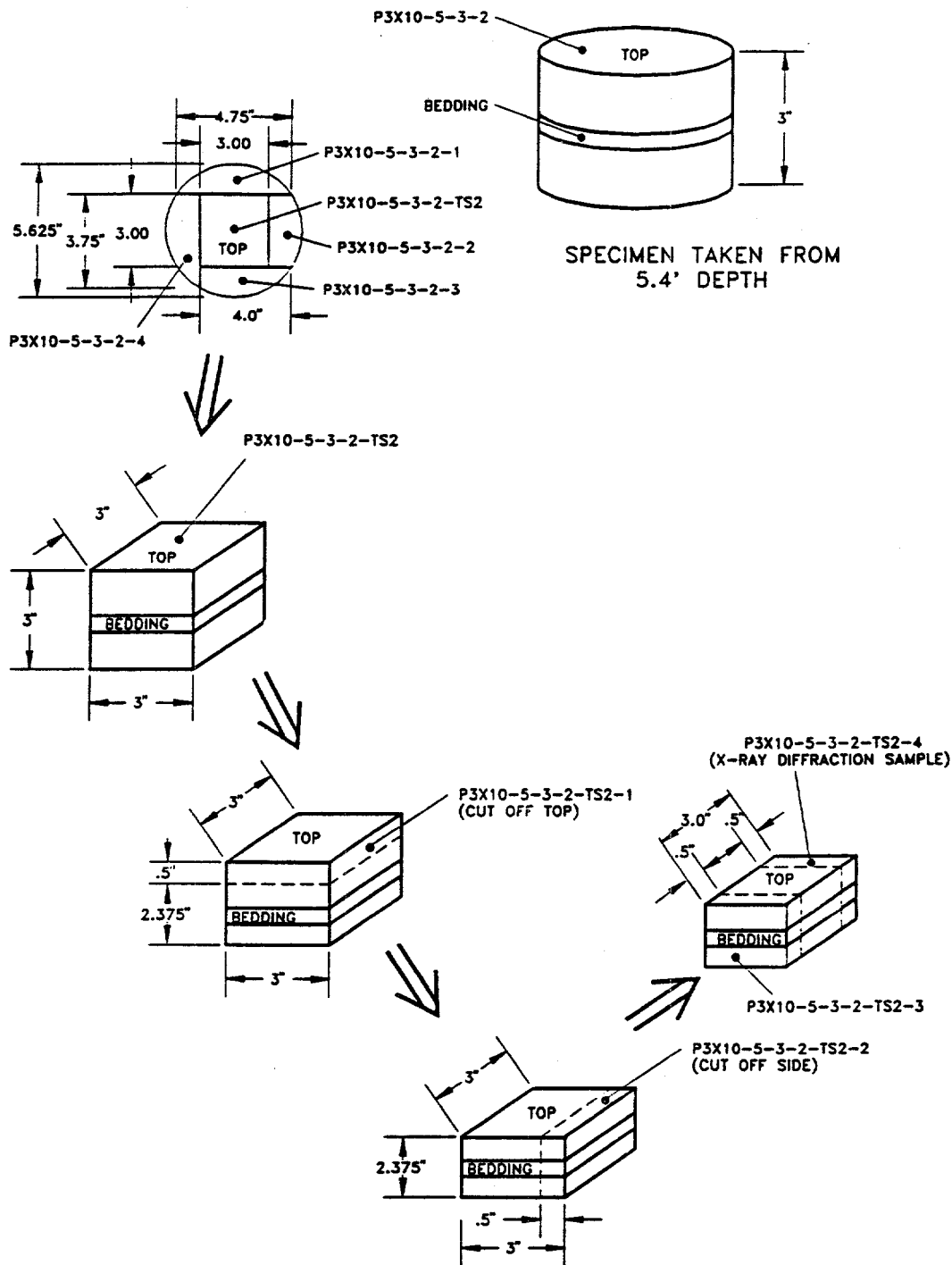
Figure 2-3. Expanded view of MB 139 anhydrite core showing locations of X-ray diffraction specimen and thin sections for TS2.
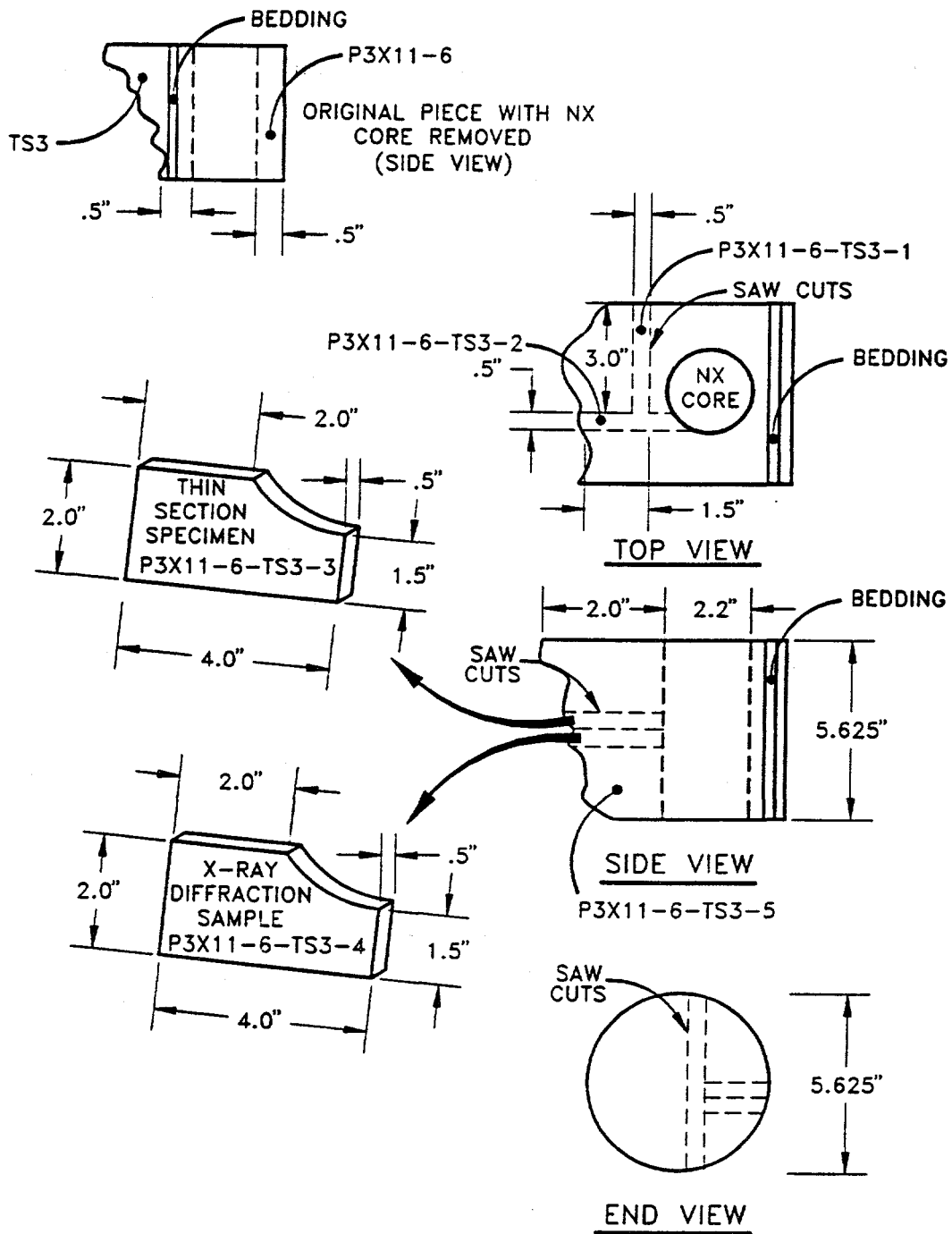
Figure 2-4. Expanded view of MB 139 anhydrite core showing locations of X-ray diffraction specimen and thin sections for TS3.

Drying Data for Specimen 1: P3X11-5-2-SP1

60C, 45% Relative Humidity

Mass/Initial Mass

1.0025

1

0.9975

0   25   50   75

Time (Days)

- Specimen SP1
□ Top: SP1-T
♦ Bottom: SP1-B
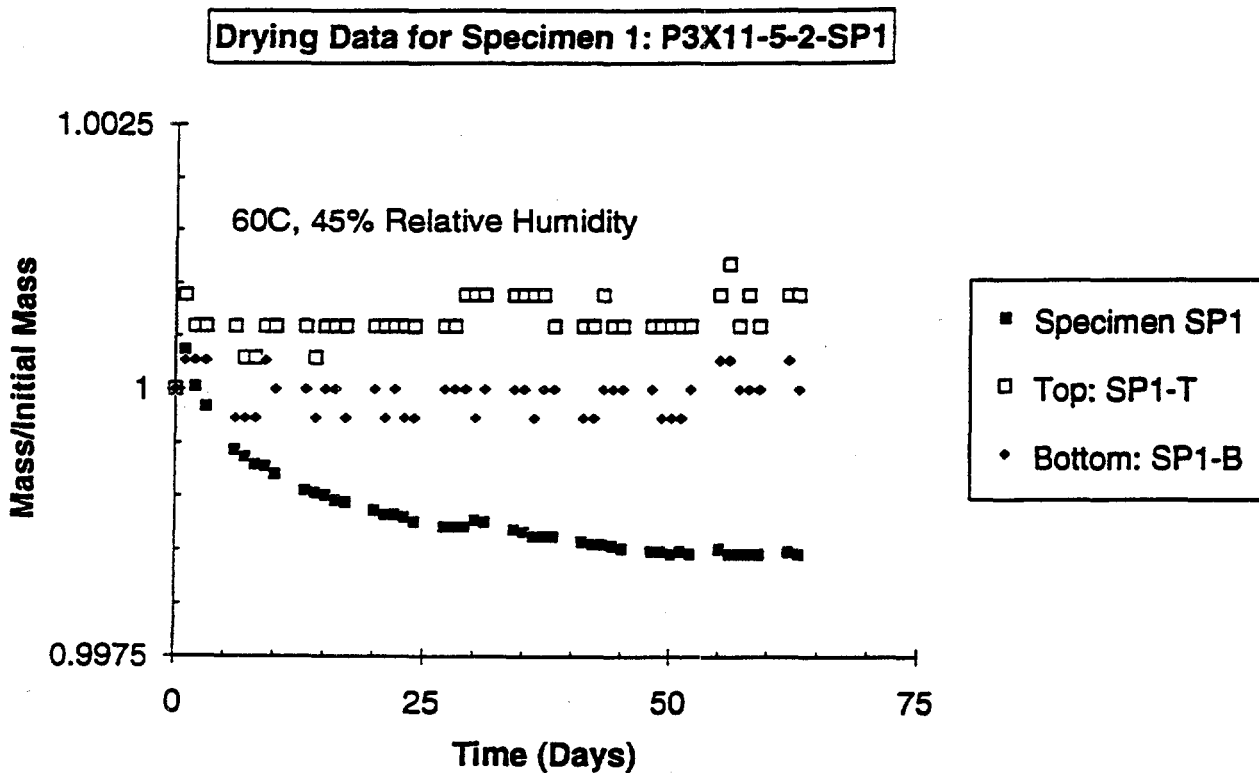
RSI-248-93-022

Figure 2-5.   Change in mass during drying at 60°C and 45 percent relative humidity for Specimen P3X11-5-2-SP1. Initial masses are 2.20445 kg, 0.03391 kg, and 0.03745 kg for the permeability specimen and the porosity specimens taken from above (SP1-T) and below (SP1-B) the permeability specimen, respectively.

Drying Data for Specimen 2: P3X10-6-SP2

60C, 45% Relative Humidity

- Specimen SP2
- Top: SP2-T
- Bottom: SP2-B
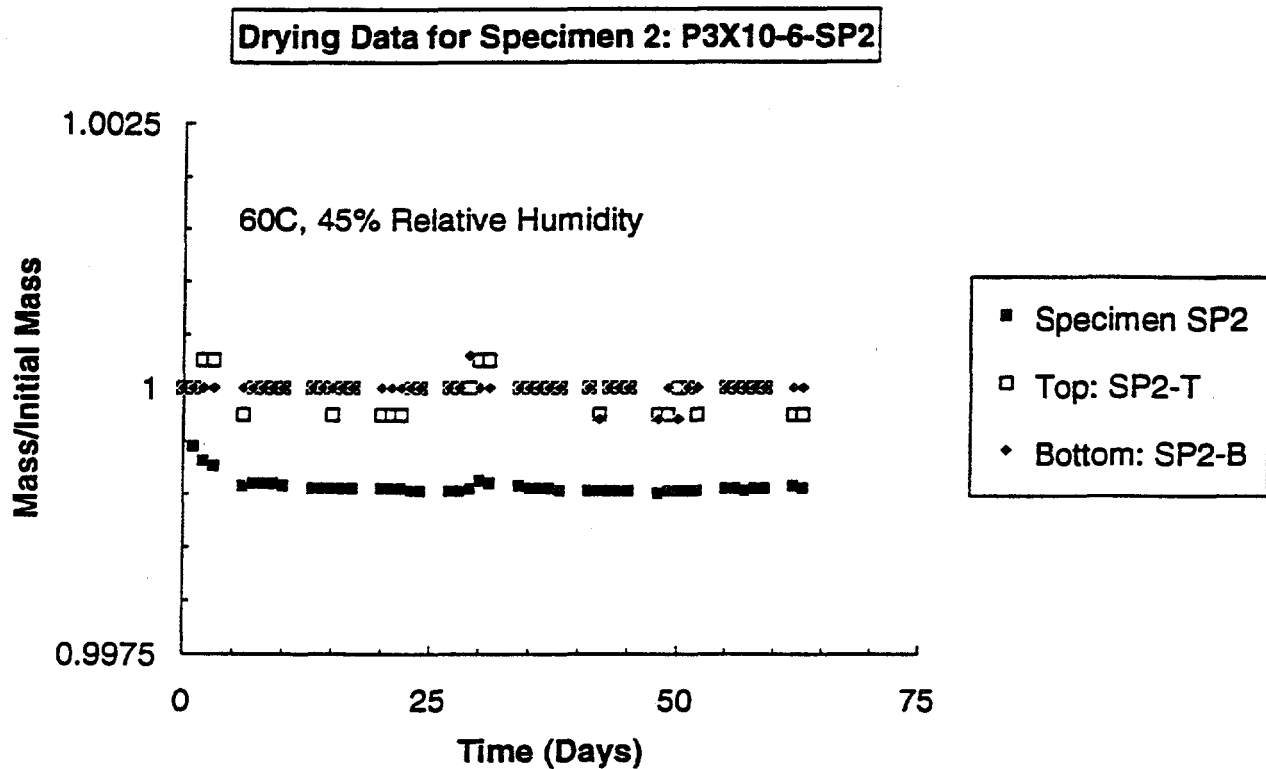
RSI-248-93-023

Figure 2-6. Change in mass during drying at 60°C and 45 percent relative humidity for Specimen P3X10-6-SP2. Initial masses are 2.15655 kg, 0.03885 kg, and 0.03367 kg for the permeability specimen and the porosity specimens taken from above (SP2-T) and below (SP2-B) the permeability specimen, respectively.

Drying Data for Specimen 3: P3X11-5-3-SP3

60C, 45% Relative Humidity

Legend:
- ■ Specimen SP3
- □ Top: SP3-T
- ◆ Bottom: SP3-B

Y-axis: Mass/Initial Mass (1.0025, 1, 0.9975)

X-axis: Time (Days) (0, 25, 50, 75)
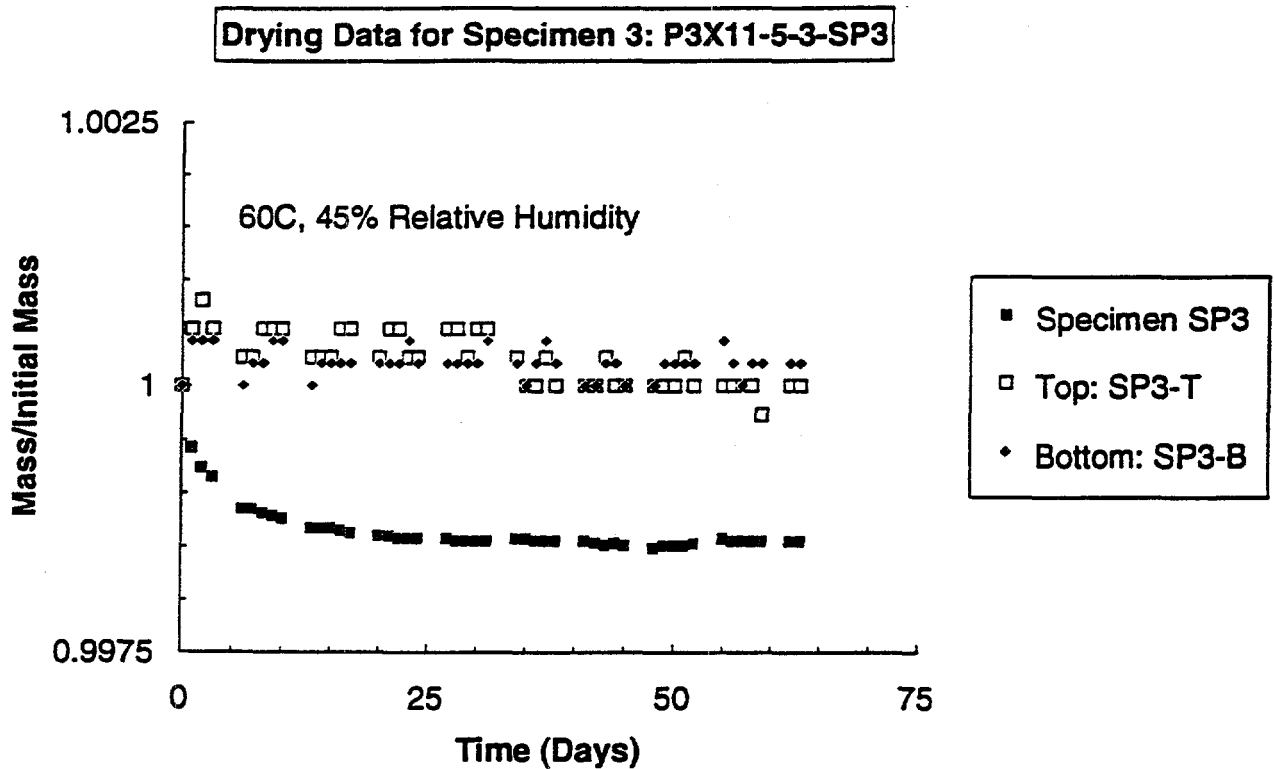
RSI-248-93-024

Figure 2-7.   Change in mass during drying at 60°C and 45 percent relative humidity for Specimen P3X11-5-3-SP3. Initial masses are 2.17060 kg, 0.03751 kg, and 0.04767 kg for the permeability specimen and the porosity specimens taken from above (SP3-T) and below (SP3-B) the permeability specimen, respectively.

3.0 EXPERIMENTAL METHODS

3.1 Specimen Characterization

Petrographic analysis and X-ray diffraction were used to determine MB 139 composition. Thin sections and X-ray diffraction samples were manufactured from the TS blocks taken from different sections of the marker bed. Three orthogonal thin sections were made from material at each location. Rectangular blocks approximately 3 inches in length, 2 to 3 inches in width, and 0.5 inches in thickness were roughed out at RE/SPEC Inc. for thin section manufacture and then sent to San Diego Petrographics for final thin section preparation. The X-ray diffraction samples were ground at RE/SPEC Inc. Six additional X-ray diffraction samples were obtained from material taken from above and below the axes of the three permeability specimens. Both types of analyses were performed by the Engineering and Mining Experiment Station at South Dakota School of Mines and Technology in Rapid City, South Dakota. The procedures that were used for petrographic analysis and X-ray diffraction work are given in Appendices B-A and B-B, respectively.

3.2 Coring-Induced Surface Damage

Two specimens were cored for this task. The first specimen, P3X11-6/1 (labeled LC3 NX core in Figure 2-1), was prepared according to standard procedures. The core was cut dry at a core barrel rotation speed of 1,300 rpm. The coring process generally requires less than 10 minutes to produce a 0.1-m-long specimen. The second specimen, P3X11-5-3/1 (labeled LC2 NX core in Figure 2-1), was cored using a slower core barrel advance rate so that the coring process required 23 minutes. The core barrel rotation speed was slowed to 1000 rpm to eliminate the chatter that occurs at this slower advance rate. This procedure was used so that damage induced along the specimen ends using the slower rate could be compared with the standard technique used for the previous core.

The cores were impregnated under vacuum with epoxy containing fluorescent red rhodamine-B dye-penetrant. The vacuum chamber contained two ports; one port was connected to the vacuum pump and the other was valved shut but was connected to a chamber containing a low viscosity epoxy (EPO-TEK 301 with a viscosity of 100 centipoise). The specimen was placed in the chamber and held under a vacuum of 680 mm Hg for 15 minutes. The valve to the epoxy chamber was then opened, allowing the epoxy to be drawn into the specimen. After the epoxy

hardened, the vacuum was removed and the epoxy was permitted to cure overnight. Each core was then sawed in half lengthwise (parallel to the core axis and parallel to bedding) and both halves were polished.

A quantitative analysis of specimens cored at different rates was performed. Each specimen was placed under a petrographic microscope and examined at a magnification of 200X. The microscope's light source was filtered so that the rhodamine-B dye fluoresced under examination. Each specimen was placed on an X-Y microscope stage so that it could be translated by moving the stage relative to a fixed vernier scale. Three lines parallel to the specimen axis were defined for each specimen; these were located along the central specimen axis and 0.5 mm from each edge. The crosshair of the microscope was translated along each line and the locations of all cracks intersected by the crosshair were recorded.

3.3 Porosity Measurements

3.3.1 Effective Porosity

Porosity measurements were conducted on six specimens manufactured from pieces immediately adjacent to the permeability test specimens. Core Laboratories performed effective porosity tests using a helium porosimeter according to the procedure given in Appendix B-C. These specimens were dried at controlled temperature and humidity conditions in the RE/SPEC Inc. laboratory as described in Chapter 2.0. To ensure that no moisture changes occurred during shipping or due to the higher humidity at the Core Laboratories Houston offices, specimen masses were measured at RE/SPEC Inc. before shipping and at Core Laboratories just after receipt and just before testing. Three metal weights were also weighed and shipped to ensure that there were no discrepancies between the outputs of the scales in the two laboratories. The largest difference in the mass measurements for the metal specimens was 0.0018 percent for the 50 g metal weight, indicating that the Core Laboratories and the RE/SPEC scales gave identical values within the accuracy of the measurements. The largest difference in the mass measurements for the anhydrite specimens was 0.0108 g and all but two were less than 0.01 g which is the resolution of the RE/SPEC Inc. scale. This indicates that there was little or no moisture change during shipping and handling.

3.3.2 Total Porosity

Total porosities were measured for the three porosity specimens made from material taken from above each permeability specimen. The procedure that was used followed ASTM D854-83, *Standard Test Method for Specific Gravity of Soils*. Specimens were placed in the humidity chamber at 60°C and 45 percent relative humidity and dried to ensure that masses were constant. The specimens were then ground until all particles passed through a 0.425-mm sieve. Ground specimens were placed in clean, dry, 100-ml flasks of known mass and again dried at 60°C and 45 percent relative humidity to ensure that masses were stable. The masses of the flasks and their contents were then measured. The flasks containing the specimens were then filled with kerosene to the calibration marks and a vacuum was applied to each flask for approximately 5 days until all air was removed. The kerosene levels in the flasks were then adjusted to reach the calibration marks and masses were measured. Each clean flask was also filled to the calibration mark with pure deaerated kerosene and the combined masses were measured. The grain densities and total void volumes were determined using Equation 3-1 which is derived in Appendix B-D.

$$\text{Porosity} = 1 - \left[\frac{\left(\dfrac{Ms_s}{0.25 \cdot L \cdot \pi \cdot D^2} \right)}{\left(\dfrac{(Mfk_1 - Mf) \cdot (Mfs_g - Mf)}{(Vf \cdot (Mfs_g - Mf + Mfk_1 - Mfs_g k_2))} \right)} \right] \quad \text{(3-1)}$$

where

Ms_s = Mass of solid specimen before grinding

L = Specimen length before grinding

D = Specimen diameter before grinding

Vf = Volume of flask to calibration mark

Mf = Mass of flask

Mfs_g = Mass of flask containing ground specimen

Mfk_1 = Mass of flask filled with deaerated kerosene to calibration mark

$Mfs_g k_2$ = Mass of flask containing ground specimen and filled with deaerated kerosene to calibration mark

3.4 Brine Production and Saturation

A standard brine was used for specimen saturation and as the permeant for liquid permeability measurements. Standard brine SB-139-95B was prepared by Twin City Testing of Rapid City, South Dakota, according to directions supplied by Sandia National Laboratories. The specified composition was designed to be 95 percent saturated with respect to the minerals in MB 139. The brine preparation instructions provided by Sandia and the laboratory notes kept by Twin City Testing during brine preparation are given in Appendix B-E. The brine was prepared in two separate batches and the laboratory notes for both are provided.

Permeability specimens were subjected to a saturation procedure after gas permeability measurements had been completed. The masses of three MB 139 specimens were measured and then specimens were submersed in a jar containing 2 gallons of clean brine. It was anticipated that specimen mass would increase while the system was under vacuum until saturation occurred. The specimens were removed from the brine after 4 days and evidence of specimen dissolution was noted. Many grains were loose and sediment had accumulated in the bottom of the jar. Some of the previously machined sharp edges of the specimens were also somewhat rounded. The specimen masses before and after saturation are given in Table 3-1. Although Specimen SP1 shows very little net change, this specimen had undoubtedly absorbed some brine which compensated for the loss of some solid mass. Samples of clean brine and brine used for saturation were sent to Sandia for analysis. The saturation procedure was terminated because of the specimen degradation and it is not known if the specimens achieved saturation.

Table 3-1. Change in Specimen Mass During Saturation Procedure

	Date	Time	Specimen Mass (g)		
			P3X11-5-2-SP1	P3X10-6-SP2	P3X11-5-3-SP3
Before Saturation	8-6-93	16:50	2200.70	2154.15	2163.85
After Saturation	8-10-93	15:20	2199.15	2101.85	2125.35
Net Change			-1.55	-52.3	-38.5

3.5 Permeability Measurements

3.5.1 Test Apparatus

3.5.1.1 LOAD FRAME

Figure 3-1 presents a cross section of a typical load frame used for permeability tests with prominent components labeled for reference. Three test frames were used in this study so that a separate frame could be devoted to each specimen. The frames use single-ended, triaxial pressure vessels. A linear actuator (hydraulic cylinder) bolted to the base of the load frame drives the loading piston, which in turn applies axial compressive force to the specimen. Confining pressure was applied to the jacketed specimens by pressurizing the sealed vessel chamber with silicone oil. A dilatometer system maintained constant confining pressure. The testing machines can apply compressive axial loads up to 1.5 MN and confining pressures up to 70 MPa. The heating system can maintain specimen temperatures up to 200°C.

A control panel houses the accumulators, hydraulic pumps, pressure intensifiers, transducer signal conditioners, temperature controllers, and confining pressure controllers for two adjacent test frames. The panels contain digital meters that display the output of the transducers. The temperature controller gives a digital output of the temperature. Mechanical pressure gages mounted in the panel give readings of oil pressure in the hydraulic cylinder.

3.5.1.2 INSTRUMENTATION

Axial force is measured by a load cell in the load train outside the pressure vessel, while confining pressure is measured by a pressure transducer in the line between the dilatometer and the pressure vessel. Temperature is measured by a thermocouple in the wall of the pressure vessel. The relationship between specimen temperature and that recorded by this thermocouple has been determined by calibration runs at several temperatures spanning the operating range. Two Linear Variable Differential Transformers (LVDTs) mounted outside the pressure vessel monitor displacement of the loading piston relative to the bottom of the pressure vessel and can be used to calculate axial strain of the specimen. Volumetric deformation is measured using a dilatometer. With this technique, volumetric deformation is determined at fixed pressure by first measuring the volume of oil that the dilatometer supplies to the pressure vessel, and then
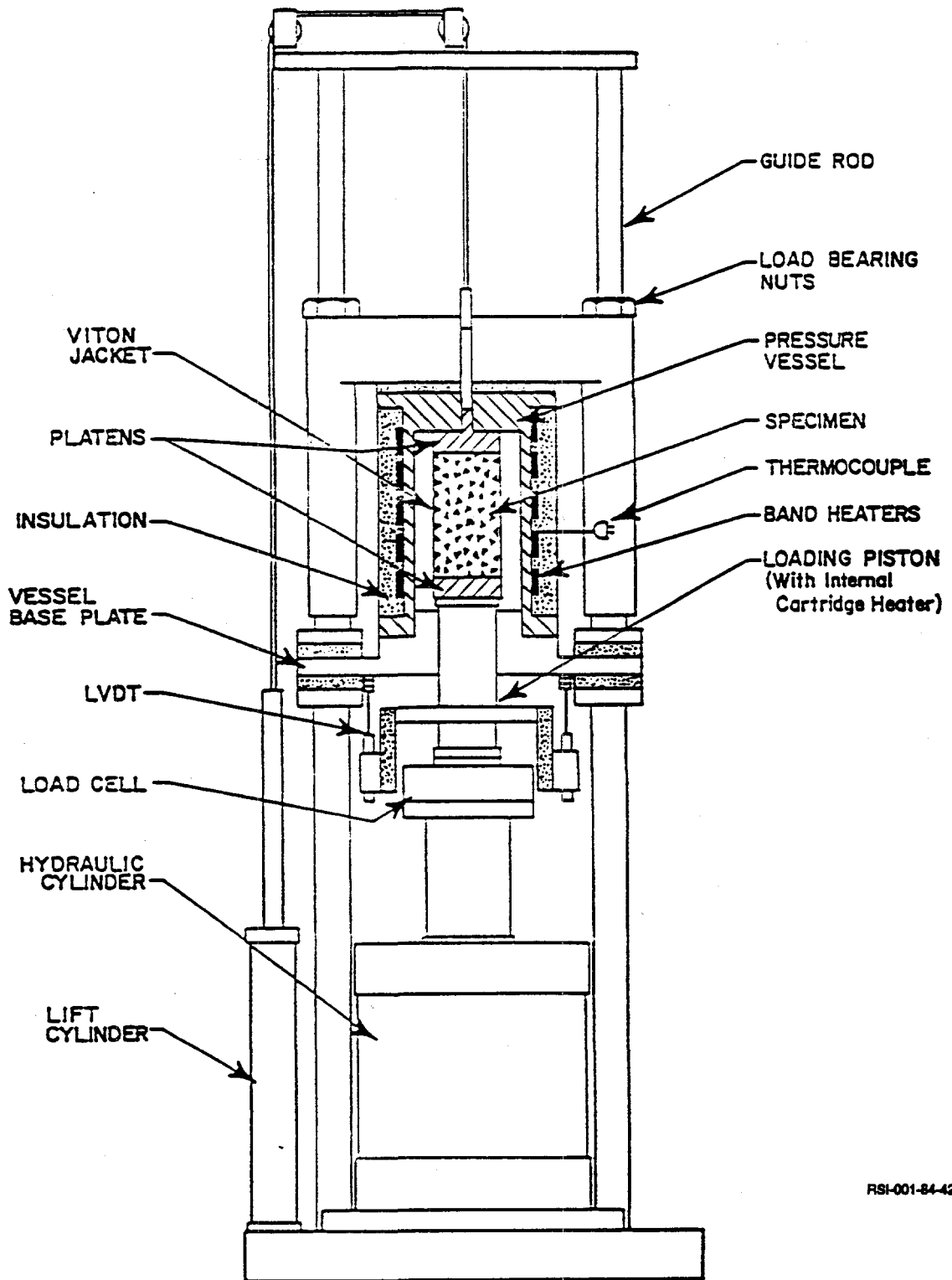
Figure 3-1. Load frame used for permeability tests.

RSI-001-84-428

compensating for the axial deformation measured by the LVDTs. A rotary potentiometer or stroke transducer is mounted on the dilatometer shaft to provide a signal proportional to the volume of oil supplied to the pressure vessel.

3.5.1.3 CONTROL

Temperature was maintained at 25°C with a manual set-point controller that regulated power to the band heaters on the vessel. The thermocouple in the pressure vessel wall supplied the feedback signal. Confining pressure was controlled by inputting the pressure transducer signal to a unit that contained two manual set points. These set points were adjusted to maintain the confining pressure constant within 20 kPa. The controller signals the intensifier to advance or retreat, depending upon whether the lower or upper set point has been reached. Axial load was controlled by a Digital Equipment Corporation PDP-11/23 microcomputer. The computer determined the current cross-sectional area of the specimen from the outputs of the deformation transducers and then adjusted the load to maintain constant stress. The deadband on load under computer control was 0.4 kN.

3.5.1.4 GAS PERMEABILITY SYSTEM

The gas permeability measurement system is shown in Figure 3-2. Nitrogen gas pressure was supplied to the lower surface of the specimen by a pressurized gas bottle. The charge pressure was controlled manually with a valve located on the gas bottle and measured by a pressure transducer. A manometer comprising two calibrated burets filled with mineral oil and connected at the base by tubing was used to measure the volume of gas exiting the specimen. As nitrogen filled the left side of the manometer, oil was forced out of the right side and into an overflow reservoir. The position of the gas/oil miniscus on the left side of the manometer was read using the calibrated markings on the buret. Using this system, the gas exit pressure increased over time as the hydraulic head increased, but the pressure increase was very small (less than 0.0045 MPa).

MANOMETER

SPECIMEN

REGULATOR VALVE

NITROGEN SUPPLY

PRESSURE TRANSDUCER
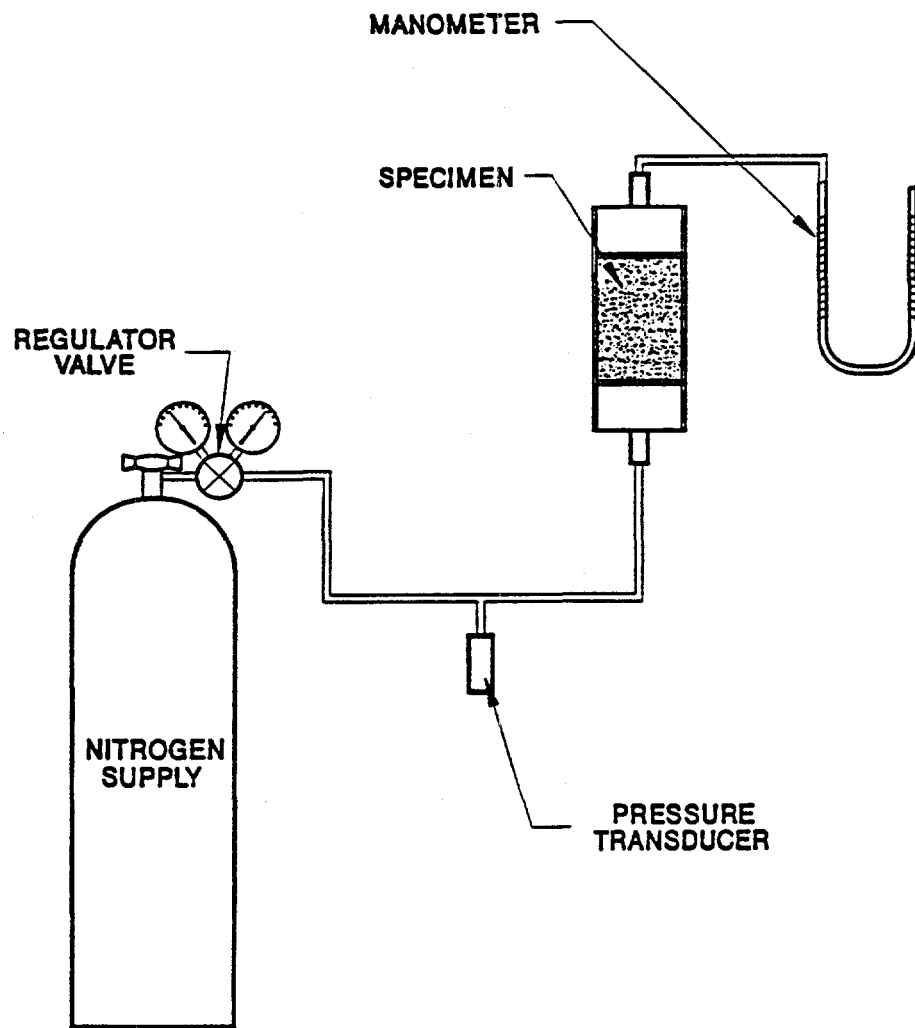
SCALE: NONE

RSI-197-92-019

Figure 3-2. Gas permeability measurement system.

3.5.1.5 BRINE PERMEABILITY SYSTEM

The brine permeability measurement system is shown in Figure 3-3. A nitrogen-driven accumulator supplied pressurized brine to the lower surface of the specimen. The charge pressure (and therefore the pressure drop across the specimen) was regulated manually with a valve located on the nitrogen bottle and was measured by a diaphragm-type pressure transducer in the hydraulic line between the accumulator and the specimen. The pressure drop in the lines between the pressure transducer and the specimen is negligible. Permeant flow through the specimen was captured and measured by a buret attached to the upper end cap of the specimen assembly. Evaporation of the permeant was prevented by placing a thin film of mineral oil on top of the permeant column in the buret (Brodsky, 1993).

3.5.1.6 SPECIMEN ASSEMBLY

The specimen assembly for all permeability tests is shown in Figure 3-4. Permeant entered the system through the lower platen, permeated the specimen, and exited through the upper vent. The spacer extended the length of the specimen assembly so that it could be easily accommodated by the testing machine. Porous felt metal disks were placed along the specimen/platen interfaces to ensure uniform permeant pressure along the specimen's upper and lower surfaces. Two Viton jackets or sleeves were used to protect specimens from the silicone oil used as a confining fluid.

3.5.1.7 CALIBRATION

The transducers used to collect force, pressure, deformation, and temperature data were calibrated using standards traceable to the National Institute of Standards and Technology and documented procedures. Each transducer was calibrated in its normal operating position on the test system so that the signal conditioners, filters, and analog-to-digital converters were included within the end-to-end calibration. Calibration constants were determined for each transducer from a linear, least-squares regression of indicated reading versus standard input. Readings were collected at 20 standard inputs equally spaced over the range of the transducer. These constants were verified immediately before testing began by comparing the predicted response of the transducer using these constants with the standard input applied in ten equally spaced steps over the calibrated range. This verification procedure was performed periodically so that drift or transducer malfunctions would be identified. Table 3-2 gives the range and resolution for these
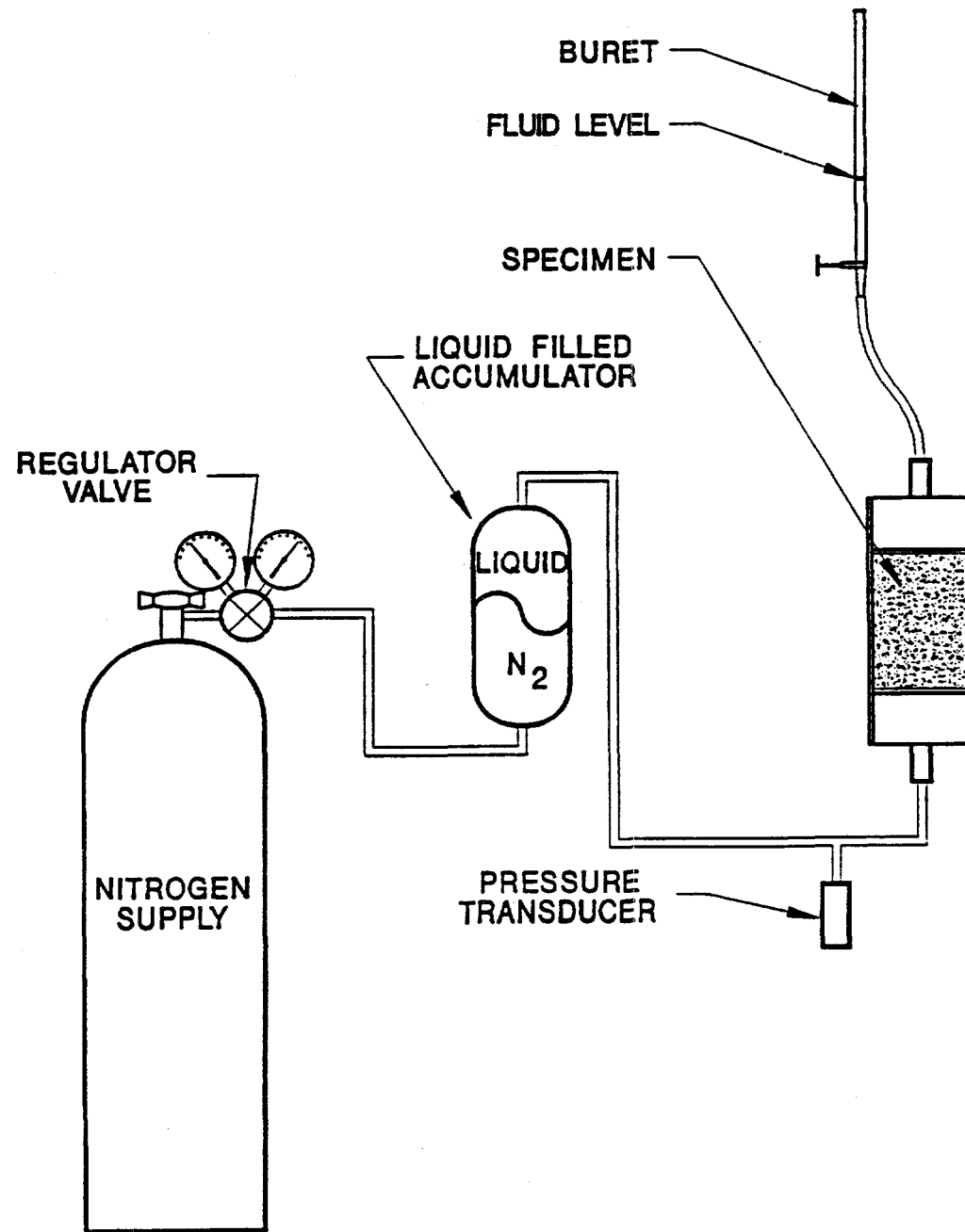
Figure 3-3. Liquid permeability apparatus.

RSI-197-92-020
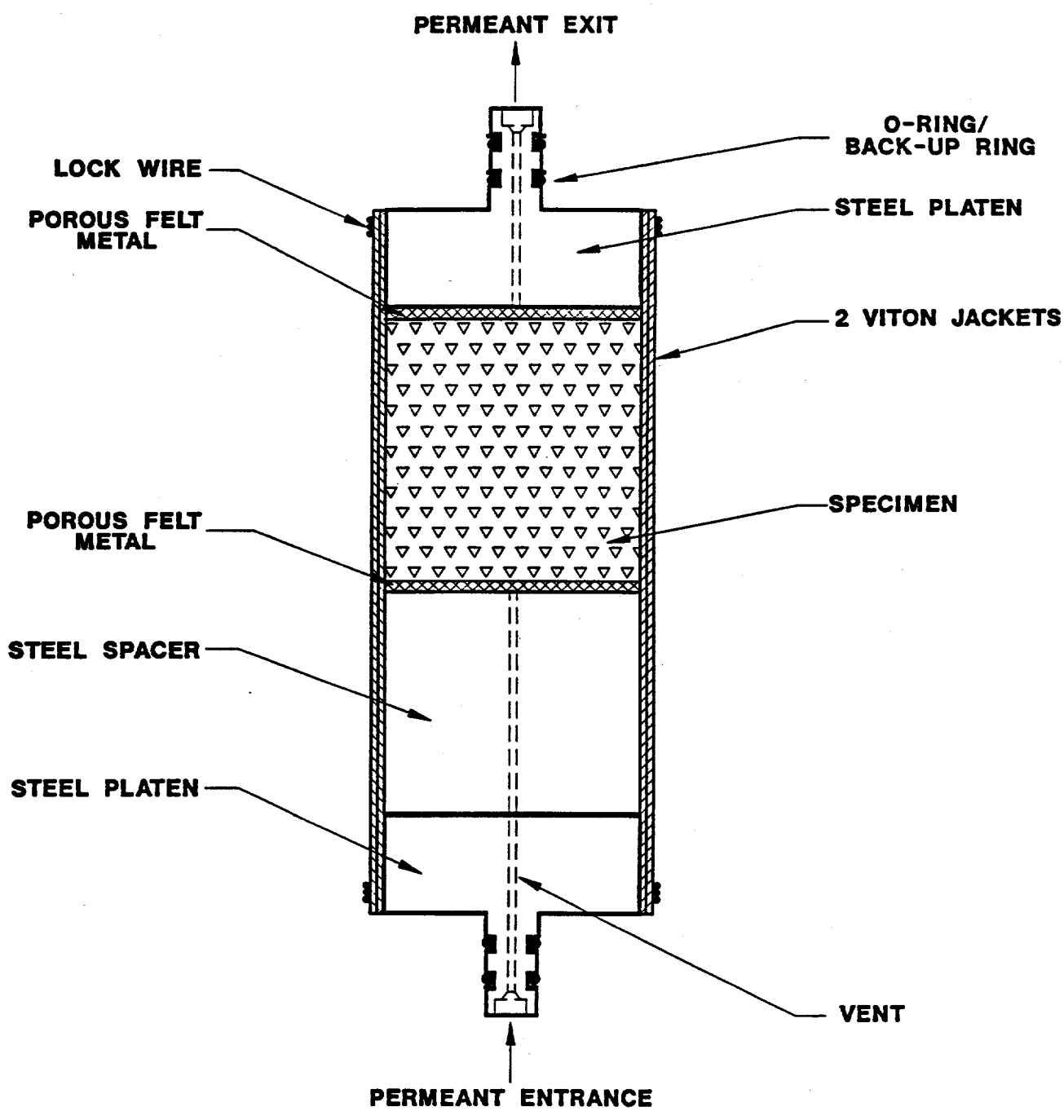
Figure 3-4. Specimen assembly for permeability tests.

transducers. Prior to testing, verifications showed that the accuracy errors for force and pressure transducers were less than 1 percent of reading and that of thermocouples was ±1°C. The accuracy specifications include both nonlinearity and repeatability. The burets used were Class A and are accurate to within 0.1 ml. All transducers were reverified after the completion of testing, and pore pressure and confining pressure transducers were also reverified midway through the testing program (after completion of gas permeability tests). Confining pressure transducers and thermocouples always reverified to within the specifications given above and shown in Table 3-2. Pore pressure transducer errors were within 1.7 percent of target values.

Table 3-2. Calibration Specifications

Measurement	Range	Resolution
Axial Force (kN)[a]	0 to 250	0.03[b]
Confining Pressure (MPa)[a]	0 to 34.5	0.004[b]
Temperature (°C)[c]	0 to 250	0.03[b]
Pore Pressure (MPa)[a]	0 to 6.895	0.0008[b]
Permeant Volume at 20°C and 0.1 MPa (ml)[d]	0 to 50	0.05

(a) Accuracy: 1 percent of reading including nonlinearity and repeatability.
(b) 14-bit analog-to-digital converter. One bit used for sign.
(c) Accuracy: ± 1°C.
(d) Accuracy: Exit buret calibrated to 0.1 ml.

3.5.2 Test Procedure for Permeability Tests

Assembled specimens were placed in load frames and the pressure vessels were lowered over the specimens. The pressure vessels were then filled with silicone oil, heated to 25°C, and pressurized to 2 MPa confining pressure. A temperature of 25°C was used rather than 20°C because heating the pressure vessel facilitates maintaining constant temperature. The temperature and pressure were allowed to stabilize for at least 12 hours. Moisture evaporation from the specimens was prevented during stabilization by closing the lower pore pressure vents and connecting oil traps to the upper vents. (An oil trap comprised flexible tubing that was attached to the upper pore pressure vent at one end and to a buret at the other end. Between the vent and the buret, the tubing was looped so that oil placed in the bottom of the loop was trapped and formed a moisture barrier.) After stabilization, data acquisition was initiated, control of the confining pressure was given to the automatic controller which signaled the dilatometer system to either inject or withdraw oil to maintain the pressure.

Nitrogen pressure was applied to the lower specimen surface for gas permeability measurements or to the brine-filled accumulator for liquid permeability measurements. Permeability was determined by measuring the steady-state flow rate of permeant through the specimen and the pressure drop across the specimen. The pressure drop was controlled throughout the permeability test by manual adjustment. The flow rate was determined manually by monitoring the gas/oil miniscus in the manometer for gas measurements and the in the buret for liquid permeability measurements.

A permeant inlet pressure of 1.0 MPa was used for the first series of permeability tests on each specimen except for the first of three gas permeability measurements for Specimen SP2 which was conducted at an inlet pressure of 1.1 MPa. Outlet pressure was atmospheric (0.1 MPa) and so the pressure drop across the specimen was 0.9 MPa (1.0 MPa for the first measurement on Specimen SP2). Gas permeability measurements proceeded reasonably quickly and so three replicate tests were performed at each test condition. After tests were completed at 1.0 MPa, the inlet pressure was decreased to 0.7 MPa and then to 0.4 MPa for measurements at pore pressure differences of 0.6 and 0.3 MPa, respectively. Confining pressure was then increased to 6 MPa and then to 10 MPa and the sequence of tests at each inlet pressure was repeated for each confining pressure. After each change in confining pressure, the system was allowed to stabilize overnight. After completion of each brine permeability test, the brine that had collected in the exit buret was collected, placed in a sample jar, and sent to Sandia National Laboratory for analysis.

3.5.3 Data Acquisition and Reduction

3.5.3.1 DATA ACQUISITION

A DEC LSI-11/23 microprocessor was used to acquire measurements of time, axial load, confining pressure, volumetric deformation, axial (piston) displacement, and temperature. The computer scanned the data channels at 15-second intervals, logged data at least every 2 hours, and wrote the data to disk on the microprocessor. The logged data were later transmitted to a separate computer for data reduction and analysis. Permeability data included time, pressure drop across the specimen, and the permeant level in the buret. These data were recorded manually and the data acquisition rate depended on the flow rate. For gas permeability tests, data were recorded generally after each 2 ml increment of gas accumulation in a 50 ml buret and so at least 20 data points were used in each permeability determination. For several tests in which gas flow

proceeded slowly, data were collected at approximately even increments of time. Flow rates were slower in the liquid permeability tests and data were recorded at approximately even increments of time.

3.5.3.2 DATA REDUCTION

Permeability to brine was determined from Darcy's law, i.e.,

$$k = \frac{\mu\, Q\, L}{A\, (P_i - P_E)} \tag{3-2}$$

where

k = Permeability (m²)

Q = Flow rate (m³ · s⁻¹)

P_E = Pressure at exit (MPa)

μ = Brine viscosity at test temperature (MPa · s)

L = Specimen Length (m)

P_i = Pressure at inflow (MPa)

A = Specimen cross sectional area (m²)

A value of 1.26 centipoise (1.26 × 10⁻⁹ MPa · s) was used for brine viscosity. Flow rates were calculated from the buret level-versus-time data by fitting with a linear least squares regression. The initial readings obtained were not used in the fit if flow rate had not yet stabilized.

Permeability to gas was determined using a modified form of Darcy's law which accounts for changes in gas density with pressure, i.e.,

$$k = \frac{2\, \mu\, L\, Q_E\, P_E}{(P_i^2 - P_E^2)\, A} \tag{3-3}$$

where

k = Permeability (m²)

Q_E = Flow rate at exit (m³ · s⁻¹)

P_E = Pressure at exit (MPa)

μ = Viscosity of gas at test temperature (MPa · s)

L = Specimen Length (m)

P_i = Pressure at inflow (MPa)

A = Specimen cross sectional area (m^2)

A value of 178 micropoise (1.78 × 10^{-11} MPa · s) was used for nitrogen viscosity (Weast, 1974). Equation 3-3 was derived from Equation 3-2 using the method given by Holcomb and Shields (1987). The flow rate given in Equation 3-2 is an average rate. Substitution of the ideal gas law,

$$P_{avg} \; Q_{avg} = P_{exit} \; Q_{exit} \qquad (3\text{-}4)$$

and

$$P_{avg} = \frac{(P_{inlet} + P_{exit})}{2} \qquad (3\text{-}5)$$

into Equation 3-2 gives Equation 3-3.

For both liquid and gas permeability tests, three values of inlet pressure were used for each confining pressure so that the relationship between flow rate and pressure difference across the specimen could be checked for linearity. A linear relationship implies that flow is laminar. The Klinkenberg correction was also applied to gas permeability data at each confining pressure by plotting permeability versus reciprocal mean pore pressure and fitting a straight line to the data. The permeability axis intercept at a reciprocal mean pressure of zero gives the equivalent liquid permeability value.

3.5.4 Shakedown Tests for Gas Permeability Measurements

Six shakedown tests were performed to evaluate the gas permeability test procedure and equipment. Two of these tests were performed on a solid aluminum specimen and four tests were performed on MB 139 anhydrite. The purpose of testing aluminum was to ensure that there were no gas leaks in the system and that the Viton jacket conformed to the specimen surface and prevented channeling of gas along the specimen/jacket interface. The first test was performed on a solid aluminum specimen at an inlet pore pressure of 0.5 MPa and a confining pressure of 1 MPa, i.e., at an effective confining pressure of 0.5 MPa. This effective confining pressure was less than that used for testing and so any problems with gas channeling along the specimen/jacket interface should have been evident; however, no gas flow was detected. The second test on aluminum contained a flattened aluminum tube inserted between the specimen and jacket that

provided a small pathway for gas flow. Using this specimen configuration a gas flow rate of approximately 3 ml · s^{-1} was measured in the manometer. All joints along the gas flow path were inspected for leaks using "Snoop," a commercial gas flow detection fluid and no leaks were detected.

The shakedown tests on MB 139 were run to evaluate the test procedure and to determine rough approximations of gas permeability values so that the appropriate instrumentation would be used for measurements. (Different flow rate detection equipment is required for different ranges of flow rates.) A single specimen was used for all four shakedown tests. The specimen was cored and finished but was not dried. The shakedown testing revealed no problems with the test procedure. The tests did show that flow rates decreased with time for the longer duration tests which was attributed to an equipment malfunction. This problem was eliminated by purchasing and installing new gas pressure regulators for the test systems.

4.0 TEST RESULTS

4.1 MB 139 Specimen Characterization

A total of nine petrographic analyses and nine X-ray diffraction analyses were performed on the marker bed material. The locations from which the specimens were taken were given in Figure 2-1. Specimens SP2 and TS2 were taken from Core P3X10 while SP1, TS1, SP3, and TS3 were taken from Core P3X11. Specimens SP1, SP2, and SP3 were taken from the upper, upper/central, and lower sections of the marker bed, respectively. Blocks TS1, TS2, and TS3 were taken from the central, upper, and lower sections, respectively.

The results of the petrographic analyses are given in Table 4-1. These data are given in terms of volume percent and were converted to weight percentages using the specific gravities in Table 4-2. The X-ray diffraction data were provided in terms of weight percent and are given in Table 4-3 along with the converted petrographic data. The complete reports for optical microscopy and X-ray diffraction analyses as supplied by the South Dakota School of Mines and Technology are given in Appendices A and B, respectively.

The mineral quantities determined by X-ray diffraction for material taken from above and below each permeability specimen were averaged and are plotted in Figure 4-1. Specimen SP1 is notably low in anhydrite and high in polyhalite. The compositions of SP2 and SP3 are more comparable. The compositions of the thin sections and the X-ray diffraction specimens taken from the thin section blocks are shown in Figures 4-2, 4-3, and 4-4 for TS1, TS2, and TS3, respectively. Specimens with identification numbers ending in "-1" and "-4" were originally perpendicular to the bedding plane while the remaining specimens were parallel to bedding. There does not appear to be any systematic difference between specimens of different orientations. The mineral quantities determined for each thin section block were averaged and the bulk compositions of the three thin section blocks are compared in Figure 4-5. Data from block TS2, from the uppermost section of the marker bed are plotted first, then TS1 and TS3 from the central and lower sections, respectively. It is evident that the specimens are primarily anhydrite. Specimens SP3 and TS3, which came from the lowermost section of the marker bed, have larger anhydrite components than do specimens SP1, SP2, TS1, and TS2. Data from blocks TS1, TS2, and TS3 indicate that the upper section of the marker bed (TS2) is enriched in halite. Specimens from the P3X10 borehole (SP2 and TS2), however, generally have more halite than those from the P3X11 borehole, making it difficult to distinguish between vertical and lateral heterogeneities. The average compositions of SP1 and TS1 are different, even though the

Table 4-1. Summary of Quantitative Polarized Light Microscopy Analyses of MB 139 Thin Sections[a]

Specimen I.D.	Anhydrite (%)	Halite (%)	Polyhalite (%)	Magnesite (%)	Carbon (%)	Total (%)
P3X11-5-3-2-TS1-1	70.4	15.9	9.6	2.0	2.2	100.1
P3X11-5-3-2-TS1-2	45.8	13.4	30.6	9.4	0.8	100.0
P3X11-5-3-2-TS1-3	48.9	26.7	14.9	8.0	1.6	100.1
P3X10-5-3-2-TS2-1	67.8	24.5	0.0	3.5	4.2	100.0
P3X10-5-3-2-TS2-2	43.1	54.8	0.0	0.6	1.6	100.1
P3X10-5-3-2-TS2-3	58.2	37.2	0.0	3.0	1.6	100.0
P3X11-6-TS3-1	95.9	1.4	0.6	0.6	0.2	98.7
P3X11-6-TS3-2	89.9	8.8	0.0	0.0	1.4	100.1
P3X11-6-TS3-3	66.7	31.9	0.0	0.4	1.0	100.0

(a)   All values are volume percentages.

specimens were in close proximity in situ. The same is true of SP3 and TS3. These data reflect a high degree of heterogeneity in the marker bed.

Table 4-2. Mineralogical Data for MB 139

Mineral	Composition	Specific Gravity
Anhydrite	$CaSO_4$	2.94[a]
Halite	$NaCl$	2.16[a]
Polyhalite	$K_2Ca_2Mg(SO_4)_4 \cdot 2H_2O$	2.78[a]
Magnesite	$MgCO_3$	3.1[a]
Carbonaceous Material	C	1.95[b]

(a) Hurlbut (1971).
(b) The median specific gravity of amorphous carbon (Weast, 1974).

4.2 Coring-Induced Surface Damage

A quantitative analysis of crack occurrence near the surfaces and center axes of specimens cored at different rates was completed using the procedure given in Section 3.2. The data are shown in Figure 4-6 for Specimen P3X11-6/1 which was cored at a standard rate, and in Figure 4-7 for Specimen P3X11-5-3/1 which was cored at the slower rate. The axes of the figures show distance in millimeters from the origin and the outline of each specimen is given. Each crack is represented by an "x," however, some data points lie so close together that they appear to overlay one another. For Specimen P3X11-6/1, an average of approximately 1.4 cracks $\cdot$ cm^{-1} were detected along the specimen edges while 0.3 cracks $\cdot$ cm^{-1} were detected along the specimen midsection. For Specimen P3X11-5-3/1, the specimen edges contained an average of 0.1 cracks $\cdot$ cm^{-1} while no cracks were detected in the midsection.

There were 4 cracks detected along the midsection traverse line for Specimen P3X11-6/1 and no cracks detected along that traverse line for Specimen P3X11-5-3/1. The two traverse lines adjacent to the specimen borders of Specimen P3X11-6/1 contained 8 and 25 cracks, respectively, while for Specimen P3X11-5-3/1 the border traverse lines contained 3 and 0 cracks, respectively. Therefore, there are 2 ± 3 cracks per traverse line for the midsection lines, and 9 ± 11 cracks per traverse line for lines adjacent to specimen borders. These data indicate that higher crack

Table 4-3. Mineral Compositions of Marker Bed 139 Specimens[a]

Specimen I.D	Anhydrite (%)	Halite (%)	Polyhalite (%)	Magnesite (%)	Carbon (%)
P3X11-5-2-SP1T	18.4	10.1	68.8	2.62	(b)
P3X11-5-2-SP1B	6.15	3.36	90.1	0.37	(b)
SP1 Average	12.3	6.7	79.5	1.5	
P3X11-5-3-2-TS1-1	74.3	12.3	9.58	2.23	1.54
P3X11-5-3-2-TS1-2	48.2	10.4	30.5	10.4	0.56
P3X11-5-3-2-TS1-3	53.1	21.3	15.3	9.16	1.15
P3X11-5-3-2-TS1-4	60.3	10.7	26.6	2.34	(b)
TS1 Average	59.0	13.7	20.5	6.04	1.08
P3X10-6-SP2T	55.4	43.5	0	1.13	(b)
P3X10-6-SP2B	44.5	43.6	11.0	0.89	(b)
SP2 Average	50.0	43.5	5.5	1.0	
P3X10-5-3-2-TS2-1	73.5	19.5	0	4.00	3.02
P3X10-5-3-2-TS2-2	50.7	47.3	0	0.74	1.25
P3X10-5-3-2-TS2-3	64.8	30.5	0	3.52	1.18
P3X10-5-3-2-TS2-4	46.8	52.5	0	0.72	(b)
TS2 Average	58.9	37.4	0	2.2	1.3
P3X11-5-3-SP3T	55.2	39.0	0	5.73	(b)
P3X11-5-3-SP3B	58.5	37.2	0	4.32	(b)
SP3 Average	56.9	38.1	0	5.0	
P3X11-6-TS3-1	97.6	1.05	0.58	0.64	0.14
P3X11-6-TS3-2	91.4	6.57	0	1.07	0.94
P3X11-6-TS3-3	73.1	25.7	0	0.46	0.73
P3X11-6-TS3-4	71.8	28.2	0	0	(b)
TS3 Average	83.5	15.4	0.15	0.54	0.60

(a) All values are weight percentages.
(b) Not reported.
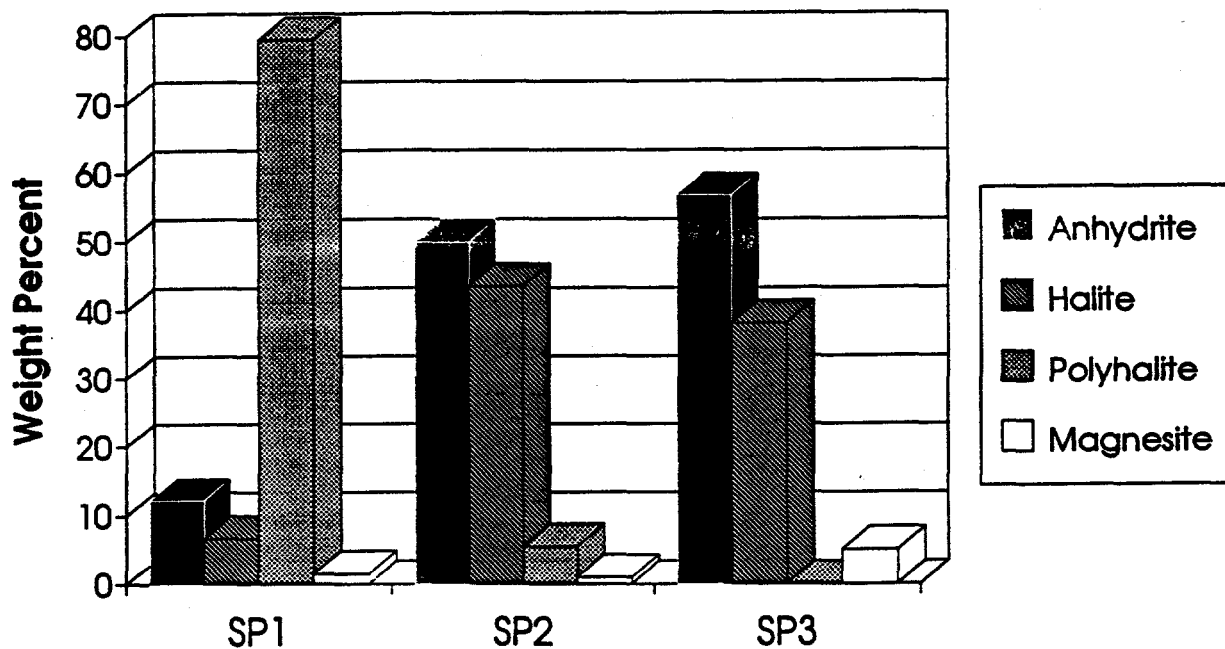
Figure 4-1. Average mineral compositions determined using X-ray diffraction for specimens taken from above and below the axes of specimens SP1, SP2, and SP3.
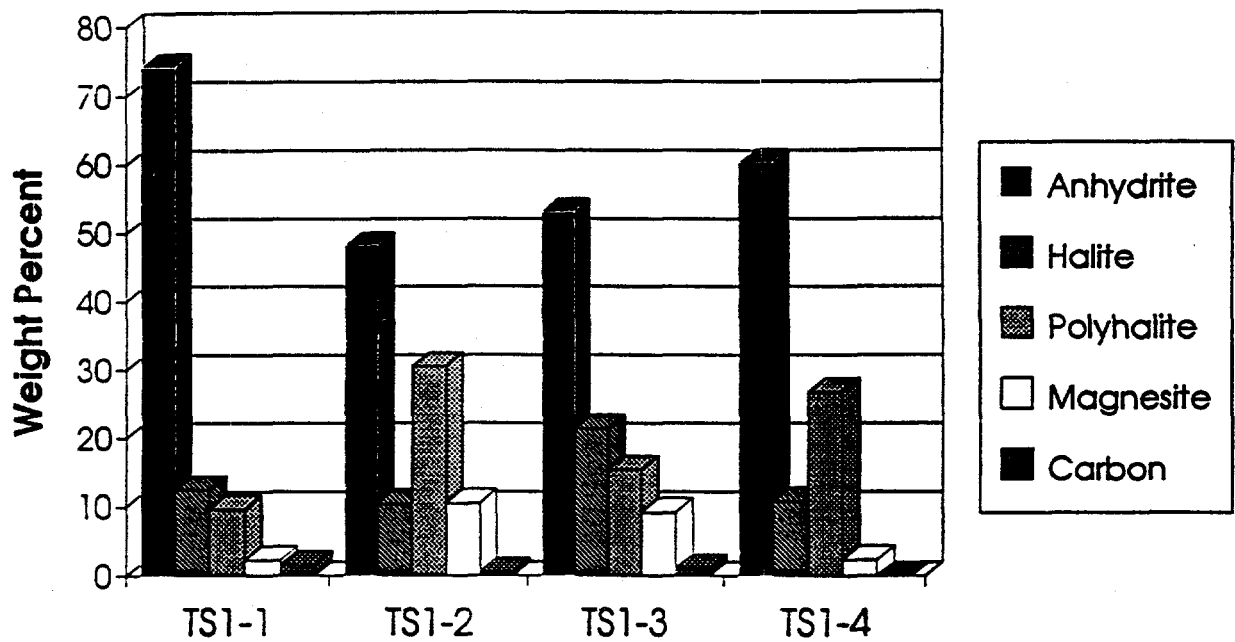
RSI-248-94-023

Figure 4-2. Mineral compositions for specimens taken from Block TS1. Petrographic analyses were used for Specimens TS1-1, TS1-2, and TS1-3; X-ray diffraction was used for Specimen TS1-4.
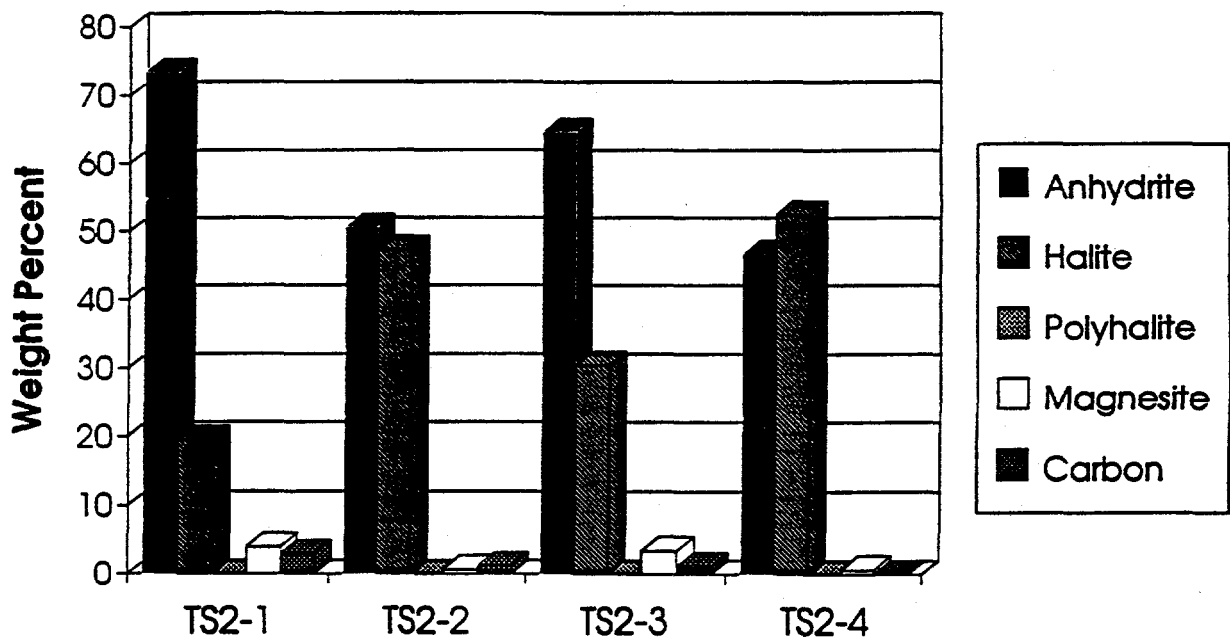
Figure 4-3. Mineral compositions for specimens taken from Block TS2. Petrographic analyses were used for Specimens TS2-1, TS2-2, and TS2-3; X-ray diffraction was used for Specimen TS2-4.
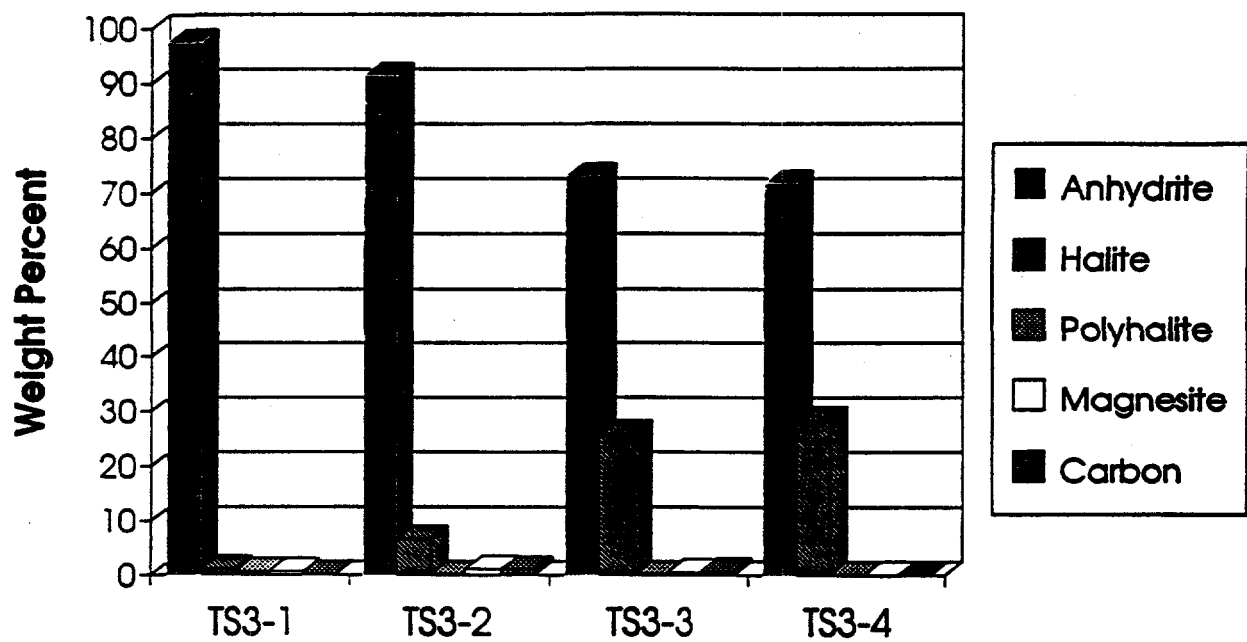
Figure 4-4. Mineral compositions for specimens taken from Block TS3. Petrographic analyses were used for Specimens TS3-1, TS3-2, and TS3-3; X-ray diffraction was used for Specimen TS3-4.
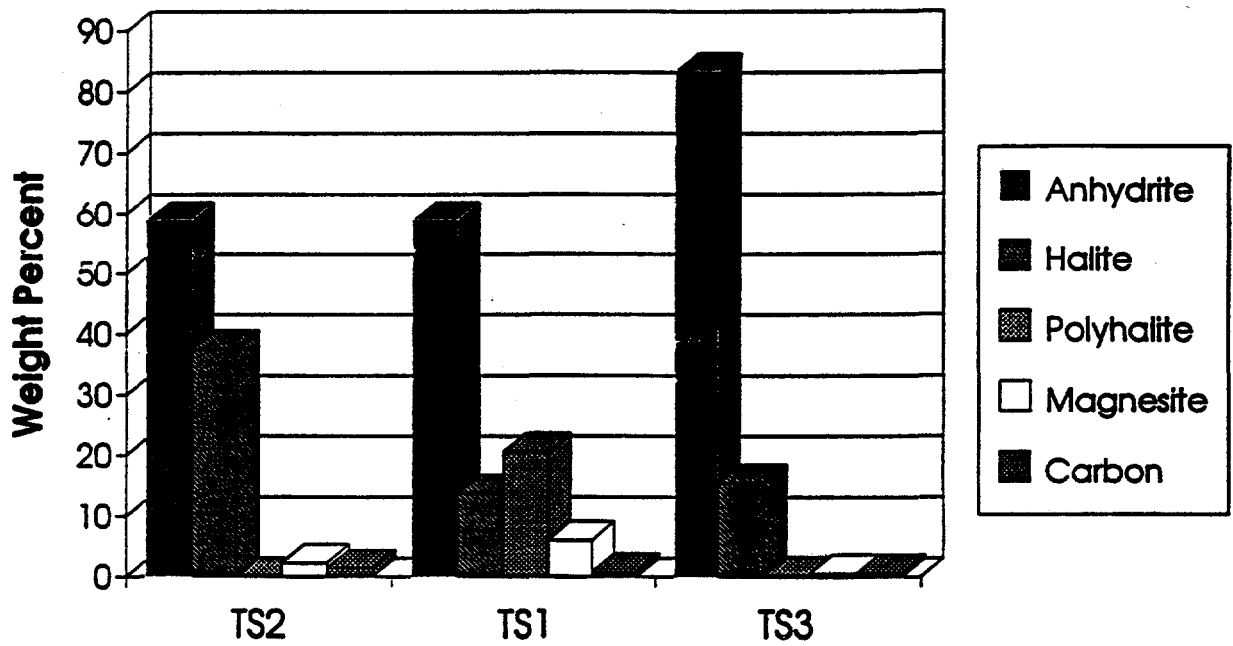
Figure 4-5. Average mineral compositions for specimens taken from Blocks TS2, TS1, and TS3 from the upper, middle, and lower sections of the marker bed, respectively.
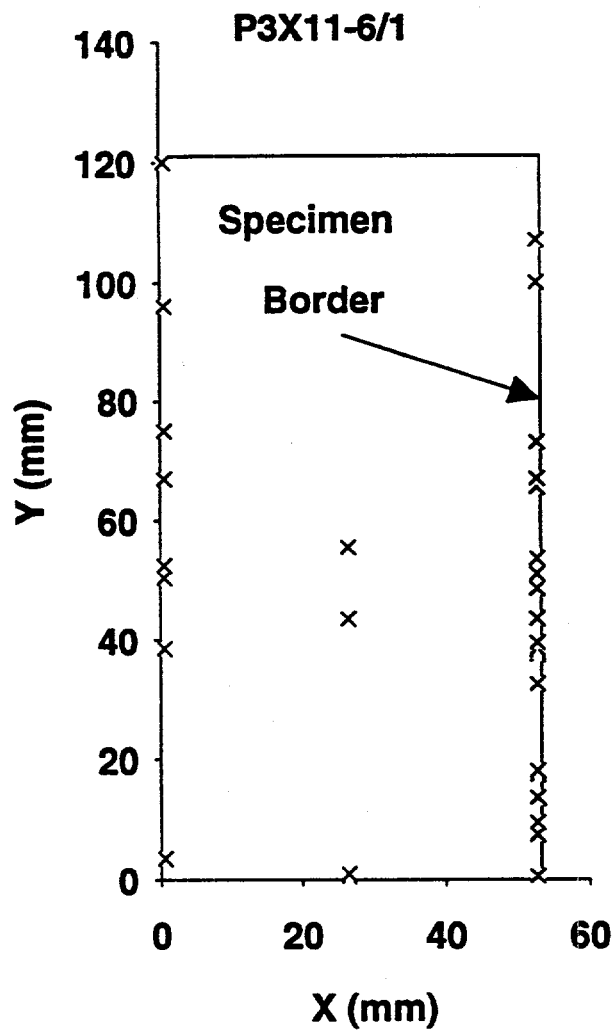
Figure 4-6. Crack occurrence on Specimen P3X11-6/1.

Figure 4-7. Crack occurrence on Specimen P3X11-5-3/1.

densities are associated with the specimen edges than with the midsection, however; the difference in crack populations is not statistically significant. Slower coring rates may reduce damage; however, differences in crack density between the two specimens may be due to specimen-to-specimen variations.

4.3 Porosity Measurements

Effective porosity and grain and bulk densities were measured for six MB 139 specimens by Core Laboratories using a helium porosimeter and the data are given in Table 4-4. Porosity varied from a low of 1.0 percent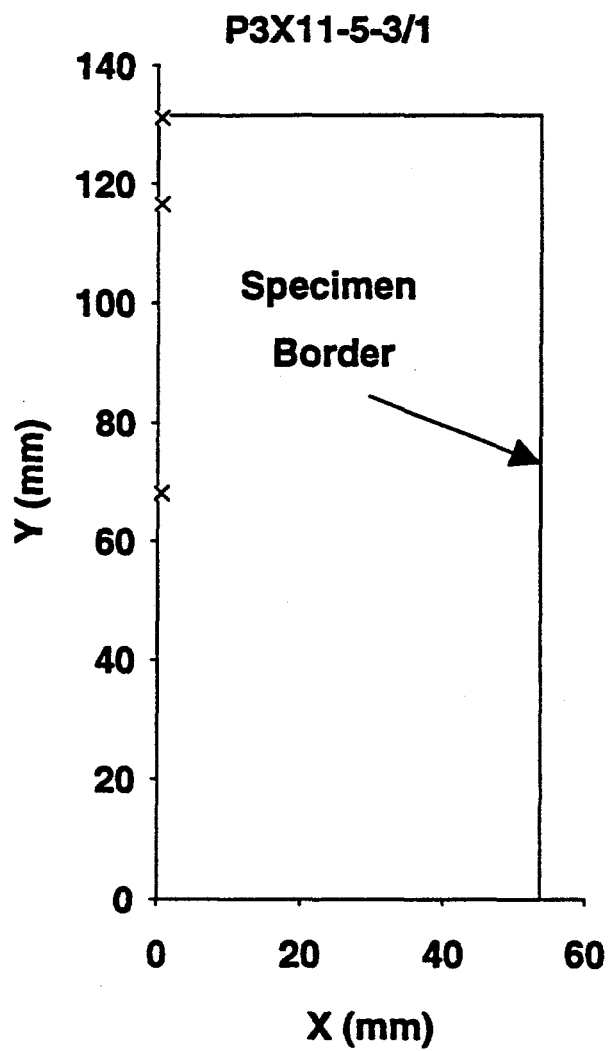 to a high of 2.1 percent. The grain densities vary from 2.53 to 2.73 g/cc while the bulk densities vary from 2.51 to 2.68 g/cc. The complete report from Core Laboratories is given in Appendix B-C.

Total porosity was measured for three of the specimens using the method given in Section 3.3.2. The densities and total porosities determined using this method and densities and effective porosities as measured for these specimens by Core Laboratories are given in Table 4-5. In all cases, the total porosities, determined using the fluid displacement technique, were greater than the effective porosities determined by Core Laboratories. In theory, the fluid displacement technique should provide higher values because grains are fractured before the measurement, providing immediate access to the specimen interior. An example of the error calculation, determined using the method given in ANSI/ASME (1986), is given in Section F1 of Appendix B-F. The errors for total porosity measurements are high because the technique relies on measuring small differences in mass among large quantities. Sampling errors were not included in the error analysis. Approximately 20-26 percent of each sample was lost during the grinding and sieving process and this may also contribute to the apparent differences between effective and total porosities.

4.4 Gas Permeability Measurements

Three nitrogen permeability tests were run at each of the test conditions given in Table 1-1. An example of the flow data obtained from each test and the linear least square fitting that was performed to obtain flow rate are given in Figure 4-8. The complete set of figures showing flow data and linear least square fits for all gas permeability tests is given in Appendix B-G. Separate plots are given for each specimen at each confining pressure and gas inlet pressure. Each plot shows the three replicate tests performed at a single set of conditions. The data for Specimens

Table 4-4. Results of Effective Porosity and Grain and Bulk Density Measurements on MB 139[a]

Specimen I.D.	Porosity (Helium) (%)	Grain Density (g/cc)	Bulk Density (g/cc)	Mass as Sent (RE/SPEC) (g)	Mass as Received (Core Labs) (g)
P3X11-5-2-SP1T	1.7	2.73	2.68	33.94	33.9326
P3X11-5-2-SP1B	2.1	2.73	2.67	37.45	37.4455
P3X10-6-SP2T	1.3	2.69	2.65	38.85	38.8394
P3X10-6-SP2B	1.1	2.57	2.54	33.67	33.6636
P3X11-5-3-SP3T	1.0	2.53	2.51	37.51	37.4992
P3X11-5-3-SP3B	1.8	2.70	2.66	47.68	47.6703

(a) Determined by Core Laboratories, Houston, Texas.

Table 4-5. Porosity, Grain Density, and Bulk Density Measurements by RE/SPEC Inc. and by Core Laboratories

Specimen ID	RE/SPEC Inc. [a]			Core Laboratories [b]		
	Porosity[c] (%)	Grain Density (g/cc)	Bulk Density (g/cc)	Porosity (%)	Grain Density (g/cc)	Bulk Density (g/cc)
P3X11-5-2-SP1T	2.76 ± 0.91	2.76	2.69	1.7	2.73	2.68
P3X10-6-SP2T	2.12 ± 0.79	2.71	2.65	1.3	2.69	2.65
P3X11-5-3-SP3T	2.20 ± 0.81	2.55	2.50	1.0	2.53	2.51

(a) Measurements of grain density and total porosity were made using a fluid displacement technique. Bulk volume was determined from specimen dimensions.

(b) Measurements of grain density and effective porosity were made using a small volume helium porosimeter. Bulk volume was determined from a mercury displacement technique.

(c) Errors bars cover the 95% uncertainty interval; i.e., the interval expected to contain the true value 95% of the time during repeated sampling.

SP1 and SP3 are very reproducible for nominally identical tests. The flow rates determined for SP2 show some scatter but are always reproducible to within a factor of 3 and generally to within a factor of 2 for nominally identical tests. Flow rates are given on each plot in the order in which the three replicate tests were performed. Flow rates and calculated permeabilities are summarized in Table 4-6 through 4-8 for the three specimens, respectively. Error analyses were performed using the method given by ANSI/ASME (1986) and an example error calculation is given in Section F2 of Appendix B-F. The 95 percent uncertainty interval for gas permeability measurements based on experimental uncertainty is approximately ± 6 percent of the measured value.

An example of flow rate plotted versus gas pressure difference across a specimen is given in Figure 4-9 for Specimen SP1 at 2 MPa confining pressure. The plot contains data obtained at the three gas inlet pressures (9 tests). The corresponding data for all gas permeability tests are given in Appendix B-H. The data are not concave towards the pressure axis, showing that flow was not turbulent.

Measurements of gas permeability are complicated by "slippage" or the Klinkenberg effect. Slippage depends upon the mean free path between molecules and results in decreased permeabilities for lower mean free paths. Because gases are compressible, mean free path
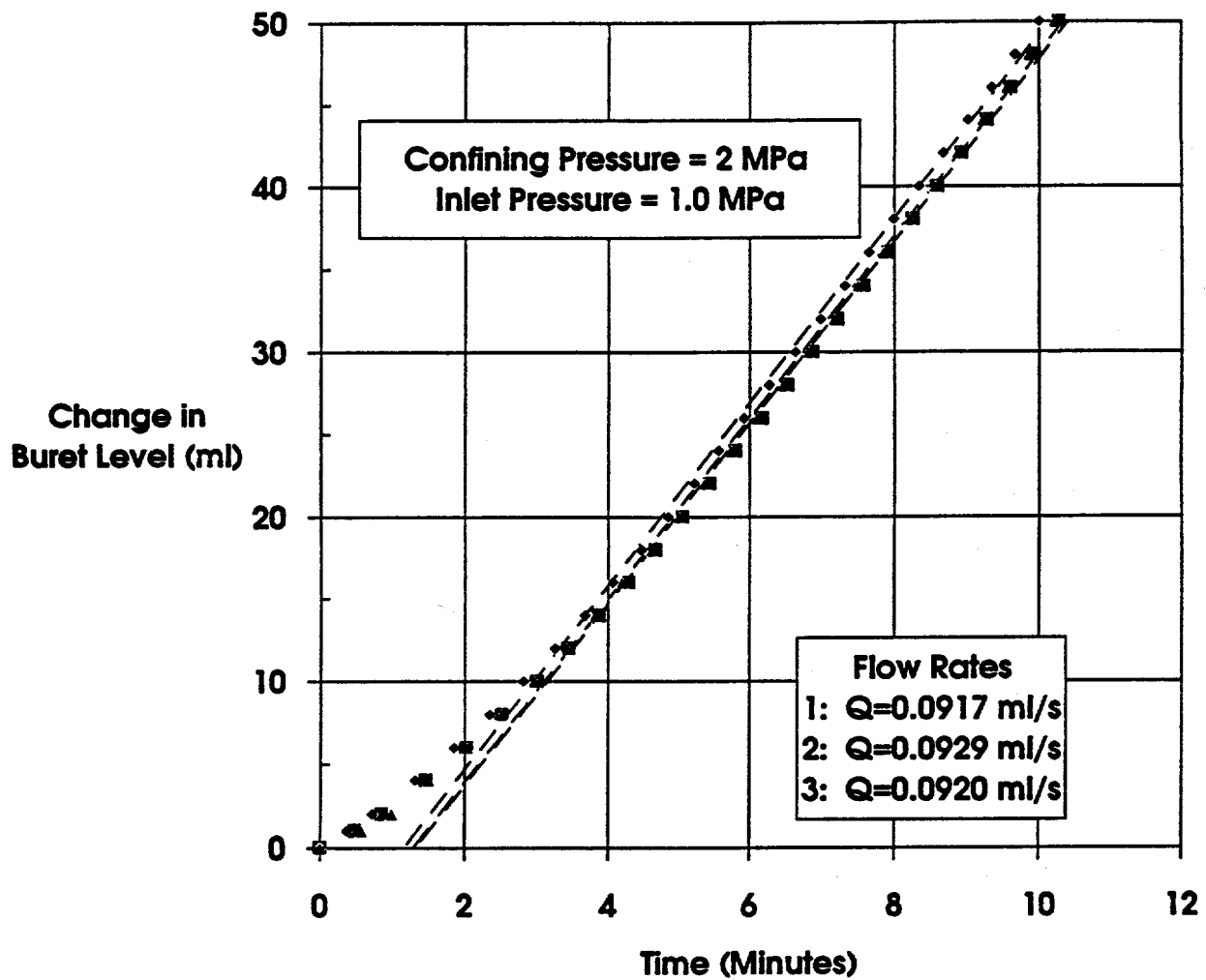
Figure 4-8. Gas volume-versus-time for test on MB 139 anhydrite Specimen P3X11-5-2-SP1 at 2 MPa confining pressure and 1 MPa gas inlet pressure. Symbols represent recorded data points and dashed lines are best fits to linear sections of data.

B-61

Table 4-6. Flow Data and Calculated Permeability to Nitrogen for Specimen P3X11-5-2-SP1

Confining Pressure (MPa)	Gas Inlet Pressure = 1.0 MPa[a]		Gas Inlet Pressure = 0.7 MPa[a]		Gas Inlet Pressure = 0.4 MPa[a]	
	Flow Rate ($10^{-8} \cdot m^3 \cdot s^{-1}$)	Permeability ($10^{-18} \cdot m^2$)	Flow Rate ($10^{-8} \cdot m^3 \cdot s^{-1}$)	Permeability ($10^{-18} \cdot m^2$)	Flow Rate ($10^{-8} \cdot m^3 \cdot s^{-1}$)	Permeability ($10^{-18} \cdot m^2$)
2	9.17	4.2	4.89	4.6	1.83	5.5
2	9.29	4.2	4.89	4.6	1.80	5.4
2	9.20	4.2	4.95	4.6	1.76	5.3
6	5.56	2.5	2.93	2.7	1.15	3.4
6	5.56	2.5	2.93	2.7	1.13	3.4
6	5.44	2.5	2.92	2.7	1.14	3.4
10	4.50	2.0	2.33	2.2	0.908	2.7
10	4.40	2.0	2.32	2.2	0.897	2.7
10	4.15	1.9	2.32	2.2	0.898	2.7

(a)   Gas outlet pressure = 0.1 MPa for all tests.

Table 4-7. Flow Data and Calculated Permeability to Nitrogen for Specimen P3X10-6-SP2

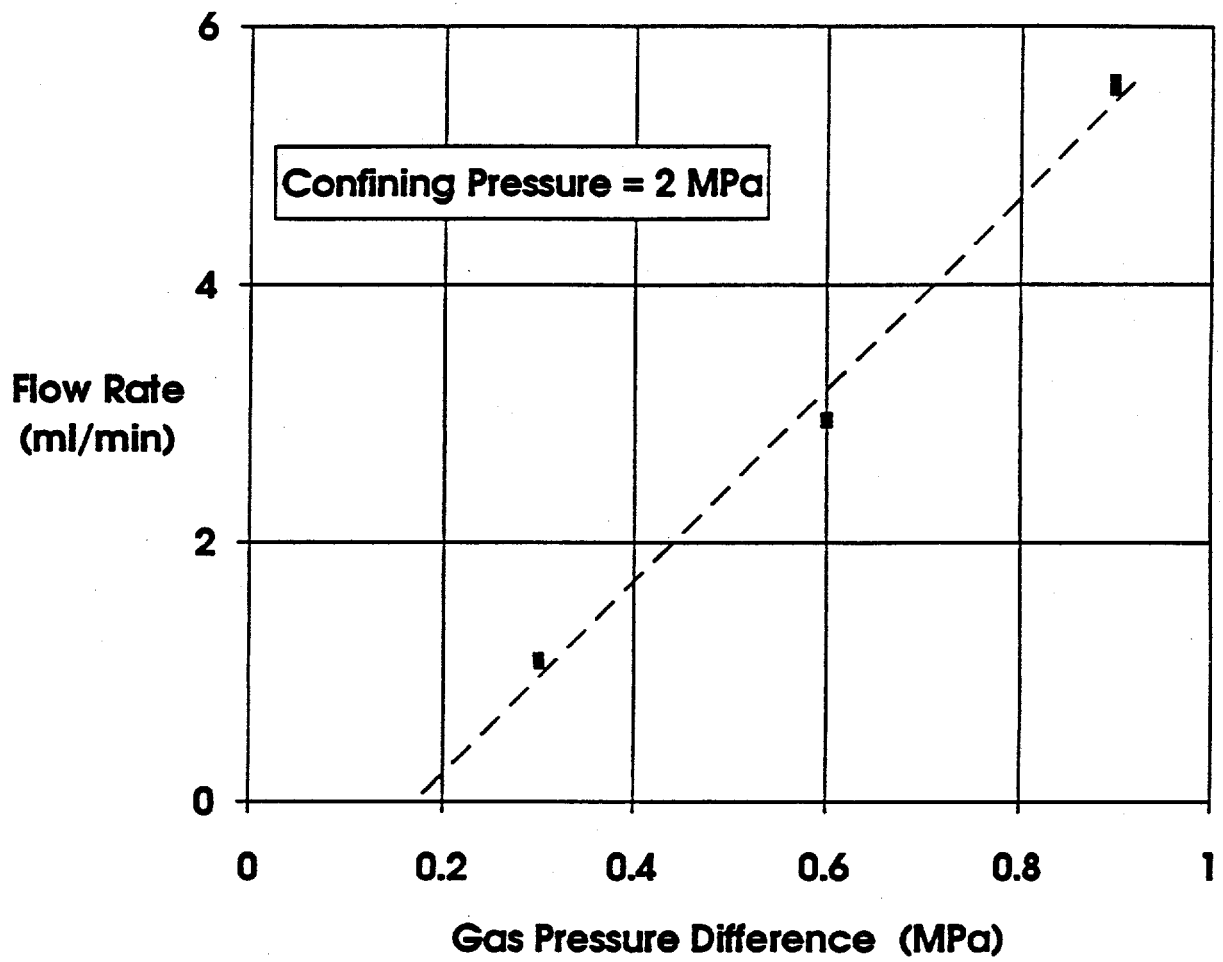| Confining Pressure (MPa)	Gas Inlet Pressure = 1.0 MPa[a]		Gas Inlet Pressure = 0.7 MPa[a]		Gas Inlet Pressure = 0.4 MPa[a]	
	Flow Rate ($10^{-8} \cdot m^3 \cdot s^{-1}$)	Permeability ($10^{-18} \cdot m^2$)	Flow Rate ($10^{-8} \cdot m^3 \cdot s^{-1}$)	Permeability ($10^{-18} \cdot m^2$)	Flow Rate ($10^{-8} \cdot m^3 \cdot s^{-1}$)	Permeability ($10^{-18} \cdot m^2$)
2	8.96[b]	3.3[b]	3.48	3.2	0.934	2.9
2	9.12	4.1	2.92	2.7	0.746	2.2
2	8.47	3.8	3.14	2.9	0.669	2.0
6	2.70	1.2	1.09	1.0	0.174	0.52
6	2.93	1.3	1.43	1.3	0.167	0.50
6	3.06	1.4	0.610	0.57	0.132	0.39
10	0.927	0.42	0.423	0.39	0.107	0.32
10	0.917	0.41	0.402	0.37	0.0718	0.21
10	1.04	0.47	0.308	0.29	0.0605	0.18

(a) Gas outlet pressure = 0.1 MPa for all tests.
(b) Gas inlet pressure = 1.1 MPa.

Table 4-8. Flow Data and Calculated Permeability to Nitrogen for Specimen P3X11-5-3-SP3

Confining Pressure (MPa)	Gas Inlet Pressure = 1.0 MPa[a]		Gas Inlet Pressure = 0.7 MPa[a]		Gas Inlet Pressure = 0.4 MPa[a]	
	Flow Rate ($10^{-8} \cdot m^3 \cdot s^{-1}$)	Permeability ($10^{-18} \cdot m^2$)	Flow Rate ($10^{-8} \cdot m^3 \cdot s^{-1}$)	Permeability ($10^{-18} \cdot m^2$)	Flow Rate ($10^{-8} \cdot m^3 \cdot s^{-1}$)	Permeability ($10^{-18} \cdot m^2$)
2	44.1	20	23.7	22	8.38	25
2	44.5	20	23.7	22	8.46	25
2	44.3	20	23.7	22	8.49	25
6	24.1	11	12.9	12	4.49	13
6	24.2	11	12.9	12	4.54	14
6	24.1	11	13.0	12	4.52	13
10	14.4	6.5	7.63	7.1	2.80	8.3
10	14.7	6.6	7.59	7.0	2.77	8.2
10	14.5	6.5	7.59	7.1	2.77	8.2

(a)   Gas outlet pressure = 0.1 MPa for all tests.

Figure 4-9. Flow rate-versus-gas pressure difference for Specimen P3X11-5-2-SP1 at 2 MPa confining pressure and all gas inlet pressures.

decreases as mean pore pressure increases and the Klinkenberg effect can become significant. The relation between gas and liquid permeabilities and mean pore pressure for a given material and non-interacting permeants was originally developed by Klinkenberg and is given as (Klinkenberg, 1941):

$$k_L = \frac{k_g}{1 + \dfrac{b}{p_m}} \qquad (4\text{-}1)$$

where

k_L = liquid permeability

k_g = gas permeability

p_m = mean pore pressure

b = Klinkenberg constant for a given gas and material

This equation can be rewritten as

$$k_g = k_L + k_L \left(\frac{b}{p_m} \right) \qquad (4\text{-}2)$$

which is the equation of a line in gas permeability versus reciprocal mean pressure coordinates. A plot of gas permeabilities versus reciprocal mean pore pressure should therefore result in a straight line and the intercept at a reciprocal mean pore pressure value of zero provides the equivalent liquid (or Klinkenberg-corrected) permeability.

Permeabilities are plotted as a function of reciprocal mean gas pressure for Specimen SP1 in Figures 4-10 through 4-12 for the three confining pressures, respectively. Data are presented in Figures 4-13 through 4-15 and Figures 4-16 through 4-18 for Specimens SP2 and SP3, respectively. The slopes and intercepts (the Klinkenberg-corrected permeabilities) are given in the figures and the Klinkenberg-corrected permeabilities are also given in Table 4-9. The data obtained for Specimens SP1 and SP3 show the expected positive slope; however, the data for Specimen SP2 (Figures 4-13 through 4-15) show greater scatter and a negative slope at all confining pressures. Although this negative slope is unexpected, the difference between the mean permeability determined at each confining pressure and the value at the intercept is always less than 1 order of magnitude. The intercepts for Specimen SP2 are not given in Table 4-9. These are not true Klinkenberg-corrected permeabilities because of the negative slope of the permeability-versus reciprocal mean pressure curves.
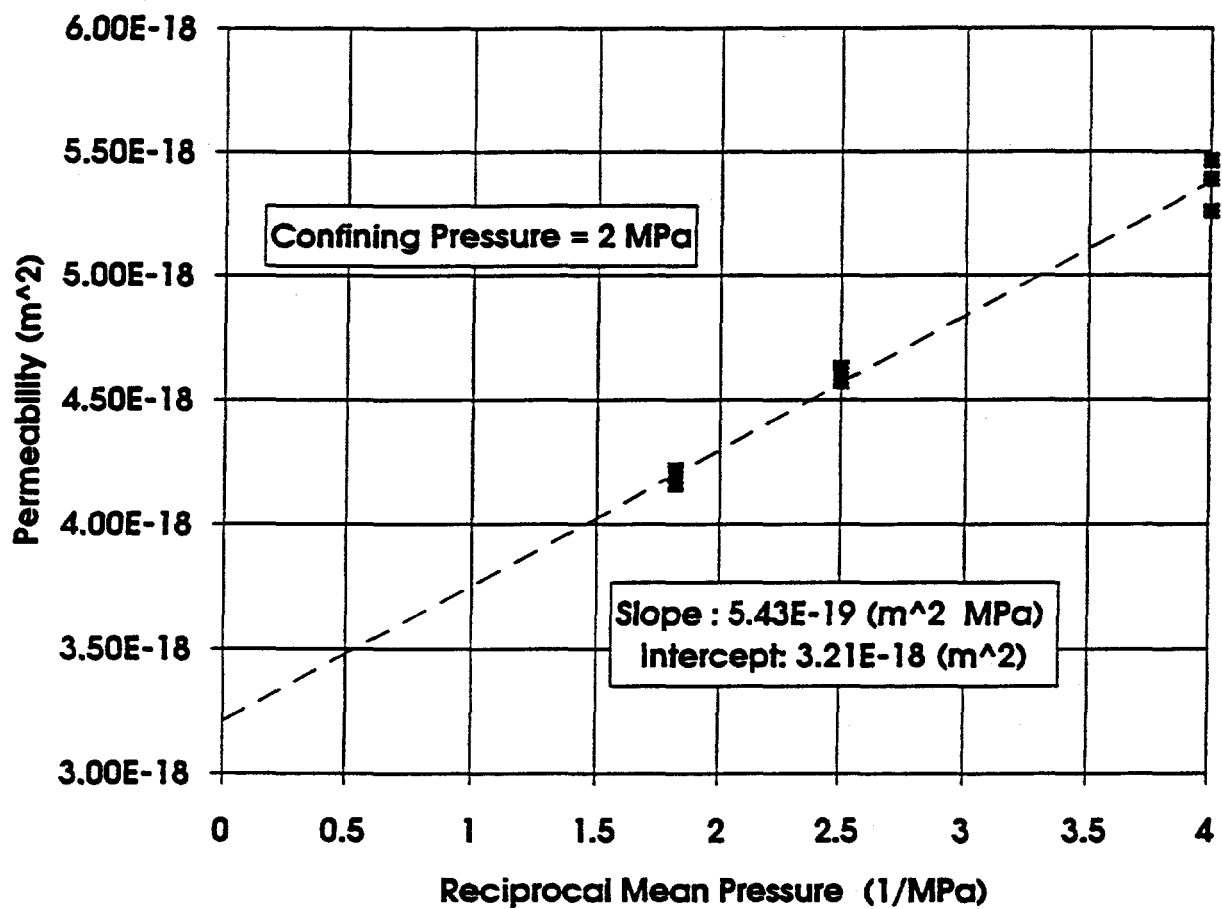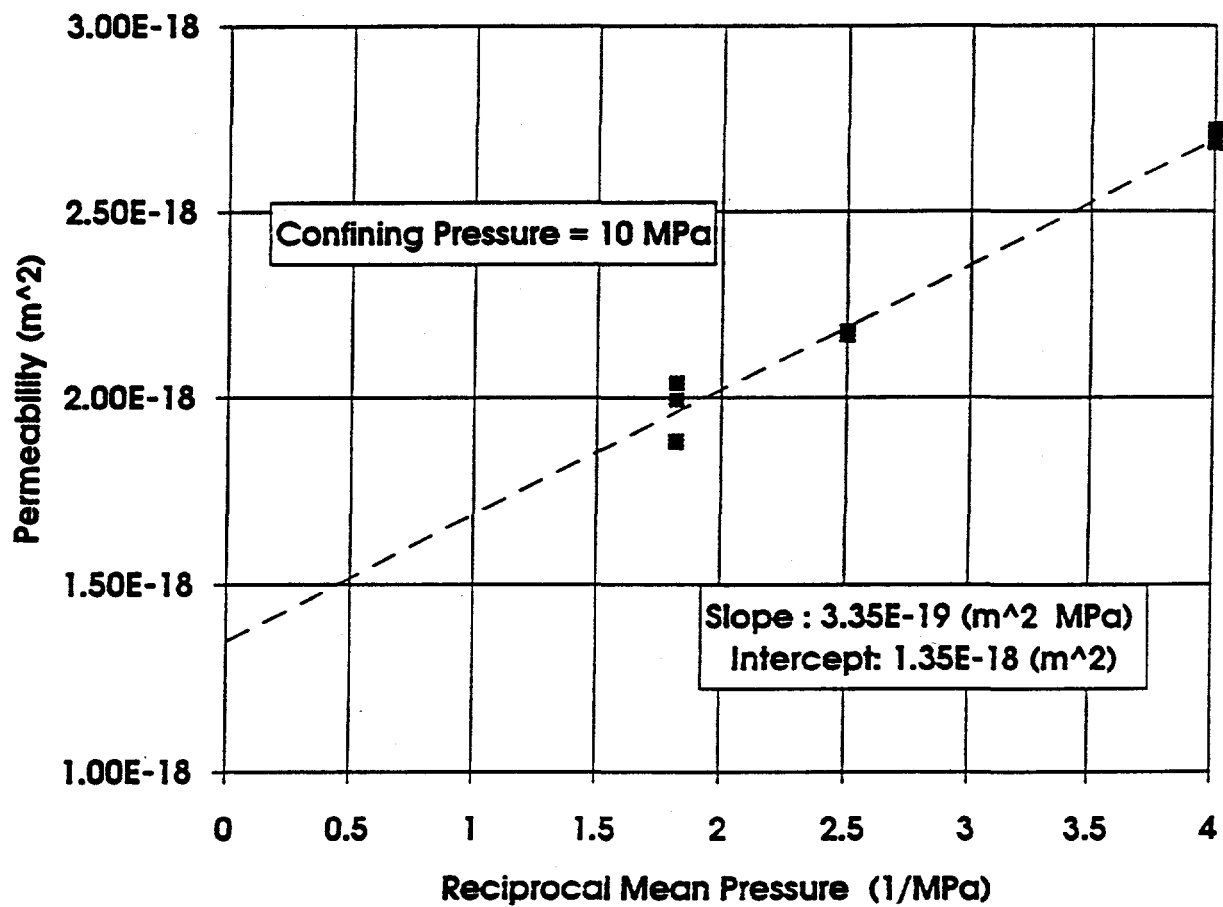
Figure 4-10. Permeability as a function of mean reciprocal gas pressure for Specimen P3X11-5-2-SP1 at 2 MPa confining pressure.
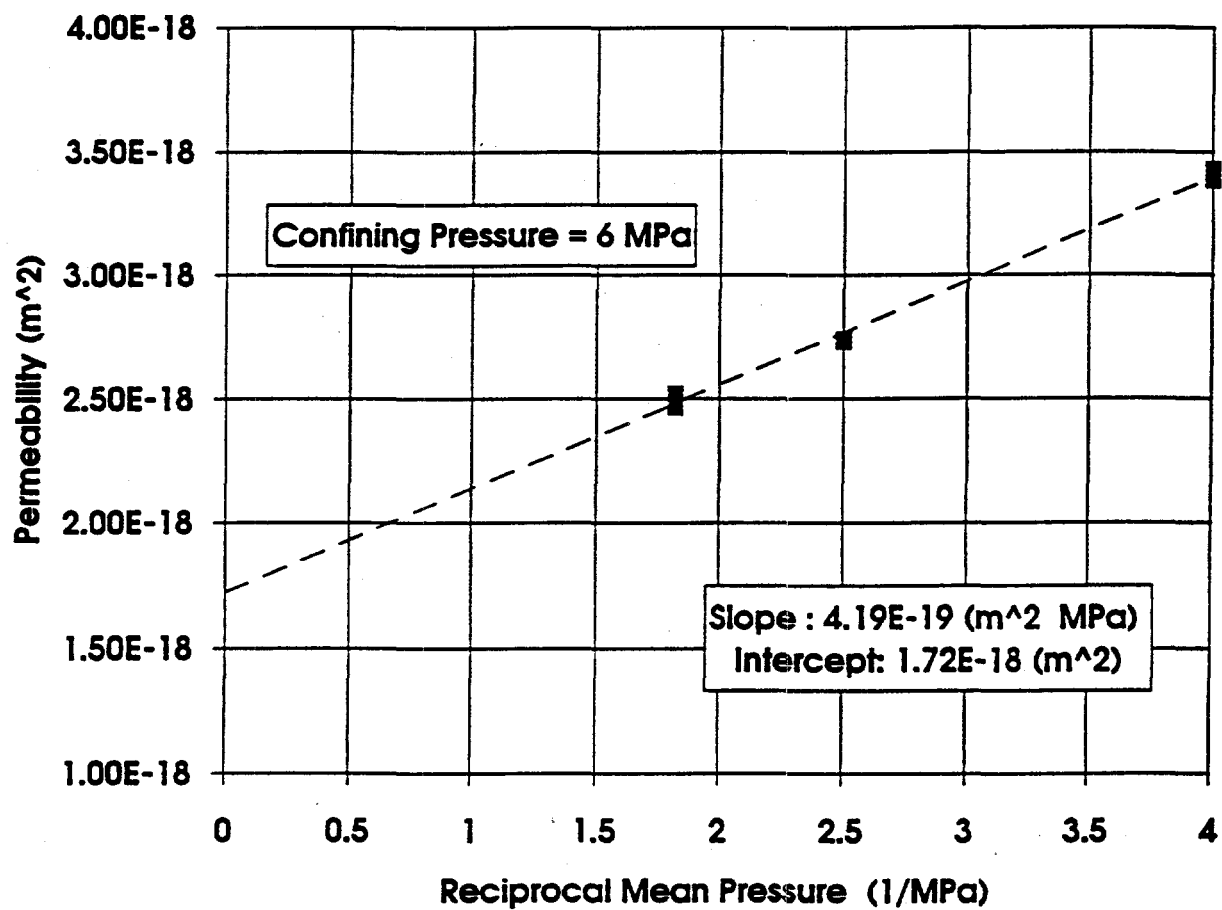
Figure 4-11. Permeability as a function of mean reciprocal gas pressure for Specimen P3X11-5-2-SP1 at 6 MPa confining pressure.

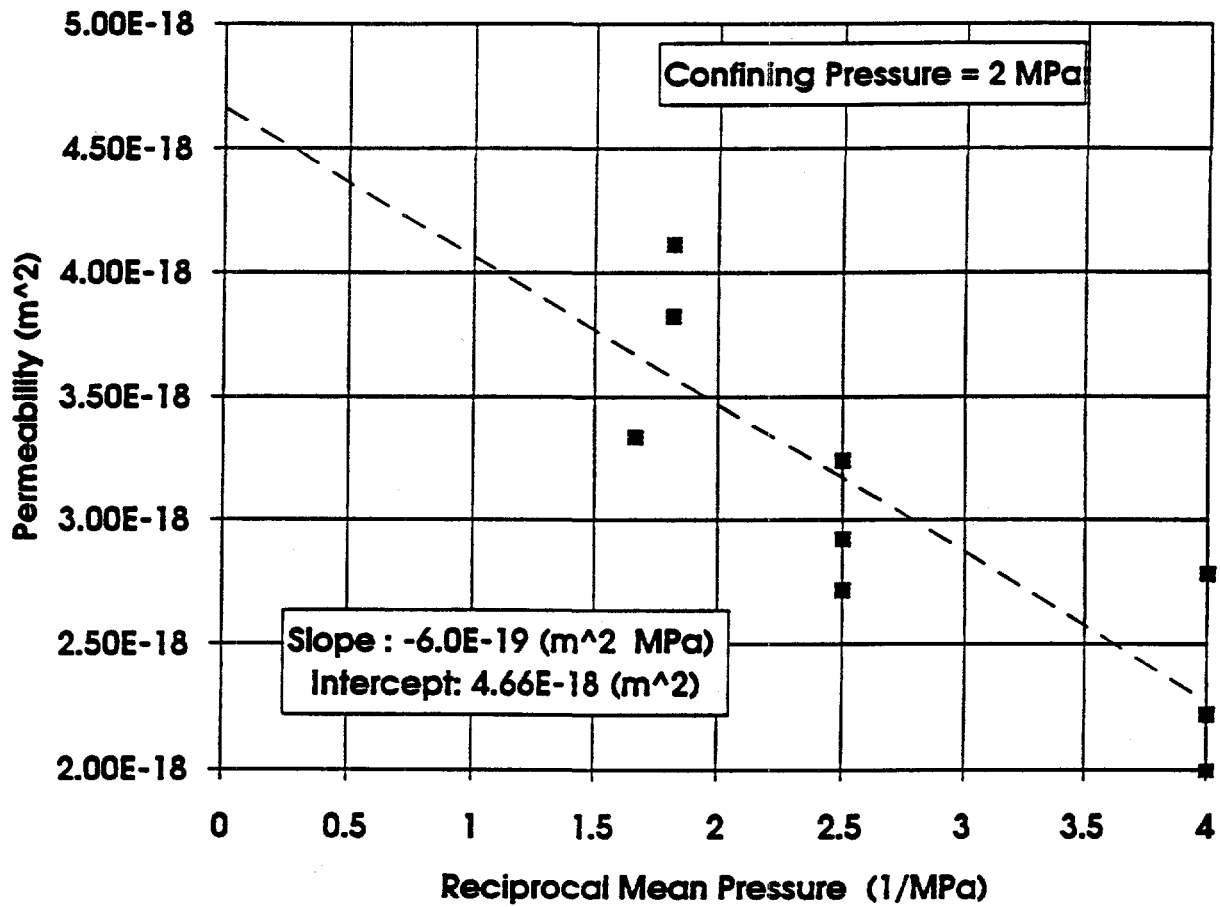Figure 4-12. Permeability as a function of mean reciprocal gas pressure for Specimen P3X11-5-2-SP1 at 10 MPa confining pressure.

Figure 4-13. Permeability as a function of mean reciprocal gas pressure for Specimen P3X10-6-SP2 at 2 MPa confining pressure.

Figure 4-14. Permeability as a function of mean reciprocal gas pressure for Specimen P3X10-6-SP2 at 6 MPa confining pressure.

Figure 4-15. Permeability as a function of mean reciprocal gas pressure for Specimen P3X10-6-SP2 at 10 MPa confining pressure.

Figure 4-16. Permeability as a function of mean reciprocal gas pressure for Specimen P3X11-5-3-SP3 at 2 MPa confining pressure.
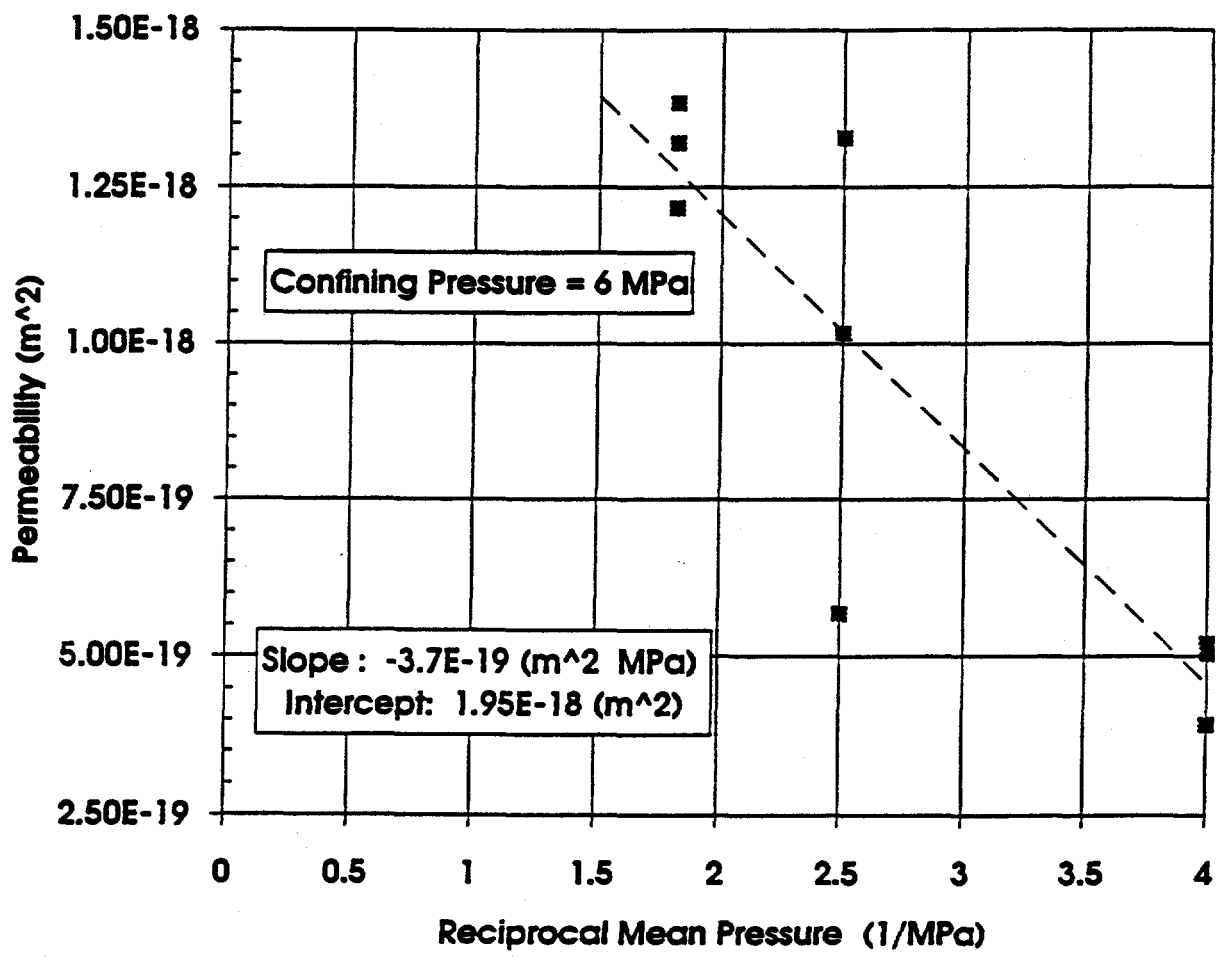
B-73

Figure 4-17. Permeability as a function of mean reciprocal gas pressure for Specimen P3X11-5-3-SP3 at 6 MPa confining pressure.

Figure 4-18. Permeability as a function of mean reciprocal gas pressure for Specimen P3X11-5-3-SP3 at 10 MPa confining pressure.
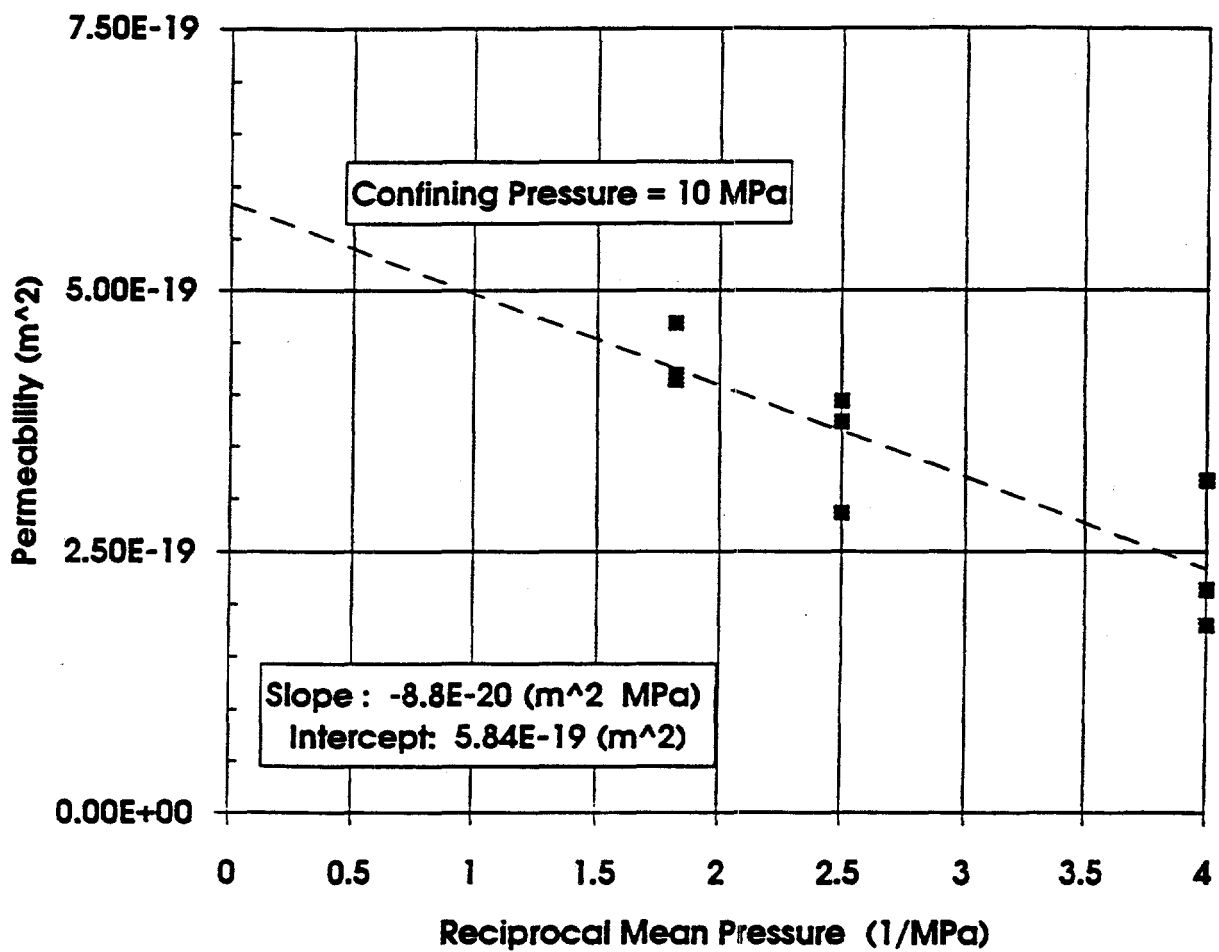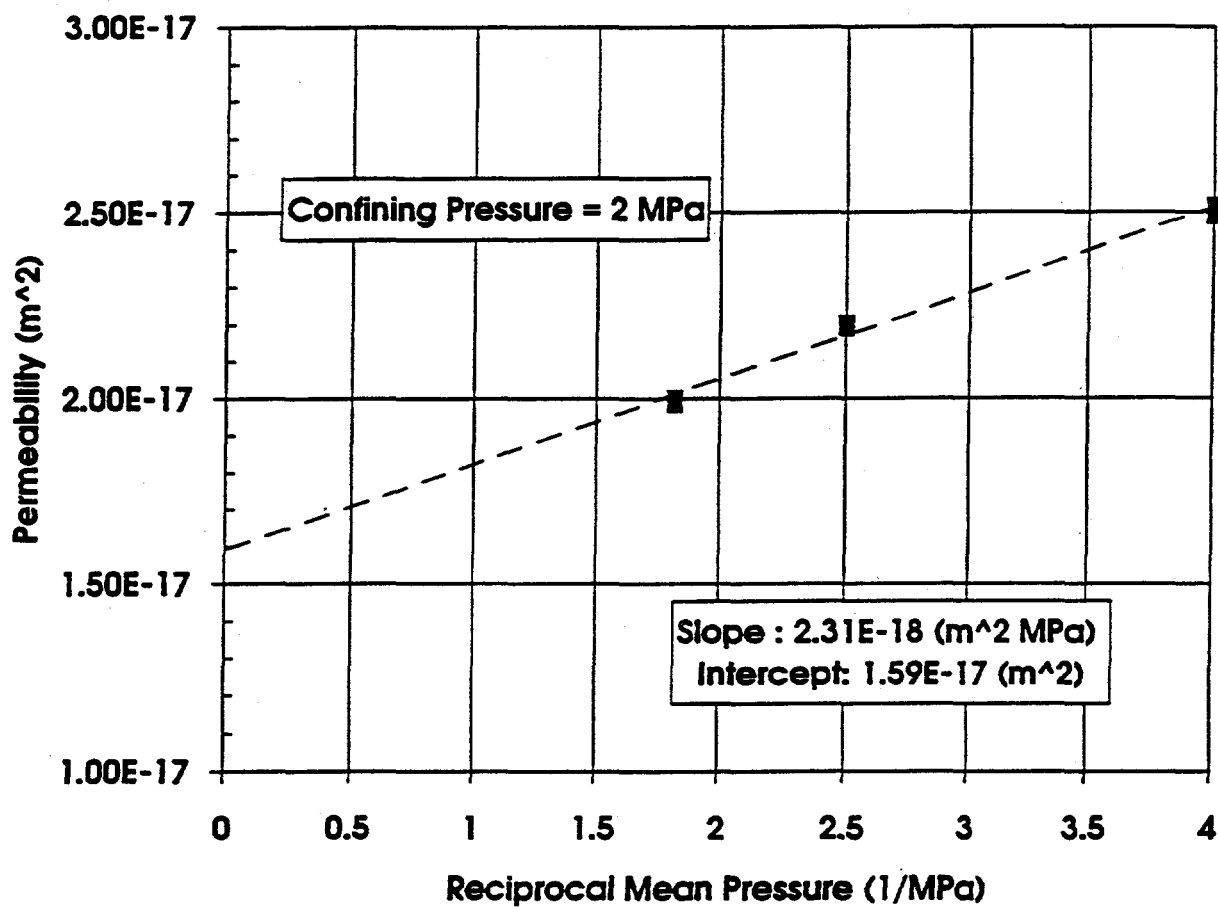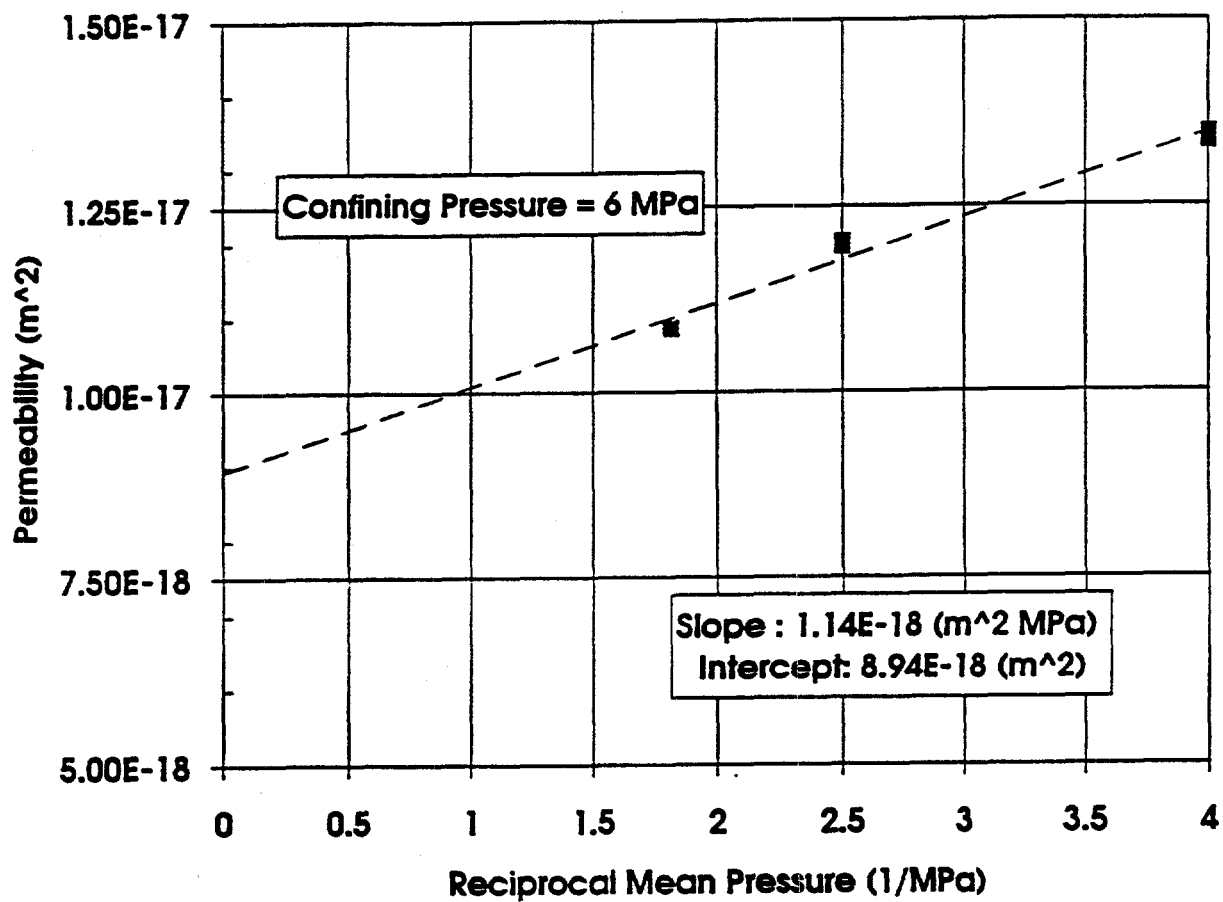
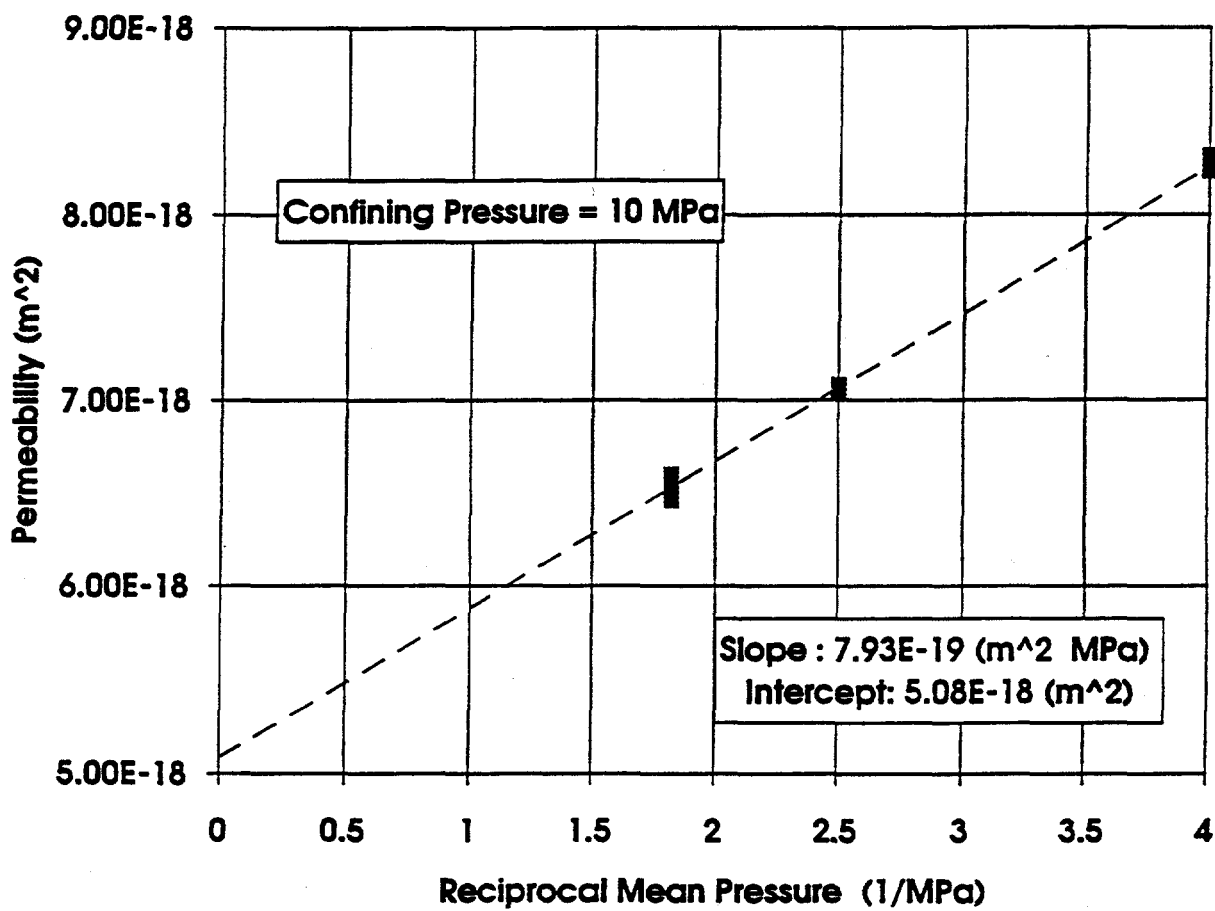Table 4-9. Klinkenberg-Corrected Permeabilities

| Confining Pressure (MPa) | Klinkenberg Corrected Permeability | |
	P3X11-5-2-SP1 (m^2)	P3X11-5-3-SP3 (m^2)
2	3.2×10^{-18}	1.6×10^{-17}
6	1.7×10^{-18}	8.9×10^{-18}
10	1.4×10^{-18}	5.1×10^{-18}

Values of b, the Klinkenberg constant for MB 139 and nitrogen gas permeant (Equation 4-2), were calculated for Specimens SP1 and SP3 from the slopes and intercepts of the Klinkenberg plots. These constants are given in Table 4-10.

Table 4-10. Klinkenberg Constants for MB 139 and Nitrogen Gas at 25°C

| Confining Pressure (MPa) | Klinkenberg Constant, b (MPa) | |
	P3X11-5-2-SP1	P3X11-5-3-SP3
2	0.17	0.15
6	0.24	0.13
10	0.25	0.16

A discussion of the role of effective confining pressure (confining pressure - pore pressure) on permeability measurements may be in part relevant to the observation of negative slopes on the Klinkenberg plots for Specimen SP2. Tables 4-6 through 4-8 show that permeability decreases as confining pressure increases. A decrease in porosity and permeability can be caused by either an increase in confining pressure at constant pore pressure or a decrease in pore pressure at constant confining pressure, as both will result in an increased effective confining pressure. The Klinkenberg effect is of opposite sign and causes permeability to decrease as pore pressure increases. The hypothesis that large effective pressures could negate observations of the Klinkenberg effect was therefore investigated, and the results are described below.

Permeability data for Specimen SP2 are plotted as a function of effective confining pressure in Figures 4-19 through 4-21 for each of the three inlet pore pressures, respectively. The slopes of these plots provide specimen-specific information on the magnitude of the change in
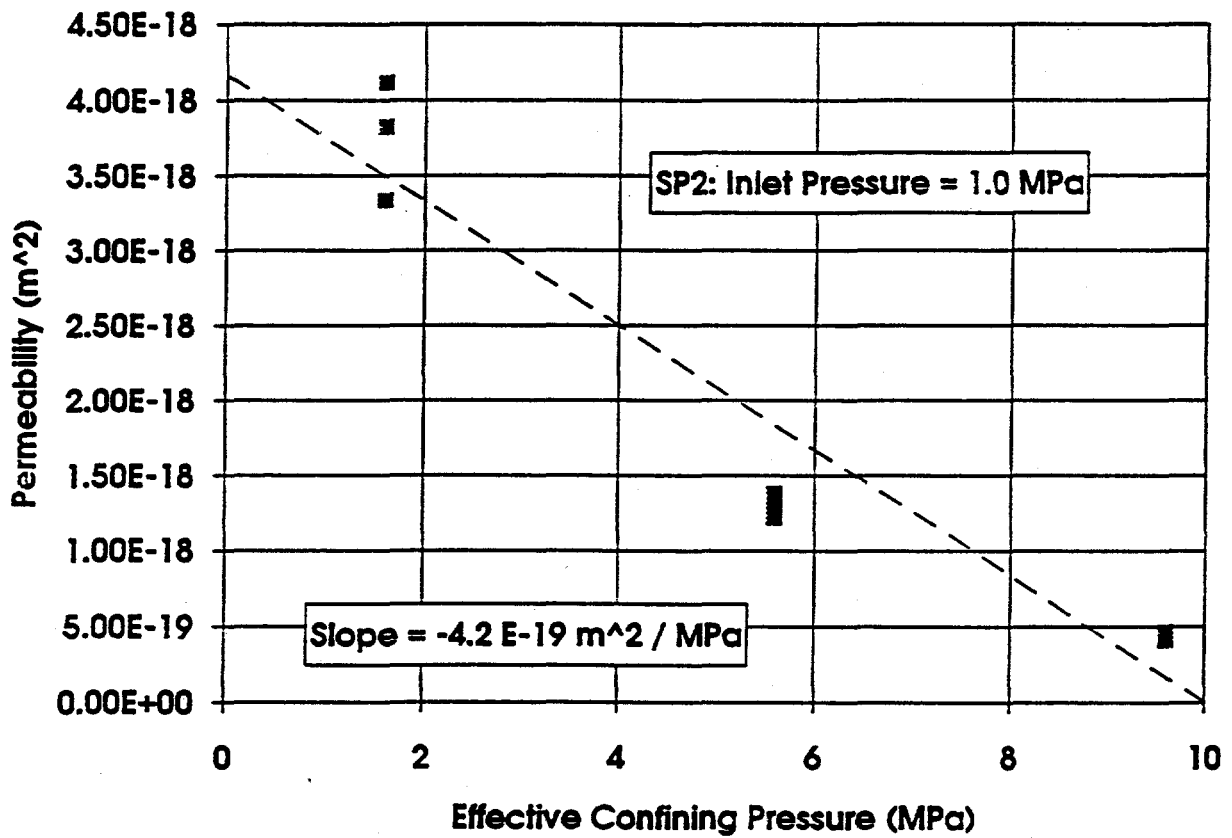
Figure 4-19. Change in permeability with increasing effective confining pressure for Specimen P3X10-6-SP2 at an inlet pore pressure of 1.0 MPa.

SP2: Inlet Pressure = 0.7 MPa

Slope = -3.3 E-19 m^2 / MPa
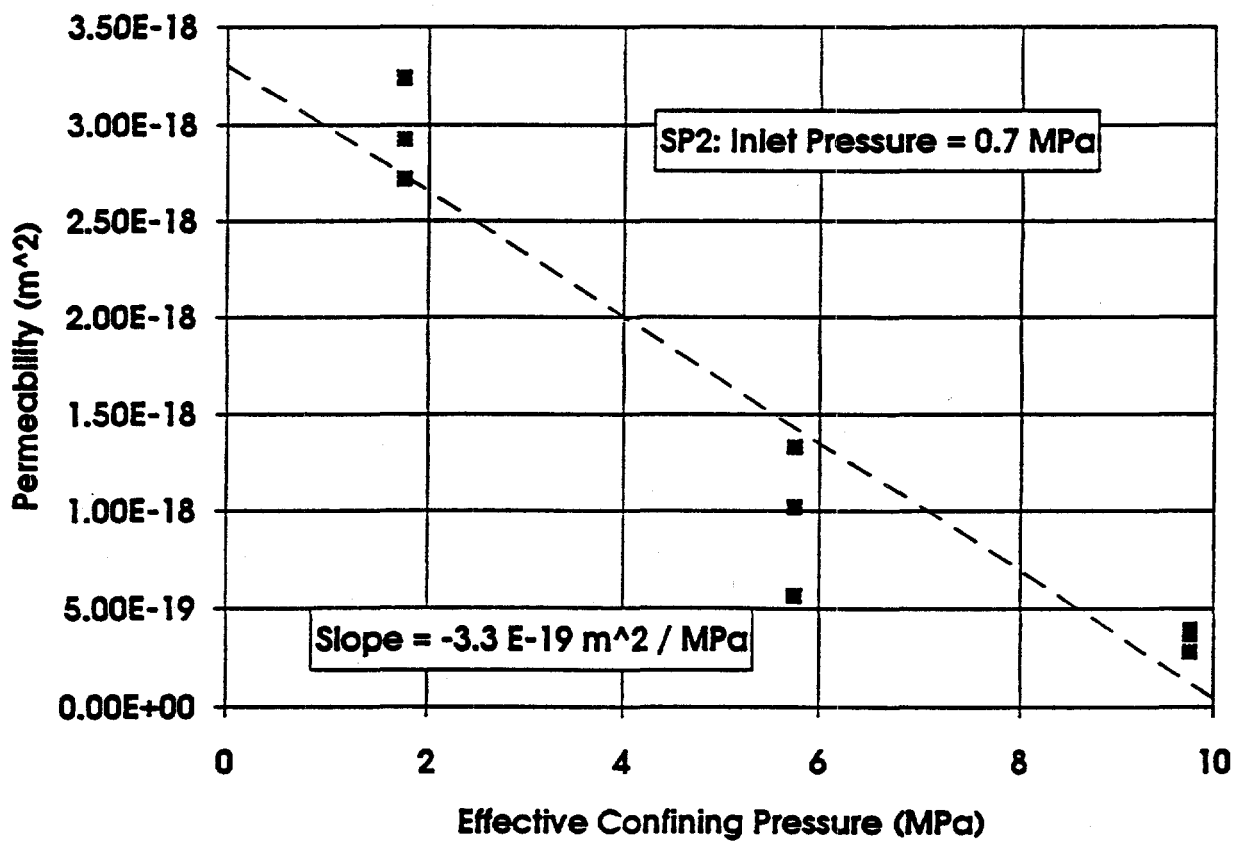
Figure 4-20. Change in permeability with increasing effective confining pressure for Specimen P3X10-6-SP2 at an inlet pore pressure of 0.7 MPa.
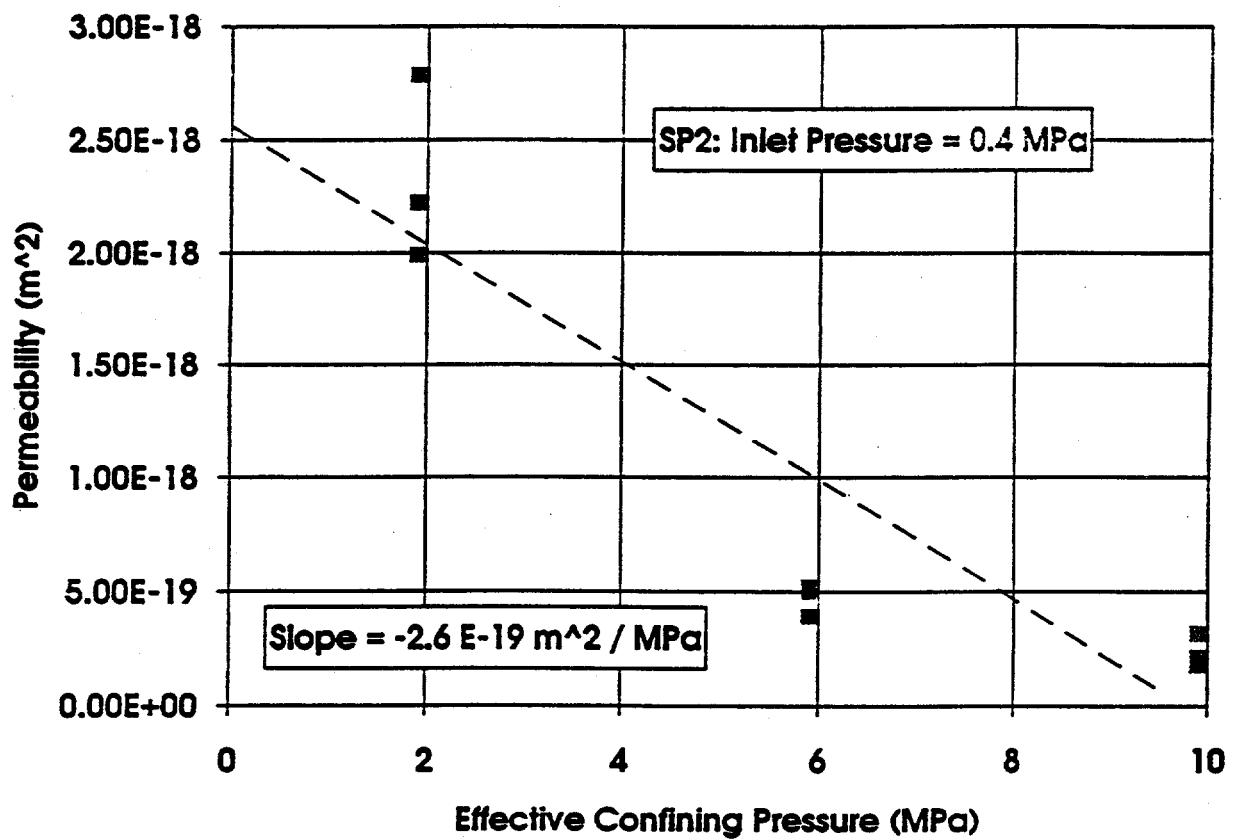
Figure 4-21. Change in permeability with increasing effective confining pressure for Specimen P3X10-6-SP2 at an inlet pore pressure of 0.4 MPa.

SP2 Confining Pressure = 2 MPa

Slope = 4.3 E-18 m^2 / MPa
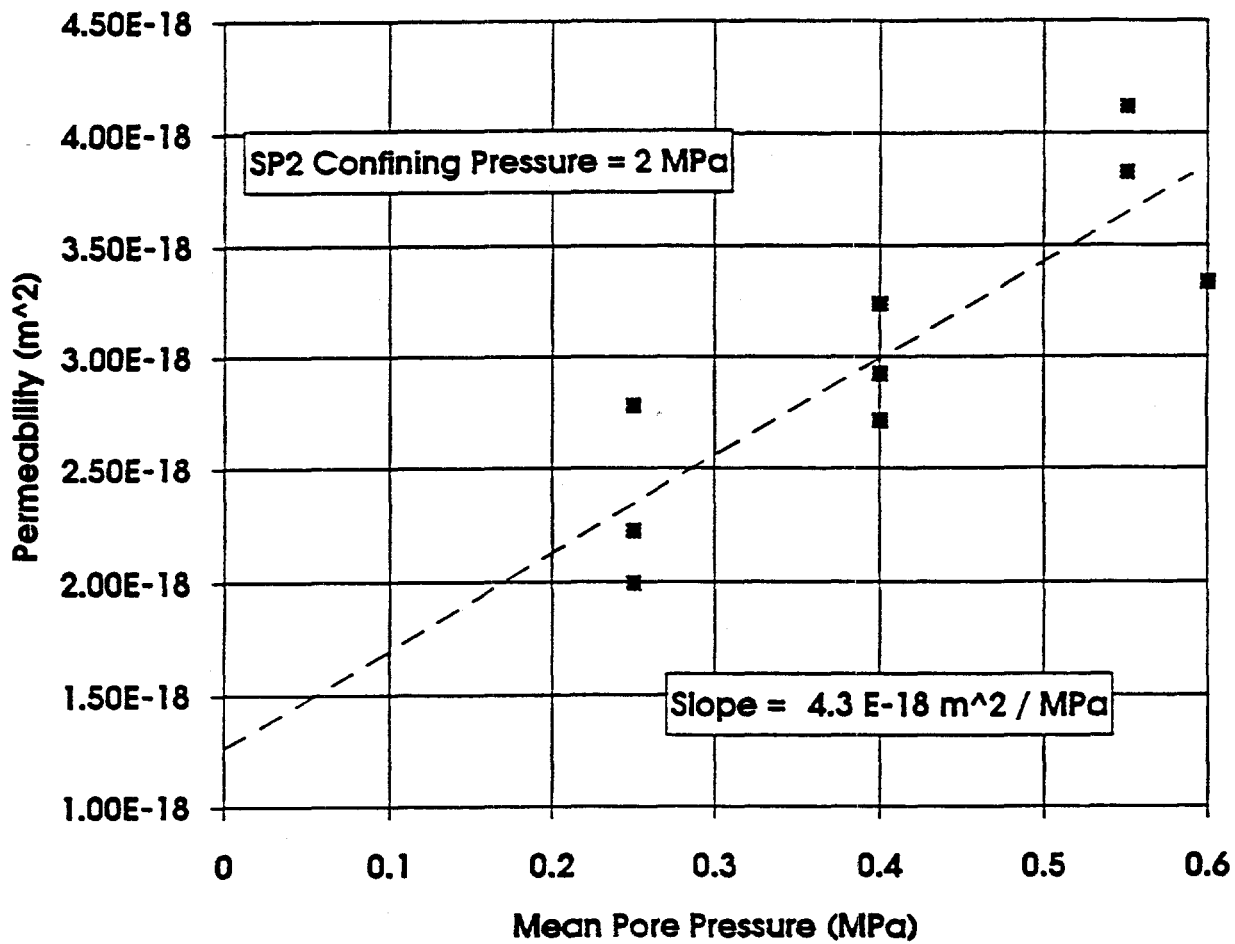
RSI-248-03-118

Figure 4-22. Change in permeability with increasing mean pore pressure for Specimen P3X10-6-SP2 at a confining pressure of 2 MPa.
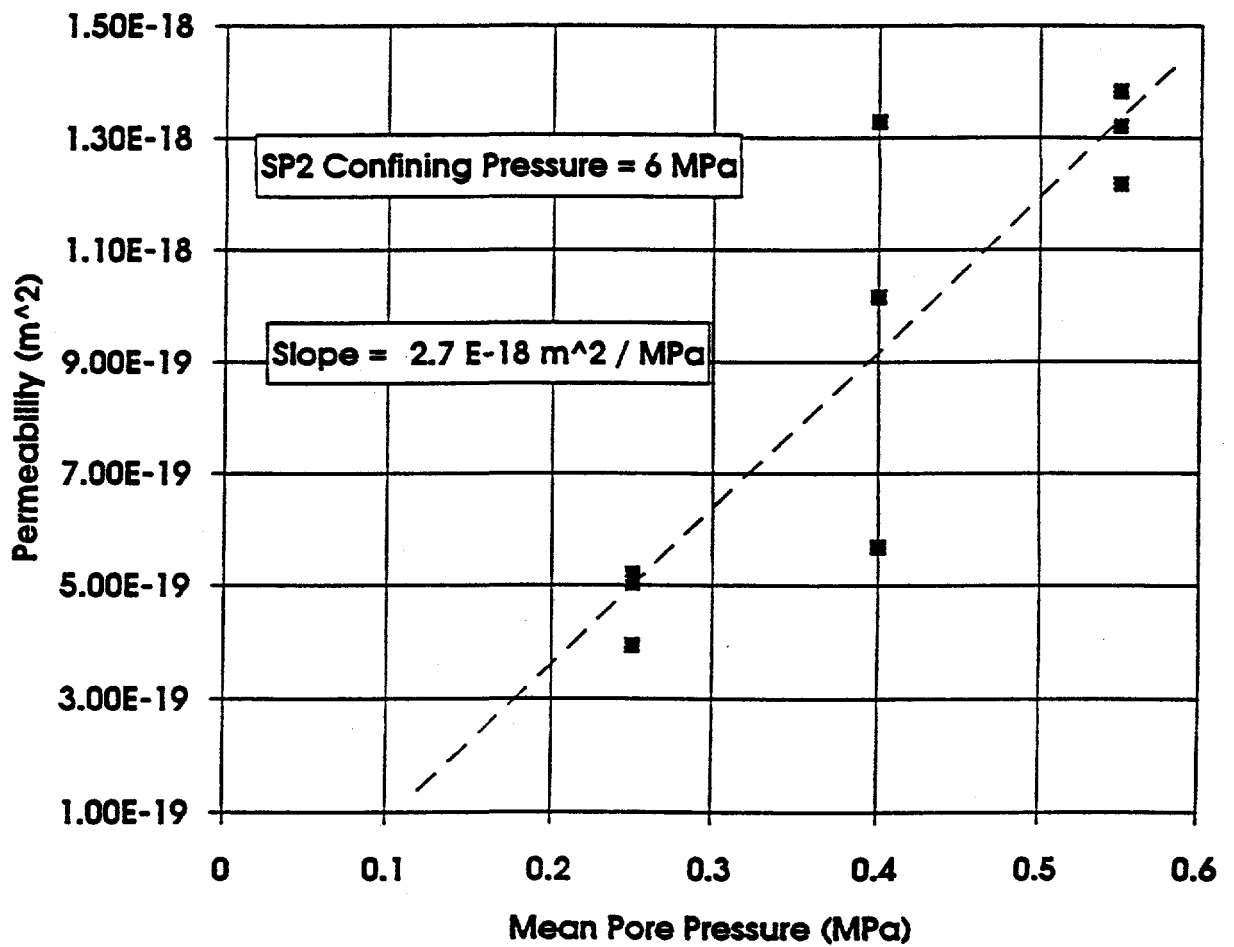
Figure 4-23. Change in permeability with increasing mean pore pressure for Specimen P3X10-6-SP2 at a confining pressure of 6 MPa.

Figure 4-24. Change in permeability with increasing mean pore pressure for Specimen P3X10-6-SP2 at a confining pressure of 10 MPa.

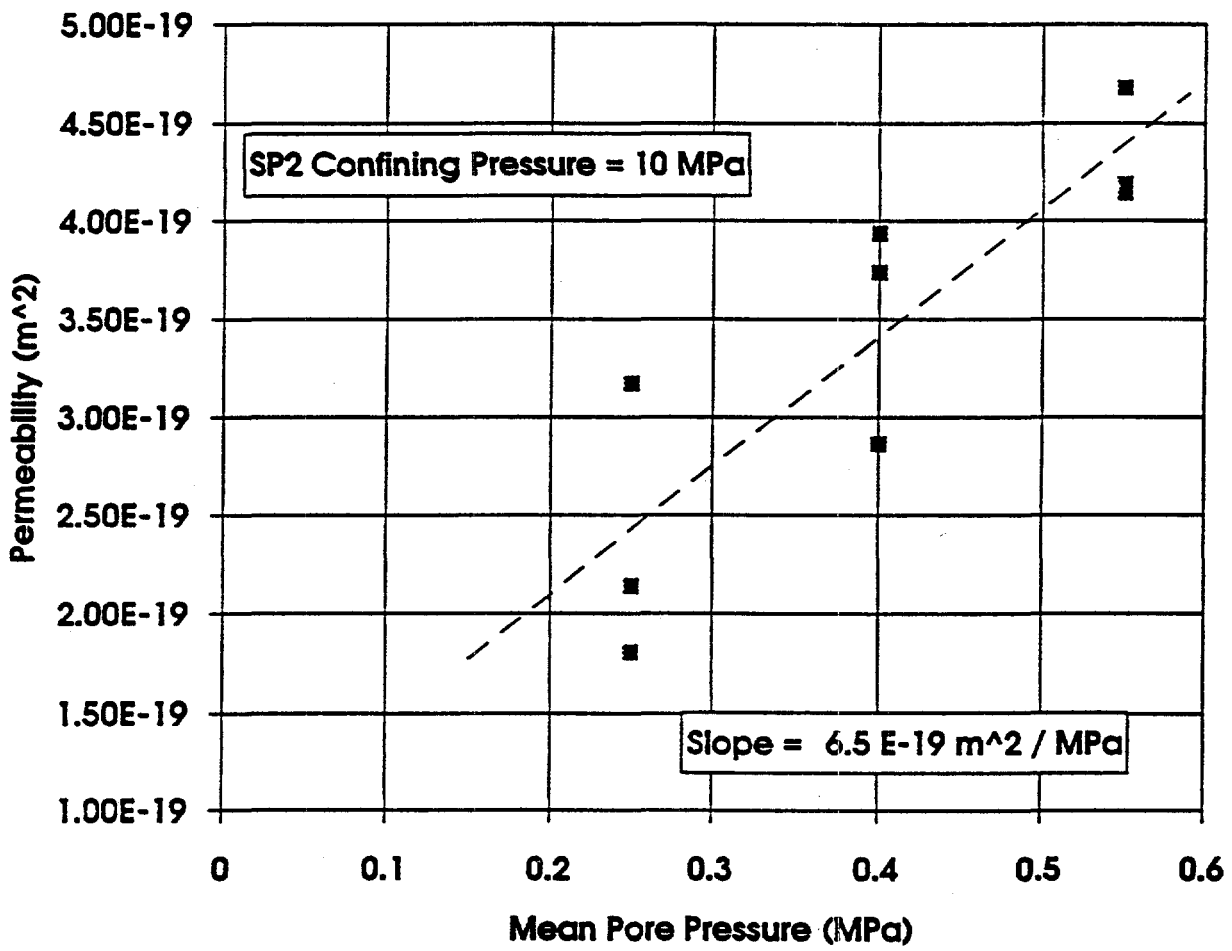permeability expected for a change in effective confining pressure. The slopes of the plots are $-4.2 \times 10^{-19} \cdot m^2 \cdot MPa^{-1}$, $-3.3 \times 10^{-19} \cdot m^2 \cdot MPa^{-1}$, and $-2.6 \times 10^{-19} \cdot m^2 \cdot MPa^{-1}$, for the three inlet pore pressures, respectively. (The average change in permeability with increasing effective confining pressure is $-3.4 \times 10^{-19} m^2 \cdot MPa^{-1}$.) The changes in permeability observed to accompany changes in mean pore pressure for Specimen SP2 are $4.3 \times 10^{-18} \cdot m^2 \cdot MPa^{-1}$, $2.8 \times 10^{-18} \cdot m^2 \cdot MPa^{-1}$, and $6.5 \times 10^{-19} \cdot m^2 \cdot MPa^{-1}$, as seen in Figures 4-22 through 4-24. The changes in permeability caused by changes in effective confining pressure shown in Figures 4-19 through 4-21 are smaller in magnitude than the changes in permeability observed as a function of mean pore pressure (Figures 4-22 through 4-24). It is therefore unlikely that permeability changes due to effective pressure obscure permeability changes due to the Klinkenberg effect. The reason for the negative slope on Figures 4-13 through 4-15 remains undetermined.

4.5 Brine Permeability Measurements

Liquid permeability tests were run according to the test matrix shown in Table 1-2. An example of the flow data obtained from each test and the linear least square fitting that was performed to obtain flow rate is given in Figure 4-25. The complete set of figures showing flow data and linear least square fits for all brine permeability tests is given in Appendix I. Separate plots are given for each specimen at each confining pressure and gas inlet pressure. Replicate tests were only run at the first set of conditions imposed on Specimen SP1. Because the specimen saturation procedure had to be terminated due to specimen dissolution, the state of specimen saturation was unknown. The replicate test was run to ensure that the specimen had reached saturation and that the flow rate was stable. The replicate tests are shown in Figure 4-25 and are very reproducible in that the slopes differ by only 3 percent. The coefficient of variation for each linear least squares fit is given in the figure. Unfortunately, a jacket leak terminated testing on this specimen before tests could be run at confining pressures of 6 MPa and 10 MPa.

Flow rates and calculated permeabilities are summarized in Tables 4-11 through 4-13 for the three specimens, respectively. An error analysis was performed for the permeability calculation using the method given in ANSI/ASME (1986) and an example is given in Section F3 of Appendix B-F. The 95 percent uncertainty interval based on experimental uncertainties is approximately ± 5 percent. Flow rates are plotted versus brine pressure difference across Specimen SP1 in Figure 4-26 for tests at 2 MPa confining pressure. These data are given for Specimens SP2 and SP3 in Appendix J. None of the data are concave towards the pressure axis, showing that flow was not turbulent.

Confining Pressure = 2 MPa
Inflow Pressure = 1.0 MPa

Flow Rates:
Q1 = 3.35E-03 ml/s +/- 0.2 %
Q2 = 3.43E-03 ml/s +/- 0.3 %
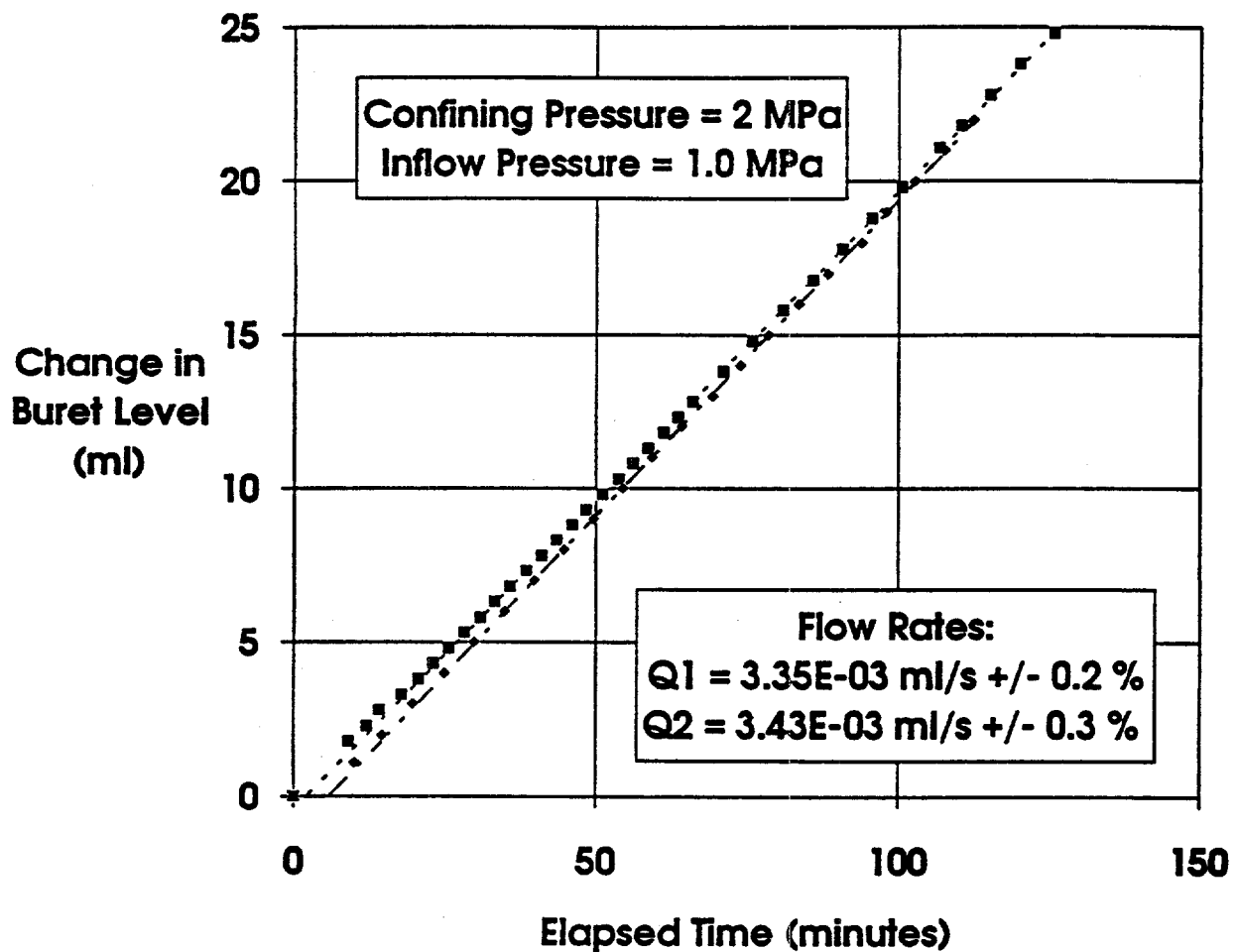
RSI-248-94-036

Figure 4-25. Change in exit buret level (brine volume)-versus-time for tests on Specimen P3X11-5-2-SP1 at 2 MPa confining pressure and 1 MPa brine inlet pressure. Symbols represent recorded data points and dashed lines are best fits to linear sections of data. The coefficients of variation for the linear least squares fits are given.

Table 4-11. Flow Data and Permeability to Brine for Marker Bed 139 Specimen SP1

Confining Pressure (MPa)	Brine Inlet Pressure[a] (MPa)	Specimen P3X11-5-2-SP1	
		Flow Rate ($m^3 \cdot s^{-1} \times 10^{-9}$)	Permeability ($m^2 \times 10^{-17}$)
2	1.0	3.35	5.9
2	1.0	3.43	6.1
2	0.7	2.02	5.3
2	0.4	0.871	4.6
6	1.0	Test Terminated by Jacket Leak	Test Terminated by Jacket Leak

(a) Brine outlet pressure = 0.1 MPa for all tests.

Table 4-12. Flow Data and Permeability to Brine for Marker Bed 139 Specimen SP2

Confining Pressure (MPa)	Brine Inlet Pressure[a] (MPa)	Specimen P3X10-6-SP2	
		Flow Rate ($m^3 \cdot s^{-1} \times 10^{-11}$)	Permeability ($m^2 \times 10^{-19}$)
2	1.0	5.29	9.3
2	0.7	2.37	6.2
2	0.4	.672	3.5
6	1.0	1.16	2.0
6	0.7	0.519	1.4
6	0.4	0.187	0.98
10	1.0	0.462	0.81
10	0.7	0.233	0.61
10	0.4	0.084	0.44

(a) Brine outlet pressure = 0.1 MPa for all tests.

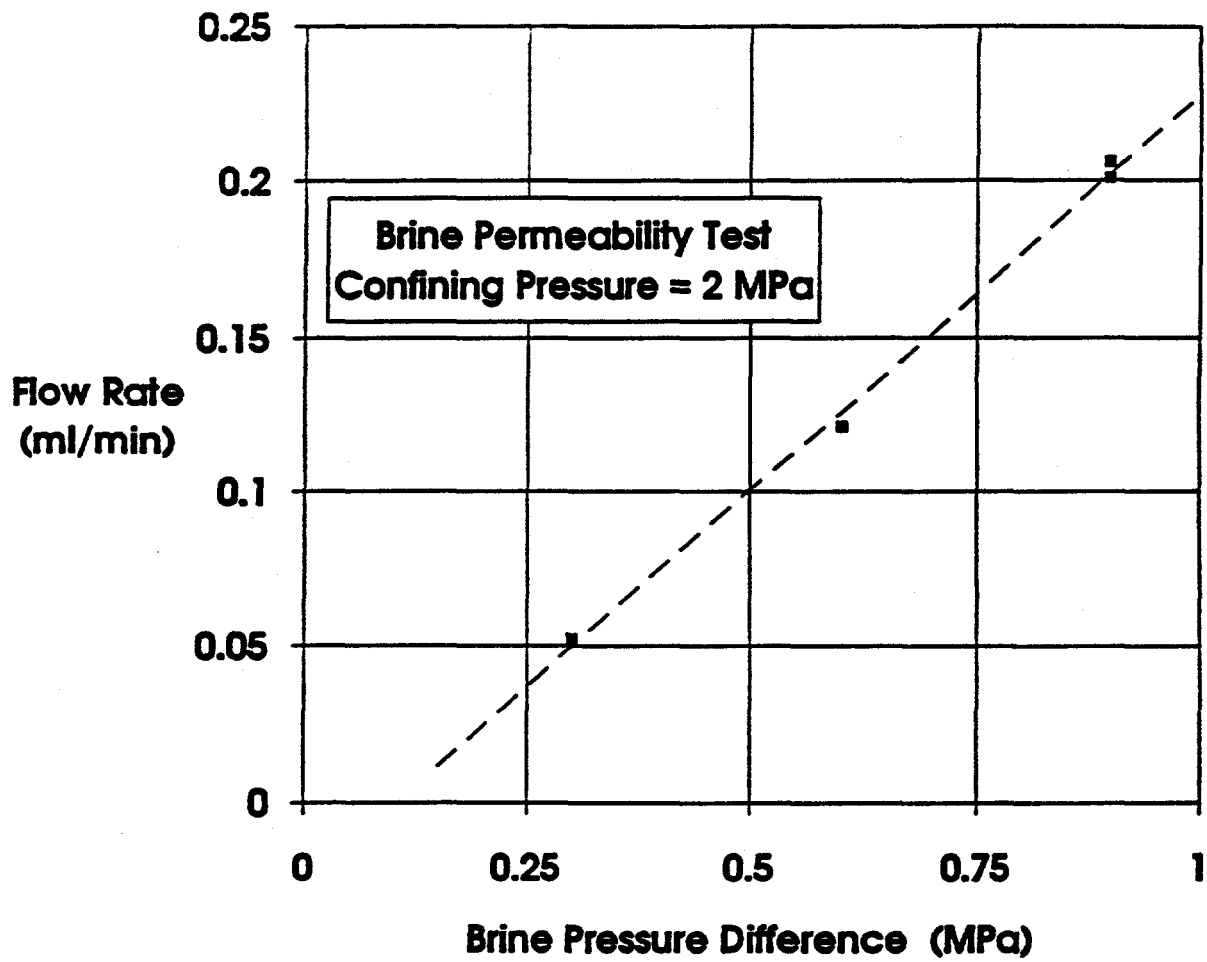Table 4-13. Flow Data and Permeability to Brine for Marker Bed 139 Specimen SP3

Confining Pressure (MPa)	Brine Inlet Pressure[a] (MPa)	Specimen P3X11-5-3-SP3	
		Flow Rate ($m^3 \cdot s^{-1}$ x 10^{-9})	Permeability (m^2 x 10^{-17})
2	1.0	5.54	9.7
2	0.7	2.99	7.9
2	0.4	1.22	6.4
6	1.0	2.61	4.6
6	0.7	1.63	4.3
6	0.4	0.617	3.2
10	1.0	1.56	2.7
10	0.7	0.981	2.6
10	0.4	0.378	2.0

(a) Brine outlet pressure = 0.1 MPa for all tests.

Brine Permeability Test
Confining Pressure = 2 MPa

Flow Rate (ml/min) vs. Brine Pressure Difference (MPa)

RSI-245-93-110

Figure 4-26. Flow rate-versus-brine pressure difference for Specimen P3X11-5-2-SP1 at 2 MPa confining pressure and all brine inlet pressures.

5.0 DISCUSSION OF RESULTS

5.1 Specimen Characterization

Some vertical and lateral heterogeneity in the marker bed can be inferred from the specimen characterization data. Specimens from the lowermost section of the marker bed, Specimens SP3T and SP3B, and samples from thin section block TS3 are enriched in anhydrite. SP3T and SP3B samples had an average anhydrite content of 57 percent as compared with averages of 12 percent for SP1T and SP1B, and 50 percent for SP2T and SP2B. Specimens from TS3 were 83 percent anhydrite, as compared with 59 percent for both TS1 and TS2. Samples from borehole P3X10 (SP2 and TS2) had the highest halite contents. Specimens SP2T and SP2B had an average halite content of 44 percent, whereas average halite content for Specimens SP1T and SP1B was 7 percent and for Specimens SP3T and SP3B was 38 percent. Specimens from thin section block TS2 averaged 37 percent halite as compared with 14 percent for TS1, and 15 percent for TS3. Comparison of data from the TS blocks shows that the uppermost section of the marker bed, TS2 from P3X10, is enriched in halite; however, it is difficult to distinguish between vertical and lateral heterogeneities in halite content from this data set.

5.2 Porosity

Effective porosity determinations were made for specimens taken from material directly above and below each permeability specimen axis. Because specimen axes were parallel to bedding, the porosity specimens were from the same horizon as each permeability specimen. Total porosities were measured only on the specimens taken from directly above the permeability specimen axis. Effective porosities ranged from a low of 1.0 percent to a high of 2.1 percent and total porosities ranged from 2.1 to 2.8 percent. The porosities of the different sections of the marker bed differ by about 1 percent porosity, which also happens to be the approximate measurement error. Because of the small sample size and large errors, any conclusions about heterogeneity in porosity are tenuous. A discussion of heterogeneity in porosity is included, however, for completeness. The uppermost section of the marker bed has the highest effective and total porosities. It has an average effective porosity of 1.9 percent, while the average effective porosity of the lower section from the same borehole was 1.4 percent. The total porosity for the uppermost section of the marker bed was 2.8 percent, while the lower section from the same borehole had a total porosity of 2.2 percent.

5.3 Permeability

Measured brine permeabilities and Klinkenberg-corrected gas permeabilities are shown in Figure 5-1 as a function of confining pressure. As expected, permeabilities decrease as confining pressure causes interconnected void space to contract. Values of Klinkenberg-corrected gas permeabilities range from $1.4 \times 10^{-18} \cdot m^2$ to $1.6 \times 10^{-17} \cdot m^2$ for MB 139 Specimens SP1 and SP3 (there are no Klinkenberg-corrected data for Specimen SP2). Brine permeability values are between $4.4 \times 10^{-20} \cdot m^2$ and $9.7 \times 10^{-17} \cdot m^2$ for the specimens tested. These values include the range of permeabilities ($8 \times 10^{-20} \cdot m^2$ to $5 \times 10^{-17} \cdot m^2$) inferred from in situ borehole tests (Davies, 1992). Brine permeabilities are higher than equivalent liquid permeabilities, probably because of the dissolution that occurred during the specimen saturation procedure. The brine and equivalent liquid permeabilities generally differ by less than one order of magnitude.

Specimen SP3 had the highest permeability, followed by Specimen SP1 even though Specimen SP1 contained a planar zone of cracks (see Section 2.1). These specimens were taken from the P3X11 borehole of MB 139 while Specimen SP2, with the lowest permeability, was taken from borehole P3X10. The differences in permeability between Specimen SP2 and Specimens SP1 and SP3 may reflect lateral rather than vertical variations in the properties of MB 139, although the two boreholes were only 0.61 m (2 feet) apart.

The test plan that guided this work included both specimen characterization and permeability determinations so that permeability differences could be correlated with differences in rock composition, porosity, and depth of origin. The lowest section of the P3X11 borehole (Specimen SP3) had the highest permeability and also the highest anhydrite content. Permeabilities are plotted versus anhydrite content in Figure 5-2. The anhydrite content given is that of the material taken from above and below the specimen axes. Only brine permeabilities determined at the lowest confining pressure are included in this figure and in Figures 5-3 through 5-8. (A jacket leak terminated brine permeability tests for Specimen SP1 and so only data obtained at comparable conditions on Specimen SP3 are included here.) The gas and brine permeabilities for borehole P3X11 (Specimens SP1 and SP3) appear to increase with anhydrite content. Anhydrite content is also high for the P3X10 specimen (Specimen SP2), however its permeability is low. Permeabilities were replotted versus the average anhydrite contents of specimens from blocks TS1, TS2, and TS3 (Figure 5-3), blocks taken from near Specimens SP1, SP2, and SP3. The composition of each thin section block is the average of four measurements whereas the compositions given in Figure 5-2 are the average of only 2 measurements. Specimen SP2 is now plotted at a much lower anhydrite content. It is possible that a larger sampling of material is required to obtain a representative composition and that once this composition is determined, a
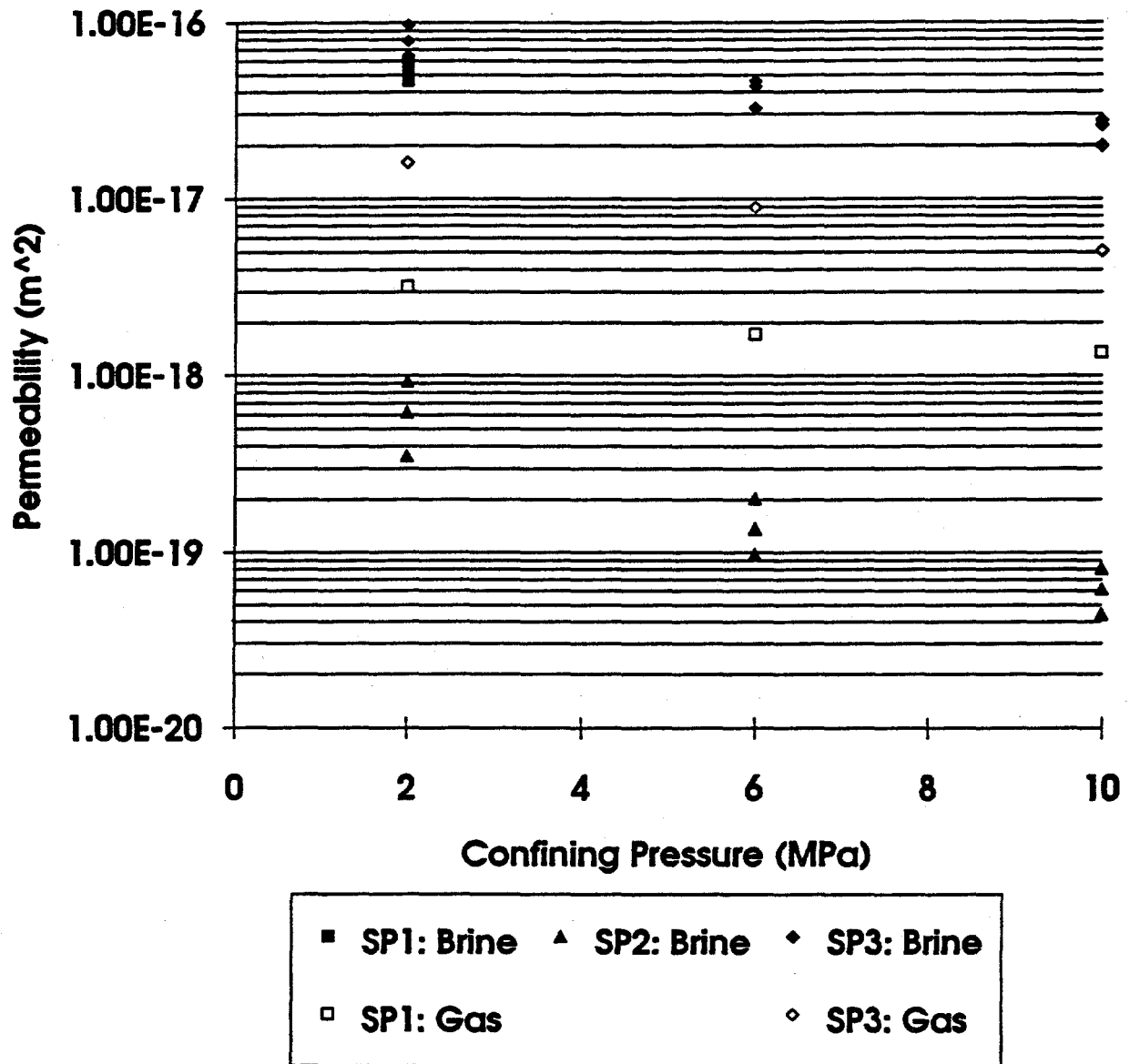
Figure 5-1. Permeability-versus-confining pressure for all tests. Klinkenberg-corrected values are given for gas permeability tests.

RSI-248-94-028

correlation between increasing permeability and increasing anhydrite content becomes more evident.

Specimen SP2 has the lowest permeability and also the highest halite content. Permeabilities are plotted versus halite content in Figure 5-4. The halite content given is that of the material taken from above and below the specimen axes. Surprisingly, the gas and brine permeabilities for borehole P3X11 increase with halite content. The halite content of the P3X10 specimen is very similar to one of the P3X11 specimens (44 percent versus 38 percent), yet its permeability is 2 orders of magnitude lower. Permeabilities were replotted versus the average halite contents of specimens from blocks TS1, TS2, and TS3 (Figure 5-5). The gas and brine permeabilities for borehole P3X11 still increase with halite content; however, with regard to the P3X10 specimen, Figure 5-5 shows the expected correlation between decreasing brine permeability and increasing halite content. It is possible that the larger sampling of material was required to obtain a representative composition. These data may imply that the high halite content in Specimen SP2 contributes to its low permeability.

Permeabilities were examined with respect to effective and total porosities and the data are given in Figures 5-6 and 5-7, respectively. Surprisingly, for the P3X11 specimens, gas and brine permeabilities decrease slightly as porosities increase. It is possible that a larger sampling of material is needed to accurately determine the porosities. The P3X10 specimen has the lowest permeability and lowest porosity, indicating that low porosity may contribute to its low permeability; however, total porosities are similar for this specimen and for one P3X11 specimen, yet they differ in permeability by 2 orders of magnitude.

Lastly, permeabilities were viewed with respect to the depth of origin of the specimen and the data are given in Figure 5-8. Gas and brine permeabilities increase with depth for specimens taken from borehole P3X11. The P3X10 specimen and one P3X11 specimen (SP1) were recovered from depths that differ by only 0.061 m, yet brine permeabilities differ by approximately 2 orders of magnitude. The specimen radii were only 0.050 m and so part of both specimens were taken from the same stratigraphic layer.

Permeabilities do not strongly correlate with any single material characteristic such as porosity, halite content, or anhydrite content; however, these material characteristics may contribute to spatial variations in permeability. Fluid flow in rock occurs through the interconnected void space. Heterogeneity of this void space either is not strongly correlated with any single material characteristic measured here, or the data obtained was insufficient in quantity for a correlation to be apparent.
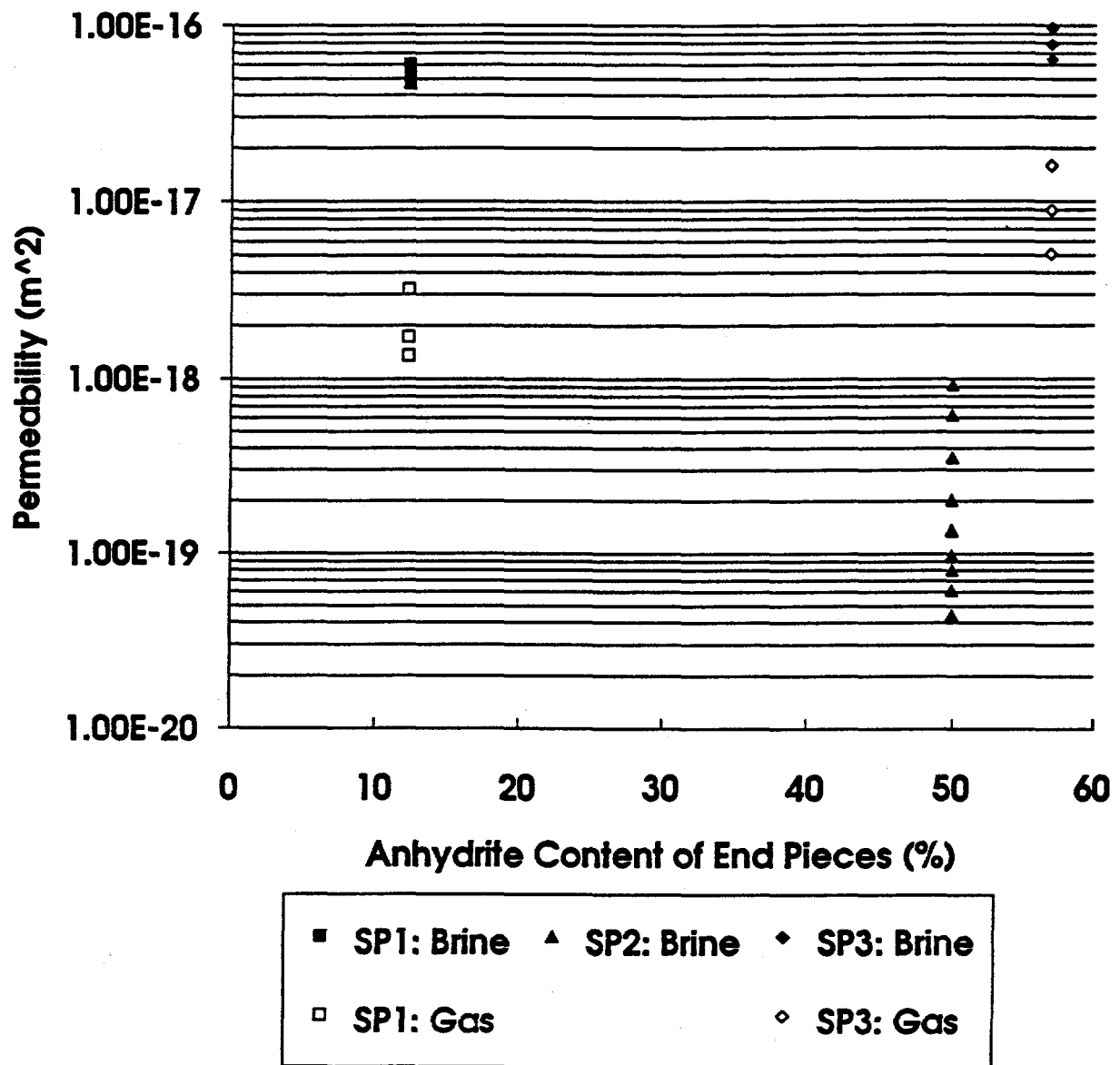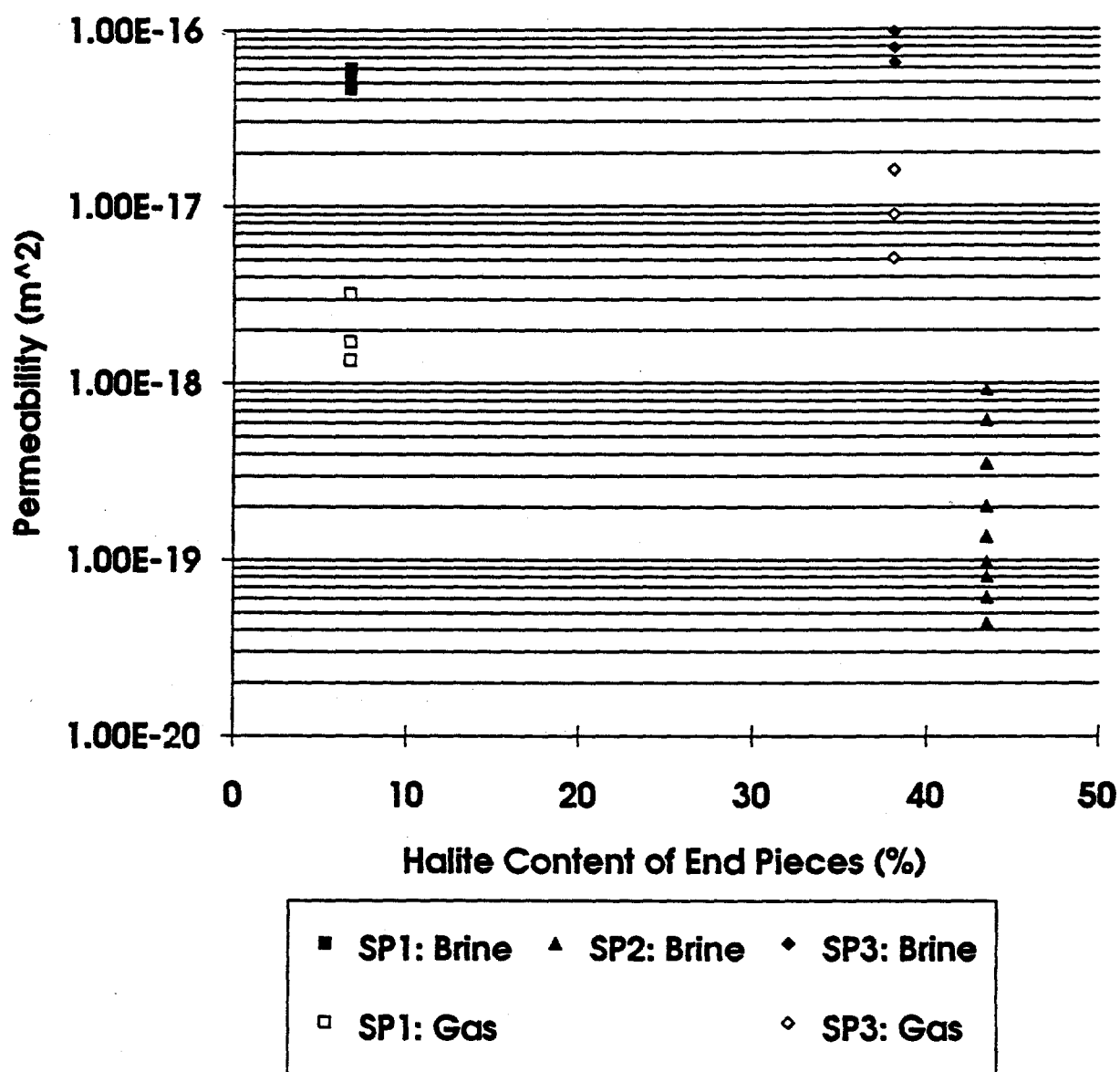
Figure 5-2. Permeability-versus-average anhydrite content of material taken from above and below specimen axes. Only data obtained at 2 MPa confining pressure are shown for Specimens SP1 and SP3.
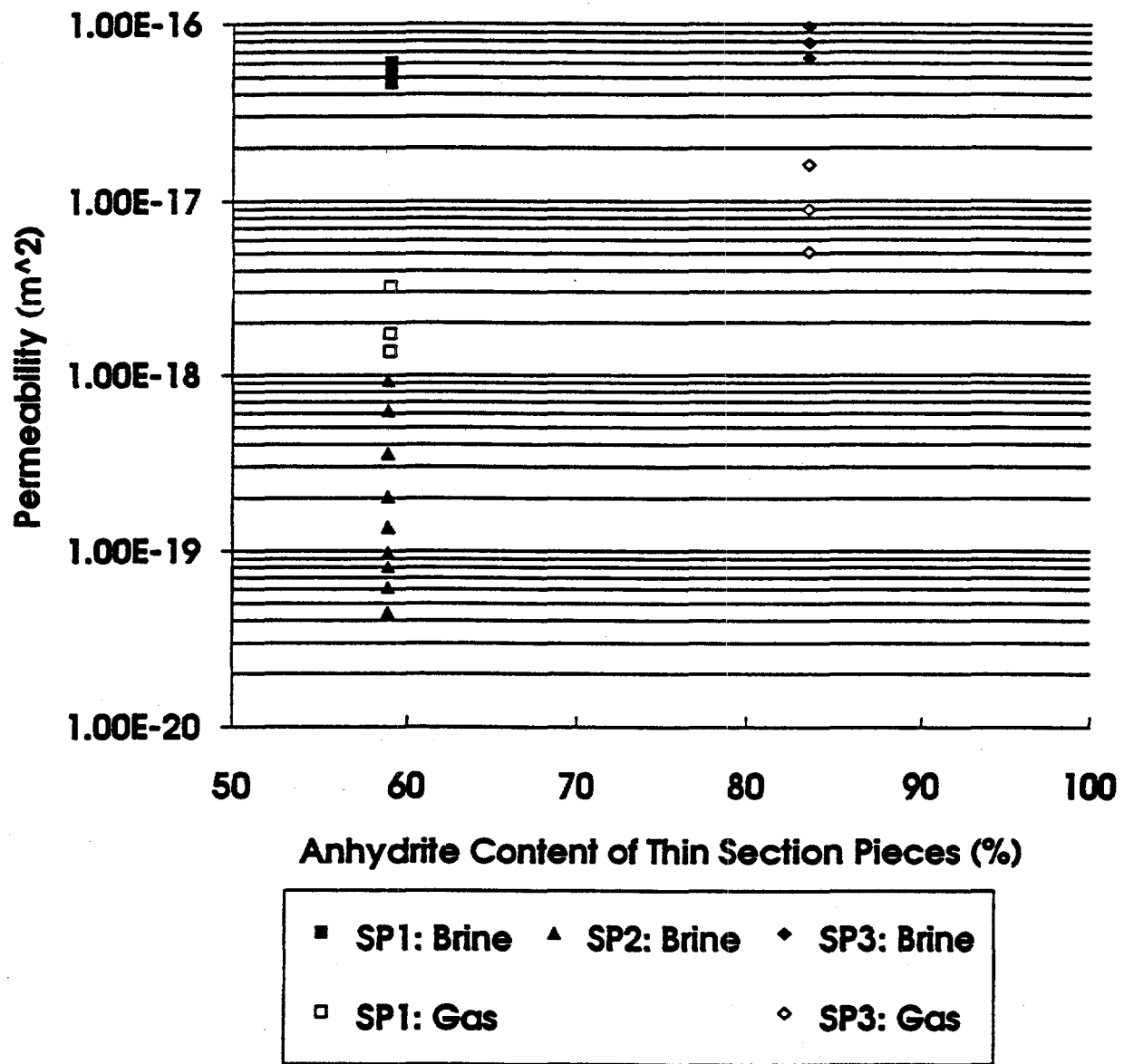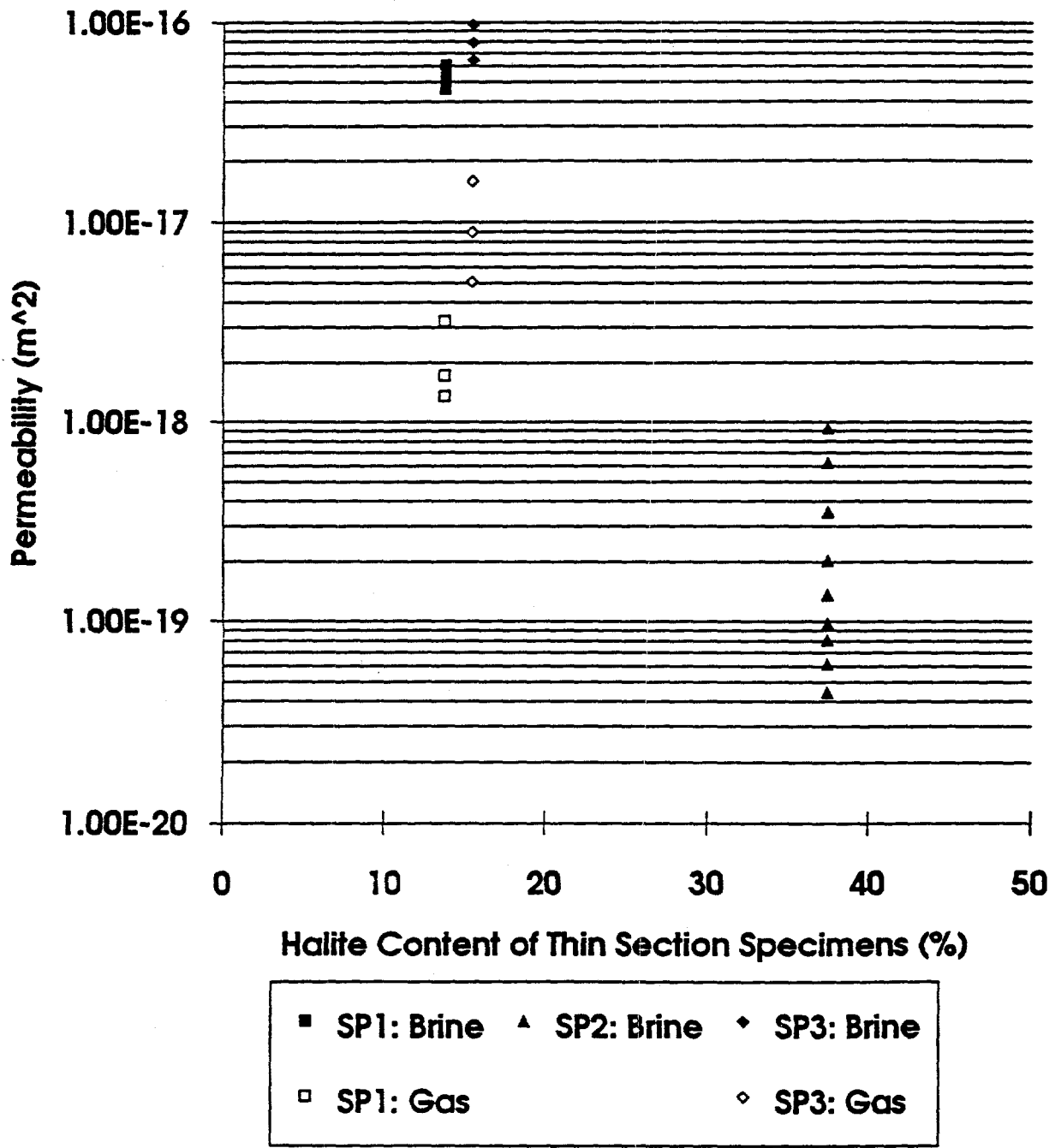
Figure 5-3. Permeability-versus-average anhydrite content of Blocks TS1, TS2, and TS3. Only data obtained at 2 MPa confining pressure are shown for Specimens SP1 and SP3.
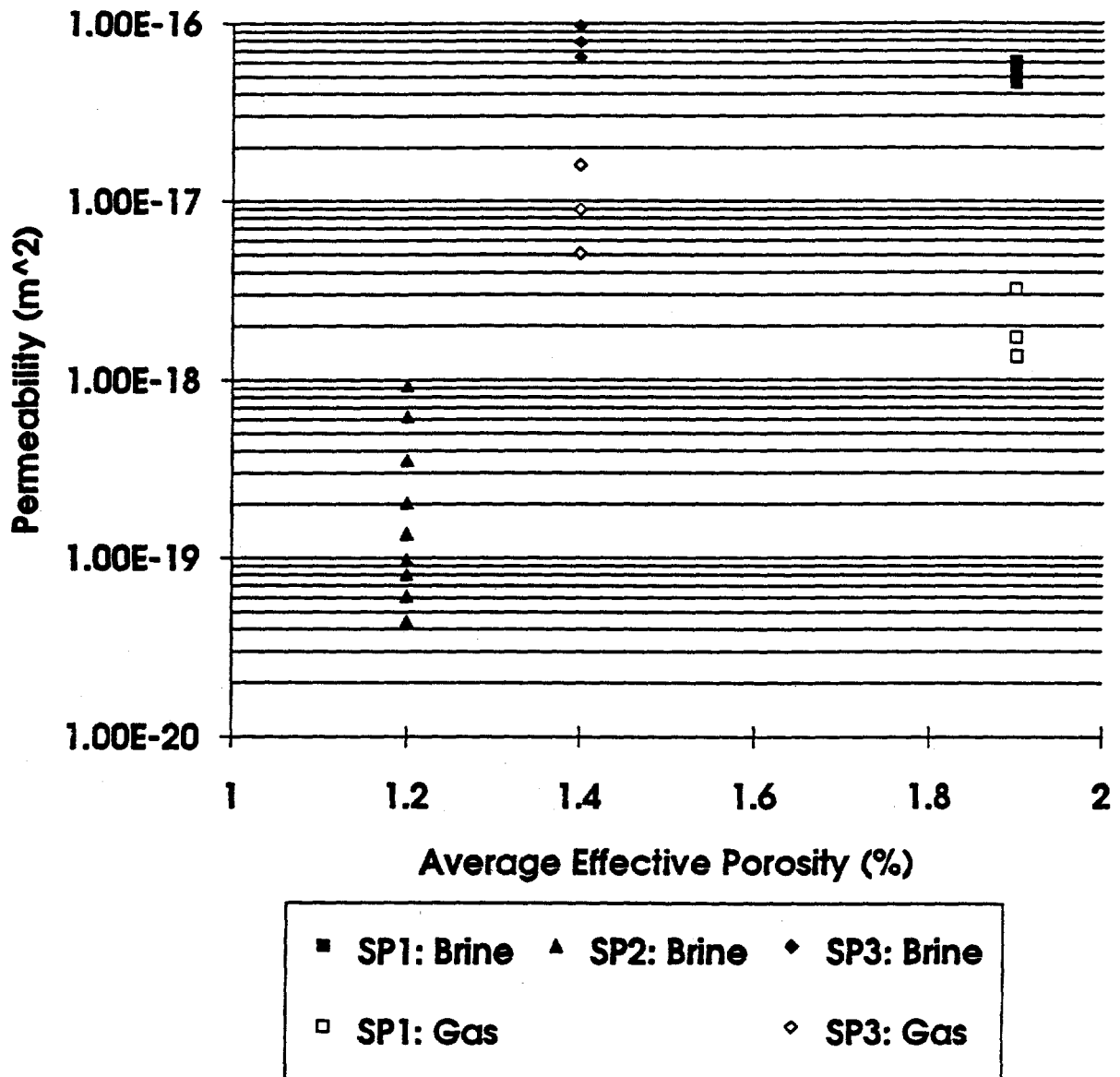
Figure 5-4. Permeability-versus-average halite content of material taken from above and below specimen axes. Only data obtained at 2 MPa confining pressure are shown for Specimens SP1 and SP3.
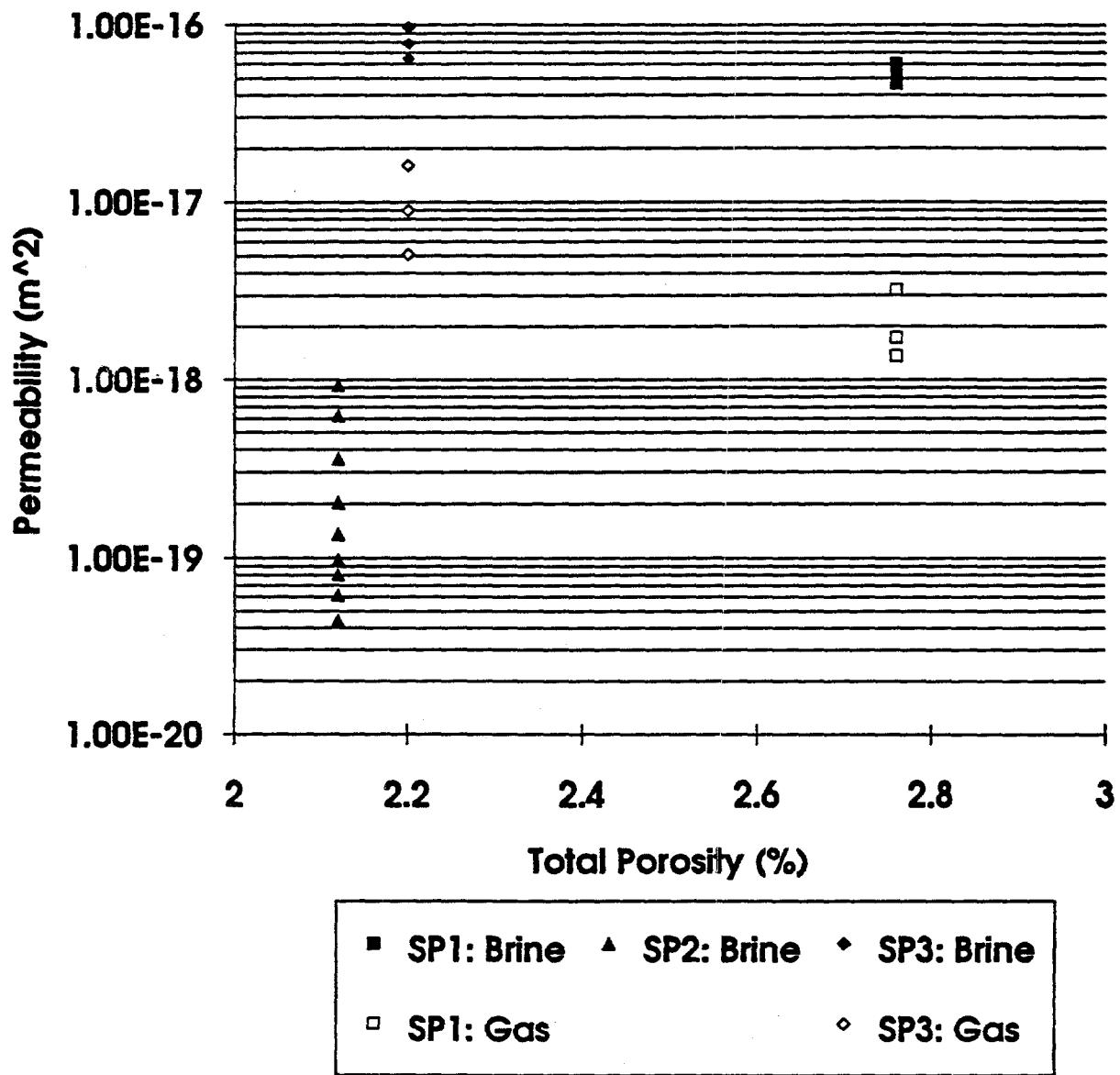
Figure 5-5. Permeability-versus-average halite content of Blocks TS1, TS2, and TS3. Only data obtained at 2 MPa confining pressure are shown for Specimens SP1 and SP3.
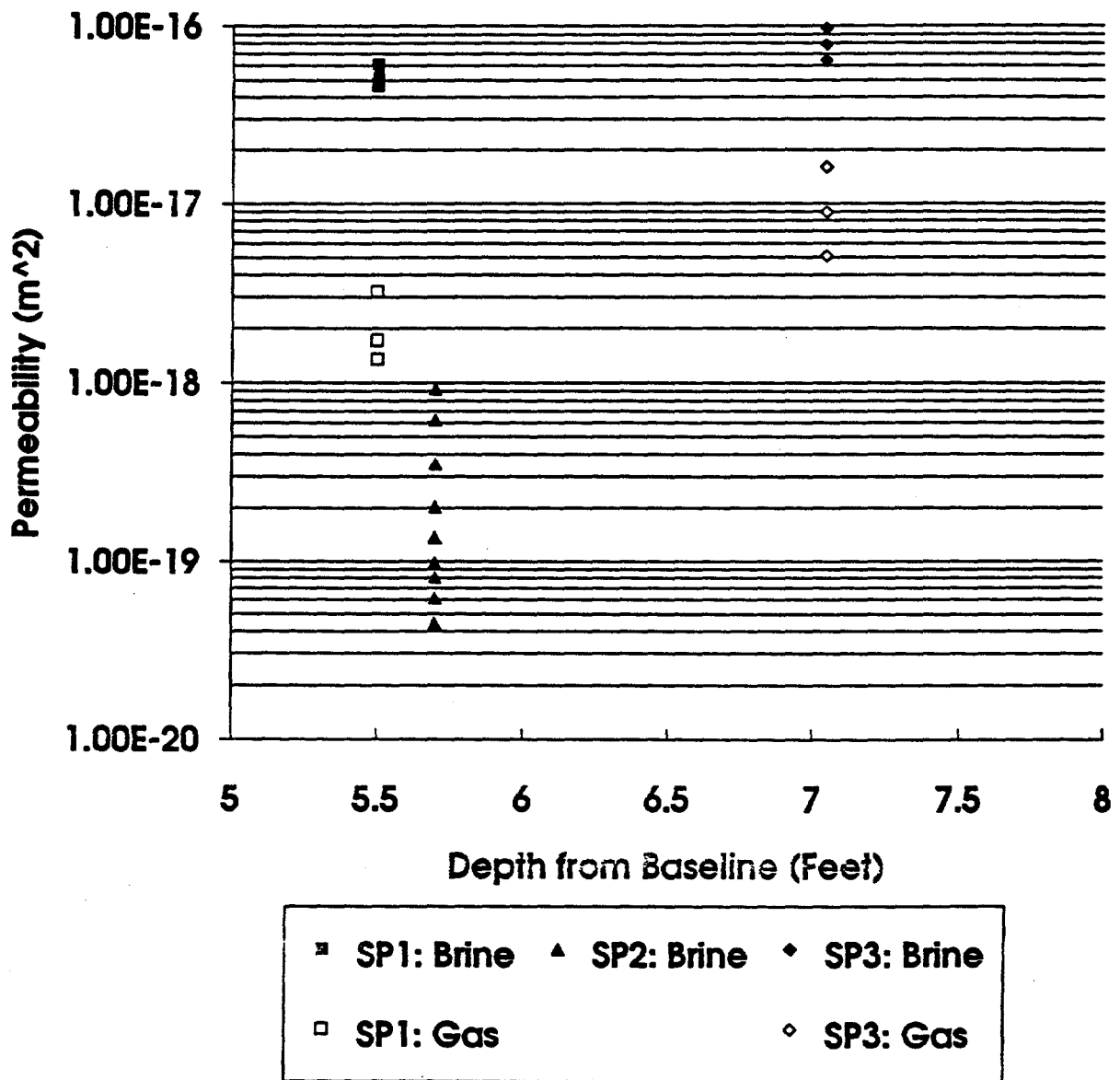
Figure 5-6. Permeability-versus-average effective porosity of specimens taken from above and below axes of permeability specimens. Only data obtained at 2 MPa confining pressure are shown for Specimens SP1 and SP3.

Figure 5-7. Permeability-versus-total porosity of specimens taken from above axes of permeability specimens. Only data obtained at 2 MPa confining pressure are shown for Specimens SP1 and SP3.

Figure 5-8. Permeability-versus-depth of origin of each specimen. Only data obtained at 2 MPa confining pressure are shown for Specimens SP1 and SP3.

6.0 SUMMARY AND CONCLUSIONS

Single-phase brine and nitrogen permeabilities were measured in the laboratory for specimens of Marker Bed 139 taken from the underground workings at the Waste Isolation Pilot Plant. The test plan was designed to provide data to evaluate the causes of spatial variations in permeabilities. Auxiliary measurements therefore included assessment of coring-induced damage, the porosities and mineralogies of materials immediately adjacent to each permeability specimen, and the mineralogies of additional specimens taken from near each permeability specimen. The same specimens were used for both gas and liquid permeability tests to facilitate comparison of results. Two of the three permeability specimens were from the upper and lower sections of borehole P3X11, and these were spaced 0.61 m apart, vertically. The third permeability specimen was from the upper/central region of adjacent borehole P3X10 and its in situ location was 0.06 m below and 0.61 m across from the uppermost specimen from borehole P3X11. Material was taken from immediately above and below the axis of each permeability specimen and used for quantitative analysis by X-ray diffraction and also for measurements of effective and total porosities. Additional blocks of material were taken from near each specimen and these were sectioned for petrographic analysis and for X-ray diffraction studies.

A quantitative analysis of crack occurrence near the surfaces and centers of cored specimens was conducted because coring-induced surface damage, if present, could affect permeability measurements. Although the data indicated that higher crack densities were associated with the specimen edges than with the midsections, the difference in crack densities was not statistically significant.

All permeability and porosity specimens were dried before testing at 60°C and 45 percent relative humidity to prevent dehydration of any clay components. Effective porosities were then measured by Core Laboratories using a helium porosimeter. These specimens were returned to RE/SPEC Inc., dried again at 60°C and 45 percent relative humidity to ensure that moisture contents were stable, and used for measurements of total porosity using gravimetric methods. Effective porosities ranged from 1.0 percent to 2.1 percent while total porosities ranged from 2.1 percent to 2.8 percent. (The errors in porosity measurements are approximately ± 1 percent porosity.) Effective and total porosities were both highest for the uppermost section of the marker bed.

A total of 81 gas permeability and 22 brine permeability measurements were made. Confining pressures of 2 MPa, 6 MPa, and 10 MPa were used and for each value of confining

pressure, permeability measurements were made at inlet pore pressures of 0.4 MPa, 0.7 MPa, and 1.0 MPa and at an outlet pore pressure of 0.1 MPa. One specimen (P3X11-5-2-SP1) experienced a jacket leak during brine permeability measurements and so no data were collected at 6 MPa and 10 MPa confining pressure. The relationship between flow rate and pore pressure difference was checked for linearity at each confining pressure to ensure that the measurements were made in the laminar flow regime. Gas permeability data were corrected for Klinkenberg effects to determine the equivalent liquid permeability at each confining pressure.

Permeabilities to nitrogen and brine each span approximately 2 to 2.5 orders of magnitude. Permeabilities to gas ranged from approximately 1.8×10^{-19} m^2 to 2.5×10^{-17} m^2 and the Klinkenberg-corrected equivalent liquid permeabilities ranged from 1.4×10^{-18} m^2 to 1.6×10^{-17} m^2. Permeabilities to brine ranged from 4.4×10^{-20} m^2 to 9.7×10^{-17} m^2. Permeabilities to brine were higher, perhaps because of some specimen dissolution that occurred during saturation and after completion of the gas permeability tests. The laboratory data include the range of permeability values indicated by field measurements, 8×10^{-20} m^2 to 5×10^{-17} m^2 (Davies et al., 1992).

These data show lateral and vertical variations in permeability for MB 139. The highest permeabilities were measured in the lowermost section of P3X11, while the lowest permeabilities were measured for the central to upper region of adjacent borehole P3X10. The data presented here are limited in extent and additional work must be performed to fully assess the causes of spatial variations in permeability. The specimen with the lowest permeability had the highest halite content and the lowest porosity; however, its porosity and halite content were not substantially different from those of the specimen with the highest permeability. The specimen with the highest permeability also had the highest anhydrite content, however, it's anhydrite content did not differ substantially from that of the specimen with the lowest permeability. Permeability values do not strongly correlate with any single material characteristic such as porosity, halite content, or anhydrite content; however, these material characteristics may contribute to spatial variations in permeability. Fluid flow in rock occurs through the interconnected void space. Heterogeneity of this void space either is not strongly correlated with any single material characteristic measured, or the data obtained was insufficient in quantity for a correlation to be apparent.

7.0 REFERENCES

ANSI/ASME, 1986. *Part 1 Measurement Uncertainty, Instruments and Apparatus.* PTC 19.1-1985. New York, NY: American Society of Mechanical Engineers.

ASTM. 1989. "Standard Test Method for Specific Gravity of Soils." *Annual Book of ASTM Standards*, Standard D854-83. Vol. 4.08. Philadelphia, PA: ASTM.

ASTM. 1989. "Standard Test Method for Permeability of Rocks by Flowing Air." *Annual Book of ASTM Standards*, Standard D4525. Vol. 4.08. Philadelphia, PA: ASTM.

Brodsky, N.S., 1993. *Hydrostatic and Shear Consolidation Tests With Permeability Measurements on Waste Isolation Pilot Plant Crushed Salt.* SAND93-7058. Albuquerque, NM: Sandia National Laboratories.

Brodsky, N.S., 1990. *The Effect of Brine Injection on the Creep of WIPP Salt During Laboratory Tests.* SAND90-2367. Albuquerque, NM: Sandia National Laboratories.

Chowdiah, P. 1988. "Influence of Water-Desaturation Technique and Stress on Laboratory Measurement of Hydraulic Properties of Tight Sandstones," *SPE Formation Evaluation.* December, 679-685.

Costin, L.S., Wawersik, W.R., 1980. *Creep Healing of Fractures in Rock Salt.* SAND80-0392. Albuquerque, NM: Sandia National Laboratories.

Gilpatrick, L.O., C.G. Baes, A.J. Shor, and C.M. Canonico, 1982. *The Permeability of Salt-Crystal Interfaces to Brine.* ORNL-5874. Oak Ridge, TN: Oak Ridge National Laboratories.

Davies, P.B., L.G. Brush, M.A. Molecke, F.T. Mendenhall, and S.W. Webb, eds., 1991. *Waste-Generated Gas at the Waste Isolation Pilot Plant: Papers Presented at the Nuclear Energy Agency Workshop on Gas Generation and Release From Radioactive Waste Repositories.* SAND91-2378. Albuquerque, NM: Sandia National Laboratories.

Howarth, S.M. 1993. *Conceptual Plan: Two-Phase Flow Laboratory Program for the Waste Isolation Pilot Plant.* SAND93-1197. Albuquerque, NM: Sandia National Laboratories.

Holcomb, D.J. and M. Shields, 1987. *Hydrostatic Creep Consolidation of Crushed Salt With Added Water.* SAND87-1990. Albuquerque, NM: Sandia National Laboratories.

Hurlbut, C.S., 1971. *Dana's Manual of Mineralogy.* New York, NY: John Wiley & Sons.

IT Corporation, 1987. *Laboratory Investigation of Crushed Salt Consolidation and Fracture Healing.* BMI/ONWI-631. Columbus, OH: Office of Nuclear Waste Isolation.

Klinkenberg, L.J., 1941. "The Permeability of Porous Media to Liquids and Gases," *API Drilling and Production Practice.* 200-213.

Stone and Webster Engineering Corporation, 1983. *Preliminary Assessment of the Healing of Fractures in Salt.* ONWI-363. Columbus, OH: Office of Nuclear Waste Isolation.

Stormont, J.C. and J.J. Daemen, 1992. "Laboratory Study of Gas Permeability Changes in Rock Salt During Deformation," *International Journal of Rock Mechanics Mining Science and Geomechanical Abstracts.* Vol. 29, No. 4, 325-342.

Sutherland, H.J. and S.P. Cave, 1980. "Argon-Gas Permeability of New Mexico Rock salt Under Hydrostatic Compression," *International Journal of Rock Mechanics Mining Science and Geomechanical Abstracts.* Vol. 17, 281-288.

Weast, R.C., ed. 1974. *Handbook of Chemistry and Physics.* Cleveland, OH: CRC Press.

APPENDIX B.A
SOUTH DAKOTA SCHOOL OF MINES AND TECHNOLOGY
PETROGRAPHIC ANALYSIS PROCEDURE AND RESULTS

ENGINEERING AND MINING EXPERIMENT STATION
REPORT OF ANALYSES
Optical Microscopy Laboratory - PLM Section

March 19, 1993

CLIENT: RE/SPEC, Inc.
            Rapid City, SD
            ATTN: Tom Pfeifle

PROCEDURES: Analysis of thin sections provided by RE/SPEC on 25mm slides. Several correlated with the XRD samples. Analysis was completed by polarizing microscopy at 100X magnification, with 550 m retardation enhancement. Counting was by areal element fraction using a Porton reticle. Six rectangles, each of area 3.256×10^{-4}, of the reticle were used. Three traverses across the section included 10 stops each, for a total of 60 Porton fields per traverse (180 per section). The percentages of table 1 are areal percentages and are equivalent to volume percentages. Because of the similar densities of the components, the percentages are approximately equivalent to weight percentages.

RESULTS:

The components found in these sections are: anhydrite, halite, polyhalite, magnesite, and carbonaceous matter (?). The latter consisted of small but areal significant specks or patches of opaque brown to black material; no orthoscopic or conoscopic properties could be obtained from this latter component; it here tentatively identified as carbon. Anhydrite was distinguished by its moderate retardation colors and good crystal shape and cleavage traces. Polyhalite was distinguished by the feathery growth habit and low (gray to first-order yellow) retardation colors. Magnesite occurred as tiny 1-5 m sized equant grains of high relief and retardation color. Halite is transparent but isotropic and could be easily distinguished from all other components; however, some of the halite appeared to have been lost during thin section preparation, leaving holes (also transparent and "isotropic") which are believed to have contained halite. Therefore, obvious holes were included in the halite count. The following table contains the summary of the volume percentages for these samples.

TABLE 1. Summary of Volume Percentages, Evaporite Thin Sections[1]

EMES ID	RE/SPEC ID	ANHYD	HALITE	POLYHA	MAGNES	CARBON
923.0854 (0849)	P3X11-5-3-2-TS1-1	70.4 ± 10.2	15.9 ± 2.6	9.6 ± 7.4	2.0 ± 0.06	2.2 ± 1.9
923.0859 (0849)	P3X11-5-3-2-TS1-2	45.8 ± 10.5	13.4 ± 2.3	30.6 ± 6.7	9.4 ± 4.2	0.8 ± 0.6
923.0855 (0849)	P3X11-5-3-2-TS1-3	48.9 ± 12.6	26.7 ± 6.8	14.9 ± 4.4	8.0 ± 3.1	1.6 ± 0.3
923.0852 (0844)	P3X10-5-3-2-TS2-1	67.8 ± 17.6	24.5 ± 19.4	0	3.5 ± 2.5	4.2 ± 0.9
923.0857 (0844)	P3X10-5-3-2-TS2-2	43.1 ± 3.7	54.8 ± 4.1	0	0.6 ± 0.03	1.6 ± 0.7
923.0858 (0844)	P3X10-5-3-2-TS2-3	58.2 ± 3.9	37.2 ± 3.9	0	3.0 ± 0.7	1.6 ± 0.3
923.0856 (0850)	P3X11-6-TS3-1	95.9 ± 3.7	1.4 ± 2.4	0.6 ± 1.1	0.6 ± 0.2	0.2 ± 0.04
923.0851 (0850)	P3X11-6-TS3-2	89.9 ± 0.8	8.8 ± 1.3	0	0	1.4 ± 0.5
923.0853 (0850)	P3X11-6-TS3-3	66.7 ± 8.5	31.9 ± 9.3	0	0.4 ± 0.7	1.0 ± 0.2

[1]   Values are volume percentages with standard deviations for the three traverse
counts given as ± below. XRD samples correlating with optical samples are given
in parentheses below EMES ID number.

APPENDIX B.B
SOUTH DAKOTA SCHOOL OF MINES AND TECHNOLOGY
X-RAY DIFFRACTION PROCEDURE AND RESULTS

B.B-1. X-RAY DIFFRACTION PROCEDURES

QUALITY ASSURANCE PROCEDURES - EMES X-RAY DIFFRACTION LABORATORY
Sept. 26, 1992

1. General Aspects

The quality assurance used in the EMES x-ray diffraction laboratory consist of sample custody procedures, sample preparation procedures, and instrument performance checks. In addition, uncertainties in analytical results are estimated using standard variance error propagation of measurement and computational errors in the full quantitative analysis (RIM) method. The XRD Laboratory manager (B.L. Davis) acts as the quality assurance officer for all XRD analytical work.

2. Sample Custody

Samples mailed or otherwise delivered to EMES are logged in according to date received and assigned an identification number. A lab work order is prepared with the i.d. numbers listed and placed with the samples in the lab cabinet. The analyst conducts the analyses in sequence of i.d. number, always maintaining proper labeling and association of filter preparations with the parent samples. Samples are stored for a minimum of 30 days before discarding, but kept longer on request. The custody log book also records date of completion of analysis and date of payment by the client.

3. Instrument Calibration Checks

3.1. X-ray Transmissometer

Weekly transmission measurements are completed on a "Quartz" filter standard. The direct-beam transmissometer attenuation plate, tube power settings, cycle number, maximum open beam intensity, filter transmission ratio, standard deviation, and operator initials and time/date of check are all recorded in the QA calibration log. Adjustments are made to correct misalignment, pulse-height-analyzer settings, or attenuation factors whenever the standard deviation of the filter standard transmission ratio for the 13 cycles exceeds 0.5%

3.2. X-ray Diffractometer

3.2.1. General Instrument alignment - A novaculite standard is scanned weekly at 100 sec/deg rate at 40/20 kV/mA power over the 101 quartz line. Pulse-height-analyzer settings, tube power, detector voltage, integrated intensity, and background integrated intensity are logged for each scan. Minor misalignment generally requires adjustments only to the graphite monochromator, more serious misalignment requires 2:1 settings and sample-height changes; this action has not been required for over 20 years.

3.2.2. Low angle alignment - A special NIST silver behenate low-angle standard has become available during the past several months. This laboratory now has prepared a standard for the Philips diffractometer that is used on all routine projects. The first low-angle adjustment was made on Sept. 19, 1992 which materially improved the sensitivity of large-spacing materials, such as glycolated smectite clays and organic compounds. Low-angle alignment will be checked on a monthly basis.

3.3. Other analytical equipment

This laboratory supports its qualitative and quantitative XRD work with polarizing light microscopy (PLM). While no periodic QA procedure is used here, some optical alignment and stage centering adjustments are made on an "as needed" basis. Electronic balances are checked periodically using standard weight sets and filter specific mass checks on Whatman GF/C 42.5-cm filters (the latter are exceptionally uniform in their composition and weight properties).

4. Analytical Procedures

4.1. General Approach

Detailed operator instructions for x-ray transmission (needed for mass absorption measurements), x-ray diffraction scanning, and data reduction from instrument computers are maintained in the laboratory. Staff have their individual copies as well. The method EMES most often uses for quantitative XRD analysis is the RIM (Reference Intensity Method); calibration curves for light filter loadings of free silica are also used. Where amorphous components are identified, mass absorption measurements (by XRT) alone, or combined with PLM measurements allow complete quantitative analysis of crystalline and amorphous components of the sample.

A flow-diagram schematically illustrating the path of a bulk sample from particle size reduction to final analysis is illustrated in Fig. 1. This particular flow diagram illustrates the procedures for small filters; large filters (8" X 10", for example) are treated similarly except that several filter circles are cut from the large filter and analyzed or ultrasonic stripping of the particles is first completed to concentrate the sample onto a smaller area.

4.2. Procedures for Free Silica (Quartz and Cristobalite)

Our capability currently exists for routine quantitative analysis for α-quartz and α-cristobalite. Tridymite analysis can be completed as well by full RIM analysis, but a calibration curve has not been developed. Quantitative analysis of free silica can be completed by two methods: (1) Full component analysis by the RIM procedures, and (2) thin-layer calibration curve analysis.

4.2.1. Reference Intensity Method (RIM)

For bulk materials the analysis procedure is:

a. Reduce the sample particles to 10-micron mean diameter or less.

b. Load the powder onto preweighed Whatman GF/C filters using aerosol (TASC) suspension (Davis, 1986). Take another weighing.

c. Complete a direct-beam x-ray transmission (XRT) measurement for mass absorption determination ((Davis and Johnson, 1987).

d. Weigh the sample again to check for losses during XRT analysis.

e. Cut the filter to 2.5-cm diameter, mount on pedestal and scan by XRD from 3^0 to 60^0 2θ at 40/20 power, $CuK\alpha$ radiation.

f. Identify components and measure intensities of analytical peaks. Determine overlaps on the component peaks used for analysis. All XRT and XRD data are entered on a RIM analysis log and entered into appropriate computer programs. Output will consists of weight fractions and associated variance errors (Davis, 1981) of all components, calculated mass absorption and density parameters, and a oxide/element table obtained from computer files for each compound found in the analysis.

For ambient filter loads the procedure is:

a. Cut the filter into 7-cm circles, dry and weigh the circles.

b. Strip the particles from the circles in a methanol bath using ultrasound.

c. Dry and weigh the stripped circles. This provides the amount of glass fiber brought down with the particles when accurate tare and load weights of the parent filter are available.

d. Deposit all or a portion of the methanol suspension onto another filter (Whatman GF/C or Metricel VM-1, depending on sample amount available).

e. Complete mass absorption analysis by either XRT or by substrate diffraction (depending on filter size and sample amount).

f. Complete scans and data analysis as in steps d-f for bulk materials.

4.2.2 Calibration procedure.

In this procedure loads must be kept to within 300 µgm cm^{-2} on teflon (PTFE) filters in order to eliminate absorption by the sample. The procedure is relatively simple, however.

a. Weigh a 37-mm PTFE filter and load with aerosol using the TASC system. Reweigh the filter to obtain total mass deposited.

b. Complete a scan of the novaculite standard at step/dwell conditions matching those of the original scan when the calibration curve was determined.

c. Complete a full scan and then a scan at 0.25^0 min^{-1} over the quartz and/or cristobalite peaks pertaining to the calibration curve.

d. Measure the integrated intensities of both quartz/cristobalite peaks and novaculite standard; correct for overlaps on the quartz peaks; adjust the intensities of the analyte peaks, if necessary to match conditions of the original novaculite standard.

B-114

e. Use the calibration curve equation to determine the specific mass of analyte present. Dividing this value by the specific mass from the tared filter and loaded filter weights provides the final weight percent analyte.

Figures 2 and 3 present the calibration curves currently used in this laboratory. Regression lines are shown, and in the case of quartz, subsequent quality control analyses points (+ symbols) indicating continued validity of the curve. For quartz R = 0.980 and for cristobalite R = 0.996.

The preferred (and least expensive) procedure, where sample amount is sufficient (or ambient filter load is large), is the full RIM procedure. The major drawback to the calibration method is that a full scan of the sample must be completed in order to identify all components for overlap corrections on the quartz or cristobalite peaks, where appropriate. Where ambient filters are analyzed and the loads are light, there may be no choice but to use the calibration method; however, in these cases long scan times are required to obtain a usable pattern for overlap corrections, which leads to considerably higher cost of analysis.

4.3. Lower Limits of Detection

Lower limits of detection are computed for full RIM analyses using relations derived from the "Adiabatic" analysis method of Chung (1974). Procedures for LLD computations have been summarized by Davis (1988). Several approaches are used, depending upon whether reference constants are available and whether the diffraction effects for the analyte are actually seen.

LLD values for quartz or cristobalite are based on the root background intensity criterion use in all counting statistics. It is given by

$$LLD = \frac{6W_i}{I_i}\sqrt{\frac{I_b}{t_t}} \tag{1}$$

An estimate of the LLD, even without a measurable peak present, can be given from a 3-σ measurement at the appropriate 2θ position.

Our experience with light ambient aerosol loadings on PTFE filters is that quartz can be detected with 0.25^0 min^{-1} scanning to within the 0.05-0.1% by weight range. Even lower values may be obtained with still slower scanning, which then becomes more costly. A study of quartz analysis by the calibration method which contains analytical results in this low weight range was completed by Davis *et al.* (1984).

5. References

The following references provide a reasonably complete documentation of the EMES XRD procedures for quantitative analysis, including sample preparation, mass absorption analysis, detection limits, and error propagation.

Chung, F.H., (1974). Quantitative Interpretation of X-ray Diffraction Patterns of Mixtures - II. Adiabatic Principle of X-ray diffraction Analysis of Mixtures. *J. Appl. Cryst.* 7, 526-531.

Davis, B.L., (1981). A Study of the Errors in X-ray Quantitative Analysis Procedures for Aerosols Collected on Filter Media. *Atm. Environ.* 15, 291-296.

Davis, B.L., (1984). Reference Intensity Quantitative Analysis using Thin-Layer Aerosol Samples. *Adv. X-ray Anal.*, 27, 339-348.

Davis, B.L., (1986). A Tubular Aerosol Suspension Chamber for the Preparation of Powder Samples for X-ray Diffraction Analysis. *Powd. Diff.*, 1, 240-243.

Davis, B.L., (1988). The Estimation of Limits of Detection in RIM Quantitative X-ray Diffraction Analysis. *Adv. X-ray Anal.*, 31, 317-323.

Davis, B.L., and L.R. Johnson (1982). On the Use of Various Filter Substrates for Quantitative Particulate Analysis by X-Ray Diffraction. *Atm. Environ.*, 16, 273-282.

Davis, B.L., and L.R. Johnson, (1987). The Use of Mass Absorption in Quantitative X-ray Diffraction Analysis. *Adv. X-ray Anal.*, 30, 333-342.

Davis, B.L., Johnson, L.R., Stevens, R.K., Courtney, W.J., and D.W. Safriet (1984). The Quartz Content and Elemental Composition of Aerosols from Selected Sites of the EPA Inhalable Particulate Network. *Atm. Environ.*, 18, 771-782.

PTFE Filters, CuKa Radiation
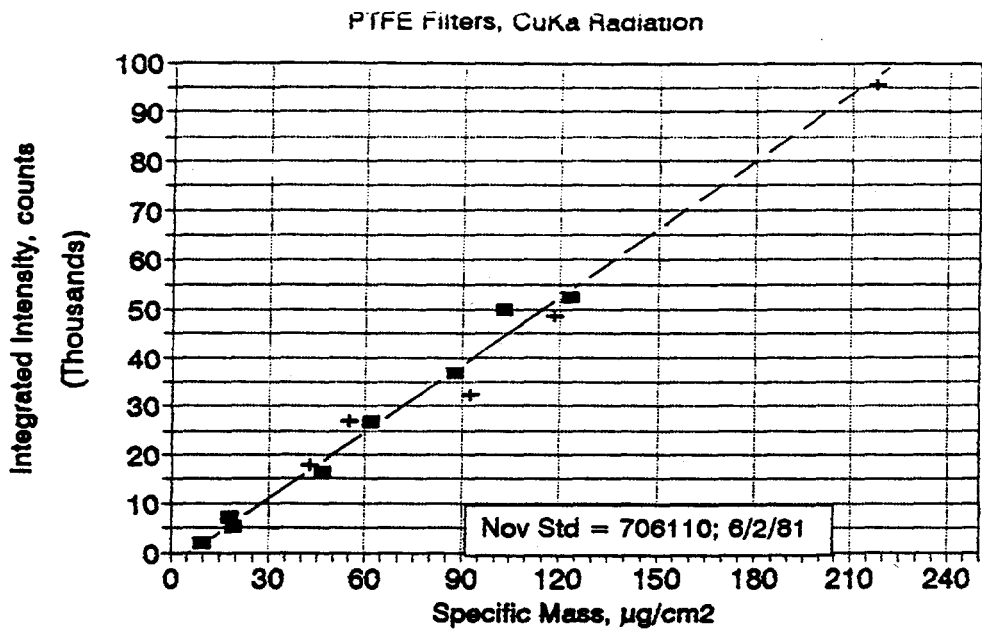
Figure 2

```
+    Quality Control Ck
```

NIOSH CRISTOBALITE CALIBRATION
PTFE Filters, CuKa Radiation
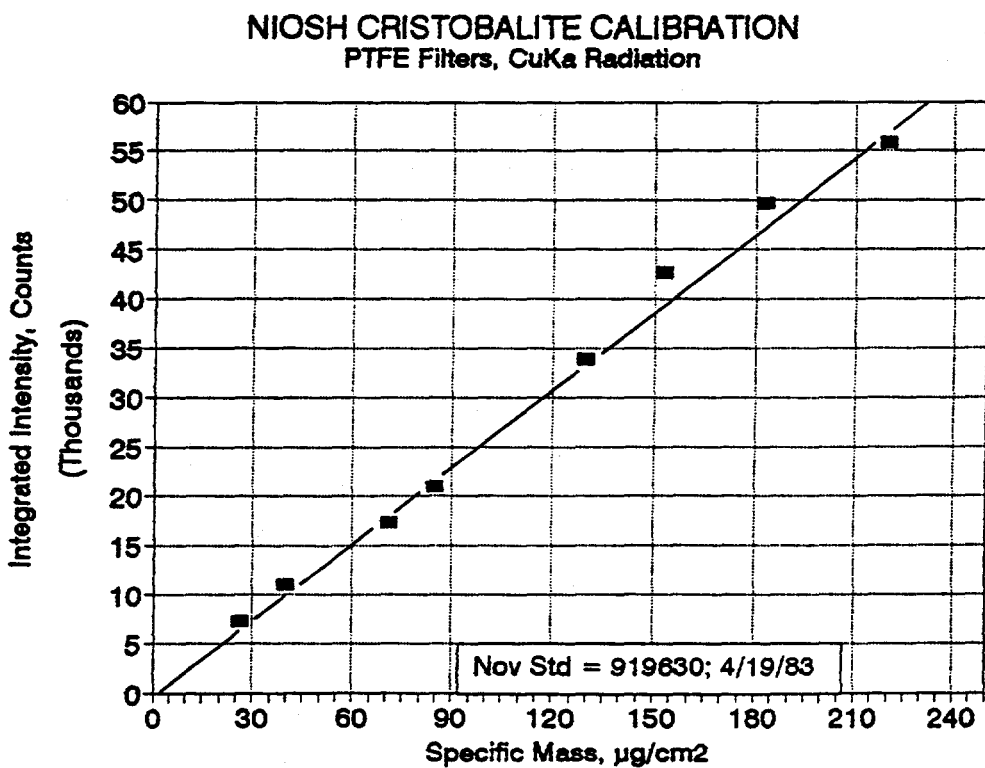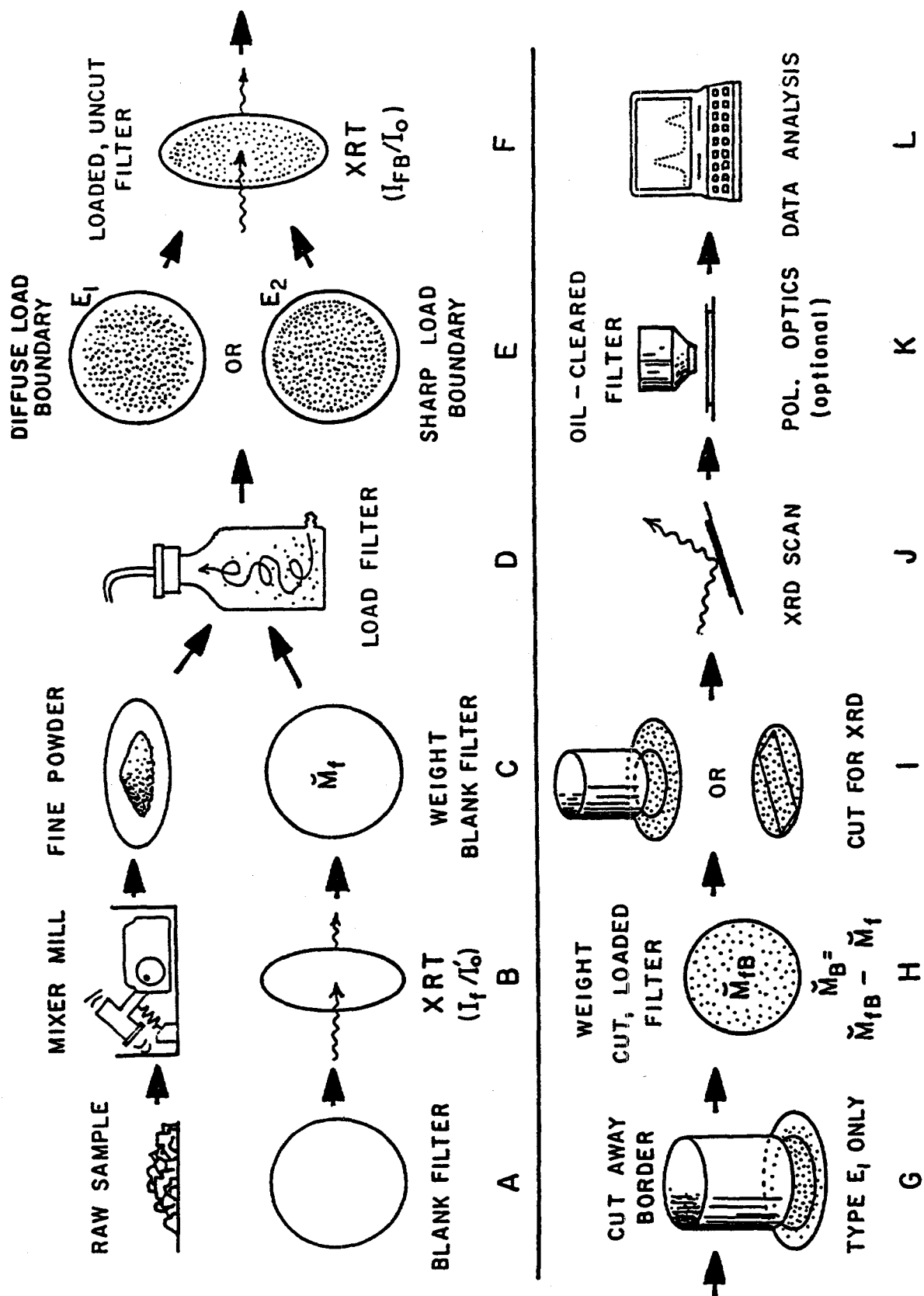
Figure 3

Figure 1 Flow diagram representing the successive steps in sample preparation and analysis. See text for step-by-step explanation.

QUALITY ASSURANCE PROCEDURE - NICOLET/SIEMENS DIFFRACTOMETER
Oct. 20, 1992

1. Background

This Nicolet/Siemens diffractometer has both transmission and diffraction capability. The transmission scanning of the Kentucky gypsum standard will be completed monthly. The brass substrate standard will completed whenever a Bragg-Brentano scan, or substrate diffraction mass absorption analysis is required. The relative infrequency of these QA scans stems from the greater mechanical alignment stability of this unit compared to the Philips unit. Whenever the scans are completed a plotter dump and integrated intensity of the prime peaks shall be collected and entered into the NICOLET QA file. Logbook entries are to be kept of each QA run as for the Philips QA scans.

2. Transmission Settings

Prime Peaks:	Gypsum 020, $2\theta = 11.59°$; d = 7.63Å Gypsum 041, $2\theta = 29.11°$; d = 3.065
Intervals:	10.50-12.98° and 27.0-34.00° 35.00-36.00° in ω
Step:	0.04° for each interval in 2θ 0.001° for each interval in ω
Dwell:	4 seconds for all scans
Corrections:	$\mu^t = 149.6$ cm^{-1} : T = 0.3mm (correction prompt ans. = yes)
Instrument:	CuKα_1, Germanium monochromator, spinner on. Power = 45 kV; 25 mA 1.0 divergence slit; 0.35 scatter slit beam stop in place and centered Counter V. = 9.0; BL = 1.0 v; WW = 6.78 v. Gain = 32; Damping = 0.4

3. Bragg-Brentano ("Reflection") Settings

Prime Peaks:	Brass 110, $2\theta = 42.63°$; d = 2.121Å Brass 201, $2\theta = 49.74°$; d = 1.833Å
Intervals:	41.00-44.00° and 48.00-51.00° in 2θ 35.00-36.00° in ω
Step:	0.04° for each interval in 2θ 0.001° for each interval in ω
Dwell:	4 seconds for all scans

Nicolet/Siemens Quality Assurance, p. 2

> Correction: No absorption correction
>
> Instrument: $CuK\alpha_1$, Germanium monochromator, spinner on.
> Power = 45 kV; 25 mA
> 1.0 divergence slit; 0.35 scatter slit
> beam stop removed; Knife stop in place
> Counter V. = 9.0; BL - 1.0 v; WW = 6.78 v.
> Gain = 32; Damping = 0.4

4. Special Precautions

Handle the standards with care. They must not be dropped or handled by the sample surface in any way. Use the magnet pencil to remove the gypsum standard from the spinner mount. Avoid scratching the brass SDIF reflection stage surface. When scanning the brass stage clean the brass surface with a Q-tip and methanol to remove vaseline.

When integrating the peak intensities place the cross-hair cursor to the left and right of each peak so that the tails are included in the intensity. Label all peaks with d-spacing and peak-height intensity before plotting.

B.B-2. X-RAY DIFFRACTION RESULTS

P3X11-5-3-3-SP3T

EMES0842 RESPEC P3X1 SP3T   THIS IS A LEVEL - 1 ANALYSIS
IFB/IO = .286804 S(IFB/IO) = .002104 IF/IO = .770598
S(IF/IO) = .003348
SPEC. FILTER MASS, MF, = .005262
SPEC. SAMPLE MASS, MB, = .013023
MEAN PARTICLE RADIUS, RZ, = .0004
MEAN SAMPLE DENSITY, RHO-Z, = 2.6

No. X-RAY COMPONENTS, N, = 3 No. OF OPTIC COMPONENTS, M, = 0
No. OF AMORPHOUS COMPONENTS, AM, = 0
No. OVERLAP SETS, OL, = 0
NO AMORPHOUS COMPONENTS IN THIS SAMPLE
FILTER TYPE = 2

COMP- 1 CODE = 28 IPK- 1 = 4921   IBG- 1 = 1008
COMP- 2 CODE = 24 IPK- 2 = 68981   IBG- 2 = 1109
COMP- 3 CODE = 284 IPK- 3 = 3927   IBG- 3 = 1322

NONE   NONE   SODIUM
ARE THE ELEMENT NAMES FOR OX FILE CODES 30, 31, AND 32
FILE REVIEW COMPLETE FOR EMES0842

MUBO(U) = 75.89402 CM2/GM MUBO(C) = 49.88233 CM2/GM
MUBO = 75.89402 CM2/GM
WHB = .9192489
MUFO = 49.52271   MUH = 73.76451 CM2/GM

INTENSITIES, CORRECTED FOR MATRIX AND TRANSPARENCY

IPK- 1 = 5314.051
IPK- 2 = 79939.68
IPK- 3 = 3567.678

FINAL INTENSITIES (IPK) CORRECTED FOR OVERLAP

IPK- 1 = 5314.051
IPK- 2 = 79939.68
IPK- 3 = 3567.678

PROVISIONAL WEIGHT FRACTIONS AND VARIANCE ERRORS
HALITE
   $W(I)- 1$ =   .3902889   +-   5.826536E-02
ANHYDRITE
   $W(I)- 2$ =   .5523928   +-   5.477093E-02
MAGNESITE
   $W(I)- 3$ =   5.731841E-02   +-   9.057642E-03

MASS ABSORPTION COEFFICIENTS AND ERRORS

MUC = 73.31308 +-   6.322203   CM2/GM
MUBO = 75.89402 +-   1.410341   CM2/GM
S(MB) = 2.143519E-04   GM/CM2
S(GAMMA) = 8.526044E-03

FINAL WEIGHT FRACTIONS AND VARIANCE ERRORS

HALITE
  W(I)- 1 =   .3902   +-   .0582
ANHYDRITE
  W(I)- 2 =   .5523   +-   .0547
MAGNESITE
  W(I)- 3 =   .0573   +-   8.999999E-03

99.98

CALCULATED SAMPLE DENSITY =   2.6   GM/CM3
SAMPLE CRYSTALLINE FRACTION =   1 +-   0

COMPOUND REDUCTION
                OXIDE   ELEMENT
SiO2   =   .0029   (.0013)
Al2O3   =   .0006   (.0003)
K2O   =   .0008   (.0007)
CaO   =   .2252   (.161)
Fe2O3   =   .0006   (.0004)
MgO   =   .0283   (.0171)
H2O   =   .0103   (.0011)
CO2   =   .0336   (9.099999E-03)
SO3   =   .3211   (.1286)
Cl   =   ----   (.2311)
SrO   =   .0006   (.0005)

ADDITIONAL ELEMENTAL COMPONENTS

Comp-1   NONE   = (0)*
Comp-2   NONE   = (0)*
Comp-3   SODIUM   = (.1477)*

OXIDE TOTAL = .6239   ELEMENT TOTAL =   .6994712
* Add these plus any C,F,Cl in ELEMENT TABLE to OXIDE TOTAL
   to obtain total weight fraction
RUN COMPLETE FOR SAMPLE   EMES0842

EMES0843 RESPEC P3X10-5-3 SP3   THIS IS A LEVEL - 1   ANALYSIS
IFB/IO = .29479 S(IFB/IO) = .002276 IF/IO = .7725
S(IF/IO) =   .003105
SPEC. FILTER MASS, MF, =   .005217
SPEC. SAMPLE MASS, MB, =   .011852
MEAN PARTICLE RADIUS, RZ, =   .0004
MEAN SAMPLE DENSITY, RHO-Z, = 2.6

No. X-RAY COMPONENTS, N, = 3   No. OF OPTIC COMPONENTS, M, = 0
No. OF AMORPHOUS COMPONENTS, AM, = 0
No. OVERLAP SETS, OL, = 0
NO AMORPHOUS COMPONENTS IN THIS SAMPLE
FILTER TYPE = 2

COMP- 1 CODE = 28 IPK- 1 = 4510   IBG- 1 = 835
COMP- 2 CODE = 24 IPK- 2 = 70260   IBG- 2 = 778
COMP- 3 CODE = 284 IPK- 3 = 2853   IBG- 3 = 892

NONE   NONE   SODIUM
ARE THE ELEMENT NAMES FOR OX FILE CODES 30, 31, AND 32
FILE REVIEW COMPLETE FOR EMES0843

MUBO(U) = 81.28323 CM2/GM MUBO(C) =   54.14616 CM2/GM
MUBO = 81.28323 CM2/GM
WHB = .9119729
MUFO = 49.47735   MUH = 78.48345 CM2/GM

INTENSITIES, CORRECTED FOR MATRIX AND TRANSPARENCY

IPK- 1 = 4876.995
IPK- 2 = 81533.86
IPK- 3 = 2595.764

FINAL INTENSITIES (IPK) CORRECTED FOR OVERLAP

IPK- 1 = 4876.995
IPK- 2 = 81533.86
IPK- 3 = 2595.764

EMES0843   RESPEC P3X10-5-3 SP3 PAGE 2
PROVISIONAL WEIGHT FRACTIONS AND VARIANCE ERRORS
HALITE
  W(I)- 1 =   .3718352   +-   5.736238E-02
ANHYDRITE
  W(I)- 2 =   .5848726   +-   5.494011E-02
MAGNESITE
  W(I)- 3 =   4.329237E-02   +-   6.861721E-03

MASS ABSORPTION COEFFICIENTS AND ERRORS

MUC = 74.20572   +-   6.304063   CM2/GM
MUBO = 81.28323   +-   1.559599   CM2/GM
S(MB) = 2.00615E-04   GM/CM2
S(GAMMA) =   8.704351E-03

EMES0843   RESPEC P3X10-5-3 SP303-19-1993 18:00:19   PAGE 3

FINAL WEIGHT FRACTIONS AND VARIANCE ERRORS

HALITE
  W(I)- 1 =   .3718   +-   .0573
ANHYDRITE   } 99.98
  W(I)- 2 =   .5848   +-   .0549
MAGNESITE
  W(I)- 3 =   .0432   +-   .0068

CALCULATED SAMPLE DENSITY = 2.62   GM/CM3
SAMPLE CRYSTALLINE FRACTION = 1 +- 0

COMPOUND REDUCTION
                 OXIDE   ELEMENT
SiO_2 = .0031   (.0014)
Al_2O_3 = .0006   (.0003)
K_2O = .0008   (.0006)
CaO = .2384   (.1703)
Fe_2O_3 = .0006   (.0004)
MgO = .0216   (.013)
H_2O = .01   (.0011)
CO_2 = .0261   (.0071)
SO_3 = .3399   (.1361)
Cl = ----   (.2202)
SrO = .0007   (.0005)

ADDITIONAL ELEMENTAL COMPONENTS

Comp-1   NONE   = (0)*
Comp-2   NONE   = (0)*
Comp-3   SODIUM   = (.1408)*

OXIDE TOTAL = .6418   ELEMENT TOTAL = .6925254
* Add these plus any C,F,Cl in ELEMENT TABLE to OXIDE TOTAL
   to obtain total weight fraction
RUN COMPLETE FOR SAMPLE EMES0843

EMES0844 RESPEC P3X10-5-3-TS2   THIS IS A LEVEL - 1 ANALYSIS
IFB/IO = .476364 S(IFB/IO) = .002124 IF/IO = .774321
S(IF/IO) = .003546
SPEC. FILTER MASS, MF, = .005157
SPEC. SAMPLE MASS, MB, = .005829
MEAN PARTICLE RADIUS, RZ, = .0004
MEAN SAMPLE DENSITY, RHO-Z, = 2.5

No. X-RAY COMPONENTS, N, = 3   No. OF OPTIC COMPONENTS, M, = 0
No. OF AMORPHOUS COMPONENTS, AM, = 0
No. OVERLAP SETS, OL, = 0
NO AMORPHOUS COMPONENTS IN THIS SAMPLE
FILTER TYPE = 2

COMP- 1 CODE = 28 IPK- 1 = 6600   IBG- 1 = 1554
COMP- 2 CODE = 24 IPK- 2 = 58466   IBG- 2 = 1176
COMP- 3 CODE = 284 IPK- 3 = 489   IBG- 3 = 1261

NONE   NONE   SODIUM
ARE THE ELEMENT NAMES FOR OX FILE CODES 30, 31, AND 32
FILE REVIEW COMPLETE FOR EMES0844

MUBO(U) = 83.34267 CM2/GM MUBO(C) = 69.08415 CM2/GM
MUBO = 83.34267 CM2/GM
WHB = .8359386
MUFO = 49.59643   MUH = 77.80621 CM2/GM

INTENSITIES, CORRECTED FOR MATRIX AND TRANSPARENCY

IPK- 1 = 7604.361
IPK- 2 = 72084.23
IPK- 3 = 479.0839

FINAL INTENSITIES (IPK) CORRECTED FOR OVERLAP

IPK- 1 = 7604.361
IPK- 2 = 72084.23
IPK- 3 = 479.0839

PROVISIONAL WEIGHT FRACTIONS AND VARIANCE ERRORS
HALITE
   W(I)- 1 = .5247543   +-   6.163265E-02
ANHYDRITE
   W(I)- 2 = .4680138   +-   6.094909E-02
MAGNESITE
   W(I)- 3 = 7.231909E-03   +-   1.52044E-03

MASS ABSORPTION COEFFICIENTS AND ERRORS

MUC = 75.83946 +-   6.792279   CM2/GM
MUBO = 83.34267 +-   2.158354   CM2/GM
S(MB) =   1.300237E-04   GM/CM2
S(GAMMA) = 6.391594E-03

11/27

EMES0844   RESPEC P3X10-5-3-TS203-19-1993   18:00:46   PAGE 3

FINAL WEIGHT FRACTIONS AND VARIANCE ERRORS

HALITE
 W(I)- 1 =   .5247   +-   .0616 ⎱
ANHYDRITE   ⎰ 99.99
 W(I)- 2 =   .468   +-   .0609 ⎱
MAGNESITE   ⎰
 W(I)- 3 =   .0072   +-   .0015 ⎰

CALCULATED SAMPLE DENSITY = 2.49 GM/CM3
SAMPLE CRYSTALLINE FRACTION = 1 +- 0

COMPOUND REDUCTION
            OXIDE   ELEMENT
SiO_2 =   .0025   (.0011)
Al_2O_3 =   .0005   (.0002)
K_2O =   .0011   (.0009)
CaO =   .1915   (.1369)
Fe_2O_3 =   .0005   (.0003)
MgO =   .0044   (.0026)
H_2O =   .013   (.0014)
CO_2 =   .0084   (.0023)
SO_3 =   .2724   (.1091)
Cl =   ----   (.3107)
SrO =   .0005   (.0004)

ADDITIONAL ELEMENTAL COMPONENTS

Comp-1   NONE   = (0)*
Comp-2   NONE   = (0)*
Comp-3   SODIUM   = (.1987)*

OXIDE TOTAL = .4947   ELEMENT TOTAL = .7652856
* Add these plus any C,F,Cl in ELEMENT TABLE to OXIDE TOTAL
   to obtain total weight fraction
RUN COMPLETE FOR SAMPLE EMES0844

EMES0845 RESPEC P3X10-6-SP2B   THIS IS A LEVEL - 1 ANALYSIS
IFB/IO = .37951 S(IFB/IO) = .002527 IF/IO = .770818
S(IF/IO) = .001983
SPEC. FILTER MASS, MF, = .005172
SPEC. SAMPLE MASS, MB, = .009531
MEAN PARTICLE RADIUS, RZ, = .0004
MEAN SAMPLE DENSITY, RHO-Z, = 2.55

No. X-RAY COMPONENTS, N, = 4   No. OF OPTIC COMPONENTS, M, = 0
No. OF AMORPHOUS COMPONENTS, AM, = 0
No. OVERLAP SETS, OL, = 2
NO AMORPHOUS COMPONENTS IN THIS SAMPLE
FILTER TYPE = 2

COMP- 1 CODE = 28 IPK- 1 = 5859   IBG- 1 = 980
COMP- 2 CODE = 24 IPK- 2 = 59722   IBG- 2 = 670
COMP- 3 CODE = 284 IPK- 3 = 739   IBG- 3 = 969
COMP- 4 CODE = 282 IPK- 4 = 7419   IBG- 4 = 1254

INTENSITY FOR PEAK OF RANK 2 IS TO BE REDUCED BY .06
OF INTENSITY OF 4 RANKED PEAK
INTENSITY FOR PEAK OF RANK 3 IS TO BE REDUCED BY .01
OF INTENSITY OF 4 RANKED PEAK

NONE   NONE   SODIUM
ARE THE ELEMENT NAMES FOR OX FILE CODES 30, 31, AND 32
FILE REVIEW COMPLETE FOR EMES0845

MUBO(U) = 74.34386 CM2/GM MUBO(C) = 55.27669 CM2/GM
MUBO = 74.34386 CM2/GM
WHB = .8928337
MUFO = 50.32928   MUH = 71.77031 CM2/GM

INTENSITIES, CORRECTED FOR MATRIX AND TRANSPARENCY

IPK- 1 = 6479.225
IPK- 2 = 70838.96
IPK- 3 = 689.1416
IPK- 4 = 8008.602

FINAL INTENSITIES (IPK) CORRECTED FOR OVERLAP

IPK- 1 = 6479.225
IPK- 2 = 70358.45
IPK- 3 = 609.0556
IPK- 4 = 8008.602

EMESO845   RESPEC P3X10-6-SP2B   PAGE 2
PROVISIONAL WEIGHT FRACTIONS AND VARIANCE ERRORS
HALITE
   W(I)- 1   =   .4359633   +-   5.941661E-02
ANHYDRITE
   W(I)- 2   =   .4454184   +-   5.043721E-02
MAGNESITE
   W(I)- 3   =   8.964619E-03   +-   1.603963E-03
POLYHALITE
   W(I)- 4   =   .1096537   +-   1.535986E-02

MASS ABSORPTION COEFFICIENTS AND ERRORS

MUC =   74.99898 +-   6.233814   CM2/GM
MUBO =   74.34386 +-   1.546049   CM2/GM
S(MB) =   1.733964E-04   GM/CM2
S(GAMMA) =   7.138277E-03

FINAL WEIGHT FRACTIONS AND VARIANCE ERRORS

HALITE
 W(I)- 1 = .4359   +-   .0594
ANHYDRITE
 W(I)- 2 = .4454   +-   .0504   } 99.98
MAGNESITE
 W(I)- 3 = .0089   +-   .0016
POLYHALITE
 W(I)- 4 = .1096   +-   .0153

CALCULATED SAMPLE DENSITY =   2.54   GM/CM3
SAMPLE CRYSTALLINE FRACTION =   1   +-   0

COMPOUND REDUCTION
              OXIDE   ELEMENT
SiO_2 = .0024   (.0011)
Al_2O_3 = .0004   (.0002)
K_2O = .018   (.015   )
CaO = .2024   (.1447)
Fe_2O_3 = .0004   (.0003)
MgO = .0124   (.0075)
H_2O = .0176   (.0019)
CO_2 = 8.599999E-03   (.0023)
SO_3 = .3173   (.1271)
Cl = ----   (.2581)
SrO = .0005   (.0004)

ADDITIONAL ELEMENTAL COMPONENTS

Comp-1   NONE   = (0)*
Comp-2   NONE   = (0)*
Comp-3   SODIUM   = (.165)*

OXIDE TOTAL = .58   ELEMENT TOTAL =   .7242136
* Add these plus any C,F,Cl in ELEMENT TABLE to OXIDE TOTAL
  to obtain total weight fraction
RUN COMPLETE FOR SAMPLE EMES0845

EMES0846   RESPEC P310X-6-SP2T   THIS IS A LEVEL - 1   ANALYSIS
IFB/IO = .465272   S(IFB/IO) = .00215   IF/IO = .771399
S(IF/IO) =   .001809
SPEC. FILTER MASS, MF, =   .005173
SPEC. SAMPLE MASS, MB, =   .007028
MEAN PARTICLE RADIUS, RZ, =   .0004
MEAN SAMPLE DENSITY, RHO-Z, =   2.55

No. X-RAY COMPONENTS, N, = 3   No. OF OPTIC COMPONENTS, M, = 0
No. OF AMORPHOUS COMPONENTS, AM, = 0
No. OVERLAP SETS, OL, = 0
NO AMORPHOUS COMPONENTS IN THIS SAMPLE
FILTER TYPE = 2

COMP- 1   CODE = 28   IPK- 1 = 5545   IBG- 1 = 1247
COMP- 2   CODE = 24   IPK- 2 = 70184   IBG- 2 = 1025
COMP- 3   CODE = 284 IPK- 3 = 778   IBG- 3 = 1187

NONE   NONE   SODIUM
ARE THE ELEMENT NAMES FOR OX FILE CODES 30, 31, AND 32
FILE REVIEW COMPLETE FOR EMES0846

MUBO(U) =   71.93848   CM2/GM MUBO(C) = 58.73722   CM2/GM
MUBO =   71.93848   CM2/GM
WHB =   .8600098
MUFO =   50.17389   MUH =   68.89166   CM2/GM

INTENSITIES, CORRECTED FOR MATRIX AND TRANSPARENCY

IPK- 1 =   6359.77
IPK- 2 =   86171.98
IPK- 3 =   757.7855

FINAL INTENSITIES (IPK) CORRECTED FOR OVERLAP

IPK- 1 =   6359.77
IPK- 2 =   86171.98
IPK- 3 =   757.7855

EMES0846   RESPEC P310X-6-SP2T   PAGE 2
PROVISIONAL WEIGHT FRACTIONS AND VARIANCE ERRORS
HALITE
   W(I)- 1 = .434615   +-   6.070437E-02
ANHYDRITE
   W(I)- 2 = .554057   +-   5.988921E-02
MAGNESITE
   W(I)- 3 = 1.132811E-02   +-   2.057948E-03

MASS ABSORPTION COEFFICIENTS AND ERRORS

MUC = 75.89401 +- 6.724433   CM2/GM
MUBO = 71.93848 +- 1.648695   CM2/GM
S(MB) = 1.440636E-04   GM/CM2
S(GAMMA) = 5.181955E-03

EMES0846   RESPEC P310X-6-SP2T 03-19-1993 18:01:32   PAGE 3

FINAL WEIGHT FRACTIONS AND VARIANCE ERRORS

HALITE
  W(I)- 1 =   .4346   +-   .0607   ⎫
ANHYDRITE   ⎬   99.99
  W(I)- 2 =   .554   +-   .0598   ⎪
MAGNESITE   ⎭
  W(I)- 3 =   .0113   +-   .002

CALCULATED SAMPLE DENSITY = 2.56   GM/CM3
SAMPLE CRYSTALLINE FRACTION = 1 +-   0

COMPOUND REDUCTION
            OXIDE   ELEMENT
SiO_2 =   .0029   (.0013)
Al_2O_3 =   .0006   (.0003)
K_2O =   .0009   (.0008)
CaO   =   .2261   (.1616)
Fe_2O_3 =   .0006   (.0004)
MgO   =   .0064   (.0038)
H_2O =   .0113   (.0012)
CO_2 =   .0099   (.0027)
SO_3 =   .3221   (.129)
Cl   =   ----   (.2574)
SrO   =   .0006   (.0005)

ADDITIONAL ELEMENTAL COMPONENTS

Comp-1   NONE   = (0)*
Comp-2   NONE   = (0)*
Comp-3   SODIUM   = (.1645)*

OXIDE TOTAL =   .5813   ELEMENT TOTAL =   .7241158
* Add these plus any C,F,Cl in ELEMENT TABLE to OXIDE TOTAL
   to obtain total weight fraction
RUN COMPLETE FOR SAMPLE EMES0846

EMES0847 RESPEC P3X11-5-2-SP1♭   THIS IS A LEVEL - 1 ANALYSIS
IFB/IO = .410545 S(IFB/IO) = .002242 IF/IO = .77084
S(IF/IO) = .006611
SPEC. FILTER MASS, MF, = .005142
SPEC. SAMPLE MASS, MB, = .008956
MEAN PARTICLE RADIUS, RZ, = .0004
MEAN SAMPLE DENSITY, RHO-Z, = 2.75

No. X-RAY COMPONENTS, N, = 4   No. OF OPTIC COMPONENTS, M, = 0
No. OF AMORPHOUS COMPONENTS, AM, = 0
No. OVERLAP SETS, OL, = 3
NO AMORPHOUS COMPONENTS IN THIS SAMPLE
FILTER TYPE = 2

COMP- 1 CODE = 282 IPK- 1 = 56034   IBG- 1 = 1830
COMP- 2 CODE = 24 IPK- 2 = 10606   IBG- 2 = 1048
COMP- 3 CODE = 27 IPK- 3 = 6714   IBG- 3 = 3121
COMP- 4 CODE = 284 IPK- 4 = 900   IBG- 4 = 1447

INTENSITY FOR PEAK OF RANK 4 IS TO BE REDUCED BY .01
OF INTENSITY OF 1 RANKED PEAK
INTENSITY FOR PEAK OF RANK 2 IS TO BE REDUCED BY .06
OF INTENSITY OF 1 RANKED PEAK
INTENSITY FOR PEAK OF RANK 3 IS TO BE REDUCED BY .03
OF INTENSITY OF 2 RANKED PEAK

NONE   NONE   SODIUM
ARE THE ELEMENT NAMES FOR OX FILE CODES 30, 31, AND 32
FILE REVIEW COMPLETE FOR EMES0847

MUBO(U) = 70.34338 CM2/GM MUBO(C) = 54.28053 CM2/GM
MUBO = 70.34338 CM2/GM
WHB = .8867326
MUFO = 50.61736   MUH = 68.10907 CM2/GM

INTENSITIES, CORRECTED FOR MATRIX AND TRANSPARENCY

IPK- 1 = 61183.26
IPK- 2 = 12716.85
IPK- 3 = 6523.361
IPK- 4 = 850.2898

FINAL INTENSITIES (IPK) CORRECTED FOR OVERLAP

IPK- 1 = 61183.26
IPK- 2 = 9045.854
IPK- 3 = 6251.986
IPK- 4 = 238.4572

EMES0847   RESPEC P3X11-5-2-SP1B PAGE 2
PROVISIONAL WEIGHT FRACTIONS AND VARIANCE ERRORS
POLYHALITE
  W(I)- 1 = .9009456   +-   1.215583E-02
ANHYDRITE
  W(I)- 2 = 6.158871E-02   +-   7.763989E-03
HALITE
  W(I)- 3 = 3.369105E-02   +-   7.57246E-03
MAGNESITE
  W(I)- 4 = 3.774721E-03   +-   6.337309E-04

MASS ABSORPTION COEFFICIENTS AND ERRORS

MUC = 69.1961 +- 6.41779   CM2/GM
MUBO = 70.34338 +- 1.732694   CM2/GM
S(MB) = 1.666558E-04   GM/CM2
S(GAMMA) = 1.016744E-02

EMES0847   RESPEC P3X11-5-2-SP103-19-1993 18:01:58   PAGE 3

FINAL WEIGHT FRACTIONS AND VARIANCE ERRORS

POLYHALITE
 W(I)- 1 = .9009   +- .0121   ⎤
ANHYDRITE   ⎥
 W(I)- 2 = .0615   +- .0077   ⎬ 99.97
HALITE   ⎥
 W(I)- 3 = .0336   +- .0075   ⎦
MAGNESITE
 W(I)- 4 = .0037   +- .0006

CALCULATED SAMPLE DENSITY = 2.76 GM/CM3
SAMPLE CRYSTALLINE FRACTION = 1 +- 0

COMPOUND REDUCTION
           OXIDE   ELEMENT
SiO2   = .0003   (.0001)
K2O   = .1408   (.1169)
CaO   = .1928   (.1377)
MgO   = .0621   (.0374)
H2O   = .0547   (.0061)
CO2   = .0022   (.0006)
SO3   = .514   (.2058)
Cl   = ----   (.0199)

ADDITIONAL ELEMENTAL COMPONENTS

Comp-1   NONE   = (0)*
Comp-2   NONE   = (0)*
Comp-3   SODIUM   = (.0127)*

OXIDE TOTAL = .9669   ELEMENT TOTAL = .5377816
* Add these plus any C,F,Cl in ELEMENT TABLE to OXIDE TOTAL
   to obtain total weight fraction
RUN COMPLETE FOR SAMPLE EMES0847

EMESO848 RESPEC P3X11-5-2-SP1T THIS IS A LEVEL - 1 ANALYSIS
IFB/IO = .388932 S(IFB/IO) = .002525 IF/IO = .771763
S(IF/IO) = .004237
SPEC. FILTER MASS, MF, = .005181
SPEC. SAMPLE MASS, MB, = .009851
MEAN PARTICLE RADIUS, RZ, = .0004
MEAN SAMPLE DENSITY, RHO-Z, = 2.7

No. X-RAY COMPONENTS, N, = 4   No. OF OPTIC COMPONENTS, M, = 0
No. OF AMORPHOUS COMPONENTS, AM, = 0
No. OVERLAP SETS, CL, = 2
NO AMORPHOUS COMPONENTS IN THIS SAMPLE
FILTER TYPE = 2

COMP- 1 CODE = 282 IPK- 1 = 41643   IBG- 1 = 1863
COMP- 2 CODE = 24 IPK- 2 = 24220   IBG- 2 = 731
COMP- 3 CODE = 28 IPK- 3 = 1215   IBG- 3 = 1238
COMP- 4 CODE = 284 IPK- 4 = 2189   IBG- 4 = 1910

INTENSITY FOR PEAK OF RANK 2 IS TO BE REDUCED BY .06
OF INTENSITY OF 1 RANKED PEAK
INTENSITY FOR PEAK OF RANK 4 IS TO BE REDUCED BY .01
OF INTENSITY OF 1 RANKED PEAK

NONE   NONE   SODIUM
ARE THE ELEMENT NAMES FOR OX FILE CODES 30, 31, AND 32
FILE REVIEW COMPLETE FOR EMESO848

MUBO(U) = 69.56381 CM2/GM MUBO(C) = 52.26043 CM2/GM
MUBO = 69.56381 CM2/GM
WHB = .8959527
MUFO = 50.00536   MUH = 67.5288 CM2/GM

INTENSITIES, CORRECTED FOR MATRIX AND TRANSPARENCY

IPK- 1 = 45062.32
IPK- 2 = 26794.08
IPK- 3 = 1346.838
IPK- 4 = 2047.132

FINAL INTENSITIES (IPK) CORRECTED FOR OVERLAP

IPK- 1 = 45062.32
IPK- 2 = 26090.34
IPK- 3 = 1346.838
IPK- 4 = 1596.508

EMES0848   RESPEC P3X11-5-2-SP1T PAGE 2
PROVISIONAL WEIGHT FRACTIONS AND VARIANCE ERRORS
POLYHALITE
   W(I)- 1   =   .6883885   +-   2.940391E-02
ANHYDRITE
   W(I)- 2   =   .184283   +-   1.944358E-02
HALITE
   W(I)- 3   =   .1011104   +-   2.242501E-02
MAGNESITE
   W(I)- 4   =   2.621802E-02   +-   3.845118E-03

MASS ABSORPTION COEFFICIENTS AND ERRORS

MUC =   69.64076 +-   5.717682   CM2/GM
MUBO =   69.56381 +-   1.519799   CM2/GM
S(MB) =   1.771482E-04   GM/CM2
S(GAMMA) =   8.502249E-03

EMES0848   RESPEC P3X11-5-2-SP103-19-1993   18:02:19   PAGE 3

FINAL WEIGHT FRACTIONS AND VARIANCE ERRORS

POLYHALITE
  W(I)- 1 = .6883   +-   .0294
ANHYDRITE
  W(I)- 2 = .1842   +-   .0194
HALITE
  W(I)- 3 = .1011   +-   .0224
MAGNESITE
  W(I)- 4 = .0262   +-   .0038

99.98 (handwritten)

CALCULATED SAMPLE DENSITY = 2.74   GM/CM3
SAMPLE CRYSTALLINE FRACTION = 1 +- 0

COMPOUND REDUCTION
                 OXIDE   ELEMENT
SiO2   =   .0009   (.0004)
Al2O3   =   .0002   (.0001)
K2O   =   .1078   (8.949999E-02)
CaO   =   .2031   (.1452)
Fe2O3   =   .0002   (.0001)
MgO   =   .0588   (.0355)
H2O   =   .0439   (.0049)
CO2   =   .0146   (.004)
SO3   =   .4724   (.1892)
Cl   =   ----   (.0598)
SrO   =   .0002   (.0001)

ADDITIONAL ELEMENTAL COMPONENTS

Comp-1   NONE   = (0)*
Comp-2   NONE   = (0)*
Comp-3   SODIUM   = (.0382)*

OXIDE TOTAL = .9020999   ELEMENT TOTAL = .5674795
* Add these plus any C,F,Cl in ELEMENT TABLE to OXIDE TOTAL
   to obtain total weight fraction
RUN COMPLETE FOR SAMPLE EMES0848

EMES0849   RESPEC P3X11-5-3-2-T   THIS IS A LEVEL - 1   ANALYSIS
IFB/IO = .292076   S(IFB/IO) = .001738   IF/IO = .769349
S(IF/IO) =   .002235
SPEC. FILTER MASS, MF, =   .005197
SPEC. SAMPLE MASS, MB, = .0129
MEAN PARTICLE RADIUS, RZ, =   .0004
MEAN SAMPLE DENSITY, RHO-Z, =   2.8

No. X-RAY COMPONENTS, N, = 4   No. OF OPTIC COMPONENTS, M, = 0
No. OF AMORPHOUS COMPONENTS, AM, = 0
No. OVERLAP SETS, OL, = 2
NO AMORPHOUS COMPONENTS IN THIS SAMPLE
FILTER TYPE = 2

COMP- 1   CODE = 282 IPK- 1 = 15563   IBG- 1 = 1171
COMP- 2   CODE = 24 IPK- 2 = 70226   IBG- 2 = 823
COMP- 3   CODE = 28 IPK- 3 = 1243   IBG- 3 = 1034
COMP- 4   CODE = 284 IPK- 4 = 1662   IBG- 4 = 1231

INTENSITY FOR PEAK OF RANK 2 IS TO BE REDUCED BY .06
OF INTENSITY OF 1 RANKED PEAK
INTENSITY FOR PEAK OF RANK 4 IS TO BE REDUCED BY .01
OF INTENSITY OF 1 RANKED PEAK

NONE   NONE   SODIUM
ARE THE ELEMENT NAMES FOR OX FILE CODES 30, 31, AND 32
FILE REVIEW COMPLETE FOR EMES0849

MUBO(U) = 75.0799 CM2/GM MUBO(C) = 49.89115 CM2/GM
MUBO = 75.0799 CM2/GM
WHB = .9185418
MUFO = 50.45423   MUH = 73.07394 CM2/GM

INTENSITIES, CORRECTED FOR MATRIX AND TRANSPARENCY

IPK- 1 =   16437.12
IPK- 2 =   81558.69
IPK- 3 =   1345.202
IPK- 4 =   1513.302

FINAL INTENSITIES (IPK) CORRECTED FOR OVERLAP

IPK- 1 =   16437.12
IPK- 2 =   80572.46
IPK- 3 =   1345.202
IPK- 4 =   1348.931

EMES0849   RESPEC P3X11-5-3-2-T PAGE 2
PROVISIONAL WEIGHT FRACTIONS AND VARIANCE ERRORS
POLYHALITE
   W(I)- 1   =   .2661801   +-   2.547559E-02
ANHYDRITE
   W(I)- 2   =   .6032845   +-   .0314958
HALITE
   W(I)- 3   =   .1070528   +-   2.328252E-02
MAGNESITE
   W(I)- 4   =   2.348271E-02   +-   3.392518E-03

MASS ABSORPTION COEFFICIENTS AND ERRORS

MUC =   73.75211   +-   4.297812   CM2/GM
MUBO =   75.0799   +-   1.341273   CM2/GM
S(MB) =   2.129089E-04   GM/CM2
S(GAMMA) =   6.621772E-03

EMES0849   RESPEC P3X11-5-3-2-T03-19-1993   18:02:47   PAGE 3

FINAL WEIGHT FRACTIONS AND VARIANCE ERRORS

POLYHALITE
  W(I)- 1 =   .2661   +-   .0254   ⎫
ANHYDRITE   ⎪
  W(I)- 2 =   .6032   +-   .0314   ⎬ 99.97
HALITE   ⎪
  W(I)- 3 =   .107   +-   .0232   ⎪
MAGNESITE   ⎭
  W(I)- 4 =   .0234   +-   .0033

CALCULATED SAMPLE DENSITY = 2.82 GM/CM3
SAMPLE CRYSTALLINE FRACTION = 1 +-   0

COMPOUND REDUCTION
              OXIDE   ELEMENT
SiO_2 =   .0032   (.0015)
Al_2O_3 =   .0006   (.0003)
K_2O =   .0418   (.0347)
CaO =   .2945   (.2104)
Fe_2O_3 =   .0006   (.0004)
MgO =   .0298   (.018)
H_2O =   .0201   (.0022)
CO_2 =   .0136   (.0037)
SO_3 =   .4913   (.1967)
Cl =   ----   (.0633)
SrO =   .0007   (.0006)

ADDITIONAL ELEMENTAL COMPONENTS

Comp-1   NONE   = (0)*
Comp-2   NONE   = (0)*
Comp-3   SODIUM   = (.0405)*

OXIDE TOTAL = .8961   ELEMENT TOTAL = .5729603
* Add these plus any C,F,Cl in ELEMENT TABLE to OXIDE TOTAL
   to obtain total weight fraction
RUN COMPLETE FOR SAMPLE EMES0849

EMES0850   RESPEC P3X11-6-TS3-4   THIS IS A LEVEL - 1   ANALYSIS
IFB/IO = .331338   S(IFB/IO) = .002254   IF/IO = .768025
S(IF/IO) =   .002917
SPEC. FILTER MASS, MF, =   .005245
SPEC. SAMPLE MASS, MB, =   .010438
MEAN PARTICLE RADIUS, RZ, =   .0004
MEAN SAMPLE DENSITY, RHO-Z, = 2.7

No. X-RAY COMPONENTS, N, = 2   No. OF OPTIC COMPONENTS, M, = 0
No. OF AMORPHOUS COMPONENTS, AM, = 0
No. OVERLAP SETS, OL, = 0
NO AMORPHOUS COMPONENTS IN THIS SAMPLE
FILTER TYPE = 2

COMP- 1 CODE = 28 IPK- 1 = 3492   IBG- 1 = 832
COMP- 2 CODE = 24 IPK- 2 = 88107   IBG- 2 = 1066

NONE   NONE   SODIUM
ARE THE ELEMENT NAMES FOR OX FILE CODES 30, 31, AND 32
FILE REVIEW COMPLETE FOR EMES0850

MUBO(U) = 80.54065 CM2/GM MUBO(C) = 56.71294   CM2/GM
MUBO = 80.54065   CM2/GM
WHB = .901226
MUFO = 50.32089   MUH = 77.55573   CM2/GM

INTENSITIES, CORRECTED FOR MATRIX AND TRANSPARENCY

IPK- 1 = 3812.065
IPK- 2 = 103203.4

FINAL INTENSITIES (IPK) CORRECTED FOR OVERLAP

IPK- 1 = 3812.065
IPK- 2 = 103203.4

EMES0850   RESPEC P3X11-6-TS3-4 PAGE 2
PROVISIONAL WEIGHT FRACTIONS AND VARIANCE ERRORS
HALITE
   W(I)- 1 = .2819145   +- 5.021604E-02
ANHYDRITE
   W(I)- 2 = .7180855   +- 5.021604E-02

MASS ABSORPTION COEFFICIENTS AND ERRORS

MUC = 77.06967 +- 5.799504   CM2/GM
MUBO = 80.54065 +- 1.604231   CM2/GM
S(MB) = 1.840312E-04   GM/CM2
S(GAMMA) = 7.791163E-03

EMES0850   RESPEC P3X11-6-TS3-403-19-1993   18:03:44   PAGE 3

FINAL WEIGHT FRACTIONS AND VARIANCE ERRORS

HALITE
  W(I)- 1 = .2819   +- .0502   } 99.99
ANHYDRITE
  W(I)- 2 = .718   +- .0502   )

CALCULATED SAMPLE DENSITY = 2.7 GM/CM3
SAMPLE CRYSTALLINE FRACTION = 1 +- 0

COMPOUND REDUCTION
            OXIDE   ELEMENT
SiO2   = .0038   (.0018)
Al2O3   = .0007   (.0004)
K2O   = .0006   (.0005)
CaO   = .2921   (.2087)
Fe2O3   = .0007   (.0005)
MgO   = .0011   (.0006)
H2O   = 8.499999E-03   (.0009)
CO2   = .0029   (.0008)
SO3   = .417   (.167)
Cl   = ----   (.1669)
SrO   = .0008   (.0007)

ADDITIONAL ELEMENTAL COMPONENTS

Comp-1   NONE   = (0)*
Comp-2   NONE   = (0)*
Comp-3   SODIUM   = (.1067)*

OXIDE TOTAL = .7282   ELEMENT TOTAL = .6561275
* Add these plus any C,F,Cl in ELEMENT TABLE to OXIDE TOTAL
  to obtain total weight fraction
RUN COMPLETE FOR SAMPLE EMES0850

APPENDIX B.C

CORE LABORATORIES' EFFECTIVE POROSITY MEASUREMENTS: PROCEDURE AND RESULTS

B.C-1. EFFECTIVE POROSITY MEASUREMENT PROCEDURE

SAMPLE PREPARATION

1. **PLUG DRYING:** Samples are dried in a convection oven at 240 degrees F. for twelve hours.

PETROPHYSICAL MEASUREMENTS

2. **GRAIN VOLUME:** Direct grain volume measurements are made using a small volume porosimeter. This instrument utilizes the principle of gas expansion as described by Boyle's law. Helium is used as the test gas. The instrument is calibrated daily and test standards are run.

3. **GRAIN DENSITY:** Calculated grain densities are obtained utilizing direct grain volume measurement and clean, dry sample weight. Grain densities are checked against lithology standards.

4. **PLUG DIMENSIONS:** Sample length and diameter are measured using metric calipers.

5. **CMS-300 OPERATIONS:** Plug Samples

> A. **PERMEABILITY "k":** Permeability is measured by flowing helium from a reference cell at the selected pressure through the core. The size of the reference cell used is optimized during a pre-test flow through. The chambers available are approximately 2,9,56, and 315 cc's. The actual size of each cell is calculated during calibration procedures. The cell combination used varies with each sample. The downstream end of the core is maintained at atmospheric pressure. The upstream pressure decline is monitored in real time, and observed by digital readout and visually displayed in either graphical or tabular form. The difference between the confining stress and the mean pore pressure during flow is the net confining stress. The stress to be used for this project will be supplied by the client.
>
> a).k-air: permeability to air at client specified overburden calculated from time pressure data.
>
> b).k-Klinkenberg: unsteady state equations used with time/pressure data to calculate the Klinkenberg slip corrected permeability at client specified overburden.

B. POROSITY: Pore volume is determined by
expansion of helium into the core sample
from a known volume source at approximately
240 psig. At pressure equilibrium, Boyle's
Law is used to compute pore volume. Porosity
is then calculated by using the pore volume
from the CMS-300 and the grain volume from
the Small Volume Porosimeter.

6. POROSITY: The bulk volume of each sample not run in the CMS-
300 will be determined using the DEB unit. This device uses
Archimedes' Principle of buoyancy to determine the bulk volume of
small samples. A pan of mercury is placed on a calibrated digital
scale with the prongs of the apparatus submerged. The scale is
zeroed. The sample is then submerged in the mercury to the same
reference point. The scale reading is divided by the density of
mercury (13.53 gm/cc approx., varies with temperature) to yield
the bulk volume. Porosities are calculated using the bulk volume
from the DEB and the grain volume from the small volume
porosimeter.

Special Instructions for Porosity
Measurements of Anhydrite

(1) Upon receipt, determine the masses of the 6 anhydrite specimens and 3 metric weights using the scale normally used for the porosity measurements. Record these masses on Table 1 under the column heading **As Received** and inform Tom Pfeifle, RE/SPEC, of the results.

(2) Perform the porosity measurements using the procedure provided.

NOTES: If the measurements of the masses of the specimens performed by Core Laboratories are significantly different from those made by RE/SPEC, the specimens may have to be dried at prescribed temperature and humidity conditions. If no differences in the measurements exist, Step 1 - Plug Drying, can be skipped. Differences of 0.01 grams (after accounting for differences in scale output using the metric weights) are considered significant.

Porosity measurements will be made at ambient pressure only. Overburden pressures should not be simulated.

(3) Following the porosity measurements, each of the six anhydrite specimens and three metric weights should be weighed. The measurements should be recorded in Table 1 under the column heading **As Sent**.

(4) Repackage the specimens and metric weights using the sealing procedure followed by RE/SPEC. Return the specimens and metric weights to RE/SPEC along with the results, Table 1, and the core receival records.

Table 1. Masses of Anhydrite Specimens and Metric Weights

Specimen I.D.	RE/SPEC Determined Mass		Core Labs Determined Mass	
	As Sent (g)	As Received (g)	As Received (g)	As Sent (g)
SP1-T				
SP1-B				
SP2-T				
SP2-B				
SP3-T				
SP3-B				
Metric Weight 10 g				
Metric Weight 20 g				
Metric Weight 50 g				
Date				

B.C-2. EFFECTIVE POROSITY MEASUREMENT RESULTS

Western Atlas International
A Litton/Dresser Company

RE/SPEC, INC.
ANHYDRITE SAMPLES
CL FILE NO.:57151-17577
FINAL REPORT

B-158

CORE LABORATORIES

April 27, 1993

RE/SPEC, Inc.
3824 Jet Drive
Rapid City, South Dakota 57701
Attn: Mr. Tom W. Pfeifle

> Core Analysis Report
> Anhydrite Samples
> CL File No. 57151-17577

Dear Mr. Pfeifle:

Six anhydrite samples were received from RE/SPEC, Inc. on April 21, 1993. The samples were analyzed by Core Laboratories personnel as directed by RE/SPEC representatives.
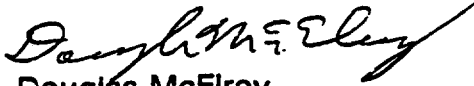
The following documentation includes: petrophysical measurements; a list of Houston laboratory personnel involved in this project; and the resultant data reported in tabular format. The type of equipment used in each procedure is also specified.
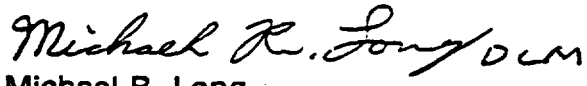
Upon completion of analysis, the samples were returned to RE/SPEC via UPS.

We appreciate your business. If we can be of further service, please call.

Very truly yours,

CORE LABORATORIES

Douglas McElroy
Laboratory Coordinator

Michael R. Long
Senior Project Analyst

TABLE OF CONTENTS

SAMPLE PREPARATION

Upon receipt, the samples were removed from the shipping pouches and inventoried. Each sample was then weighed and the weights recorded to .0001 gram. Three metric weights were received with the samples. These were also weighed to .0001 gram. All weights were recorded on data sheet provided by client.

PETROPHYSICAL MEASUREMENTS

1. GRAIN VOLUME: Direct grain volume measurements were made using a small volume porosimeter. This instrument utilizes the principle of gas expansion as described by Boyle's law. Helium was used as the test gas. The instrument was calibrated daily and test standards were run.

2. GRAIN DENSITY: Calculated grain densities were obtained utilizing direct grain volume measurement and clean, dry sample weight. Grain densities were checked against lithology standards.

3. POROSITY: The bulk volume of each sample was determined using the DEB unit. This device uses Archimedes' principle of buoyancy to determine the bulk volume of small samples. A pan of mercury is placed on a calibrated digital scale with the prongs of the apparatus submerged. The scale is zeroed. The sample is then submerged in the mercury to the same reference point. The scale reading is divided by the density of mercury (13.53 gm/cc approx., varies with temperature) to yield the bulk volume. Porosities were calculated using the bulk volume from the DEB and the grain volume from the small volume porosimeter. T

4. BULK DENSITY: Calculated bulk densities were obtained using the clean, dry sample weight and the Archimedes' bulk volume.

5. POST-ANALYSIS WEIGHTS: Upon completion of all other measurements, samples and metric weights were re-weighed and the results recorded on client data sheet.

SAMPLE DISPOSITION

Upon completion of petrophysical measurements, all samples and metric weights were re-packaged and returned to client.

CORE LABORATORIES

Company : RE/SPEC INC.
Well : Anhydrite Samples
Location :
Co,State :

Field :
Formation :
Coring Fluid :
Elevation :

CORE ANALYSIS RESULTS

SAMPLE NUMBER	POROSITY (HELIUM) %	GRAIN DENSITY gm/cc	BULK DENSITY gm/cc	DESCRIPTION
1	1.7	2.73	2.68	SP1-T
2	2.1	2.73	2.67	SP1-B
3	1.3	2.69	2.65	SP2-T
4	1.1	2.57	2.54	SP2-B
5	1.0	2.53	2.51	SP3-T
6	1.8	2.70	2.66	SP3-B

APPENDIX A: LIST OF PROJECT ANALYSTS and PERSONNEL

PETROLEUM SERVICES MANAGER   FEDERICA M. MANNI
LABORATORY COORDINATOR   DOUG McELROY
SENIOR PROJECT ANALYST   MICHAEL R. LONG
TECHNICAL SALES REPRESENTATIVE   TOM SWISHER

APPENDIX B: REPORT DISTRIBUTION

RE/SPEC, INC.
ANHYDRITE SAMPLES
CL FILE NO.:57151-17577

3 cc   Mr. Tom F. Pfeifle
RE/SPEC, Inc.
3824 Jet Drive
Rapid City, South Dakota 57701

Table 1. Masses of Anhydrite Specimens and Metric Weights

Specimen I.D.	RE/SPEC Determined Mass		Core Labs Determined Mass	
	As Sent (g)	As Received (g)	As Received (g)	As Sent (g)
SP1-T	33.94	33.94	33.9326	33.9433
SP1-B	37.45	37.45	37.4455	37.4558
SP2-T	38.85	38.84	38.8374	38.8421
SP2-B	33.67	33.66	33.6636	33.6670
SP3-T	37.51	37.49	37.4992	37.4970
SP3-B	47.68	47.67	47.6703	47.6676
Metric Weight 10 g	10.00	10.00	7.9999	10.0000
Metric Weight 20 g	20.00	20.00	19.9998	20.0002
Metric Weight 50 g	50.00	50.00	49.9991	50.0000
Date	4-15-93	5-7-93	4-22-73	4-25-93

APPENDIX B.D
DERIVATION OF EQUATION FOR POROSITY CALCULATION BASED ON FLUID DISPLACEMENT MEASUREMENTS

Attachment 1

Derivation of Equation for Porosity Using
Fluid Displacement Measurements

The equation to be derived is porosity given in terms of the quantities measured using the fluid displacement technique:

$$\text{Porosity} = 1 - \left[\frac{\left(\dfrac{Ms_s}{0.25 \cdot L \cdot \pi \cdot D^2} \right)}{\left(\dfrac{(Mfk_1 - Mf) \cdot (Mfs_g - Mf)}{(Vf \cdot (Mfs_g - Mf + Mfk_1 - Mfs_g k_2))} \right)} \right] \quad (1)$$

where the measured quantities are

Ms_s	=	Mass of solid specimen before grinding
L	=	Specimen length before grinding
D	=	Specimen diameter before grinding
Vf	=	Volume of flask to calibration mark
Mf	=	Mass of flask
Mfs_g	=	Mass of flask containing ground specimen
Mfk_1	=	Mass of flask filled with deaerated kerosene to calibration mark
$Mfs_g k_2$	=	Mass of flask containing ground specimen and filled with deaerated kerosene to calibration mark

Let

Mk_1	=	Mass of kerosene required to fill empty flask
Mk_2	=	Mass of kerosene required to fill the flask containing the ground specimen
Ms_g	=	Mass of ground specimen
ρ_b	=	Bulk density of solid specimen
ρ_g	=	Grain density
ρ_k	=	Kerosene density
Vg	=	Grain volume of solid specimen
Vb	=	Bulk volume of solid specimen
Vs_g	=	Volume of ground specimen

It follows from these defined quantities that

$$Vs_g = \frac{Mk_1 - Mk_2}{\rho_k} \tag{2}$$

$$Ms_g = Mfs_g - Mf \tag{3}$$

$$\rho_k = \frac{Mfk_1 - Mf}{Vf} \tag{4}$$

$$\rho_b = \frac{Ms_s}{0.25 \cdot \pi \cdot L \cdot D^2} \tag{5}$$

$$\rho_g = \frac{Ms_s}{Vg} = \frac{Ms_g}{Vs_g} \tag{6}$$

The derivation begins with

$$Porosity = \frac{Bulk\ Specimen\ Volume\ -\ Grain\ Volume}{Bulk\ Specimen\ Volume} \tag{7}$$

or

$$P = \frac{Vb - Vg}{Vb} \tag{8}$$

Multiply and divide by Ms_s to obtain

$$P = 1 - \frac{Ms_s \cdot Vg}{Ms_s \cdot Vb} = 1 - \frac{\rho_b}{\rho_g} \tag{9}$$

Substitute Equation 6 into Equation 9 to obtain

$$P = 1 - \frac{\rho_b \cdot Vs_g}{Ms_g} \tag{10}$$

Expressions for Ms_g, and ρ_b are given in Equations 3 and 5. An expression is needed for Vs_g in terms of the quantities directly measured using the fluid displacement technique. Begin with Equation 2:

$$Vs_g = \frac{Mk_1 - Mk_2}{\rho_k} $$

Add and subtract Mf from the right hand side numerator to obtain

$$Vs_g = \frac{Mfk_1 - Mfk_2}{\rho_k} \tag{11}$$

Add and subtract Ms_g from the right hand side numerator to obtain

$$Vs_g = \frac{Mfk_1 - Mfs_g k_2 + Ms_g}{\rho_k} \tag{12}$$

Substituting expressions for Ms_g, ρ_k, ρ_b, and Vs_g (Equations 3 through 5 and Equation 12) into Equation 10 completes the derivation of Equation 1.

APPENDIX B.E
BRINE MANUFACTURE

B.E-1. PROCEDURE SUPPLIED BY SANDIA NATIONAL LABORATORIES

Date: 07 June 1993

To: Susan Howarth, 6119

            Karen Robinson

From: Karen Robinson, 6119

Subject: Preparation of Standard Brine SB-139-95B

SUMMARY
This memo describes the preparation of the standard brine SB-139-95B. I am
giving quite a bit of detail in case you want to use this to generate a brine-
preparation procedure for future use. In brief, I prepared 1 liter of brine,
adjusted the pH to ~6.1 with HCl, and split the brine into two 500-mL lots.
You sent one bottle to Chem Nuclear Geotech for analysis; the other bottle is
being stored in 823/2079.

RECIPE
Craig Novak supplied a recipe for an average QPB brine, a brine expected to be
saturated with respect to the minerals in Marker Bed 139. The brine described
here is slightly undersaturated and contains 95% of the salts recommended by
Craig.

Table 1a shows the "95%" recipe and the amounts of salts actually weighed out.
Table 1b shows the calculated composition based on the "95%" recipe and the
calculated composition based on the amounts of salts actually weighed out.

PROCEDURE
Detailed notes about the preparation are in my lab notebook (Lab Notebook No.
WIPP 04, pp.21-23); those notes are summarized in Attachment 1.

Reagents
Reagent grade salts were used. All salts were used "as is" from the bottle
(that is, they were not dried in the lab oven).

Deionized water from the Barnstead Nanopure A deionizer was used.

Standard pH buffer solutions were prepared from pHydrion buffer capsules.

Trace-metal grade hydrochloric acid was used to adjust the pH.

Equipment
Reagents were weighed out using the Mettler AE163 balance. The balance was
calibrated before use with the internal calibration weight. The calibration
was checked with selected standard weights. Details can be found in the
balance log book (Lab Notebook No. WIPP 02, p. 25).

Glassware included a 1000-mL class-A volumetric flask and a powder funnel.

Plasticware included weighing boats, 500-mL polyethylene bottles, *various* plastic beakers, and a teflon stirring rod.

Other equipment included a Thermolyne Nuova 7 stir plate; a magnetic stir bar and stir-bar retriever; and a Sentron model 2001 pH system (meter and probe).

Preparation
In brief, the required amounts of salts were dissolved in deionized water in the volumetric flask; dissolution was speeded by using the magnetic stirrer. The volume was adjusted to 1000 mL in the volumetric flask. The pH was then adjusted by adding ~4 mL of HCl. The solution was then transferred to two 500-mL polyethylene bottles. The step-by-step details are in Attachment 1.

Note that although the final volume of the solution was ~1004 mL (after the pH was adjusted), I used a volume of 1000 mL to calculated the concentrations of the solutes.

WORK REMAINING

As we discussed, I will also prepare one liter of the "saturated" recipe. This work has been delayed somewhat because there wasn't enough NaCl in the lab. More was ordered and has recently arrived. I expect to have the brine prepared and the memo documenting its preparation written by Friday, June 18.

\karen\misc\sb-139-b.1

copy to: 6119 C. F. Novak
           6119 K. L. Robinson

TABLE 1a: Recipes -- Amounts of Salts Needed and Weighed Out

Salt	Amount needed for 1 liter of "95%" soln (grams)	Amount weighed out for SB-139-95B (grams)
NaHCO3	0.00127	*
CaCl2·2H2O	1.2156	1.2144
MgSO4	18.9250	18.9238
MgCl2·6H2O	124.076	124.0775
KCl	30.7753	30.7727
NaCl	193.8998	193.8973
Na2B4O7	6.6523	6.6519
NaBr	1.7819	1.7837

* Don't have appropriate equipment to accurately measure 0.00127 g of a salt.

Table 1b: Brine Compositions -- Target and Calculated

Species	Calc'd Comp. "95%" Recipe (mg/L)	Calc'd Comp SB-139-95B* (mg/L)
HCO3	0.922	**
Cl	176106	176100
SO4	15103	15100
Na	78198	78200
K	16141	16140
Ca	331	330
Mg	18657	18660
B	1430	1430
Br	1384	1390

 * Concentrations rounded to nearest 10 mg/L.
** Probably equilibrated with atmosphere.

ATTACHMENT 1: Preparation of SB-139-95B

04/30/93: Put ~200 mL deionized water and small magnetic stir bar into 1000-mL
         volumetric flask.
         Weighed Na2B4O7; transferred quantitatively to vol. flask.
         Began stirring. Stirred for ~3 hrs. Left standing over weekend.
         Weighed other salts (CaCl2·2H2O, MgCl2·6H2O, KCl, NaCl, MgSO4, NaBr)
         into plastic beakers. Covered with parafilm.
05/03/93: Resumed stirring.
         Quantitatively transferred chloride salts (CaCl2·2H2O, MgCl2·2H2O,
         KCl, NaCl) to vol. flask.
         Added deionized water to fill flask ~two-thirds.
         Stirred ~2 hrs.
         Quantitatively transferred remaining salts (MgSO4, NaBr) to
         vol. flask.
         Continued stirring. At end of work day turned off stirrer and left
         to stand overnight.
05/04/93: Removed stir bar with magnetic stir-bar retriever. Rinsed with
         deionized water, adding all rinse water to flask.
         Diluted with deionized water to volume and inverted to mix
         thoroughly.
         Calibrated pH system with standard buffers 7 and 4. Checked
         calibration with standard buffer 6.4.
         Measured initial pH of solution as 7.0.
         Alternately added aliquots of HCl, mixed the solution by inverting
         the vol. flask, and checked the pH of the solution. After ~4 mL of
         HCl were added (in 6 unequal increments) the pH of the solution was
         6.14.
         The final volume of the solution was ~1004 mL. Note that
         concentrations of solutes were calculated using a volume of 1000 mL.
         The solution was transferred to two 500-mL polyethylene bottles.
         One was given to S. Howarth for shipping to ChemNuclear Geotech for
         chemical analysis. The other is currently stored in 823/2079.

B.E-2. LABORATORY NOTES SUPPLIED BY TWIN CITY TESTING

Huntingdon
Consulting Engineers ● *Environmental Scientists*

August 3, 1993

RE/SPEC
Attn: Nancy S. Bradsky, Ph.D.
3824 Jet Drive
Rapid City, SD 57709

Preparation of Brine Solution

7/30/93: Weigh all salts into glass beakers and covered with plastic film. Set up large stirrer and 5 gallon vessel added 2000 ml of deionized water to vessel and started stirrer. Salts were quantitatively added in the following order: $MgCl_2 \cdot 6H_2O$, NaCl, KCl, $CaCl_2 \cdot 2H_2O$, $NaHCO_3$, $MgSO_4 \cdot 7H_2O$, Na_2B_4O , NaBr. Added deionized water to approximately 16 liters total volume. Covered and allowed to stir over the weekend.

8/2/93: Stopped stirrer and allowed to stand for three hours. Salts were not fully dissolved. Resumed stirring and added 2000 ml deionized water. Allowed to stir overnight.

8/3/93: Stopped stirrer. Diluted to final volume of 19 liters (5 gallons) by transferring solution to 19-1000 ml vol. flasks. Deionized water was added to make up deficient volume. Vol. flasks were then emptied back into 5 gallon vessel for mixing and pH adjustment. Calibrated pH meter with standard buffers 7 and 4. Initial pH of the solution measured 7.50. Added aliquots of conc. HCl to a pH of 5.96, added aliquots of 10N NaOH to a final pH of 6.16. Volume of conc. HCl added was 54 ml. Volume of 10N NaOH added was 7 ml. Final volume of solution was 19061 ml. Solution was transferred to five 1 gallon polyethylene bottles.

Amounts of Salts Needed and Weighed

Salt	Amount Needed for 19 liters of Brine, grams	Amount weighed, grams
$NaHCO_3$	0.0241	0.0242
$CaCl_2 \cdot 7H_2O$	23.0964	23.0965
*$MgSO_4 \cdot 7H_2O$	735.623	735.620
$MgCl_2 \cdot 6H_2O$	2357.444	2357.4450
KCl	584.731	584.7308
NaCl	3684.0962	3684.0962
Na_2B_4O	126.3937	126.3939
NaBr	33.8561	33.8563

* Recipe for brine solution called for $MgSO_4$ - $MgSO_4 \cdot 7H_2O$ was used and the weight adjusted to allow for H_2O present.

B-182

September 3, 1993

RE/SPEC
Attn: Nancy S. Brodsky, Ph.D.
3824 Jet Drive
Rapid City, SD 57709

Preparation of Brine Solution

8/30/93: Weigh all salts into glass beakers and covered with plastic film. Set up large stirrer and 5 gallon vessel added 2000 ml of deionized water to vessel and started stirrer. Salts were quantitatively added in the following order: $MgCl_2 \cdot 6H_2O$, NaCl, KCl, $CaCl_2 \cdot 2H_2O$, $NaHCO_3$, $MgSO_4 \cdot 7H_2O$, Na_2B_4O , NaBr. Added deionized water to approximately 16 liters total volume. Covered and allowed to stir.

9/3/93: Stopped stirrer and allowed to stand for three hours. All salts were dissolved. Diluted solution to final volume of 19 liters (5 gallons) by transferring to 19 -1000 ml vol. flasks. Deionized water was added to make up deficient volume. Vol. flasks were then emptied back into 5 gallon vessel for mixing and pH adjustment. Calibrated pH meter with standard buffers 7 and 4. Initial pH of the solution measured 7.50. Added aliquots of conc. HCl to a pH of 6.18. Volume of conc. HCl added was 48.5 ml. Solution was transferred to five (5) one (1) gallon polyethylene bottles.

Amounts of Salts Needed and Weighed

Salt	Amount Needed for 19 liters of Brine, grams	Amount weighed, grams
$NaHCO_3$	0.0241	0.0242
$CaCl_2 \cdot 7H_2O$	23.0964	23.0963
*$MgSO_4 \cdot 7H_2O$	735.623	735.623
$MgCl_2 \cdot 6H_2O$	2357.444	2357.4440
KCl	584.731	584.7311
NaCl	3684.0962	3684.0962
Na_2B_4O	126.3937	126.3939
NaBr	33.8561	33.8561

* Recipe for brine solution called for $MgSO_4$ - $MgSO_4 \cdot 7H_2O$ was used and the weight adjusted to allow for H_2O present.

APPENDIX B.F
ERROR ANALYSES

B.F-1. ERROR ANALYSIS FOR TOTAL POROSITY MEASUREMENTS

Attachment 2

CALCULATION OF ERRORS FOR TOTAL POROSITY MEASUREMENTS.

Application: Contract 248b calculation of total porosity using fluid displacement
technique. Used ANSI/ASME PTC 19.1-1985. "Part I Measurement
Uncertainty ; Instruments and Apparatus".

Mathcad file: Syntax:

:= User is defining a value or function

= Mathcad is returning a calculated value

units such as "length" and "mass" are returned by mathcad.

SPECIMEN P3X11-5-2-SP1-T

Input Values:

$Mss := .03394 \cdot kg$ Bulk mass of specimen, before grinding

$L := 0.4192 \cdot .0254 \cdot m$ Specimen length, before grinding

$D := 1.5297 \cdot .0254 \cdot m$ Specimen diameter, before grinding

$Mfk := .12297 \cdot kg$ Mass of flask with kerosene to cal. mark

$Mf := 0.04301 \cdot kg$ Mass of flask alone

$Vf := .0001 \cdot m^3$ Volume of flask to cal. mark

$Mgsf := .06998 \cdot kg$ Mass of ground specimen in flask

$Mfsk := .14214 \cdot kg$ Mass of flask with ground specimen and kerosene to calibration mark

$$Porosity := 1 - \frac{\dfrac{Mss}{0.25 \cdot L \cdot \pi \cdot D^2}}{\left[\dfrac{(Mfk - Mf) \cdot (Mgsf - Mf)}{Vf \cdot (Mgsf - Mf + Mfk - Mfsk)} \right]} \qquad Porosity = 0.02764$$

$vol := 0.25 \cdot \pi \cdot L \cdot D^2$ $vol = 1.26248 \cdot 10^{-5} \cdot length^3$

$blkden := \dfrac{Mss}{vol}$ $blkden = 2688.35737 \cdot mass \cdot length^{-3}$

Calculate Sensitivity Factors, Sx

Define sensitivity factors for each input parameter:

$$SMss := \frac{d}{dMss}\left[\frac{\dfrac{-Mss}{0.25\cdot\pi\cdot L\cdot D^2}}{\dfrac{(Mfk-Mf)\cdot(Mgsf-Mf)}{Vf\cdot(Mgsf-Mf+Mfk-Mfsk)}}+1\right]$$

$$SL := \frac{d}{dL}\left[\frac{\dfrac{-Mss}{0.25\cdot\pi\cdot L\cdot D^2}}{\dfrac{(Mfk-Mf)\cdot(Mgsf-Mf)}{Vf\cdot(Mgsf-Mf+Mfk-Mfsk)}}+1\right]$$

$$SD := \frac{d}{dD}\left[\frac{\dfrac{-Mss}{0.25\cdot\pi\cdot L\cdot D^2}}{\dfrac{(Mfk-Mf)\cdot(Mgsf-Mf)}{Vf\cdot(Mgsf-Mf+Mfk-Mfsk)}}+1\right]$$

$$SMfk := \frac{d}{dMfk}\left[\left[\frac{\dfrac{-Mss}{0.25\cdot\pi\cdot L\cdot D^2}}{\dfrac{(Mfk-Mf)\cdot(Mgsf-Mf)}{Vf\cdot(Mgsf-Mf+Mfk-Mfsk)}}\right]+1\right]$$

$$SMf := \frac{d}{dMf}\left[\left[\frac{\dfrac{-Mss}{0.25\cdot\pi\cdot L\cdot D^2}}{\dfrac{(Mfk-Mf)\cdot(Mgsf-Mf)}{Vf\cdot(Mgsf-Mf+Mfk-Mfsk)}}\right]+1\right]$$

$$SVf := \frac{d}{dVf}\left[\left[\frac{\dfrac{-Mss}{0.25\cdot\pi\cdot L\cdot D^2}}{\dfrac{(Mfk-Mf)\cdot(Mgsf-Mf)}{Vf\cdot(Mgsf-Mf+Mfk-Mfsk)}}\right]+1\right]$$

$$SMgsf := \frac{d}{dMgsf}\left[\left[\frac{\dfrac{-Mss}{0.25\cdot\pi\cdot L\cdot D^2}}{\dfrac{(Mfk-Mf)\cdot(Mgsf-Mf)}{Vf\cdot(Mgsf-Mf+Mfk-Mfsk)}}\right]+1\right]$$

$$SMfsk := \frac{d}{dMfsk}\left[\left[\frac{\dfrac{-Mss}{0.25\cdot\pi\cdot L\cdot D^2}}{\dfrac{(Mfk-Mf)\cdot(Mgsf-Mf)}{Vf\cdot(Mgsf-Mf+Mfk-Mfsk)}}\right]+1\right]$$

B-189

Summary of Sensitivity Factors, List of Returned Values:

$SMss = -28.64943 \cdot mass^{-1}$

$SMgsf = -88.5978 \cdot mass^{-1}$

$SMf = 76.43194 \cdot mass^{-1}$

$SMfk = -112.45597 \cdot mass^{-1}$

$SL = 91.29315 \cdot length^{-1}$

$SVf = -9723.61758 \cdot length^{-3}$

$SD = 50.0475 \cdot length^{-1}$

$SMfsk = 124.66176 \cdot mass^{-1}$

List Errors Associated With Each Input Parameter

$me := 0.5 \cdot 10^{-5} \cdot kg$ Maximum error in mass measurement, scale. Applicable to Mss, Mf, Mfk, Mgsf, Mfsk

$fe := 5 \cdot 10^{-8} \cdot m^3 \cdot \dfrac{Mfk - Mf}{Vf}$ Max. error in mass measurement due to 0.05 ml imprecision in filling flask to calibration mark with kerosene. Applicable to Mfk, Mgsf, Mfsk

$fe = 0.00004 \cdot mass$

$le := 0.0012 \cdot .0254 \cdot m$ Maximum error in specimen length (total indicated runnout). Applicable to L

$de := .0004 \cdot .0254 \cdot m$ Maximum error in specimen diameter (total indicated runnout). Applicable to D.

$ve := 1 \cdot 10^{-7} \cdot m^3$ Maximum error in flask volume (1/10 ml). Applicable to Vf.

CALCULATE UNCERTAINTIES

BIAS LIMIT = B

$$B := \sqrt{(me)^2 \cdot \left(SMss^2 + SMf^2\right) + (le \cdot SL)^2 + (de \cdot SD)^2 + (ve \cdot SVf)^2 + \left(SMfk^2 + SMfsk^2 + SMgsf^2\right) \cdot (fe + me)^2}$$

$B = 0.00906$

Root sum of squares uncertainty = URss:

$URss := \sqrt{B^2}$ $URss = 0.00906$

For Reference: Full equation for URss is
    URss= sqrt(B^2+(t*S)^2)
where S is the precision error and t is an index
found in statistics charts. The t index decreases
with increasing degrees of freedom. All calibration
error are bias errors. Errors that can be reduced
with repeated measurments are precision errors.

Relative error, as a percent of porosity:

$Porosity = 0.02764$ $Rel\_Err\_pcnt := \dfrac{100 \cdot URss}{Porosity}$ $Rel\_Err\_pcnt = 32.76848$

B.F-2. ERROR ANALYSIS FOR GAS PERMEABILITY MEASUREMENTS

CALCULATION OF ERRORS FOR GAS PERMEABILITY MEASUREMENTS.

Application: Contract 248b calculation of gas permeability.
Used ANSI/ASME PTC 19.1-1985. "Part I Measurement
Uncertainty ; Instruments and Apparatus".

Mathcad file: Syntax:

:= User is defining a value or function

= Mathcad is returning a calculated value

units such as "length" and "mass" are returned by mathcad.

Definitions:

$$N := \frac{kg \cdot m}{sec^2}$$

$$MPa := \frac{10^6 \cdot N}{m^2}$$

GENERIC SPECIMEN

Input Values:

$$Q := \frac{20 \cdot 10^{-6} \cdot m^3}{86400 \cdot sec}$$ Flow rate

$$L := 0.1 \cdot m$$ Specimen length

$$D := 0.1 \cdot m$$ Specimen diameter

$$Pe := 0.1 \cdot MPa$$ Exit pore pressure

$$Pin := 0.4 \cdot MPa$$ Inlet pore pressure (low value gives worst case error)

$$u := 1.78 \cdot 10^{-11} \cdot MPa \cdot sec$$ Viscosity of nitrogen gas

$$A := 0.25 \cdot \pi \cdot D^2$$

$$Perm := \frac{2 \cdot Q \cdot Pe \cdot u \cdot L}{\left(Pin^2 - Pe^2\right) \cdot A}$$ $$Perm = 6.995 \cdot 10^{-20} \cdot length^2$$

Calculate Sensitivity Factors, Sx

Define sensitivity factors for each input parameter:

$$SQ := \frac{d}{dQ} \frac{2 \cdot Q \cdot Pe \cdot u \cdot L}{\left(Pin^2 - Pe^2\right) \cdot A}$$

$$SQ = 3.0218 \cdot 10^{-10} \cdot length^{-1} \cdot time$$

$$SPe := \frac{d}{dPe} \frac{2 \cdot Q \cdot Pe \cdot u \cdot L}{\left(Pin^2 - Pe^2\right) \cdot A}$$

$$SPe = 7.9276 \cdot 10^{-25} \cdot mass^{-1} \cdot length^3 \cdot time^2$$

$$SPin := \frac{d}{dPin} \frac{2 \cdot Q \cdot Pe \cdot u \cdot L}{\left(Pin^2 - Pe^2\right) \cdot A}$$

$$SPin = -3.7306 \cdot 10^{-25} \cdot mass^{-1} \cdot length^3 \cdot time^2$$

$$Su := \frac{d}{du} \frac{2 \cdot Q \cdot Pe \cdot u \cdot L}{\left(Pin^2 - Pe^2\right) \cdot A}$$

$$Su = 3.9298 \cdot 10^{-15} \cdot mass^{-1} \cdot length^3 \cdot time$$

$$SL := \frac{d}{dL} \frac{2 \cdot Q \cdot Pe \cdot u \cdot L}{\left(Pin^2 - Pe^2\right) \cdot A}$$

$$SL = 6.995 \cdot 10^{-19} \cdot length$$

$$SD := \frac{d}{dL} \frac{2 \cdot Q \cdot Pe \cdot u \cdot L}{\left(Pin^2 - Pe^2\right) \cdot \left(0.25 \cdot \pi \cdot D^2\right)}$$

$$SD = 6.995 \cdot 10^{-19} \cdot length$$

Summary of Relative Sensitivity Factors:

$$SQr := SQ \cdot \frac{Q}{Perm}$$
$$SLr := SL \cdot \frac{L}{Perm}$$
$$SQr = 1$$

$$SPer := SPe \cdot \frac{Pe}{Perm}$$
$$SLr = 1$$

$$SDr := SD \cdot \frac{D}{Perm}$$

$$SPinr := SPin \cdot \frac{Pin}{Perm}$$
$$SDr = 1$$

$$SPer = 1.1333$$

$$SPinr = -2.1333$$

$$Sur := Su \cdot \frac{u}{Perm}$$

$$Sur = 1$$

List Errors Associated With Each Input Parameter

$\text{Peerr} := 0.01 \cdot \text{Pe}$

$\text{Pinerr} := 0.01 \cdot \text{MPa}$

Errors in pore pressures; taken from transducer reverification data

$\text{Qerr} := Q \cdot 0.02$

Maximum error in flow rate - taken from errors to linear least square fits to data.

$\text{Lerr} := 0.0005 \cdot 0.0254 \cdot \text{m}$

Measurement errors in specimen dimensions

$\text{Derr} := 0.005 \cdot 0.0254 \cdot \text{m}$

$\text{uerr} := \dfrac{.07}{6} \cdot \text{u}$

Holcomb and Shields report that argon changes 7 percent over a 6 MPa pressure change. The maximum pressure change across the specimen here is 1.0 MPa. Therefore an error of 7/6 percent is used.

CALCULATE UNCERTAINTIES

B is the bias limit:

$$B := \sqrt{(\text{SPin} \cdot \text{Pinerr})^2 + (\text{SPe} \cdot \text{Peerr})^2 + (\text{SQ} \cdot \text{Qerr})^2 + (\text{SL} \cdot \text{Lerr})^2 + (\text{SD} \cdot \text{Derr})^2 + (\text{Su} \cdot \text{uerr})^2}$$

$$B = 4.1445 \cdot 10^{-21} \cdot \text{length}^2$$

Root sum of squares uncertainty = URss:

$$\text{URss} := \sqrt{B^2} \qquad\qquad \text{URss} = 4.1445 \cdot 10^{-21} \cdot \text{length}^2$$

For Reference: Full equation for URss is
URss= sqrt(B^2+(t*S)^2)
where S is the precision error and t is an index found in statistics charts. The t index decreases with increasing degrees of freedom. All calibration error are bias errors. Errors that can be reduced with repeated measurments are precision errors.

Relative error, as a percent of porosity:

$$\text{Perm} = 6.995 \cdot 10^{-20} \cdot \text{length}^2 \qquad \text{Rel\_Err\_pcnt} := \dfrac{100 \cdot \text{URss}}{\text{Perm}} \qquad \text{Rel\_Err\_pcnt} = 5.9251$$

B.F-3. ERROR ANALYSIS FOR BRINE PERMEABILITY MEASUREMENTS

CALCULATION OF ERRORS FOR BRINE PERMEABILITY MEASUREMENTS.

Application: Contract 248b calculation of gas permeability.
Used ANSI/ASME PTC 19.1-1985. "Part I Measurement
Uncertainty ; Instruments and Apparatus".
Mathcad file: Syntax:

:= User is defining a value or function

= Mathcad is returning a calculated value

units such as "*length" and "*mass" are returned by mathcad.

Definitions:

$$N := \frac{kg \cdot m}{sec^2}$$

$$MPa := \frac{10^6 \cdot N}{m^2}$$

GENERIC SPECIMEN

Input Values:

$$Q := 1 \cdot 10^{-9} \cdot \frac{m^3}{sec}$$ Flow rate

$$L := 0.1015 \cdot m$$ Specimen length

$$D := 0.1015 \cdot m$$ Specimen diameter

$$Pg := 0.3 \cdot MPa$$ Inlet gage pore pressure

$$u := 1.26 \cdot 10^{-9} \cdot MPa \cdot sec$$ Viscosity of brine (Stroup and Senseny, 1987) - no data for MB 139 brine recipe.

Where

$$A := 0.25 \cdot \pi \cdot D^2$$ Specimen cross-sectional area

$$Pe := 0.1 \cdot MPa$$ Exit pore pressure

$$Pin := Pg + Pe$$

$$Perm := \frac{Q \cdot u \cdot L}{(Pin - Pe) \cdot A}$$

$$Perm = 5.2686 \cdot 10^{-17} \cdot length^2$$

$$Perm := \frac{Q \cdot u \cdot L}{(Pg) \cdot A}$$

$$Perm = 5.2686 \cdot 10^{-17} \cdot length^2$$

CALCULATION OF ERRORS FOR BRINE PERMEABILITY MEASUREMENTS.

Application: Contract 248b calculation of gas permeability.
Used ANSI/ASME PTC 19.1-1985. "Part I Measurement
Uncertainty ; Instruments and Apparatus".
Mathcad file: Syntax:

:= User is defining a value or function

= Mathcad is returning a calculated value

units such as "*length" and "*mass" are returned by mathcad.

Definitions:

$$N := \frac{kg \cdot m}{sec^2}$$

$$MPa := \frac{10^6 \cdot N}{m^2}$$

GENERIC SPECIMEN

Input Values:

$$Q := 1 \cdot 10^{-9} \frac{m^3}{sec}$$ Flow rate

$$L := 0.1015 \cdot m$$ Specimen length

$$D := 0.1015 \cdot m$$ Specimen diameter

$$Pg := 0.3 \cdot MPa$$ Inlet gage pore pressure

$$u := 1.26 \cdot 10^{-9} \cdot MPa \cdot sec$$ Viscosity of brine (Stroup and Senseny, 1987) - no data for MB 139 brine recipe.

Where

$$A := 0.25 \cdot \pi \cdot D^2$$ Specimen cross-sectional area

$$Pe := 0.1 \cdot MPa$$ Exit pore pressure

$$Pin := Pg + Pe$$

$$Perm := \frac{Q \cdot u \cdot L}{(Pin - Pe) \cdot A}$$

$$Perm = 5.2686 \cdot 10^{-17} \cdot length^2$$

$$Perm := \frac{Q \cdot u \cdot L}{(Pg) \cdot A}$$

$$Perm = 5.2686 \cdot 10^{-17} \cdot length^2$$

Calculate Sensitivity Factors, Sx

Define sensitivity factors for each input parameter:

$$SQ := \frac{d}{dQ} \frac{Q \cdot u \cdot L}{(Pg) \cdot A}$$

$$SQ = 5.2686 \cdot 10^{-8} \cdot length^{-1} \cdot time$$

$$SPg := \frac{d}{dPg} \frac{Q \cdot u \cdot L}{(Pg) \cdot A}$$

$$SPg = -1.7562 \cdot 10^{-22} \cdot mass^{-1} \cdot length^3 \cdot time^2$$

$$Su := \frac{d}{du} \frac{Q \cdot u \cdot L}{(Pg) \cdot A}$$

$$Su = 4.1814 \cdot 10^{-14} \cdot mass^{-1} \cdot length^3 \cdot time$$

$$SL := \frac{d}{dL} \frac{Q \cdot u \cdot L}{(Pg) \cdot A}$$

$$SL = 5.1907 \cdot 10^{-16} \cdot length$$

$$SD := \frac{d}{dL} \frac{Q \cdot u \cdot L}{(Pg) \cdot (0.25 \cdot \pi \cdot D^2)}$$

$$SD = 5.1907 \cdot 10^{-16} \cdot length$$

Summary of Relative Sensitivity Factors:

$$SQr := SQ \cdot \frac{Q}{Perm} \qquad SQr = 1$$

$$SPgr := SPg \cdot \frac{Pg}{Perm} \qquad SPgr = -1$$

$$Sur := Su \cdot \frac{u}{Perm} \qquad Sur = 1$$

$$SLr := SL \cdot \frac{L}{Perm} \qquad SLr = 1$$

$$SDr := SD \cdot \frac{D}{Perm} \qquad SDr = 1$$

List Errors Associated With Each Input Parameter

$Pgerr := 0.01 \cdot MPa$ — Maximum error in pore pressure gage reading; taken from transducer reverification data

$Qerr := 0.03 \cdot Q$ — Maximum error in flow rate (3%) - taken from standard error in linear fit to data.

$Lerr := 0.0005 \cdot 0.0254 \cdot m$

$Derr := 0.005 \cdot 0.0254 \cdot m$ — Measurement errors in specimen dimensions

$uerr := 0.01 \cdot 10^{-9} \cdot MPa \cdot sec$ — Used precision of reported viscosity.

CALCULATE UNCERTAINTIES

B is the bias limit:

$$B := \sqrt{(SPg \cdot Pgerr)^2 + (SQ \cdot Qerr)^2 + (SL \cdot Lerr)^2 + (SD \cdot Derr)^2 + (Su \cdot uerr)^2}$$

$$B = 2.4003 \cdot 10^{-18} \cdot length^2$$

Root sum of squares uncertainty = URss:

$$URss := \sqrt{B^2} \qquad\qquad URss = 2.4003 \cdot 10^{-18} \cdot length^2$$

> For Reference: Full equation for URss is
> URss= sqrt(B^2+(t*S)^2)
> where S is the precision error and t is an index
> found in statistics charts. The t index decreases
> with increasing degrees of freedom. All calibration
> error are bias errors. Errors that can be reduced
> with repeated measurments are precision errors.

Relative error, as a percent of permeability:

$$Perm = 5.2686 \cdot 10^{-17} \cdot length^2 \qquad Rel\_Err\_pcnt := \frac{100 \cdot URss}{Perm}$$

$$Rel\_Err\_pcnt = 4.556$$

APPENDIX B.G
FLOW-VERSUS-TIME DATA FOR ALL GAS PERMEABILITY TESTS

Figures

Figures (Continued)

Figures (Continued)

Figure G-1. Gas volume-versus-time for tests on Specimen P3X11-5-2-SP1 at 2 MPa confining pressure and 1.0 MPa gas inlet pressure. Symbols represent recorded data points and dashed lines are best fits to linear sections of data.
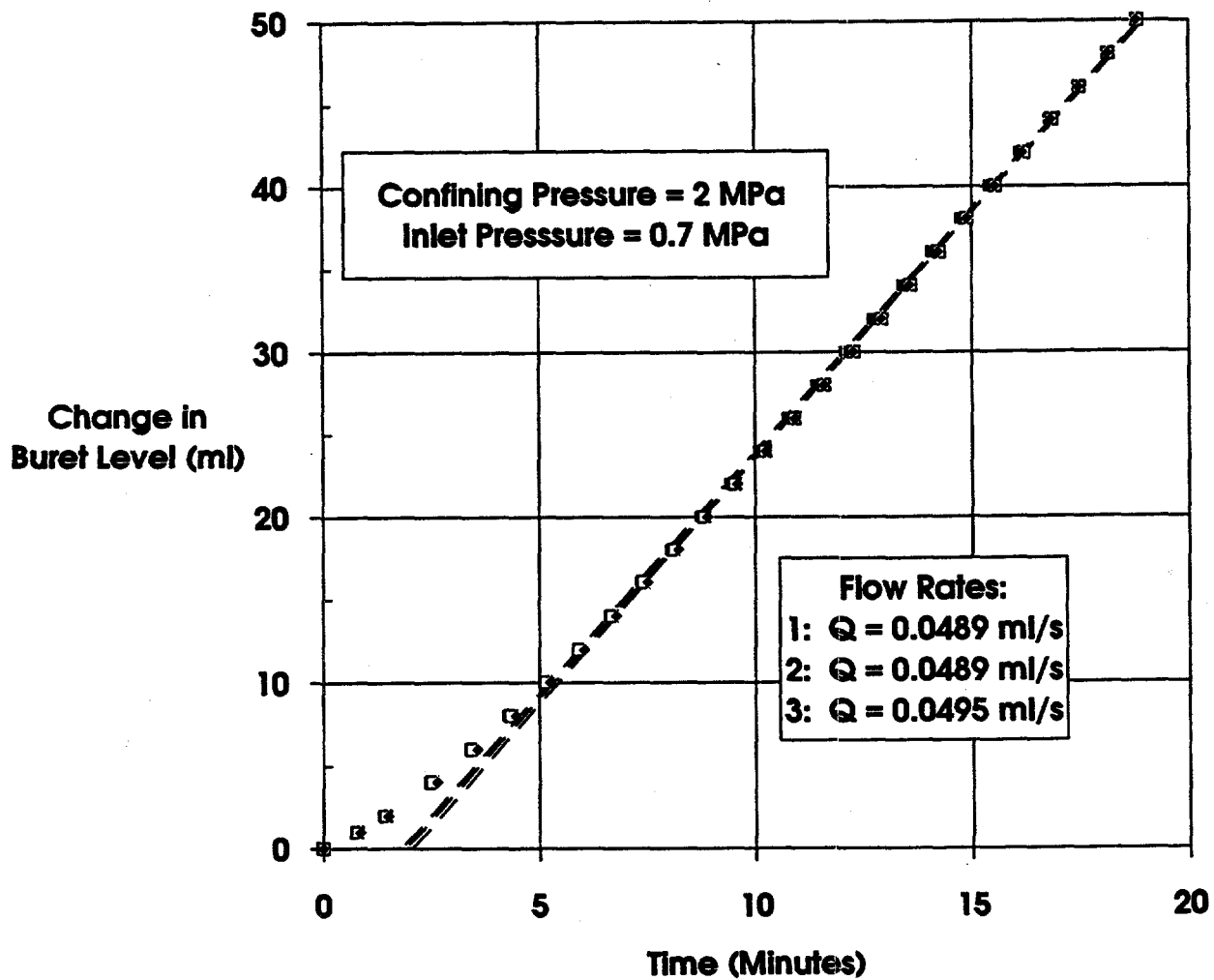
Figure G-2. Gas volume-versus-time for tests on Specimen P3X11-5-2-SP1 at 2 MPa confining pressure and 0.7 MPa gas inlet pressure. Symbols represent recorded data points and dashed lines are best fits to linear sections of data.
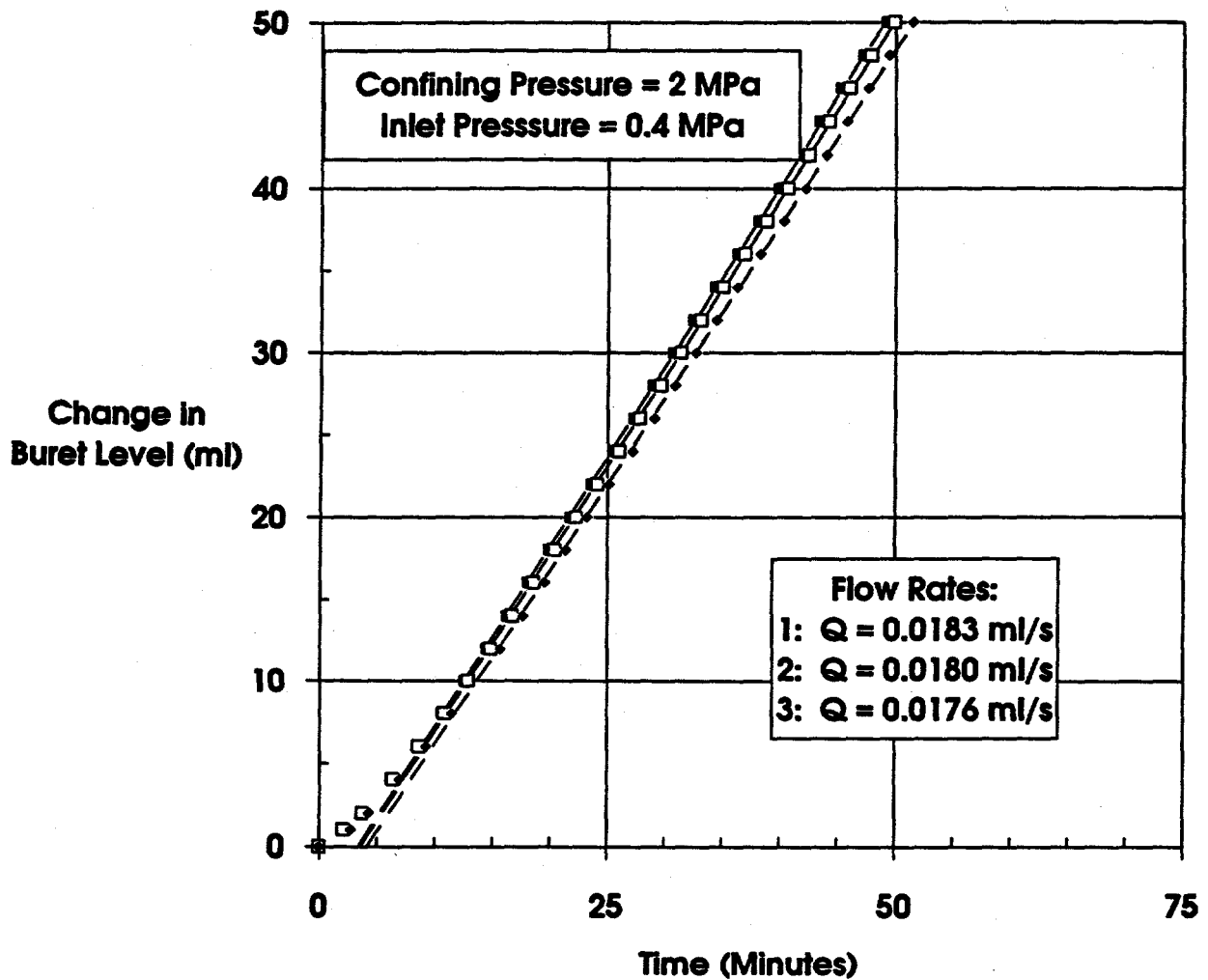
B-210

Figure G-3. Gas volume-versus-time for tests on Specimen P3X11-5-2-SP1 at 2 MPa confining pressure and 0.4 MPa gas inlet pressure. Symbols represent recorded data points and dashed lines are best fits to linear sections of data.
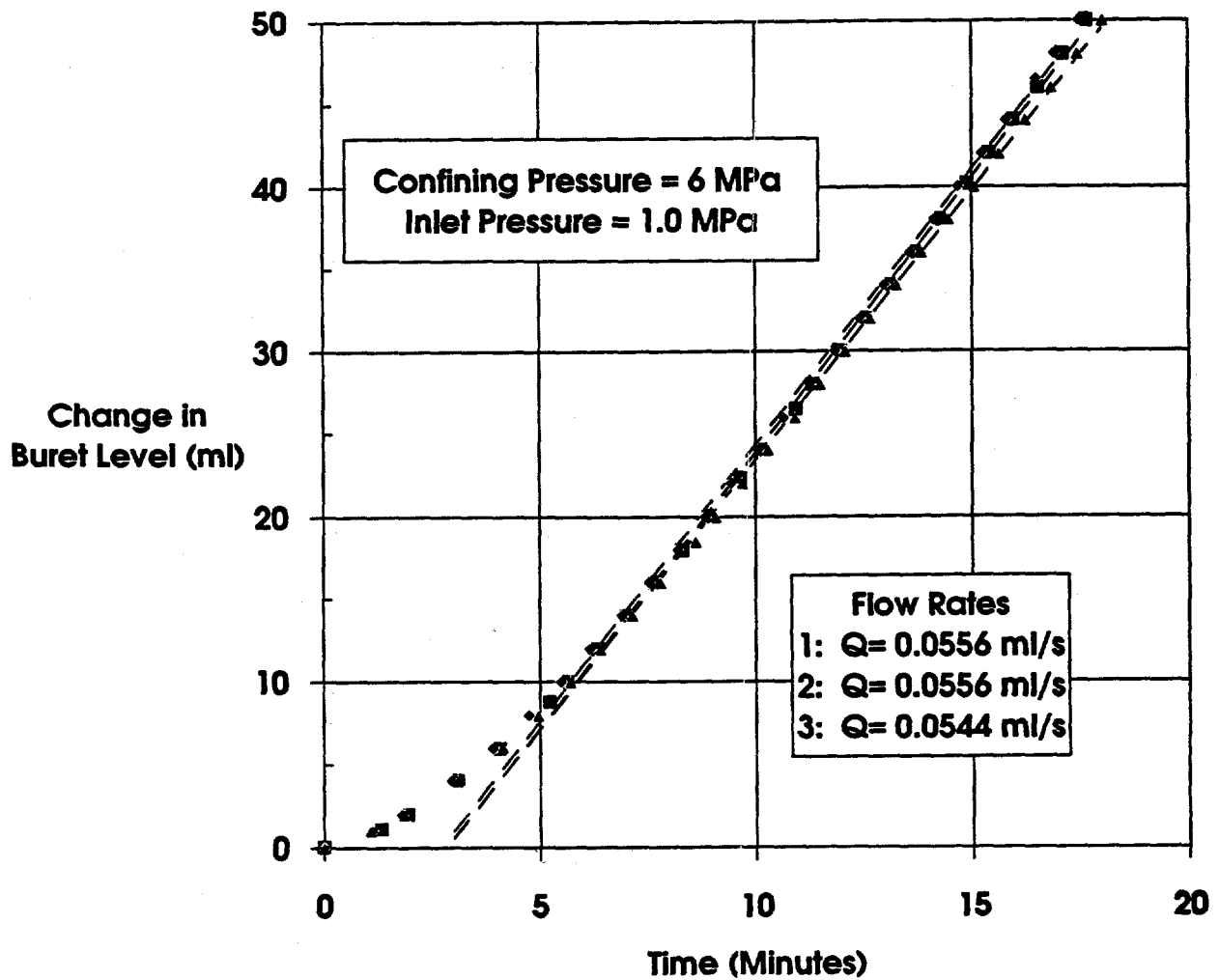
Figure G-4. Gas volume-versus-time for tests on Specimen P3X11-5-2-SP1 at 6 MPa confining pressure and 1.0 MPa gas inlet pressure. Symbols represent recorded data points and dashed lines are best fits to linear sections of data.
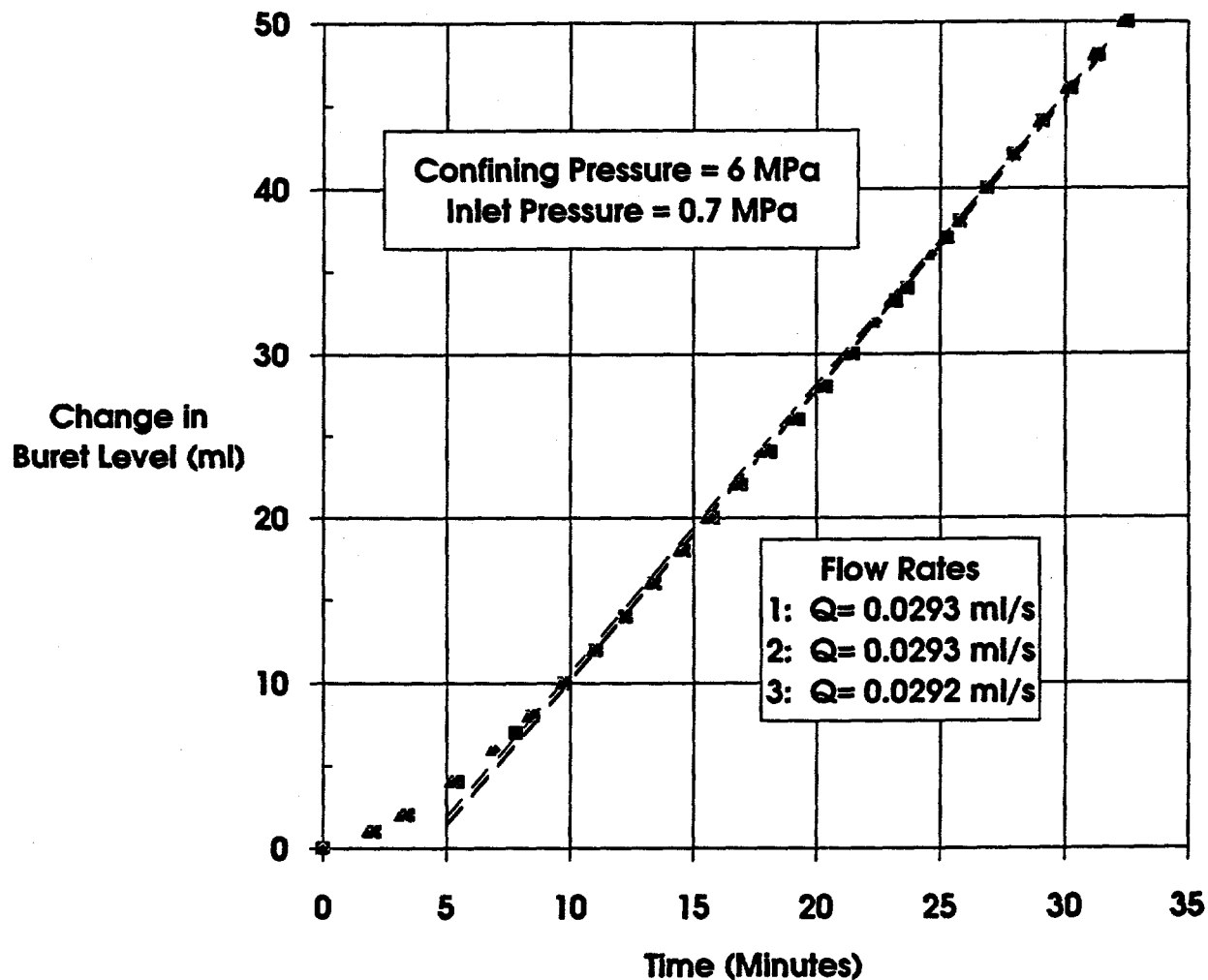
Figure G-5. Gas volume-versus-time for tests on Specimen P3X11-5-2-SP1 at 6 MPa confining pressure and 0.7 MPa gas inlet pressure. Symbols represent recorded data points and dashed lines are best fits to linear sections of data.
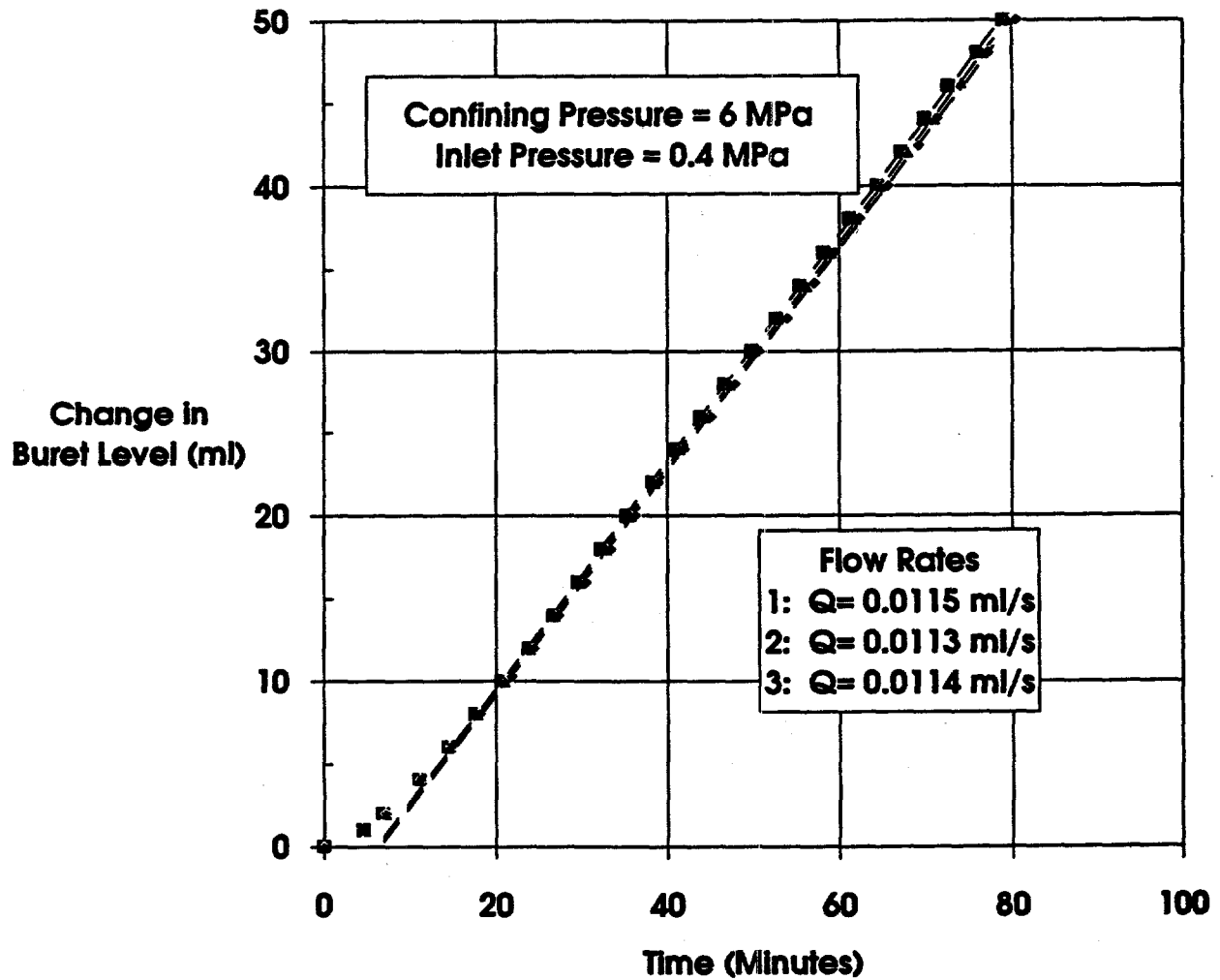
B-213

Figure G-6. Gas volume-versus-time for tests on Specimen P3X11-5-2-SP1 at 6 MPa confining pressure and 0.4 MPa gas inlet pressure. Symbols represent recorded data points and dashed lines are best fits to linear sections of data.

Confining Pressure = 10 MPa
Inlet Pressure = 1.0 MPa

Flow Rates
1: Q= 0.0450 ml/s
2: Q= 0.0440 ml/s
3: Q= 0.0415 ml/s
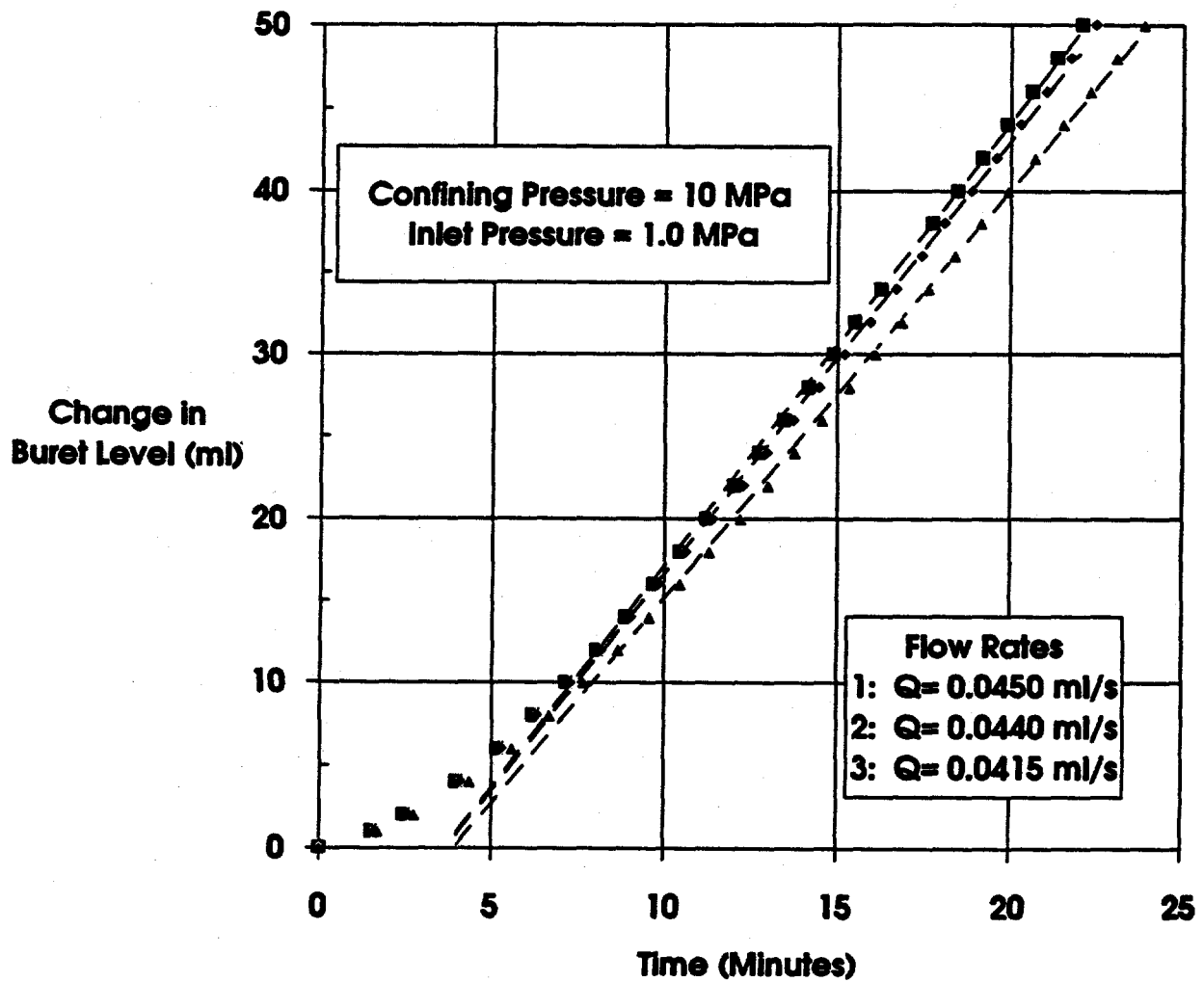
RSI-248-93-064

Figure G-7. Gas volume-versus-time for tests on Specimen P3X11-5-2-SP1 at 10 MPa confining pressure and 1.0 MPa gas inlet pressure. Symbols represent recorded data points and dashed lines are best fits to linear sections of data.
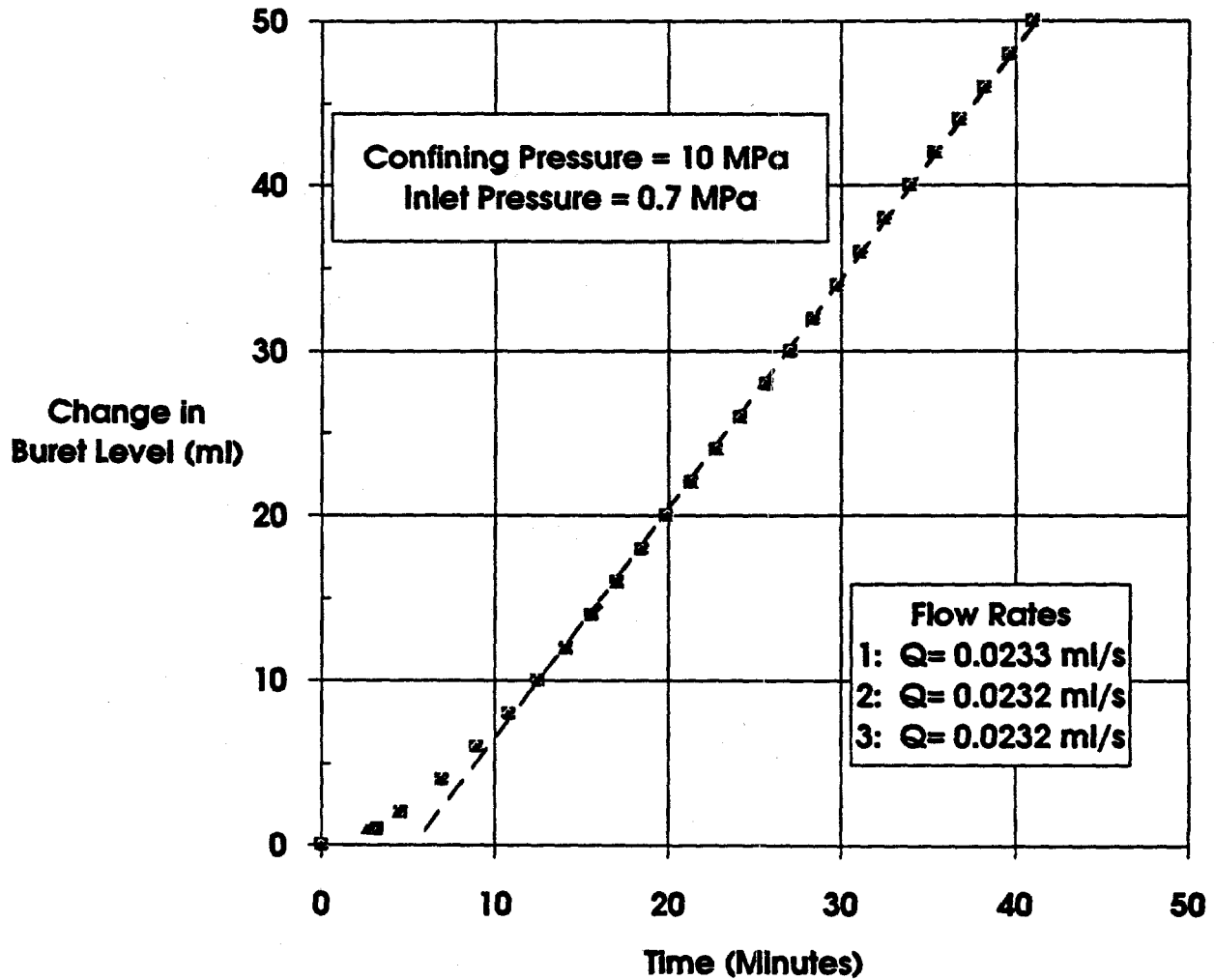
Figure G-8. Gas volume-versus-time for tests on Specimen P3X11-5-2-SP1 at 10 MPa confining pressure and 0.7 MPa gas inlet pressure. Symbols represent recorded data points and dashed lines are best fits to linear sections of data.
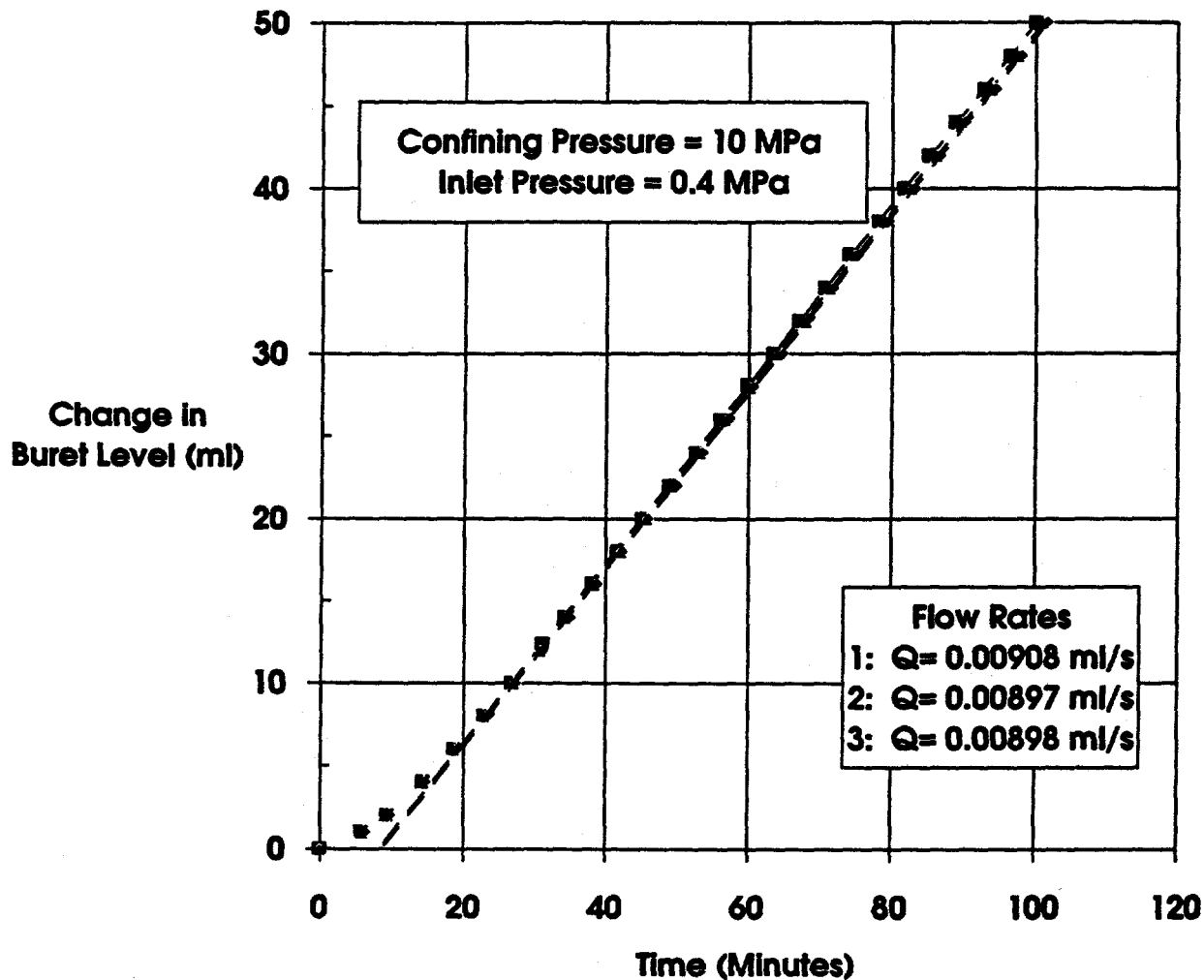
Figure G-9. Gas volume-versus-time for tests on Specimen P3X11-5-2-SP1 at 10 MPa confining pressure and 0.4 MPa gas inlet pressure. Symbols represent recorded data points and dashed lines are best fits to linear sections of data.
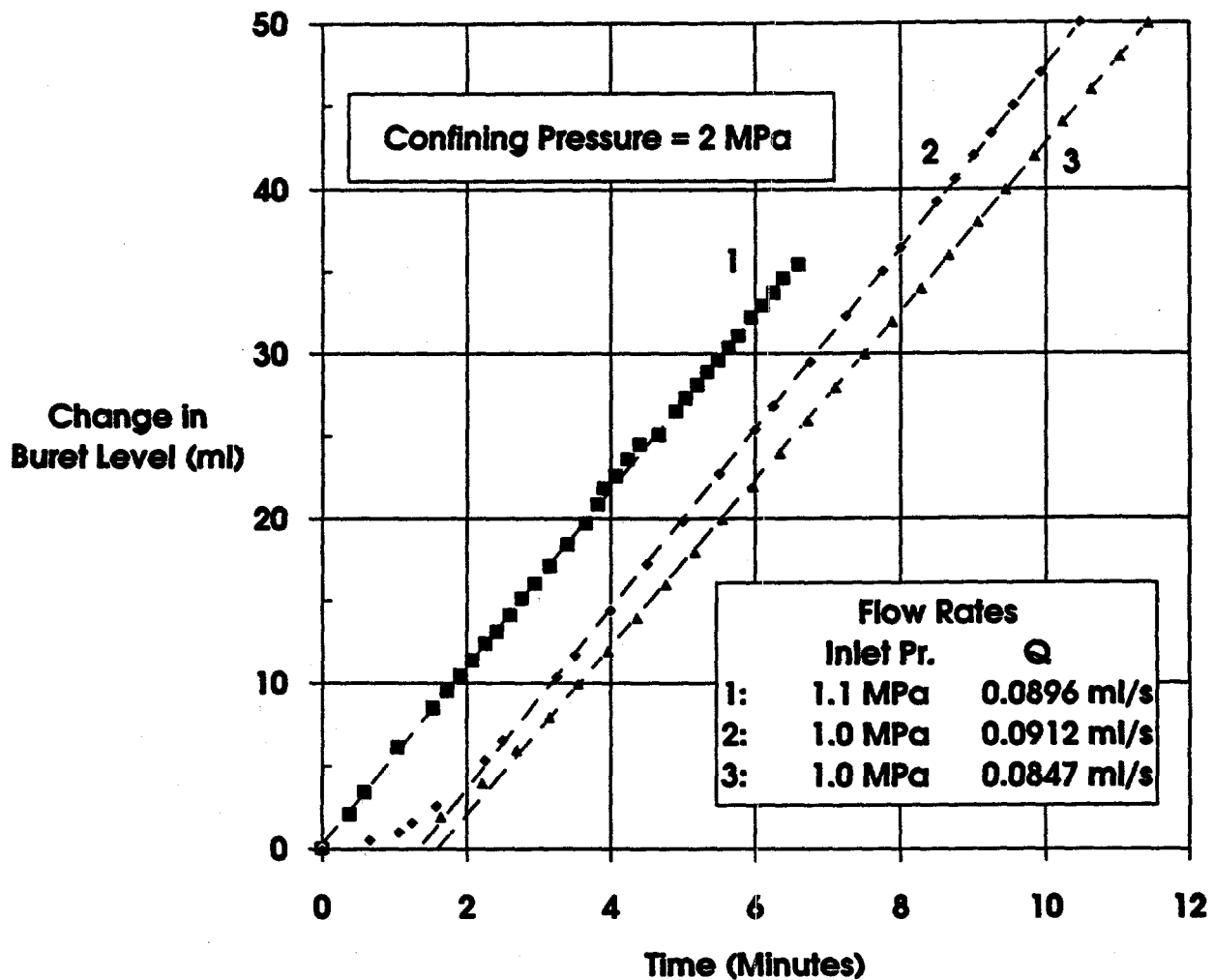
B-217

Figure G-10. Gas volume-versus-time for tests on Specimen P3X10-6-SP2 at 2 MPa confining pressure and 1.0 MPa gas inlet pressure. Symbols represent recorded data points and dashed lines are best fits to linear sections of data.
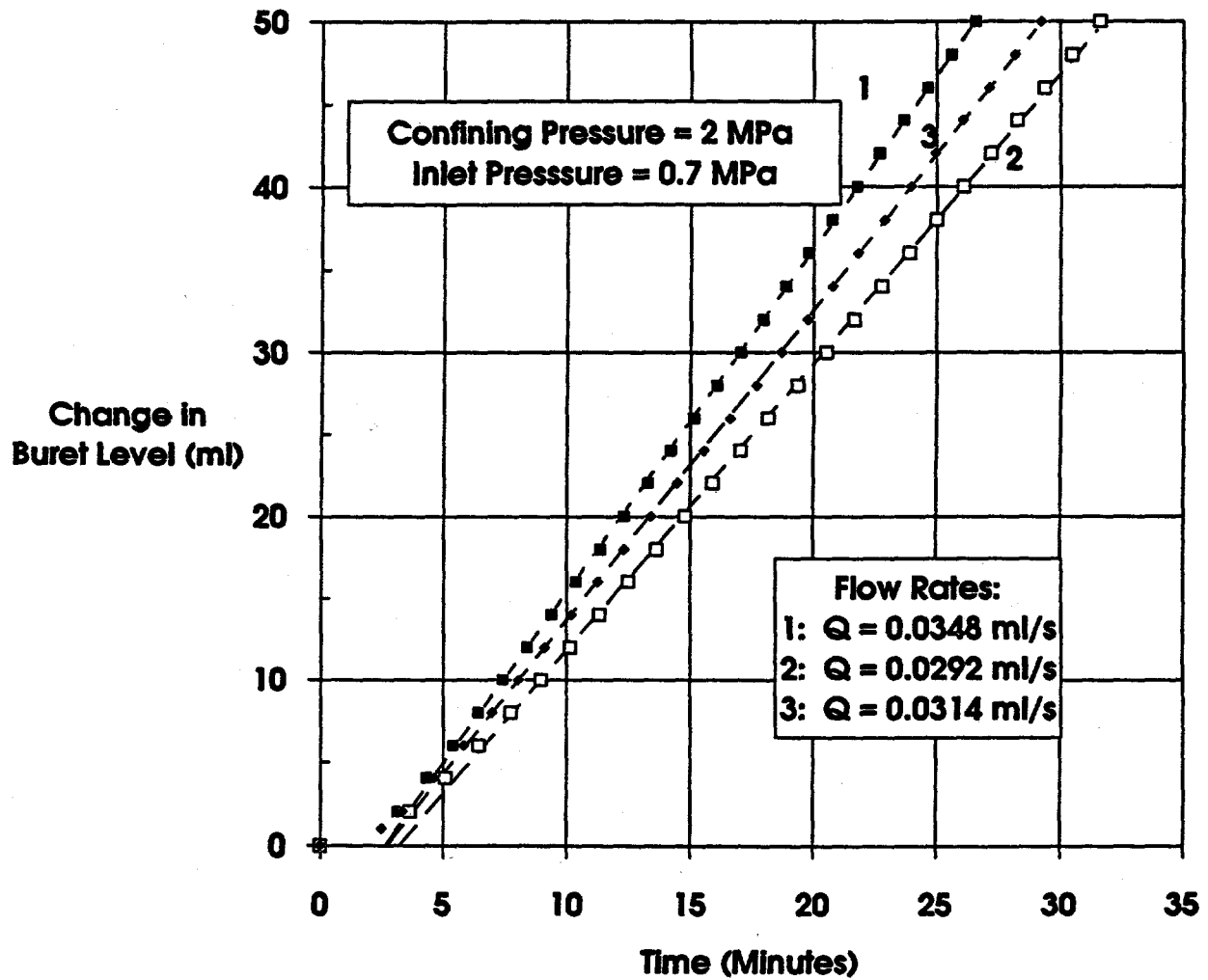
Figure G-11. Gas volume-versus-time for tests on Specimen P3X10-6-SP2 at 2 MPa confining pressure and 0.7 MPa gas inlet pressure. Symbols represent recorded data points and dashed lines are best fits to linear sections of data.
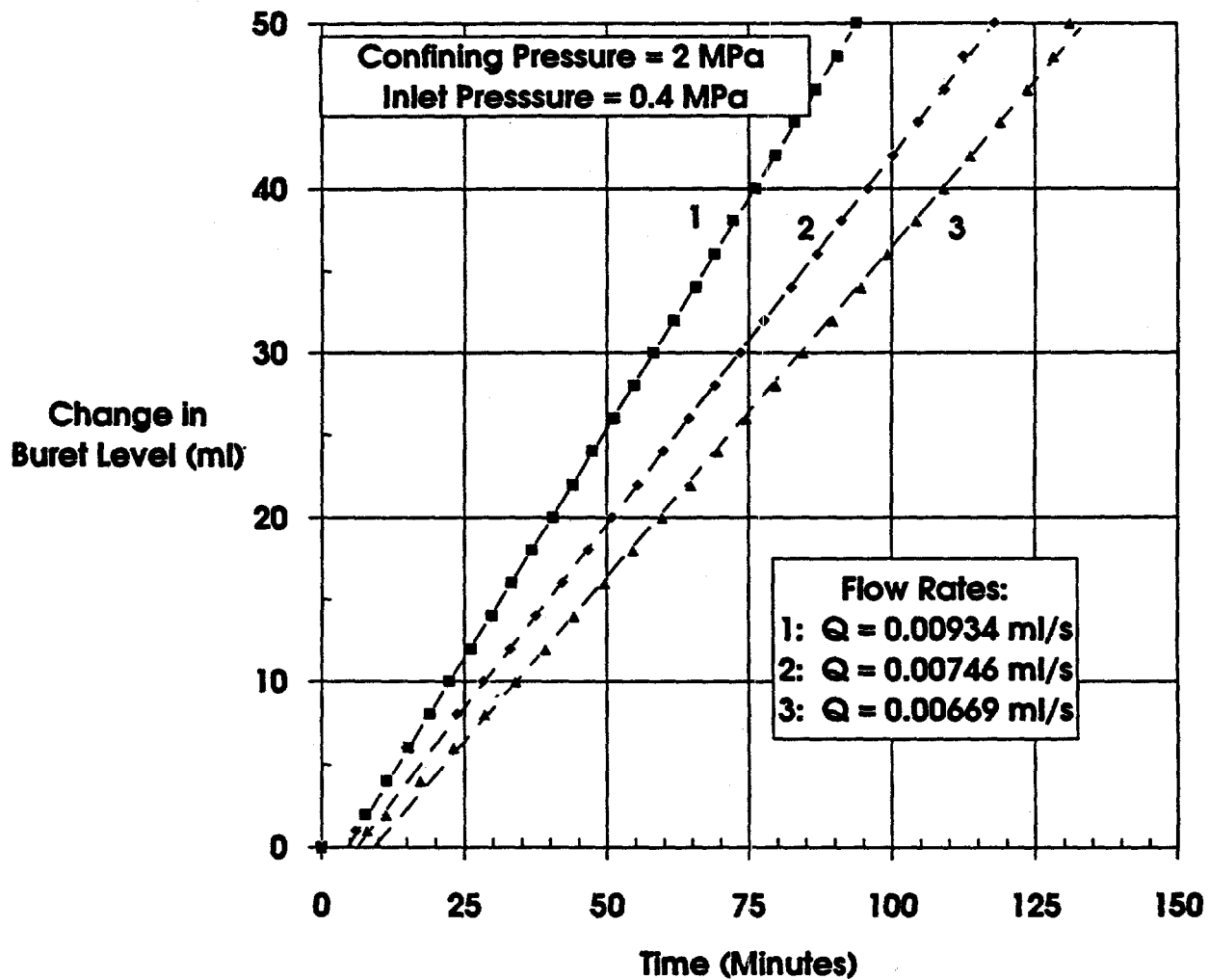
Figure G-12. Gas volume-versus-time for tests on Specimen P3X10-6-SP2 at 2 MPa confining pressure and 0.4 MPa gas inlet pressure. Symbols represent recorded data points and dashed lines are best fits to linear sections of data.
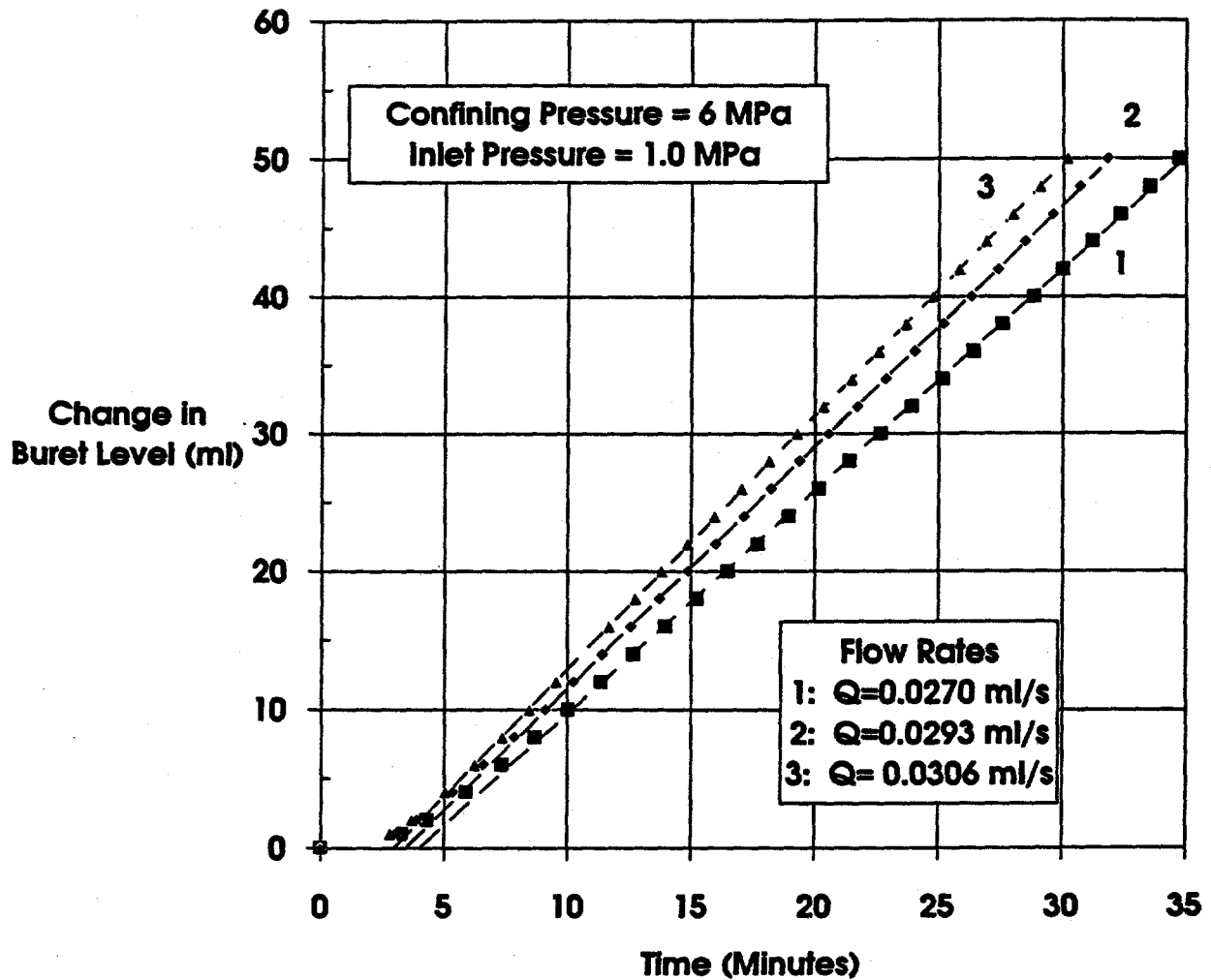
B-220

Figure G-13. Gas volume-versus-time for tests on Specimen P3X10-6-SP2 at 6 MPa confining pressure and 1.0 MPa gas inlet pressure. Symbols represent recorded data points and dashed lines are best fits to linear sections of data.
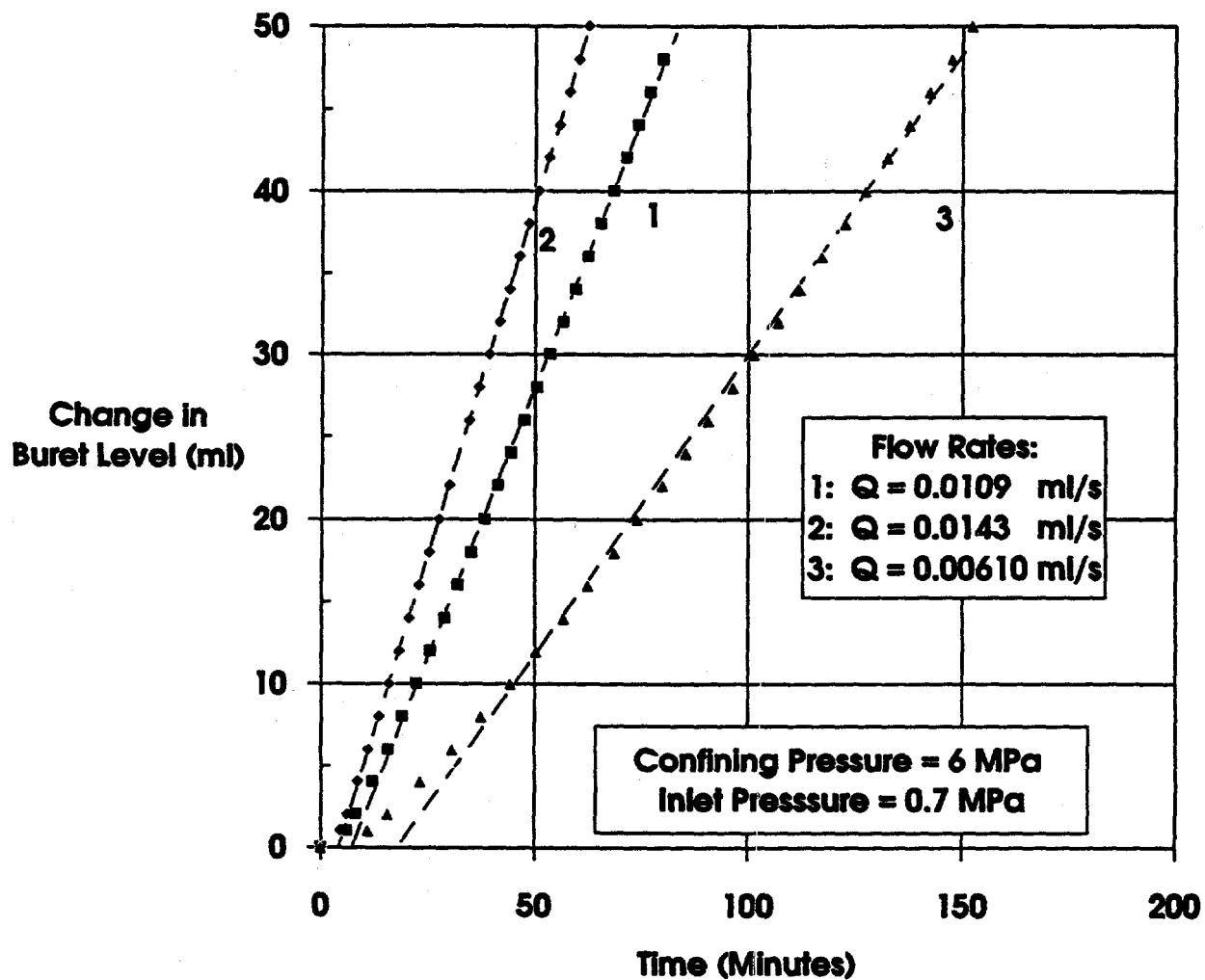
Figure G-14. Gas volume-versus-time for tests on Specimen P3X10-6-SP2 at 6 MPa confining
pressure and 0.7 MPa gas inlet pressure. Symbols represent recorded data points
and dashed lines are best fits to linear sections of data.
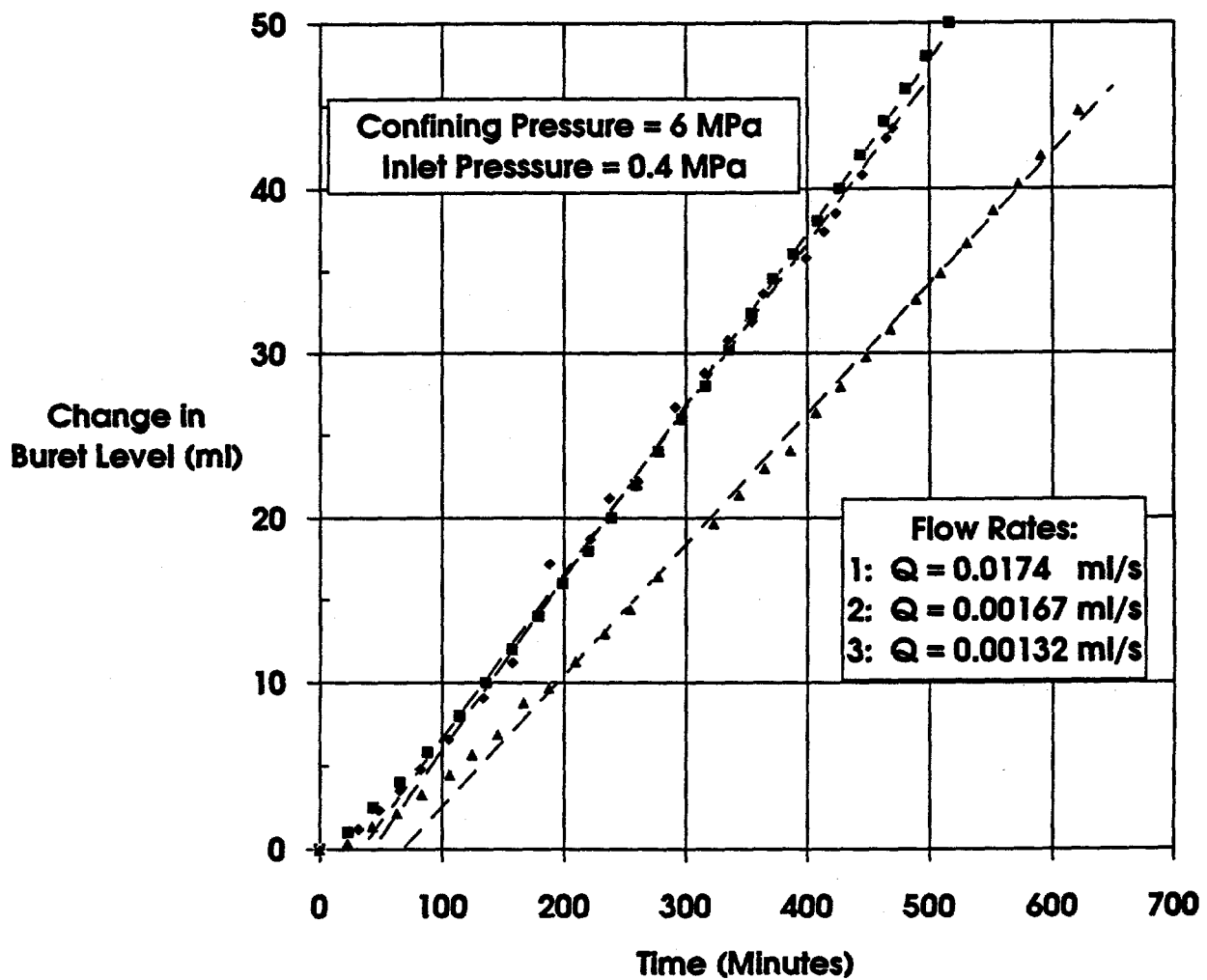
Figure G-15. Gas volume-versus-time for tests on Specimen P3X10-6-SP2 at 6 MPa confining pressure and 0.4 MPa gas inlet pressure. Symbols represent recorded data points and dashed lines are best fits to linear sections of data.
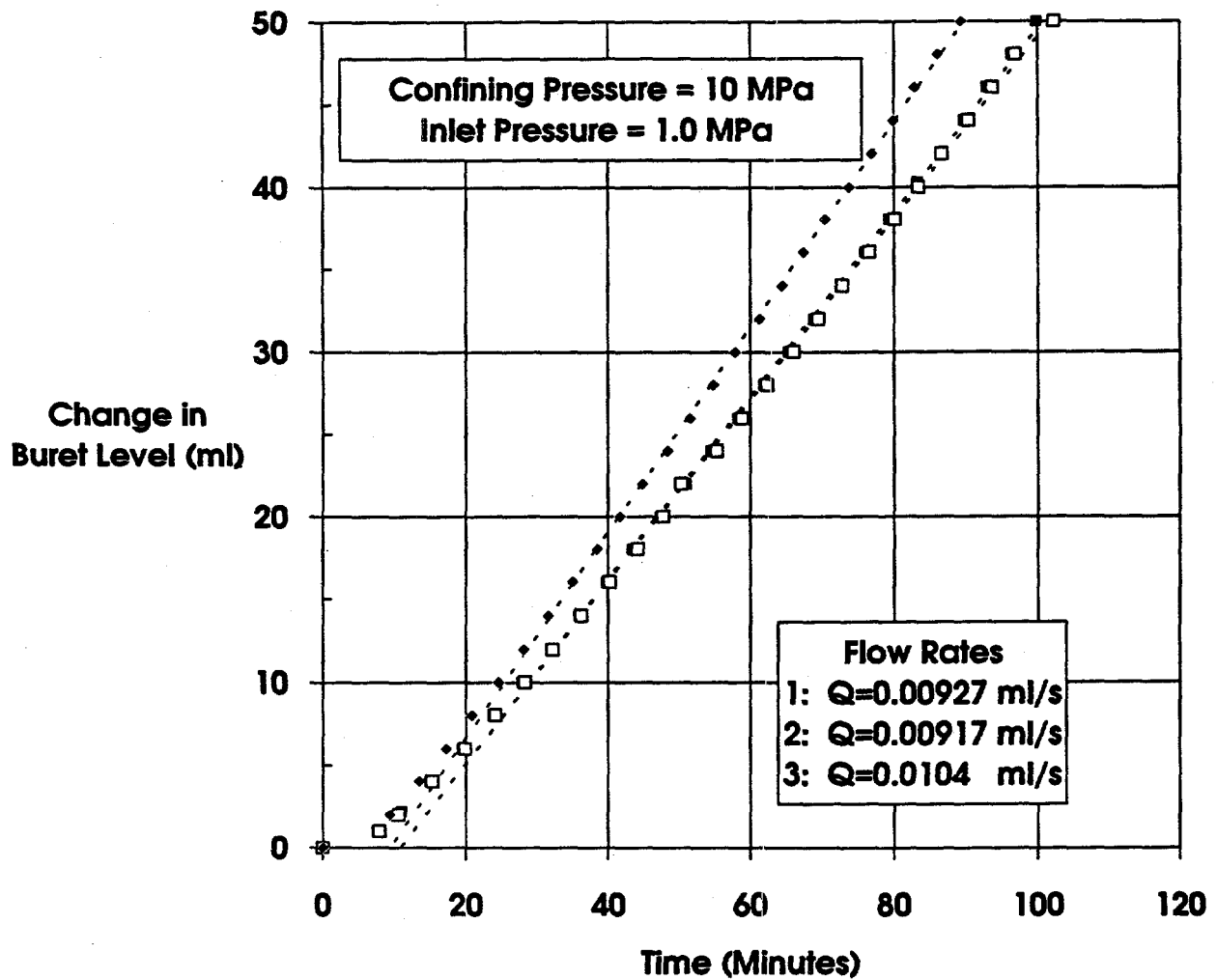
Figure G-16. Gas volume-versus-time for tests on Specimen P3X10-6-SP2 at 10 MPa confining pressure and 1.0 MPa gas inlet pressure. Symbols represent recorded data points and dashed lines are best fits to linear sections of data.
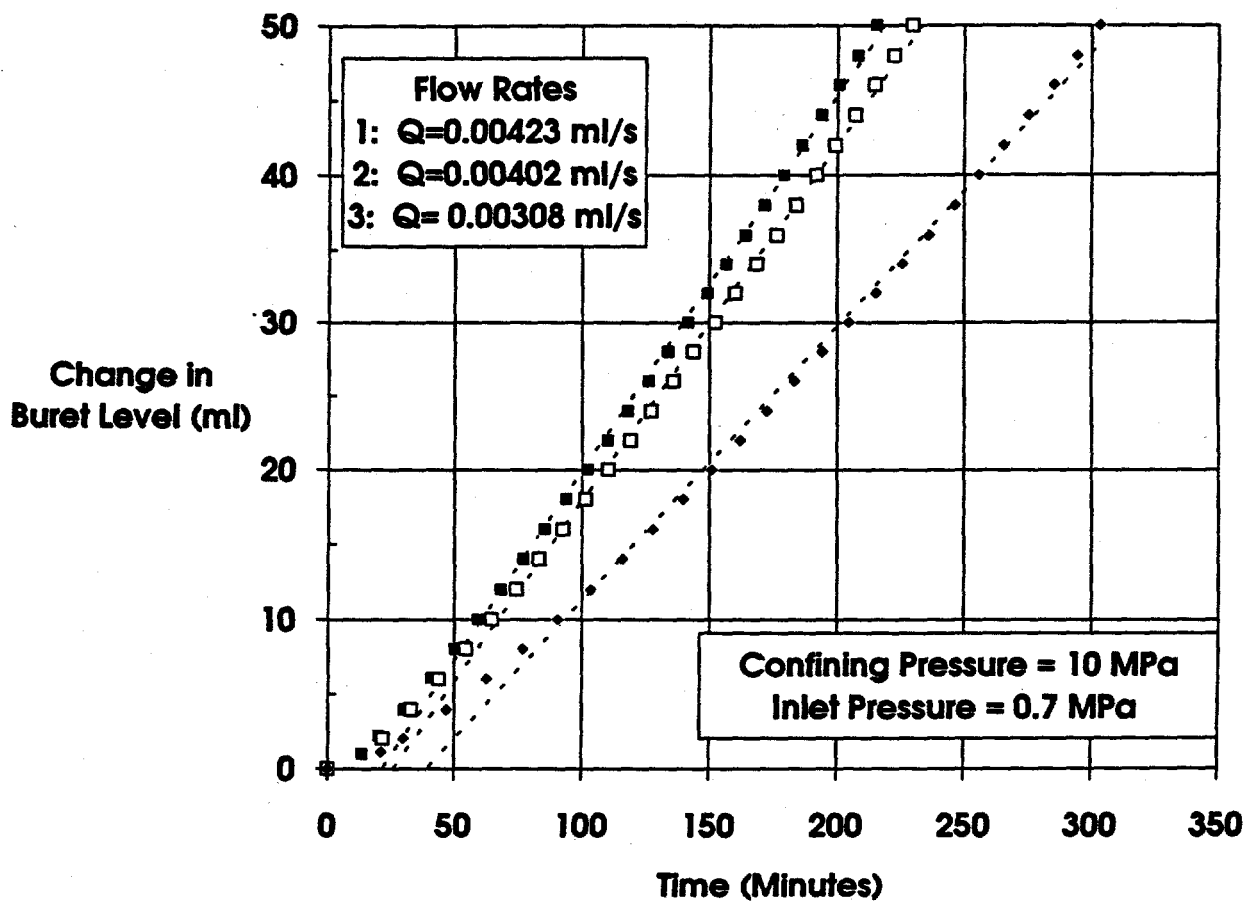
Figure G-17. Gas volume-versus-time for tests on Specimen P3X10-6-SP2 at 10 MPa confining pressure and 0.7 MPa gas inlet pressure. Symbols represent recorded data points and dashed lines are best fits to linear sections of data.
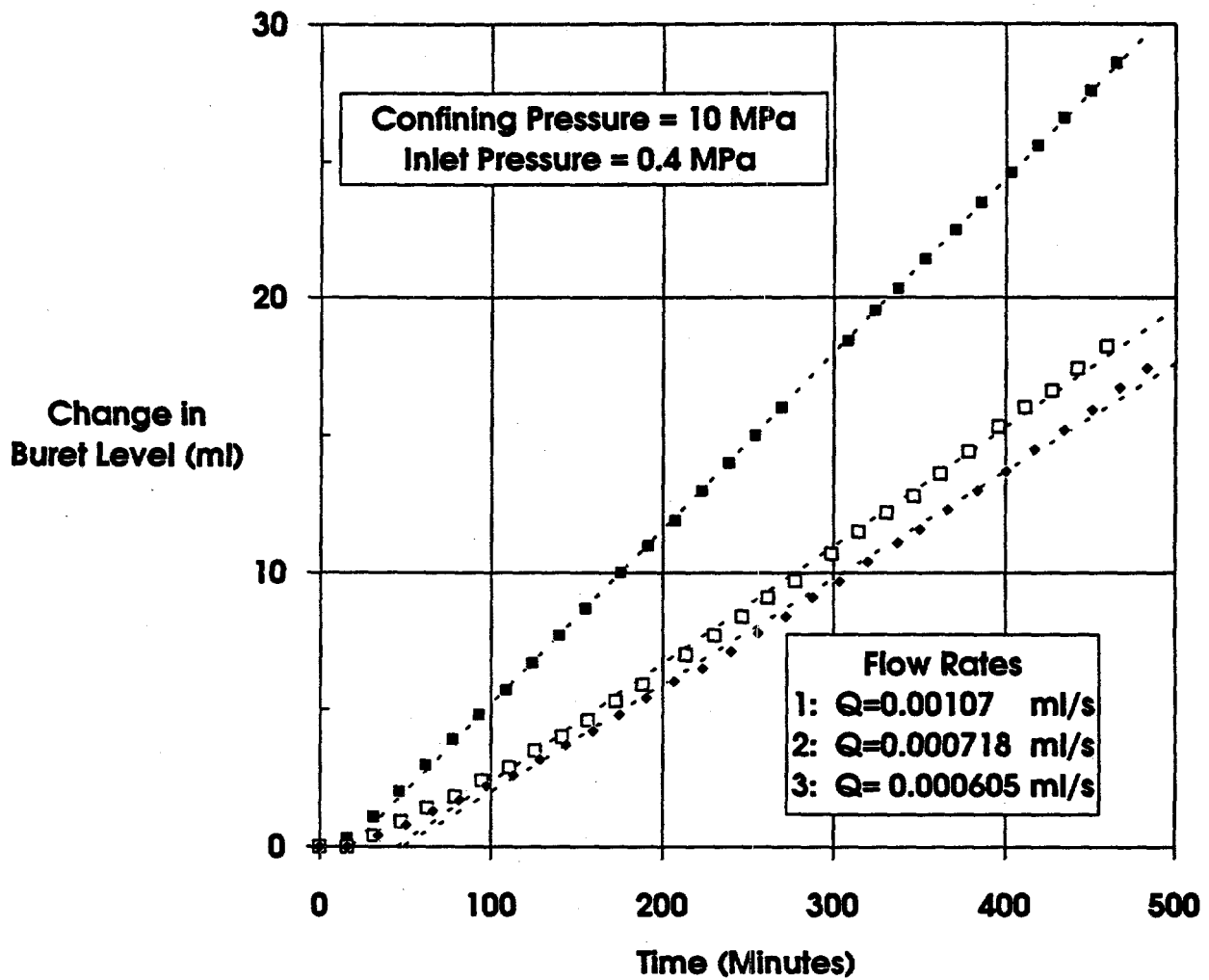
Figure G-18. Gas volume-versus-time for tests on Specimen P3X10-6-SP2 at 10 MPa confining pressure and 0.4 MPa gas inlet pressure. Symbols represent recorded data points and dashed lines are best fits to linear sections of data.
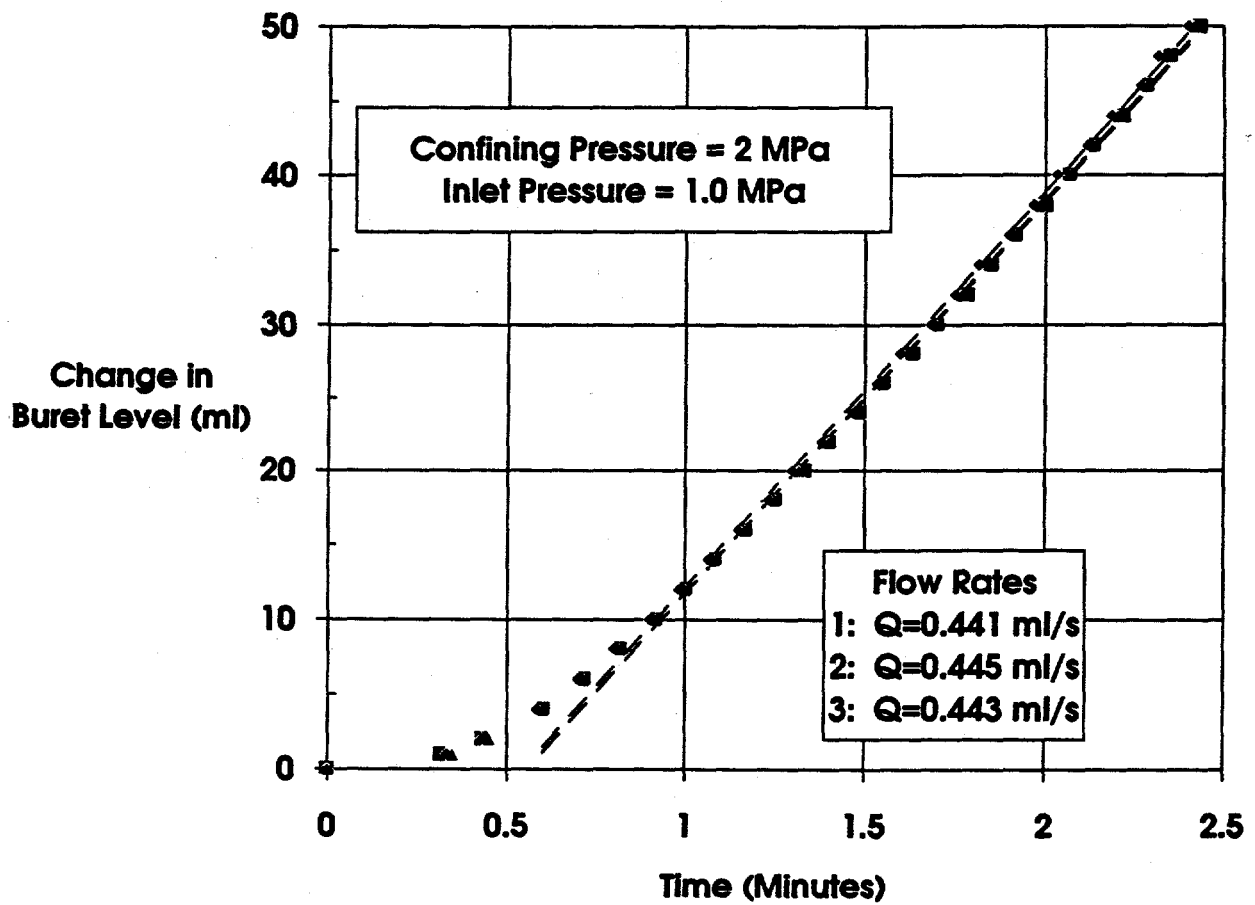
Figure G-19. Gas volume-versus-time for tests on Specimen P3X11-5-3-SP3 at 2 MPa confining pressure and 1.0 MPa gas inlet pressure. Symbols represent recorded data points and dashed lines are best fits to linear sections of data.
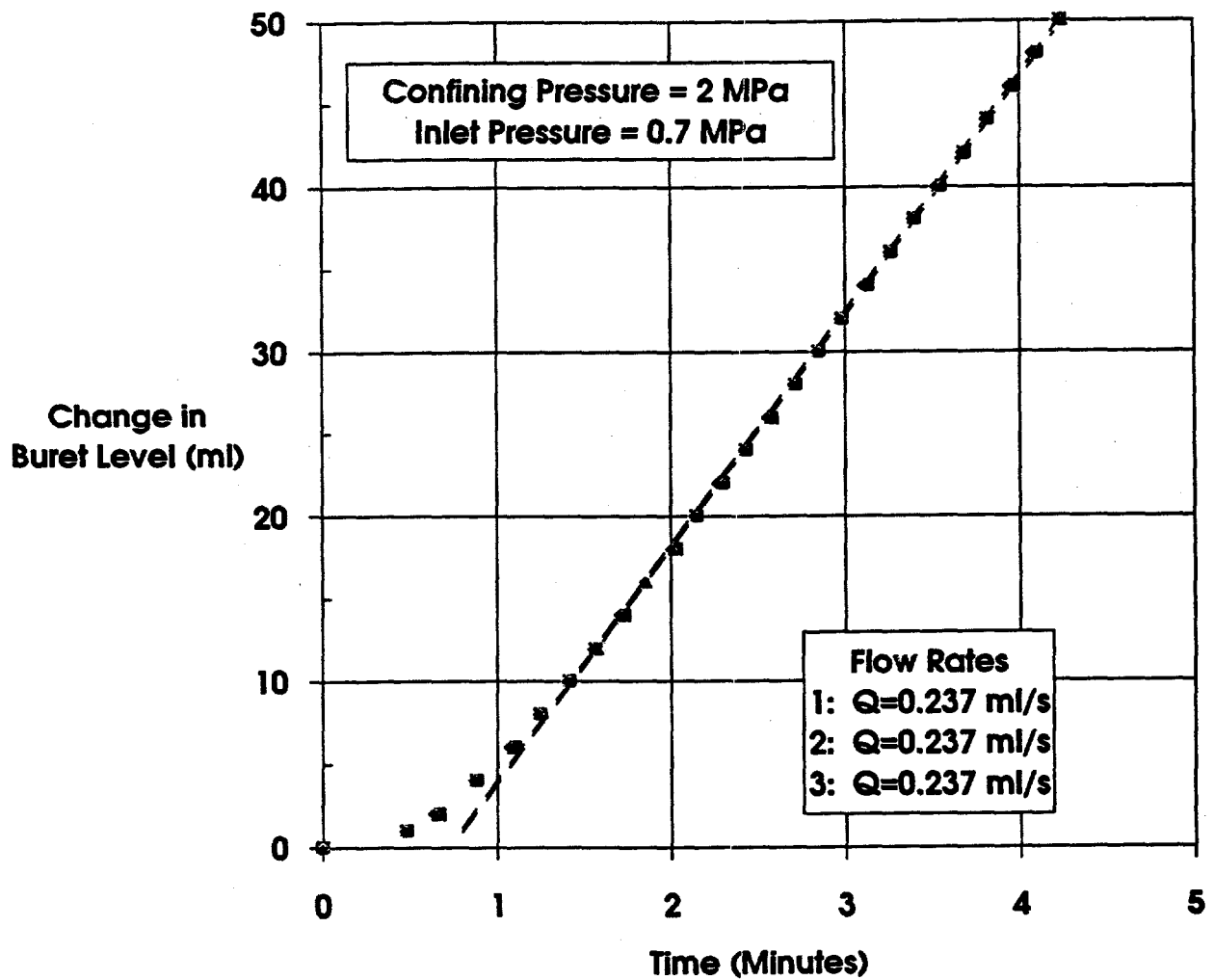
B-227

Figure G-20. Gas volume-versus-time for tests on Specimen P3X11-5-3-SP3 at 2 MPa confining pressure and 0.7 MPa gas inlet pressure. Symbols represent recorded data points and dashed lines are best fits to linear sections of data.
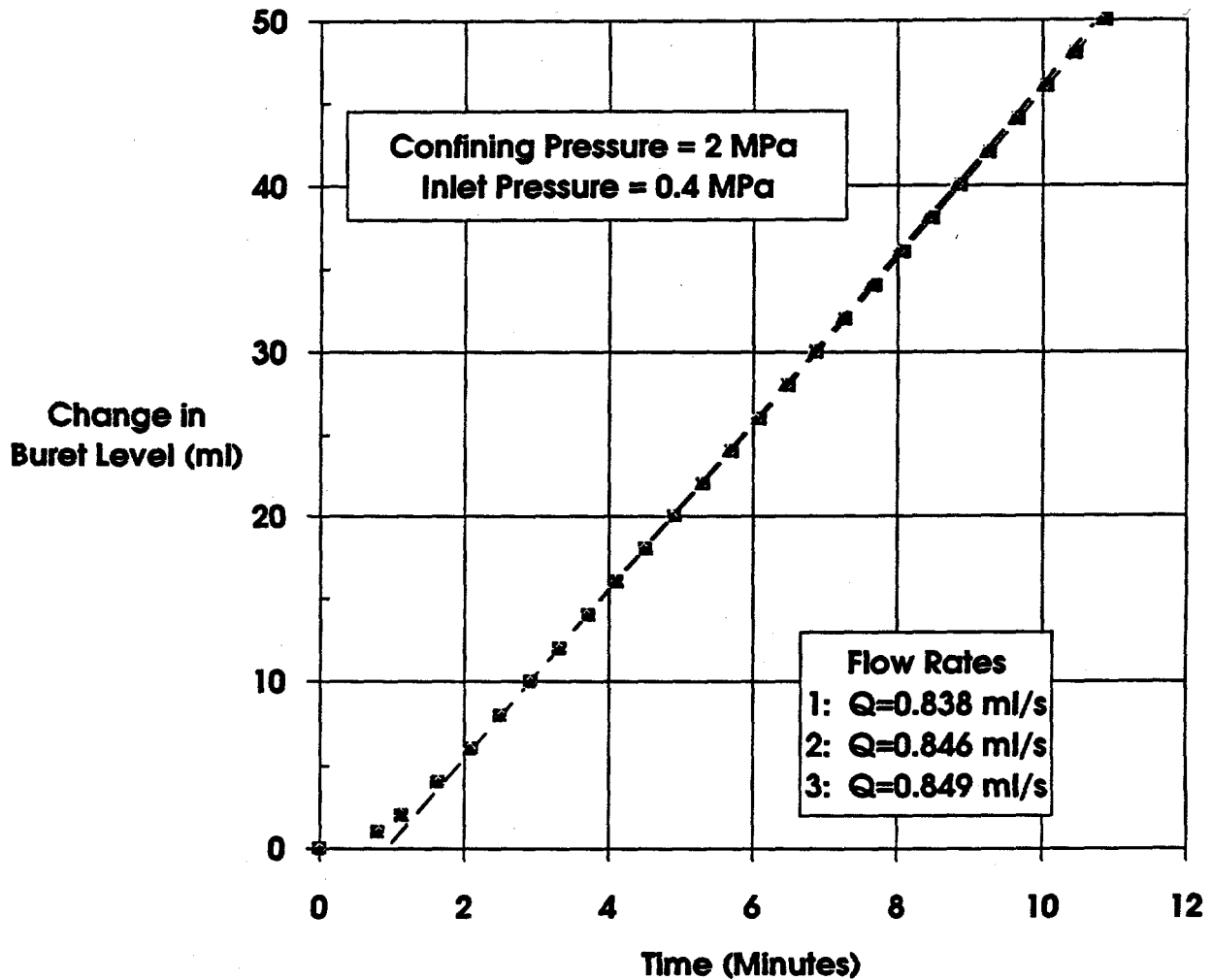
Figure G-21. Gas volume-versus-time for tests on Specimen P3X11-5-3-SP3 at 2 MPa confining
pressure and 0.4 MPa gas inlet pressure. Symbols represent recorded data points
and dashed lines are best fits to linear sections of data.
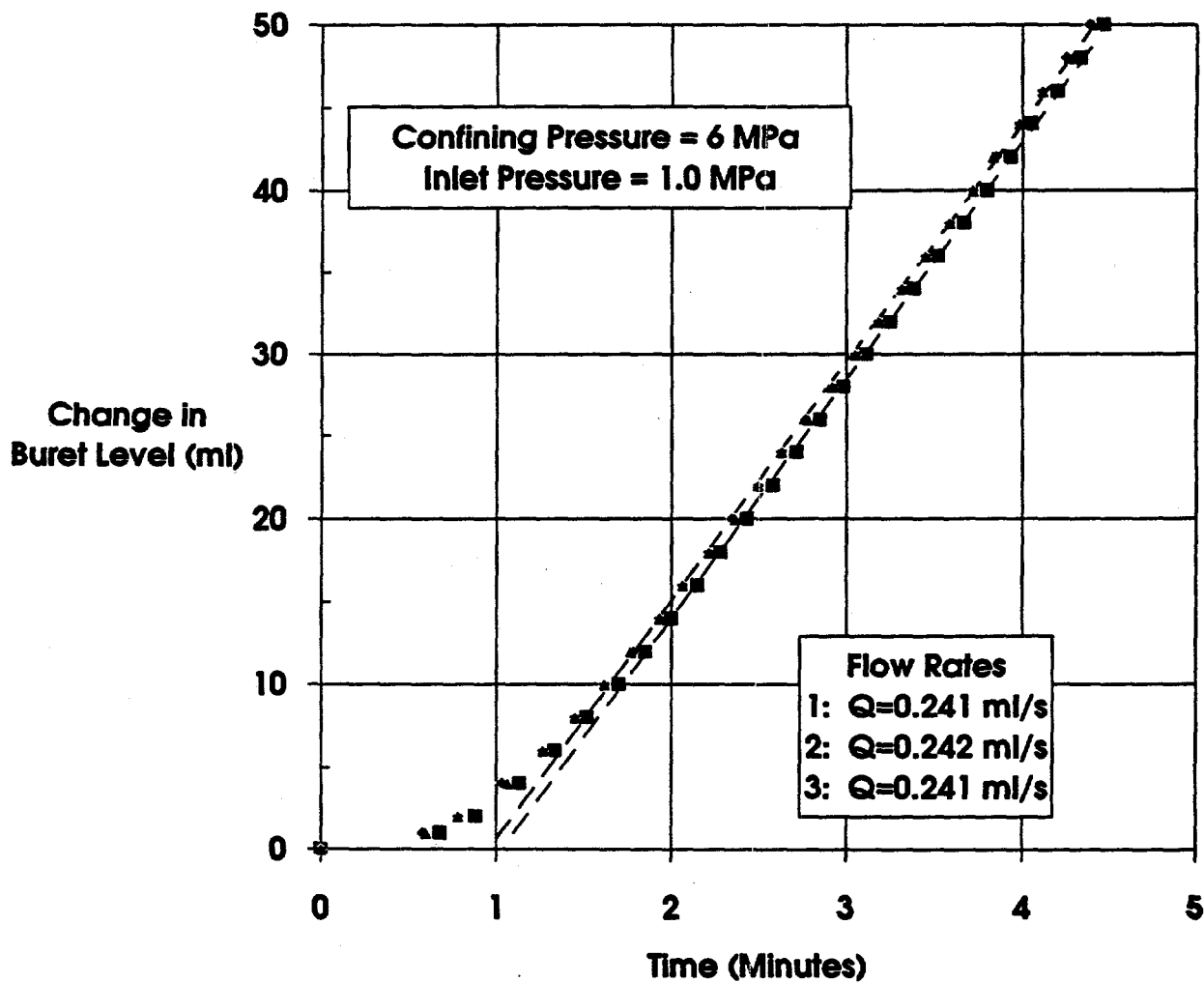
Figure G-22. Gas volume-versus-time for tests on Specimen P3X11-5-3-SP3 at 6 MPa confining pressure and 1.0 MPa gas inlet pressure. Symbols represent recorded data points and dashed lines are best fits to linear sections of data.
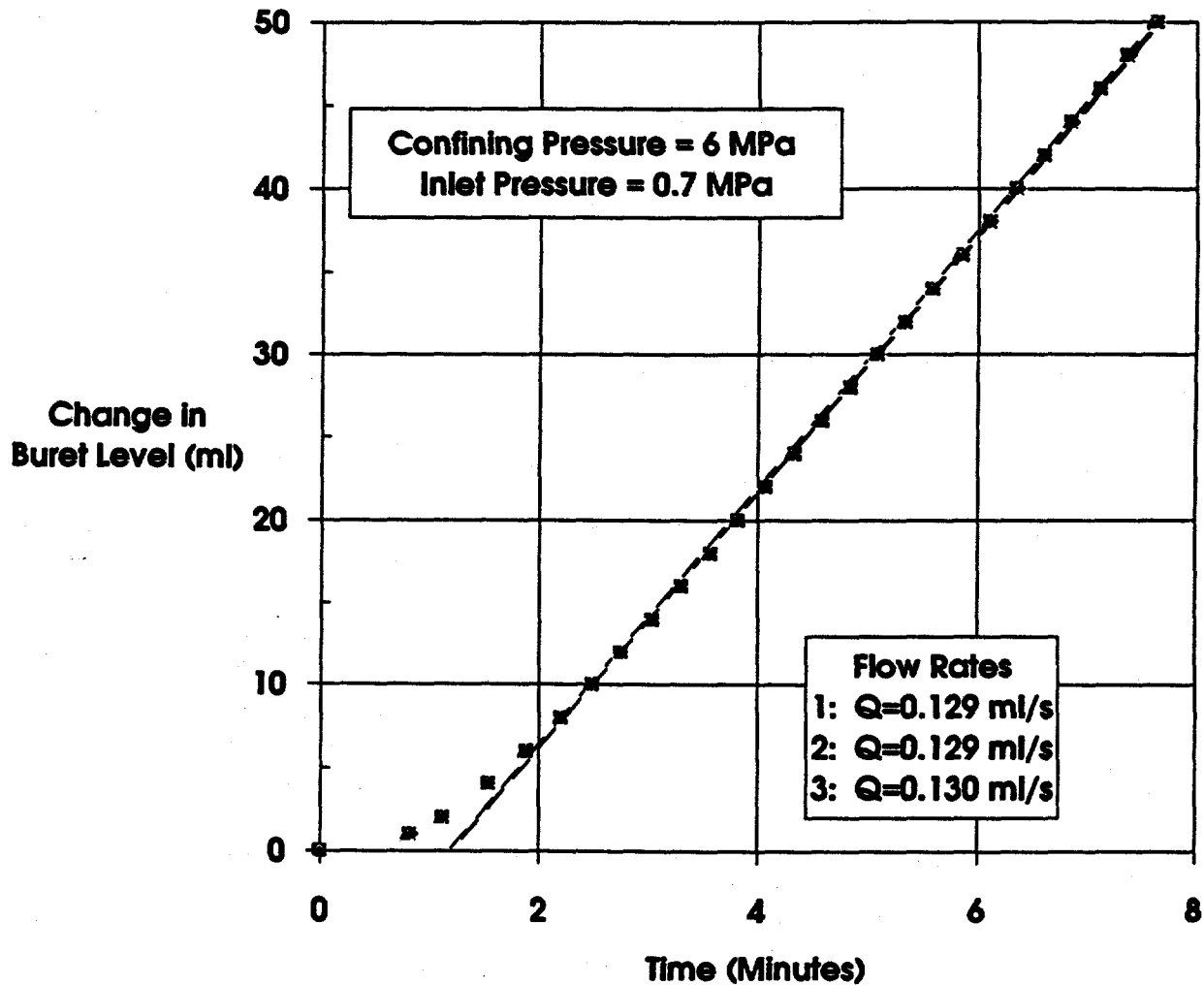
Figure G-23. Gas volume-versus-time for tests on Specimen P3X11-5-3-SP3 at 6 MPa confining pressure and 0.7 MPa gas inlet pressure. Symbols represent recorded data points and dashed lines are best fits to linear sections of data.
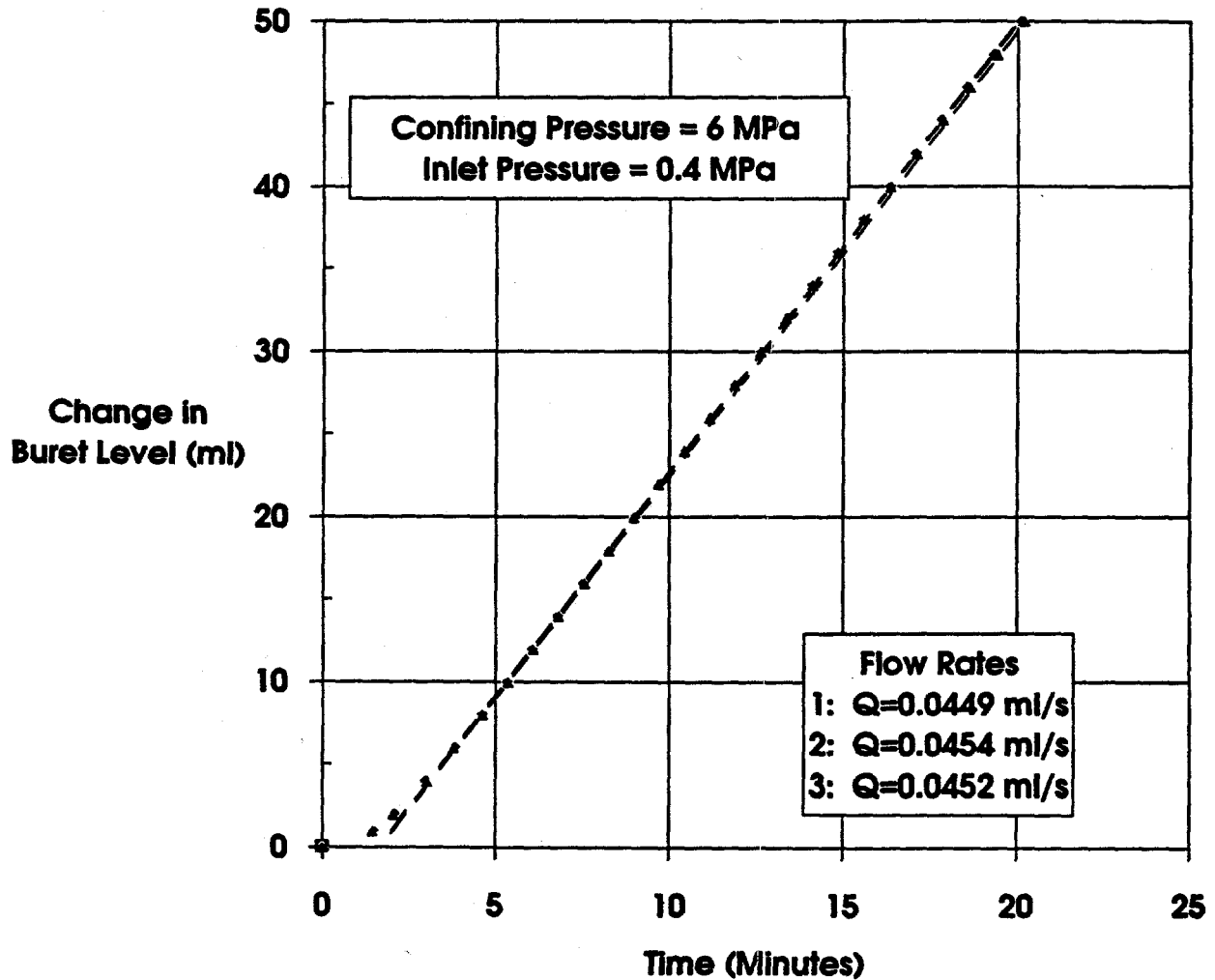
B-231

Figure G-24. Gas volume-versus-time for tests on Specimen P3X11-5-3-SP3 at 6 MPa confining pressure and 0.4 MPa gas inlet pressure. Symbols represent recorded data points and dashed lines are best fits to linear sections of data.
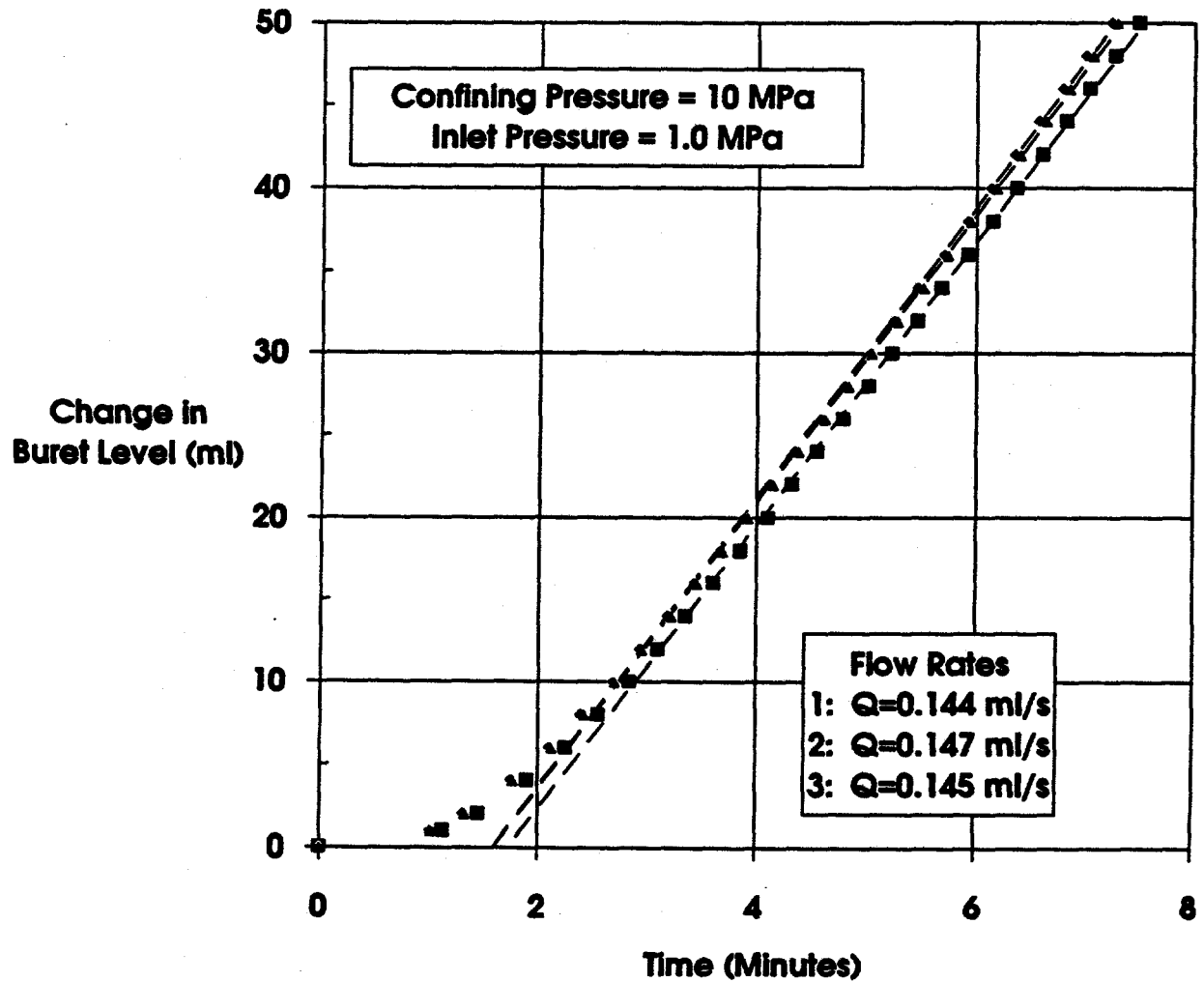
Figure G-25. Gas volume-versus-time for tests on Specimen P3X11-5-3-SP3 at 10 MPa confining pressure and 1.0 MPa gas inlet pressure. Symbols represent recorded data points and dashed lines are best fits to linear sections of data.
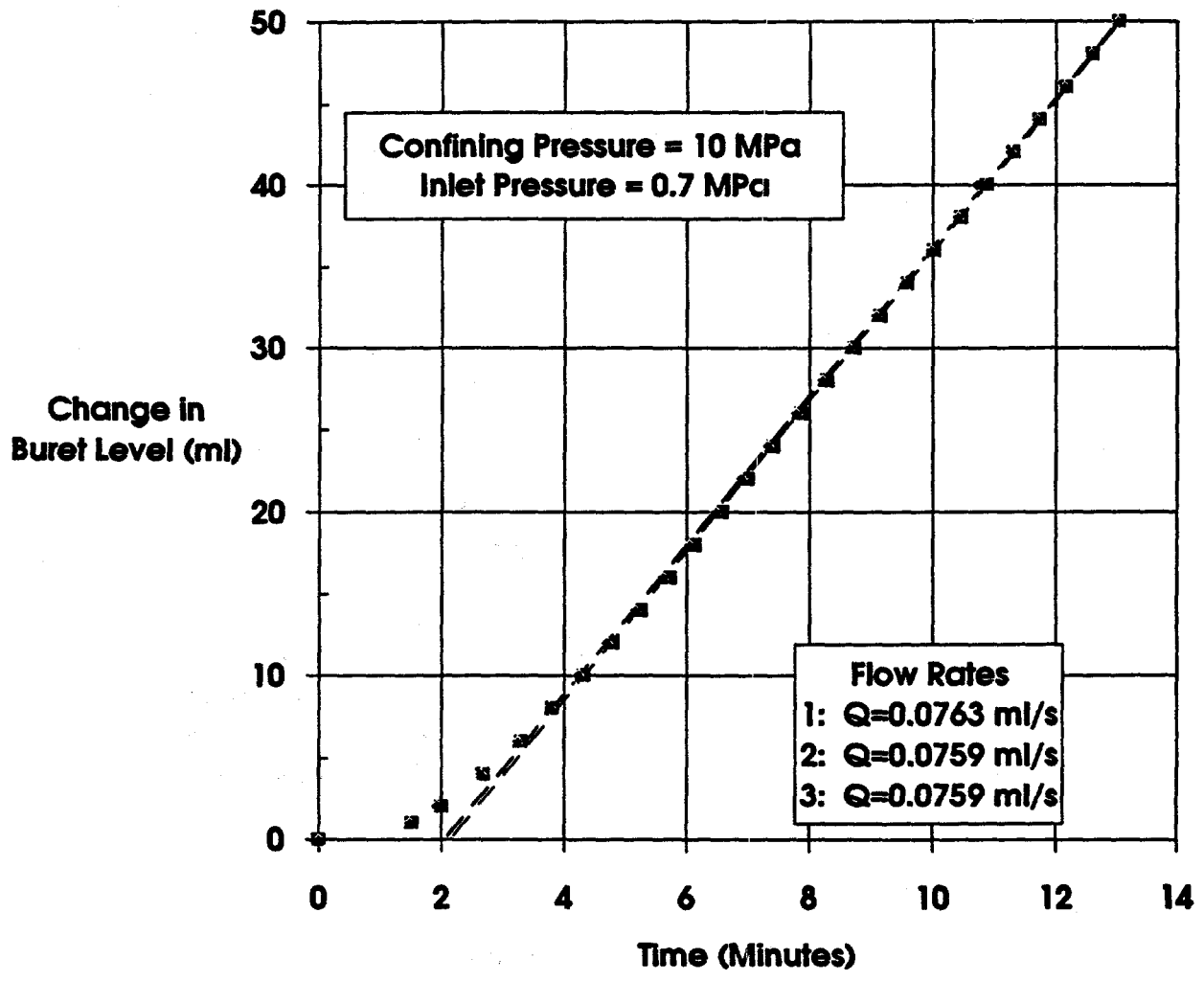
Figure G-26. Gas volume-versus-time for tests on Specimen P3X11-5-3-SP3 at 10 MPa confining pressure and 0.7 MPa gas inlet pressure. Symbols represent recorded data points and dashed lines are best fits to linear sections of data.
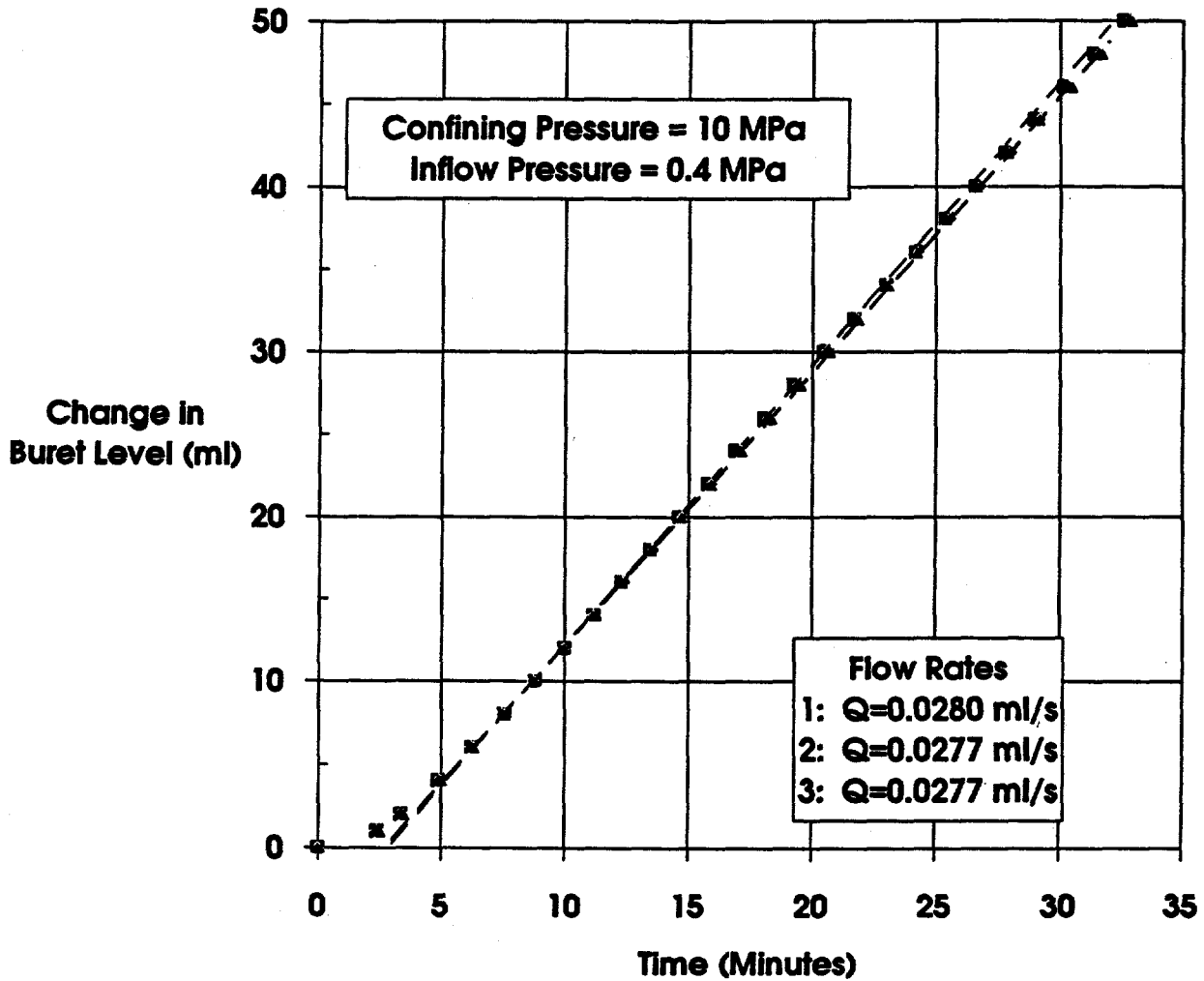
Figure G-27. Gas volume-versus-time for tests on Specimen P3X11-5-3-SP3 at 10 MPa confining pressure and 0.4 MPa gas inlet pressure. Symbols represent recorded data points and dashed lines are best fits to linear sections of data.

APPENDIX B.H. FLOW RATE-VERSUS-PORE PRESSURE DIFFERENCE ACROSS SPECIMEN FOR GAS PERMEABILITY TESTS

Figures

Confining Pressure = 2 MPa

Flow Rate (ml/min)

Gas Pressure Difference (MPa)

RSI-248-03-085

Figure H-1. Flow rate-versus-gas pressure difference difference for Specimen P3X11-5-2-SP1 at 2 MPa confining pressure and all gas inlet pressures.
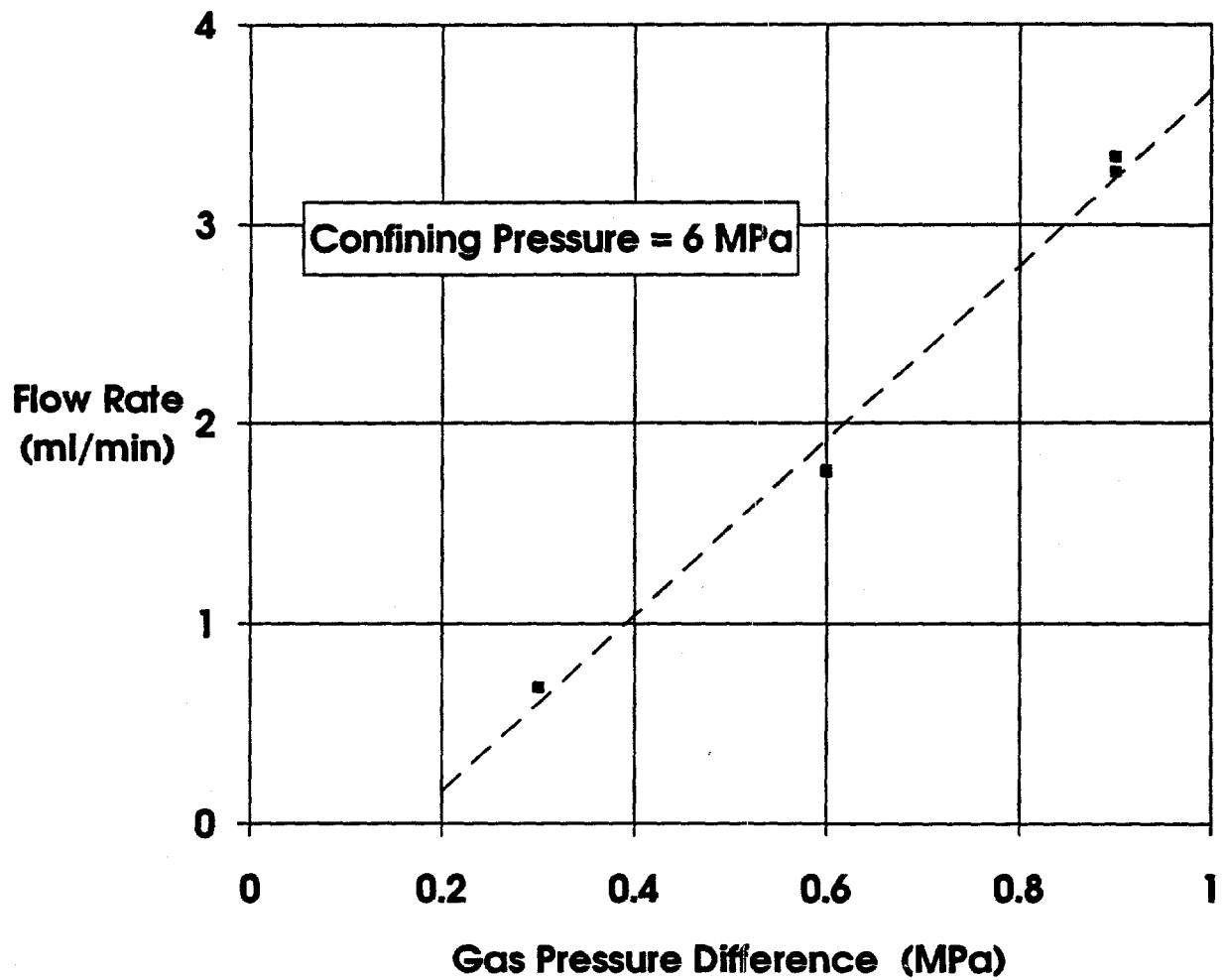
Figure H-2. Flow rate-versus-gas pressure difference difference for Specimen P3X11-5-2-SP1 at 6 MPa confining pressure and all gas inlet pressures.

Confining Pressure = 10 MPa
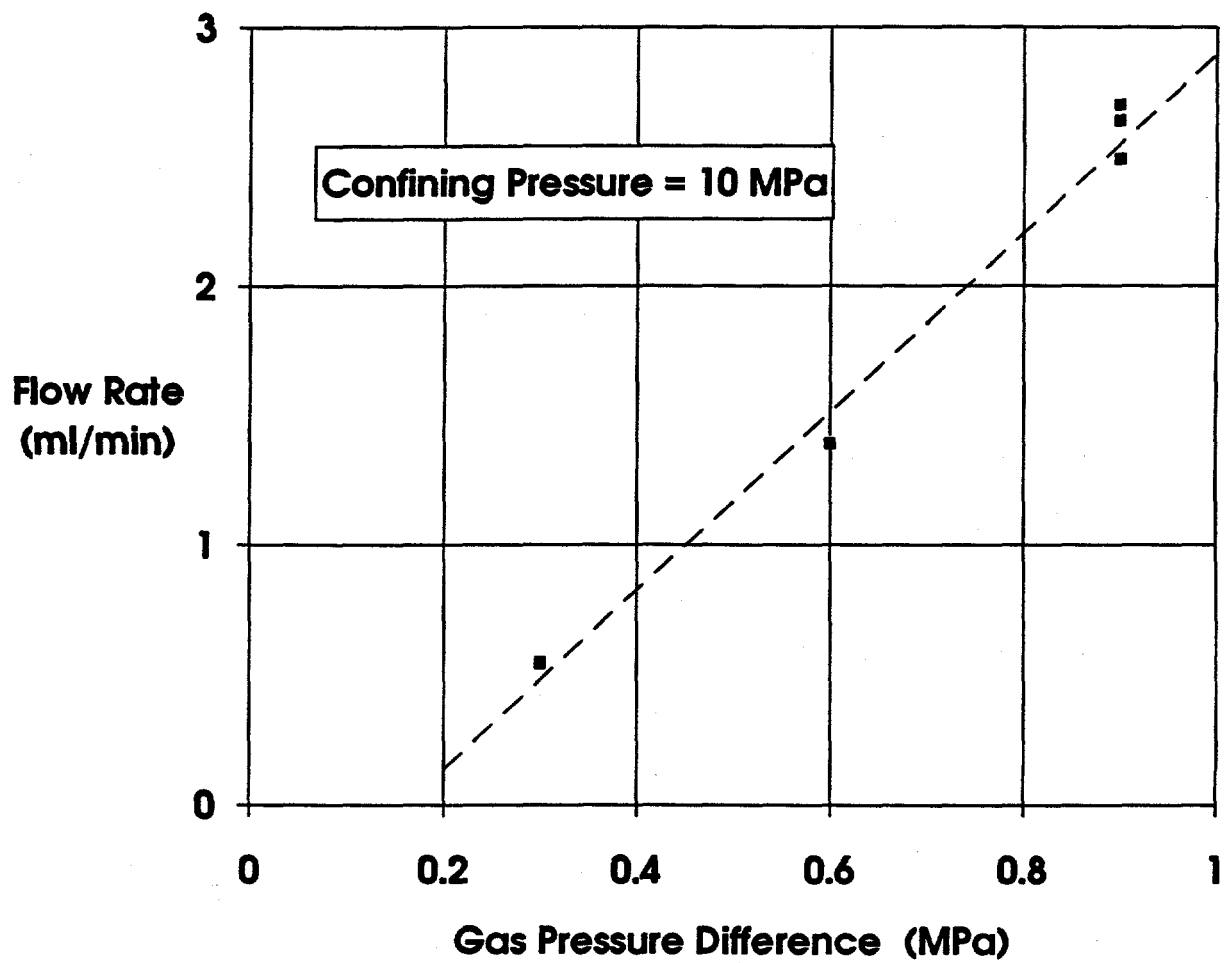
RSI-248-93-087

Figure H-3. Flow rate-versus-gas pressure difference difference for Specimen P3X11-5-2-SP1 at 10 MPa confining pressure and all gas inlet pressures.
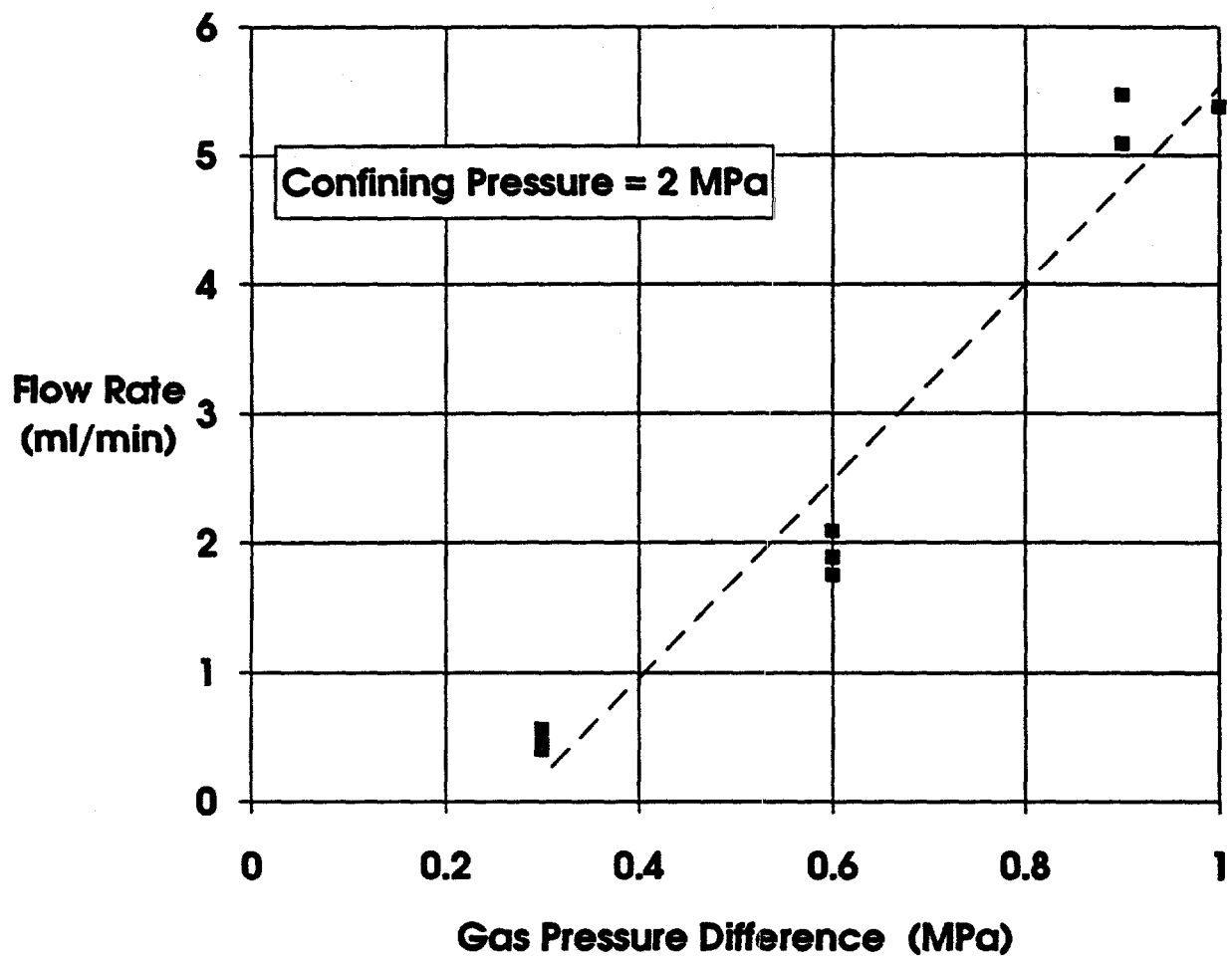
Figure H-4. Flow rate-versus-gas pressure difference difference for Specimen P3X10-6-SP2 at 2 MPa confining pressure and all gas inlet pressures.
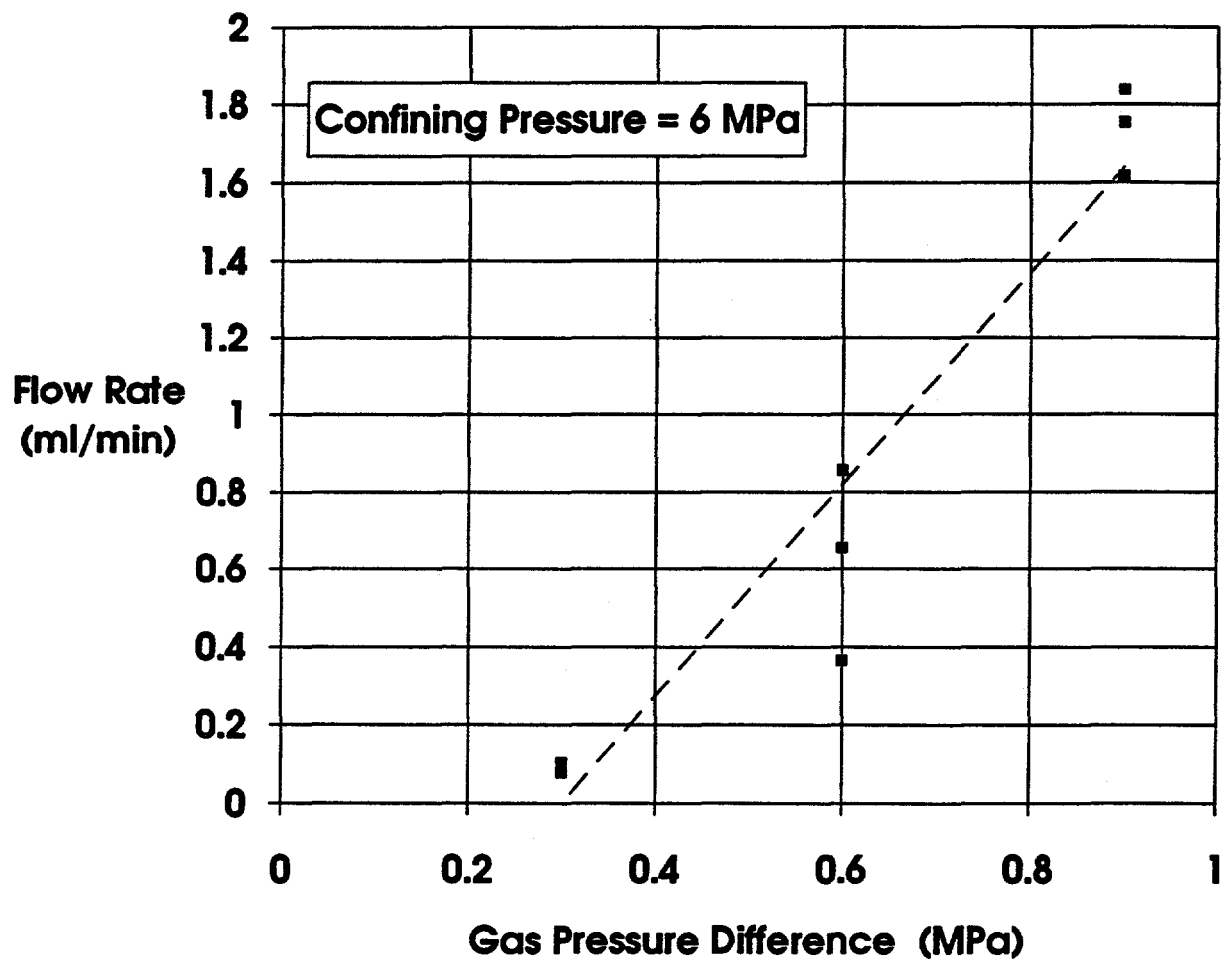
Figure H-5. Flow rate-versus-gas pressure difference difference for Specimen P3X10-6-SP2 at 6 MPa confining pressure and all gas inlet pressures.
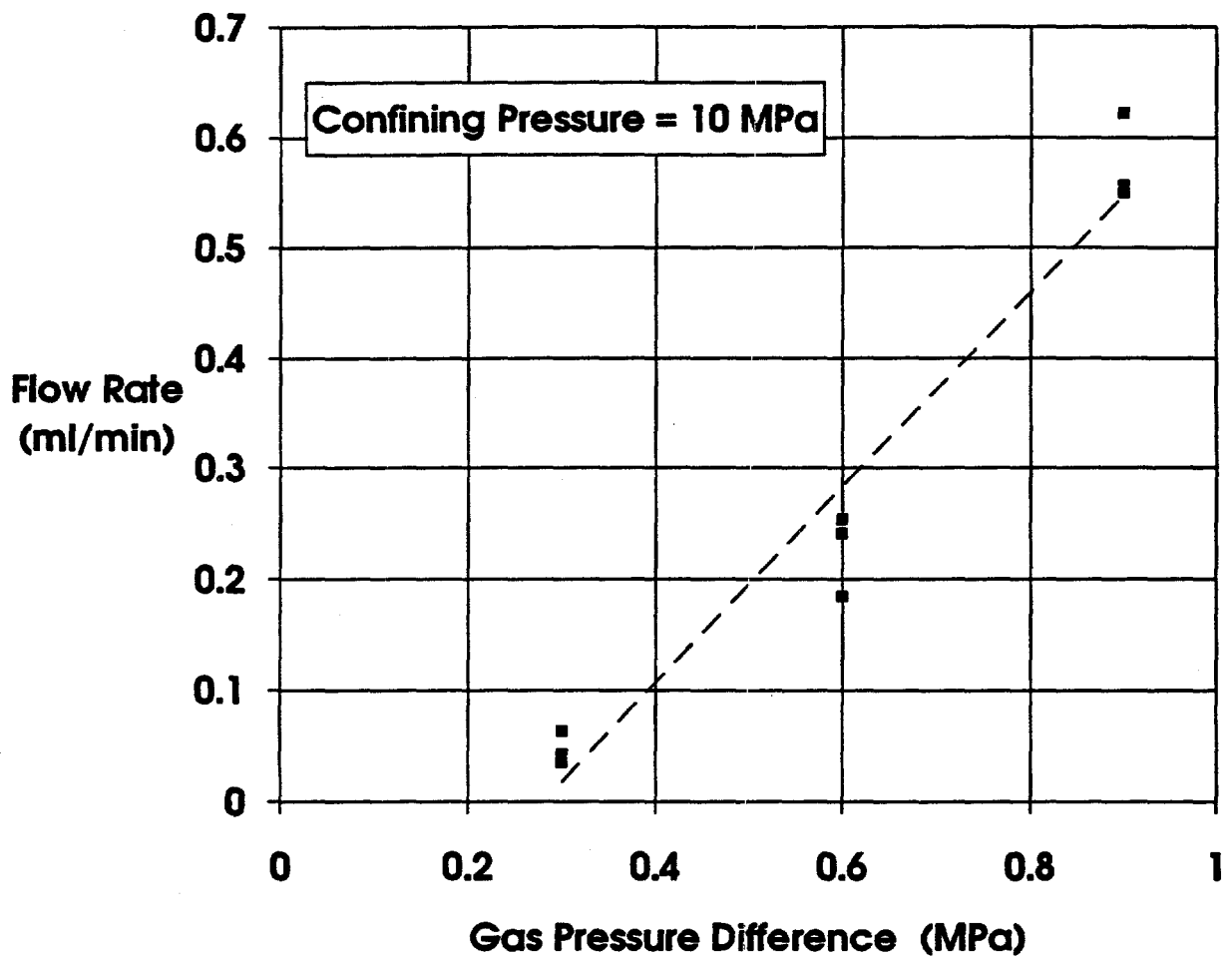
RSI-248-93-090

Figure H-6. Flow rate-versus-gas pressure difference difference for Specimen P3X10-6-SP2 at 10 MPa confining pressure and all gas inlet pressures.

Confining Pressure = 2 MPa

Flow Rate (ml/min) vs Gas Pressure Difference (MPa)
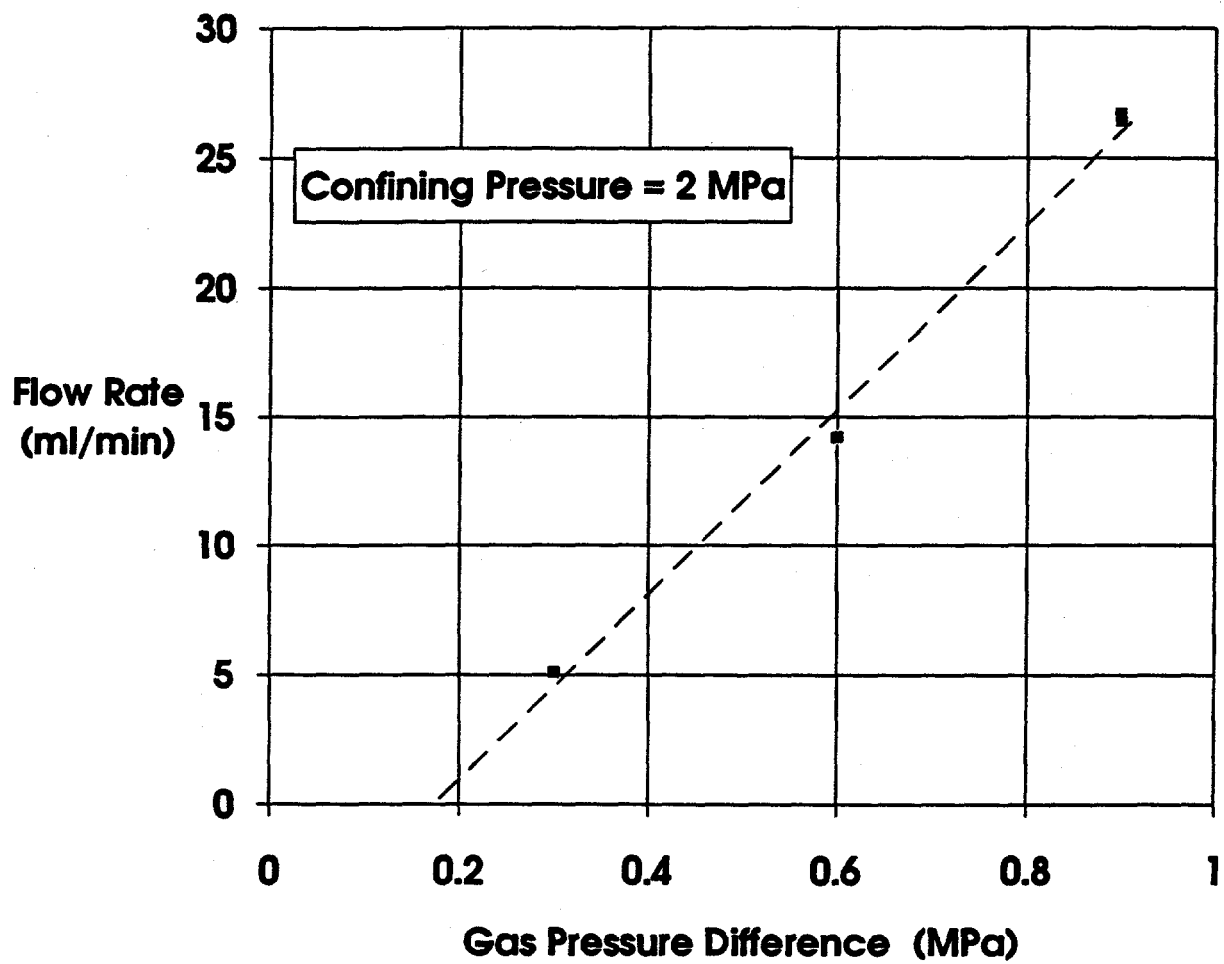
RSI-248-83-091

Figure H-7.   Flow rate-versus-gas pressure difference difference for Specimen P3X11-5-3-SP3 at 2 MPa confining pressure and all gas inlet pressures.
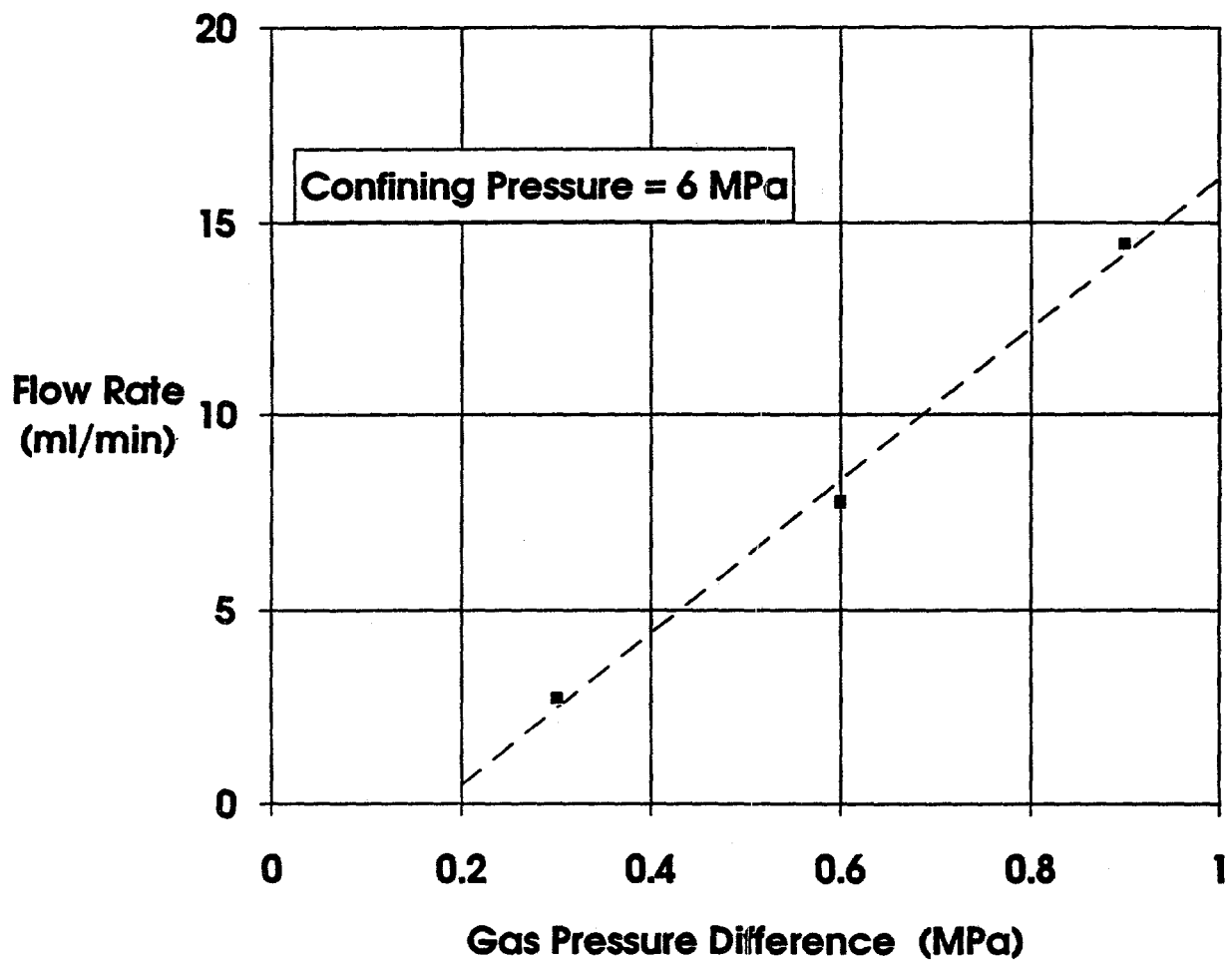
Figure H-8. Flow rate-versus-gas pressure difference difference for Specimen P3X11-5-3-SP3 at 6 MPa confining pressure and all gas inlet pressures.

Confining Pressure = 10 MPa

Flow Rate (ml/min)

Gas Pressure Difference (MPa)
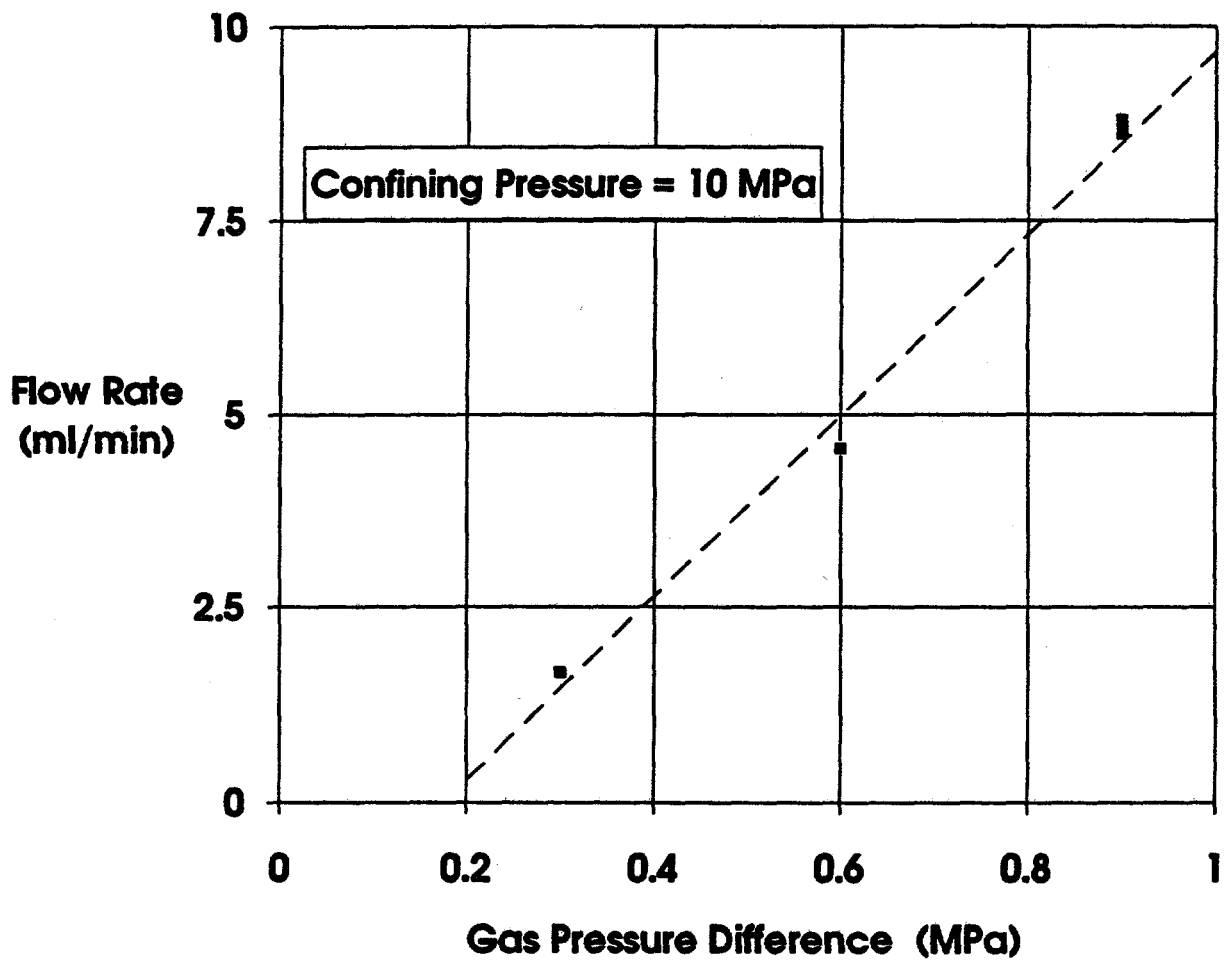
RSI-248-93-093

Figure H-9. Flow rate-versus-gas pressure difference difference for Specimen P3X11-5-3-SP3 at 10 MPa confining pressure and all gas inlet pressures.

APPENDIX B.I
FLOW-VERSUS-TIME DATA FOR ALL BRINE PERMEABILITY TESTS

Figures

Figures (continued)

Figures (continued)

Confining Pressure = 2 MPa
Inflow Pressure = 1.0 MPa

Flow Rates:
Q1 = 3.35E-03 ml/s +/- 0.2 %
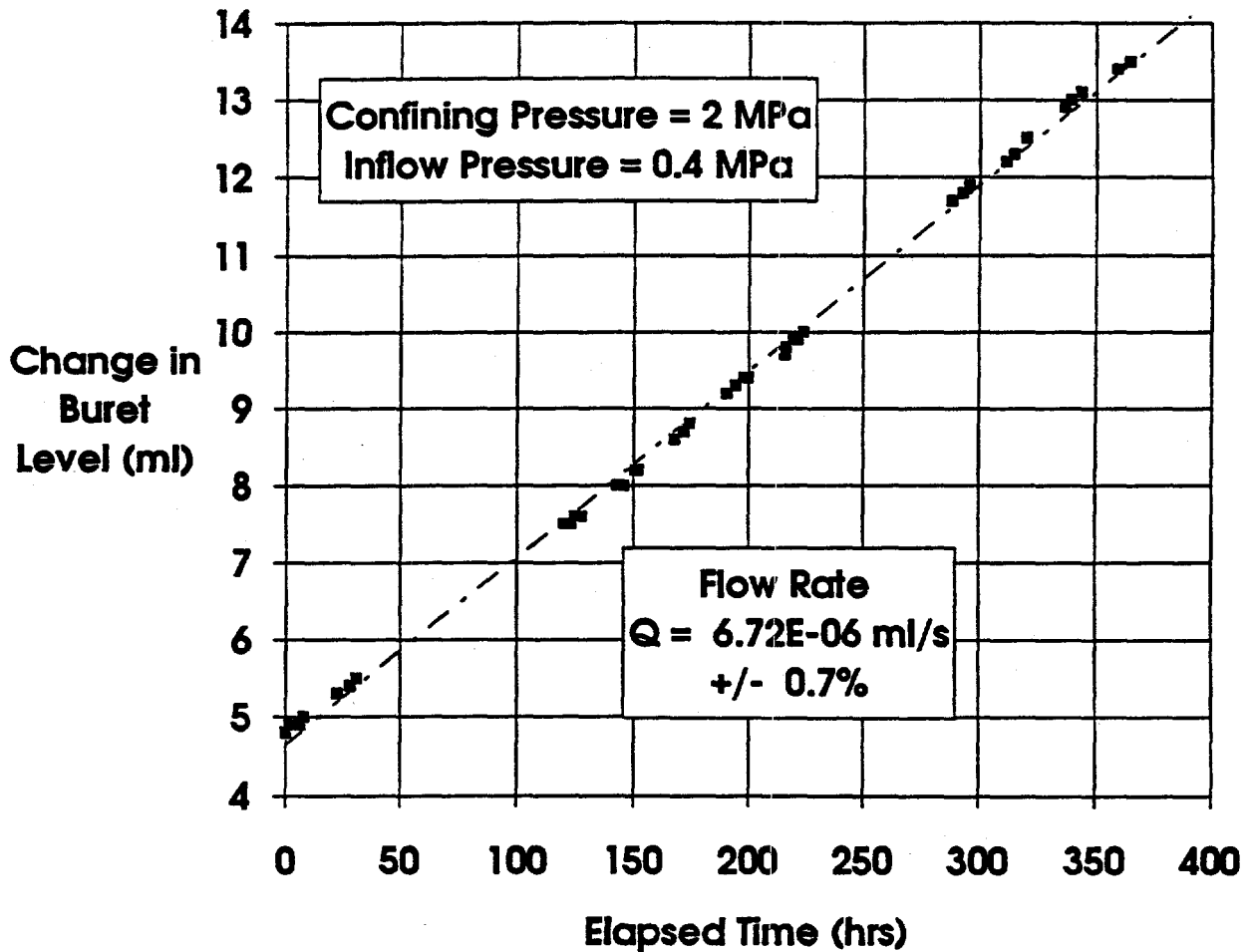Q2 = 3.43E-03 ml/s +/- 0.3 %

RSI-249-94-001

Figure I-1. Change in exit buret level (brine volume)-versus-time for tests on Specimen P3X11-5-2-SP1 at 2 MPa confining pressure and 1.0 MPa brine inlet pressure. Symbols are recorded data points; dashed lines are best fits to linear sections of data. Coefficient of variation for linear least square fits are given.
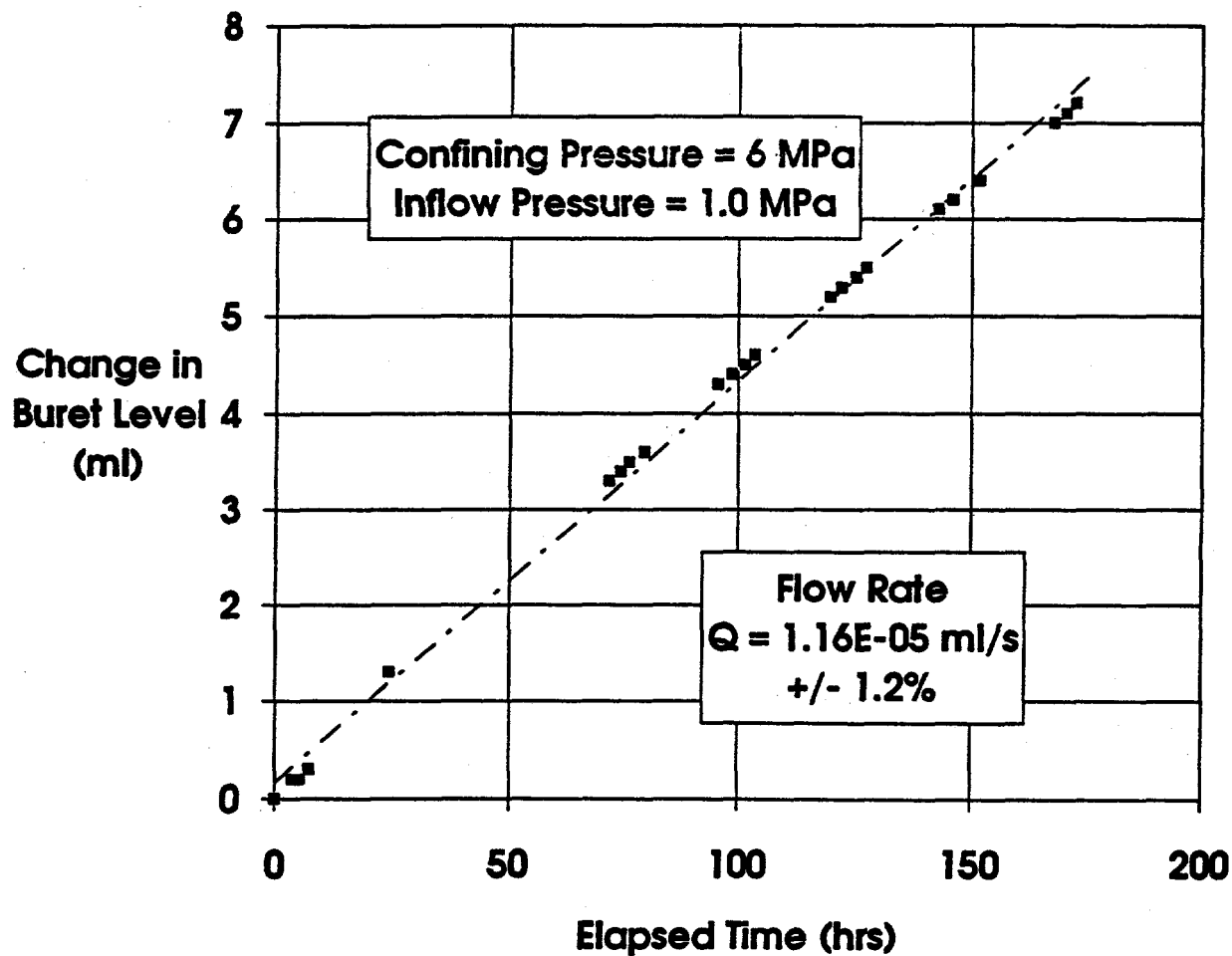
Confining Pressure = 2 MPa
Inflow Pressure = 0.7 MPa

Flow Rate:
Q = 2.02E-03 ml/s
+/- 0.2%
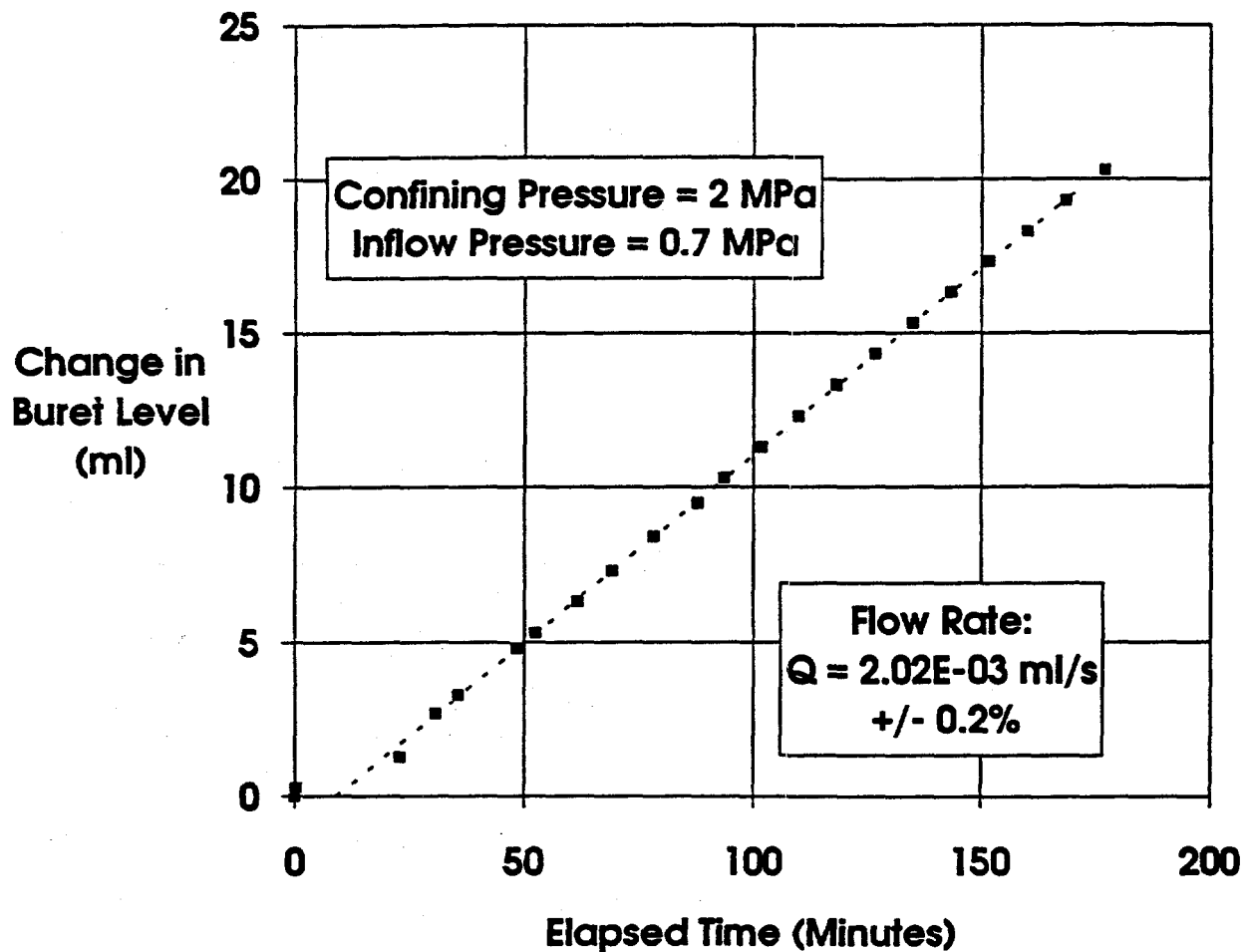
RSI-248-94-002

Figure I-2.   Change in exit buret level (brine volume)-versus-time for tests on Specimen
P3X11-5-2-SP1 at 2 MPa confining pressure and 0.7 MPa brine inlet pressure.
Symbols are recorded data points; dashed lines are best fits to linear sections of
data. Coefficient of variation for linear least square fits are given.

B-258

Confining Pressure = 2 MPa
Inflow Pressure = 0.4 MPa

Flow Rate:
Q = 8.71E-04 ml/s
+/- 0.2 %
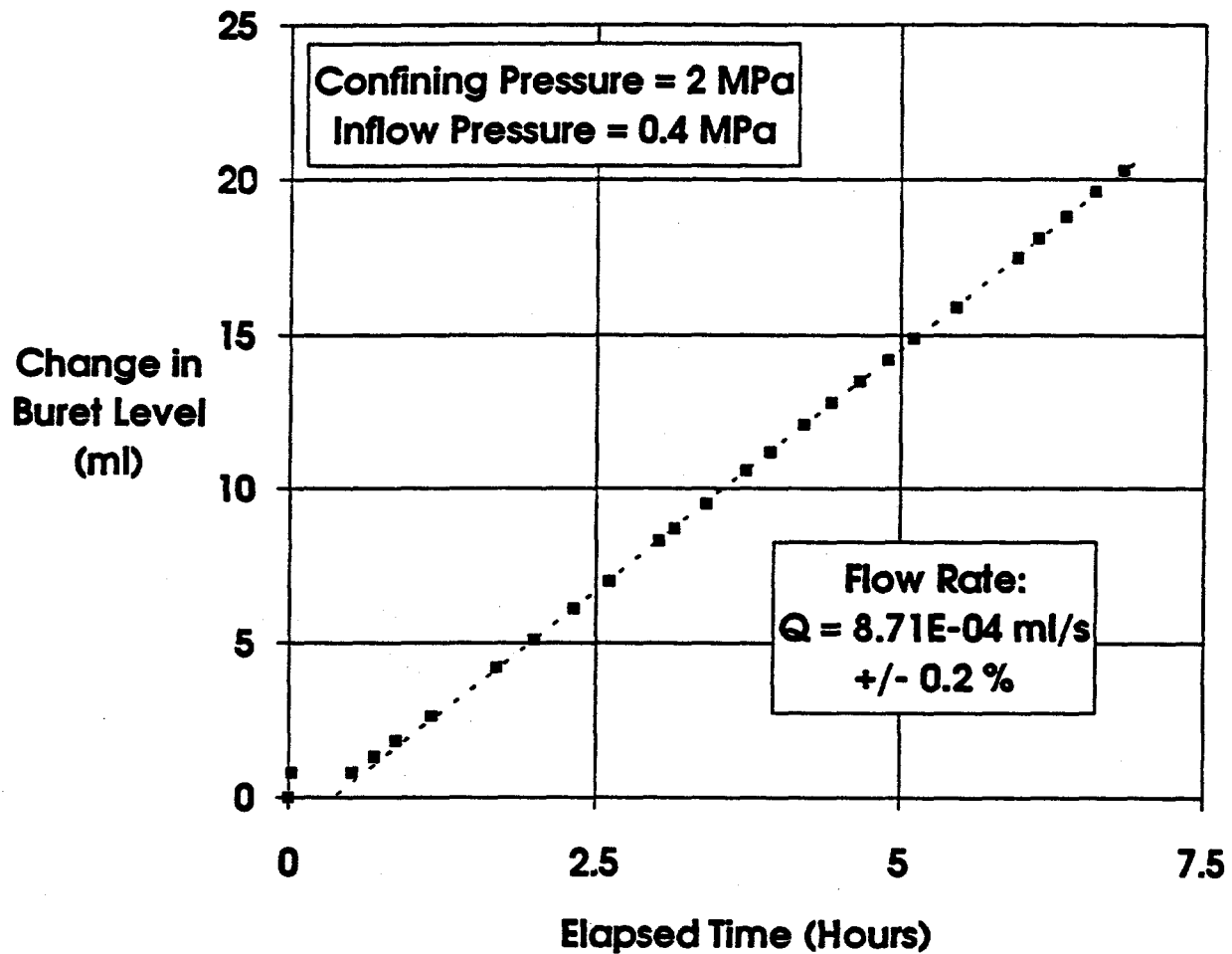
RSI-248-94-003

Figure I-3. Change in exit buret level (brine volume)-versus-time for tests on Specimen P3X11-5-2-SP1 at 2 MPa confining pressure and 0.4 MPa brine inlet pressure. Symbols are recorded data points; dashed lines are best fits to linear sections of data. Coefficient of variation for linear least square fits are given.
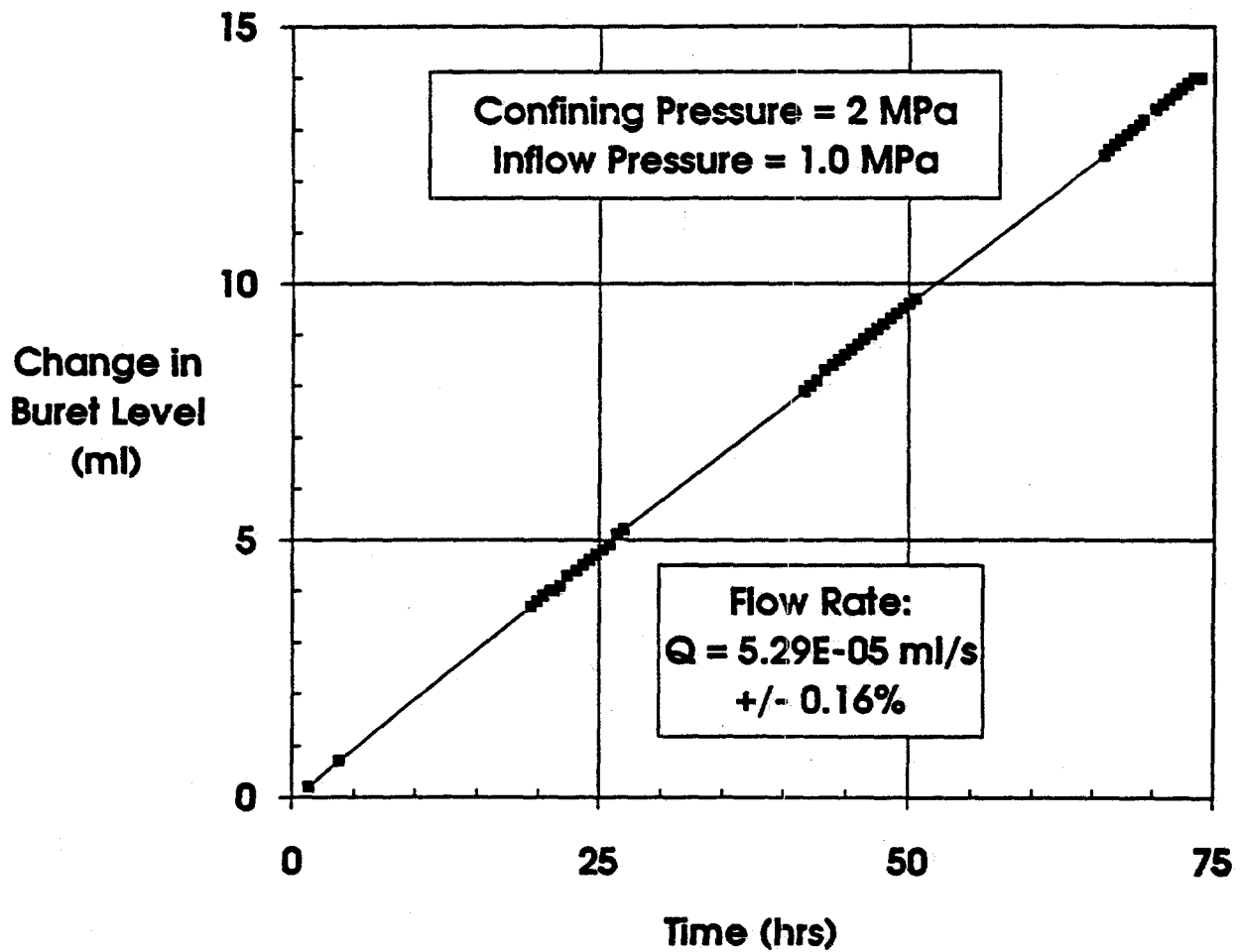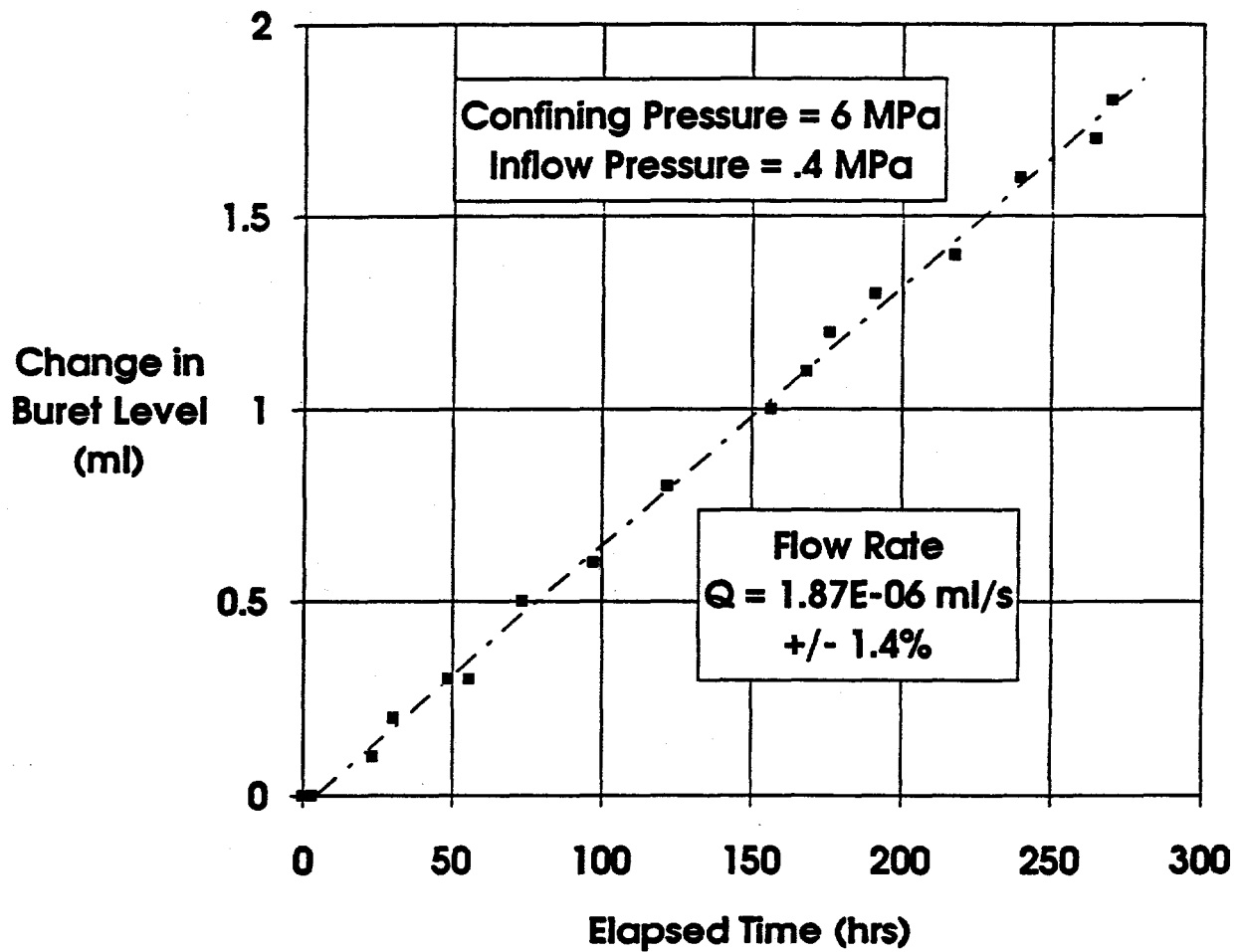
Figure I-4. Change in exit buret level (brine volume)-versus-time for tests on Specimen P3X10-6-SP2 at 2 MPa confining pressure and 1.0 MPa brine inlet pressure. Symbols are recorded data points; dashed lines are best fits to linear sections of data. Coefficient of variation for linear least square fits are given.
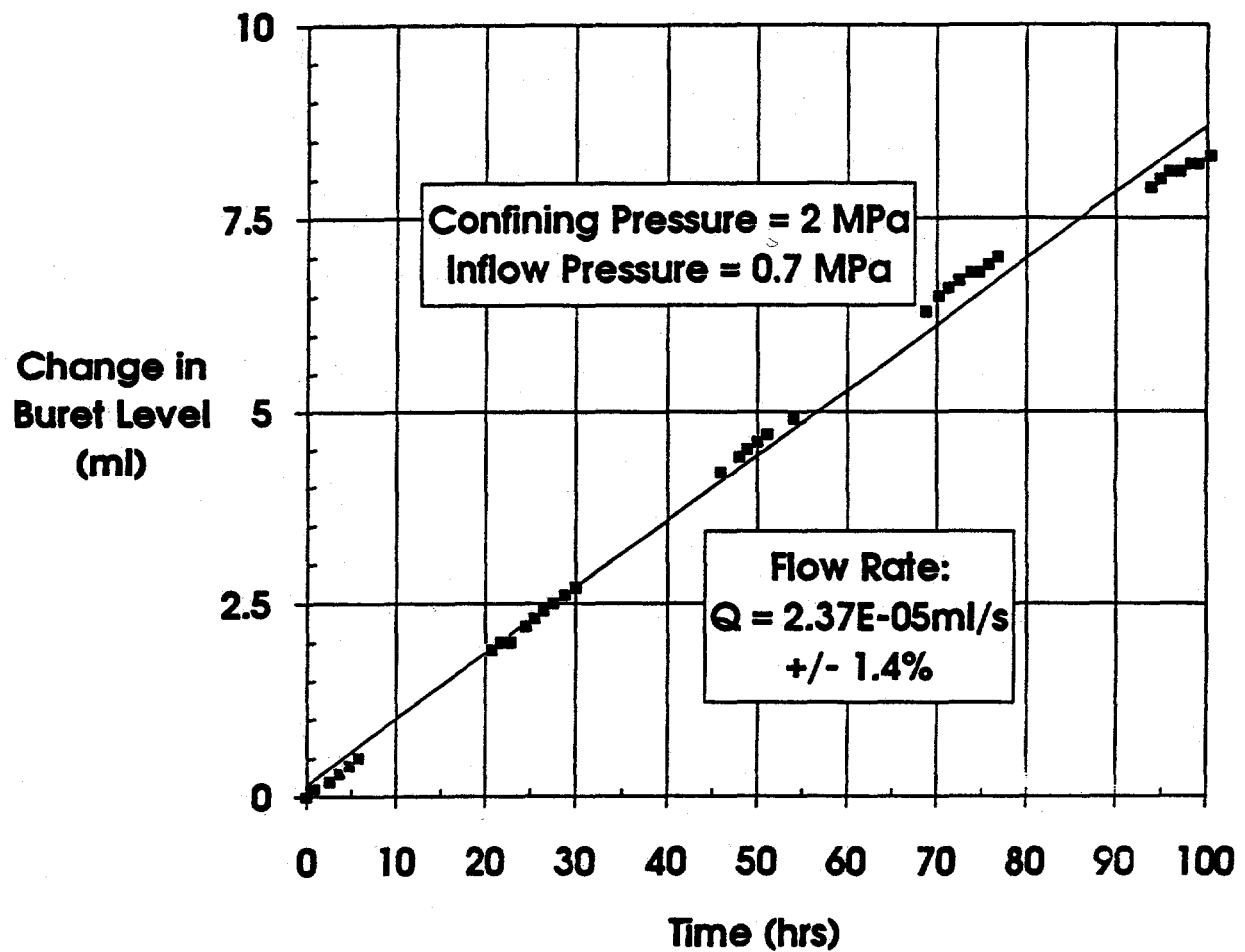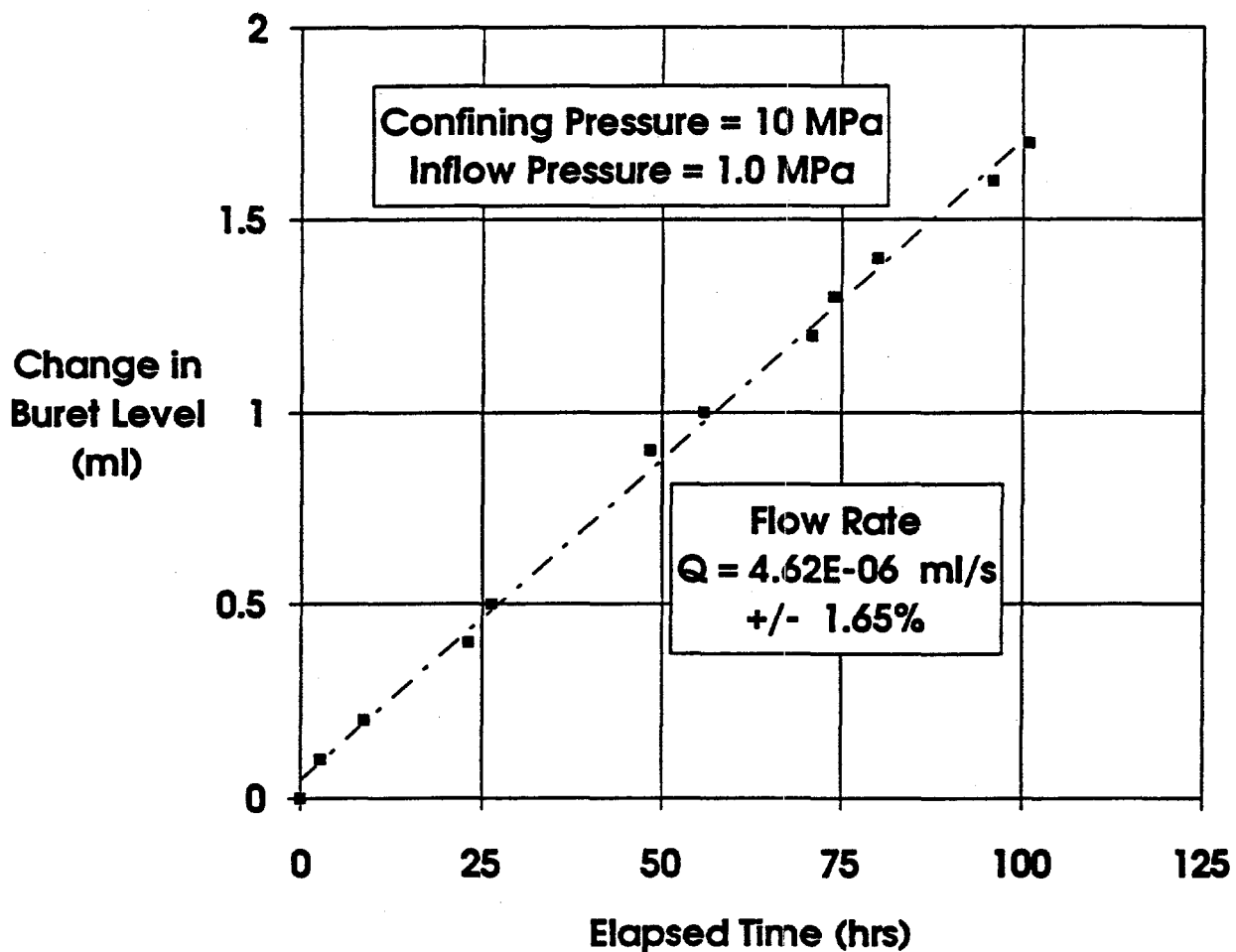
Figure I-5.   Change in exit buret level (brine volume)-versus-time for tests on Specimen
P3X10-6-SP2 at 2 MPa confining pressure and 0.7 MPa brine inlet pressure.
Symbols are recorded data points; dashed lines are best fits to linear sections of
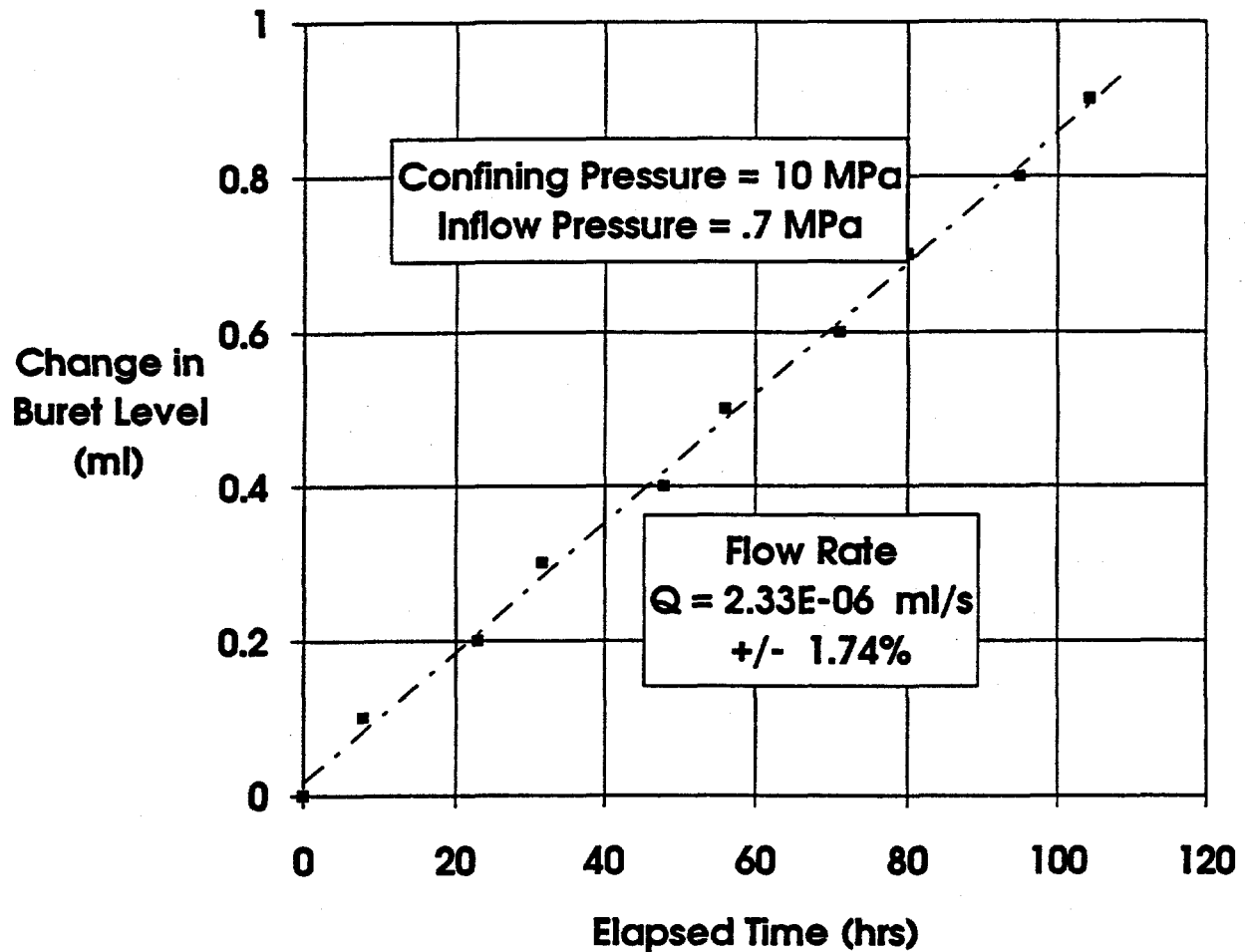data.   Coefficient of variation for linear least square fits are given.

Figure I-6. Change in exit buret level (brine volume)-versus-time for tests on Specimen P3X10-6-SP2 at 2 MPa confining pressure and 0.4 MPa brine inlet pressure. Symbols are recorded data points; dashed lines are best fits to linear sections of data. Coefficient of variation for linear least square fits are given.

Figure I-7. Change in exit buret level (brine volume)-versus-time for tests on Specimen P3X10-6-SP2 at 6 MPa confining pressure and 1.0 MPa brine inlet pressure. Symbols are recorded data points; dashed lines are best fits to linear sections of data. Coefficient of variation for linear least square fits are given.
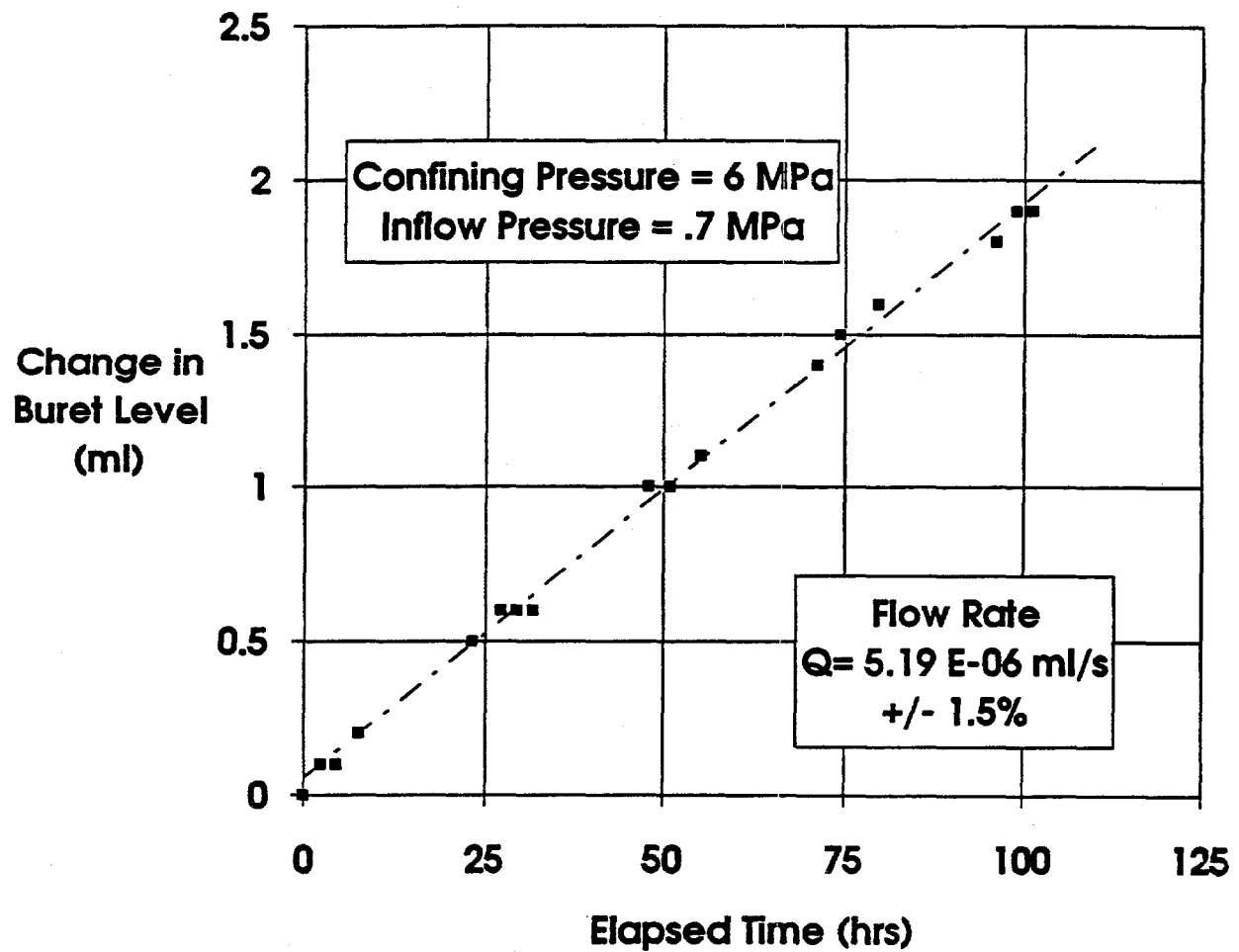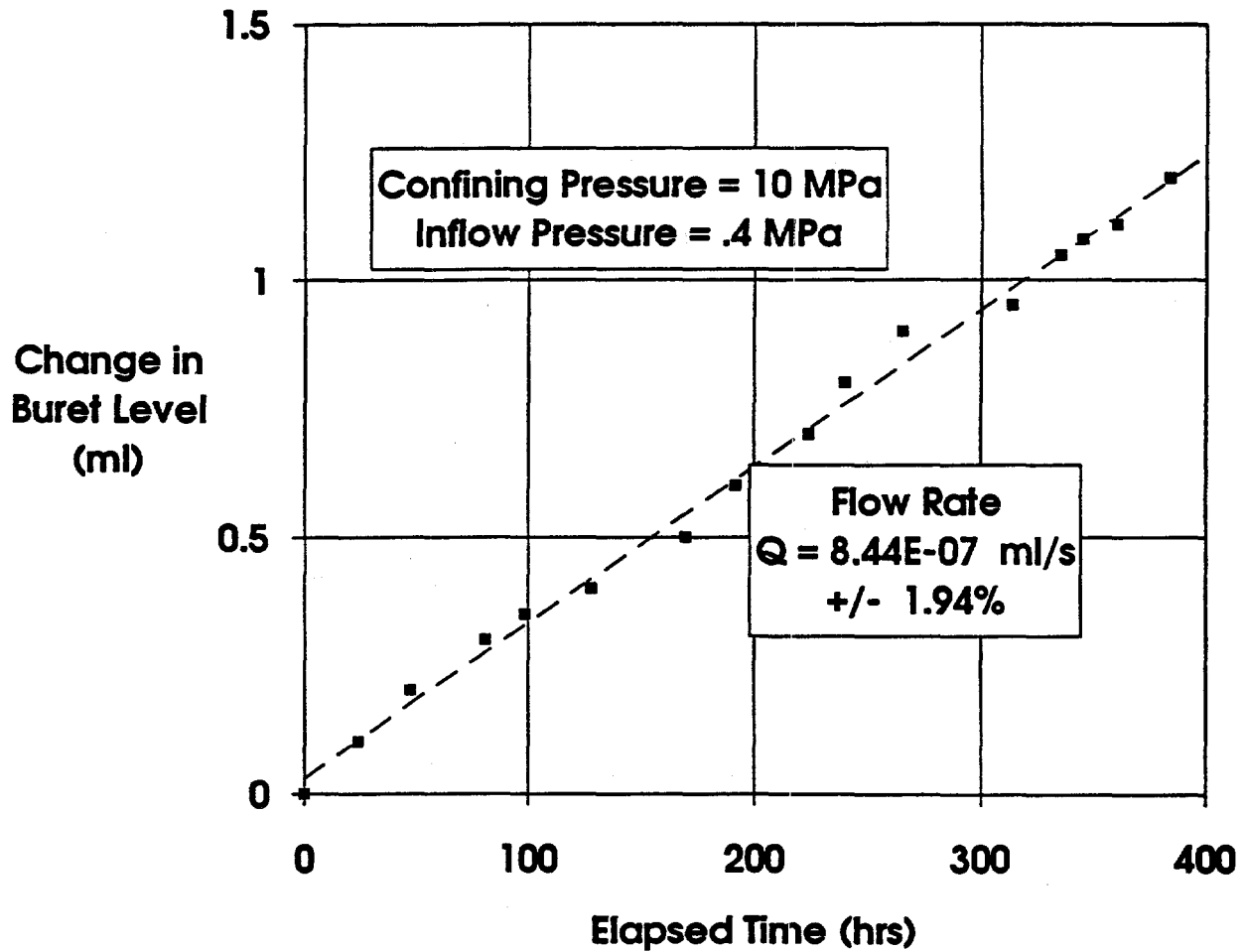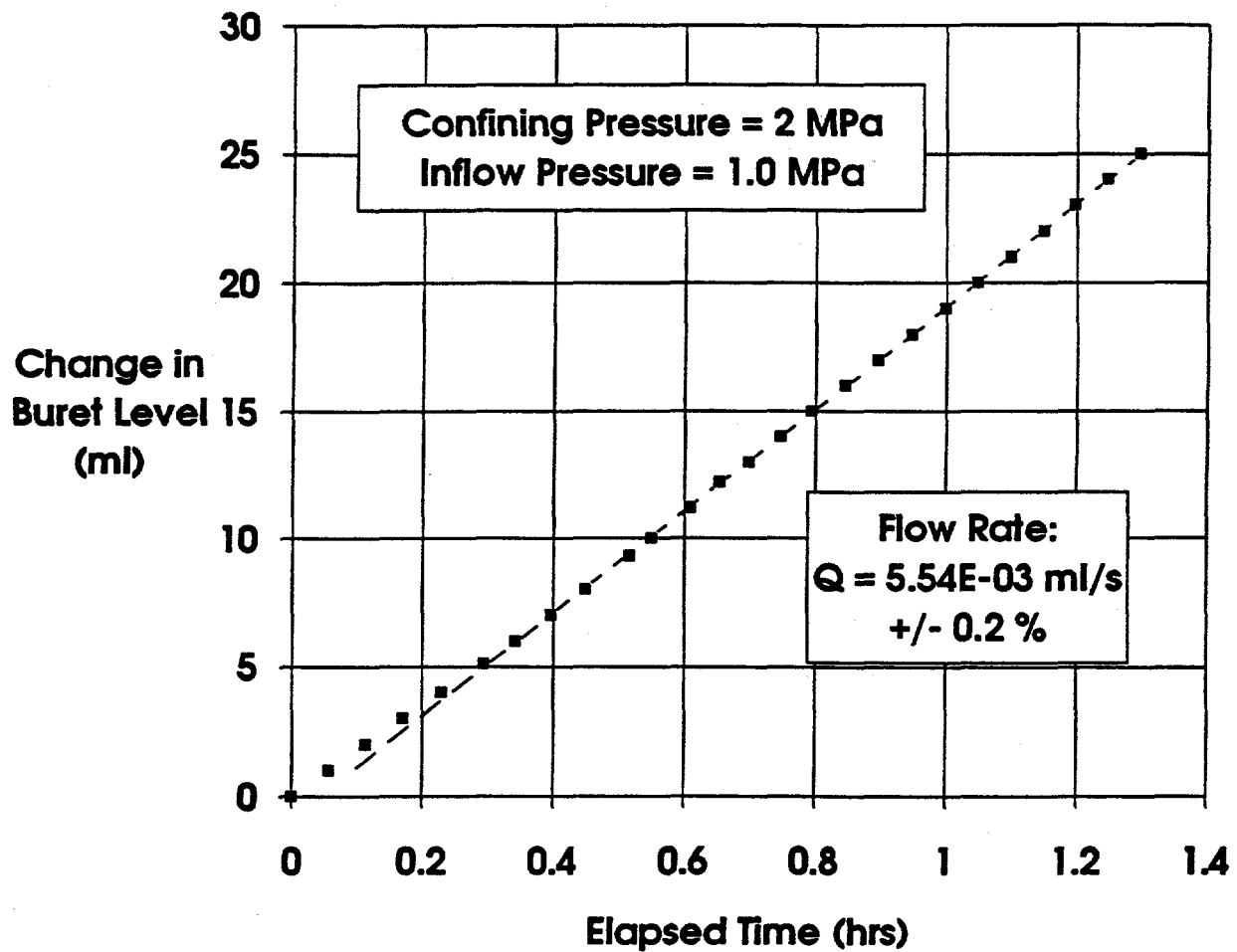
Figure I-8.   Change in exit buret level (brine volume)-versus-time for tests on Specimen P3X10-6-SP2 at 6 MPa confining pressure and 0.7 MPa brine inlet pressure. Symbols are recorded data points; dashed lines are best fits to linear sections of data.   Coefficient of variation for linear least square fits are given.

Confining Pressure = 6 MPa
Inflow Pressure = .4 MPa
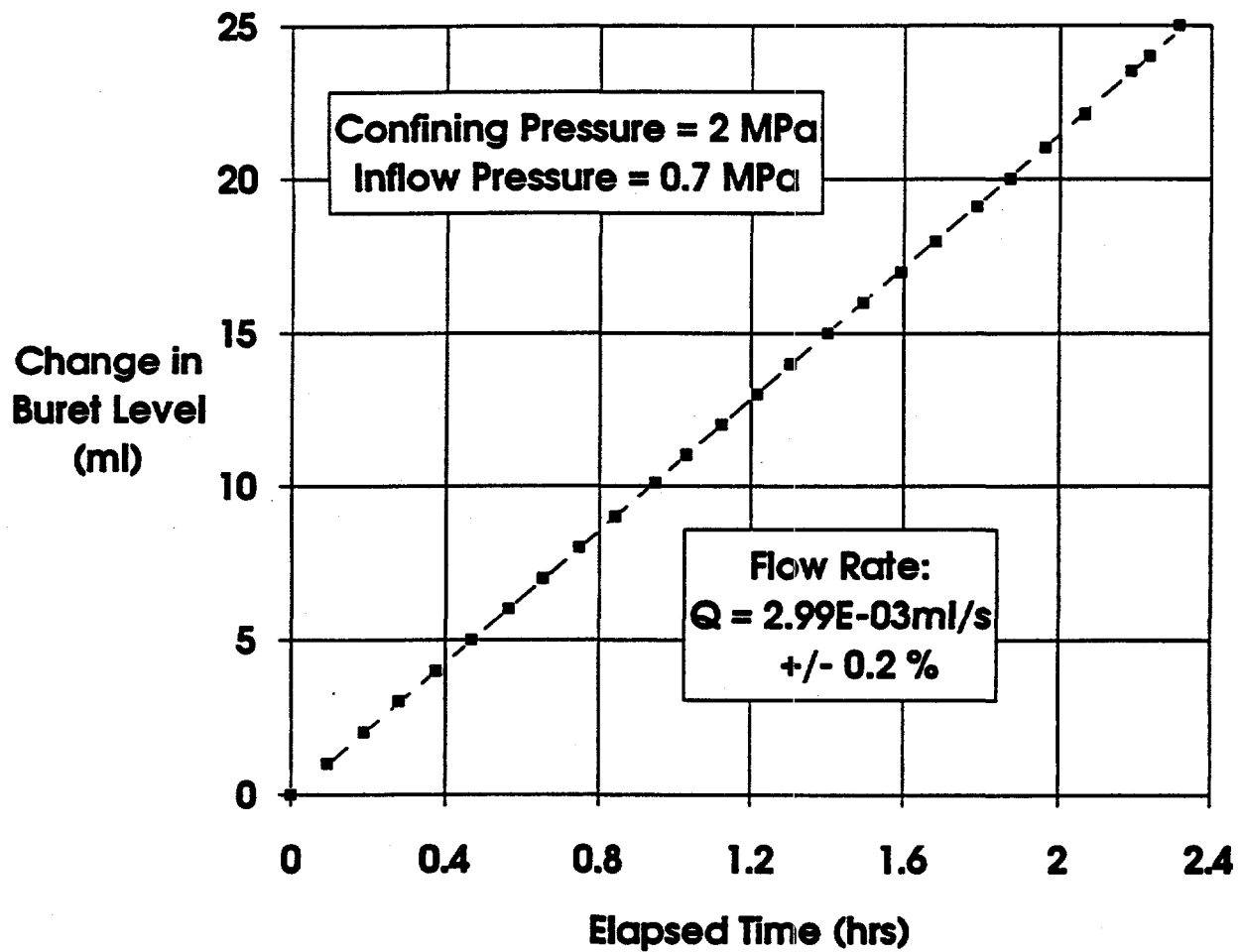
Flow Rate
Q = 1.87E-06 ml/s
+/- 1.4%

RSI-248-94-009

Figure I-9. Change in exit buret level (brine volume)-versus-time for tests on Specimen P3X10-6-SP2 at 6 MPa confining pressure and 0.4 MPa brine inlet pressure. Symbols are recorded data points; dashed lines are best fits to linear sections of data. Coefficient of variation for linear least square fits are given.

Confining Pressure = 10 MPa
Inflow Pressure = 1.0 MPa

Flow Rate
Q = 4.62E-06 ml/s
+/- 1.65%

Change in Buret Level (ml)

Elapsed Time (hrs)

Figure I-10.   Change in exit buret level (brine volume)-versus-time for tests on Specimen
P3X10-6-SP2 at 10 MPa confining pressure and 1.0 MPa brine inlet pressure.
Symbols are recorded data points; dashed lines are best fits to linear sections of
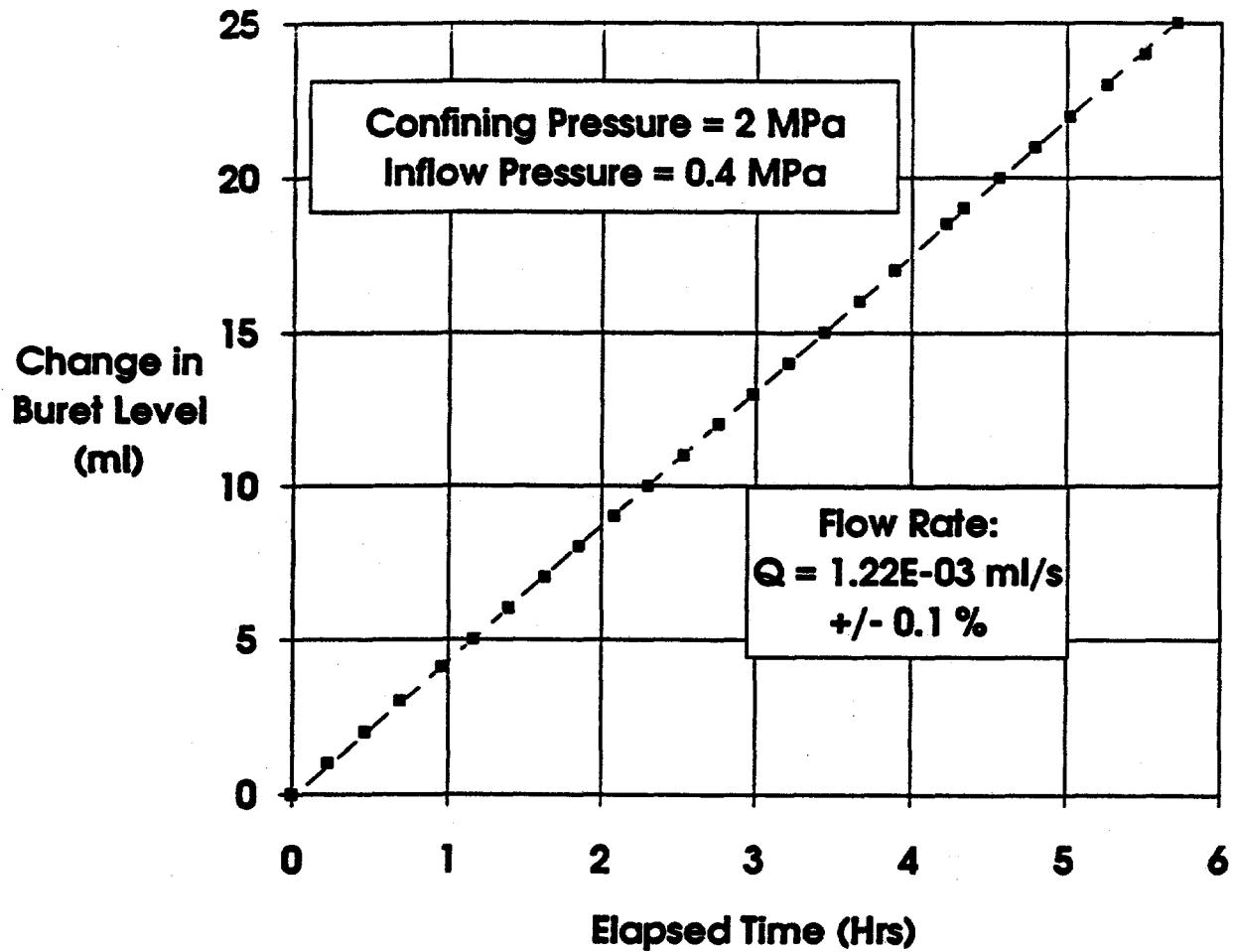data.   Coefficient of variation for linear least square fits are given.

Confining Pressure = 10 MPa
Inflow Pressure = .7 MPa

Flow Rate
Q = 2.33E-06 ml/s
+/- 1.74%

Figure I-11. Change in exit buret level (brine volume)-versus-time for tests on Specimen P3X10-6-SP2 at 10 MPa confining pressure and 0.7 MPa brine inlet pressure. Symbols are recorded data points; dashed lines are best fits to linear sections of data. Coefficient of variation for linear least square fits are given.
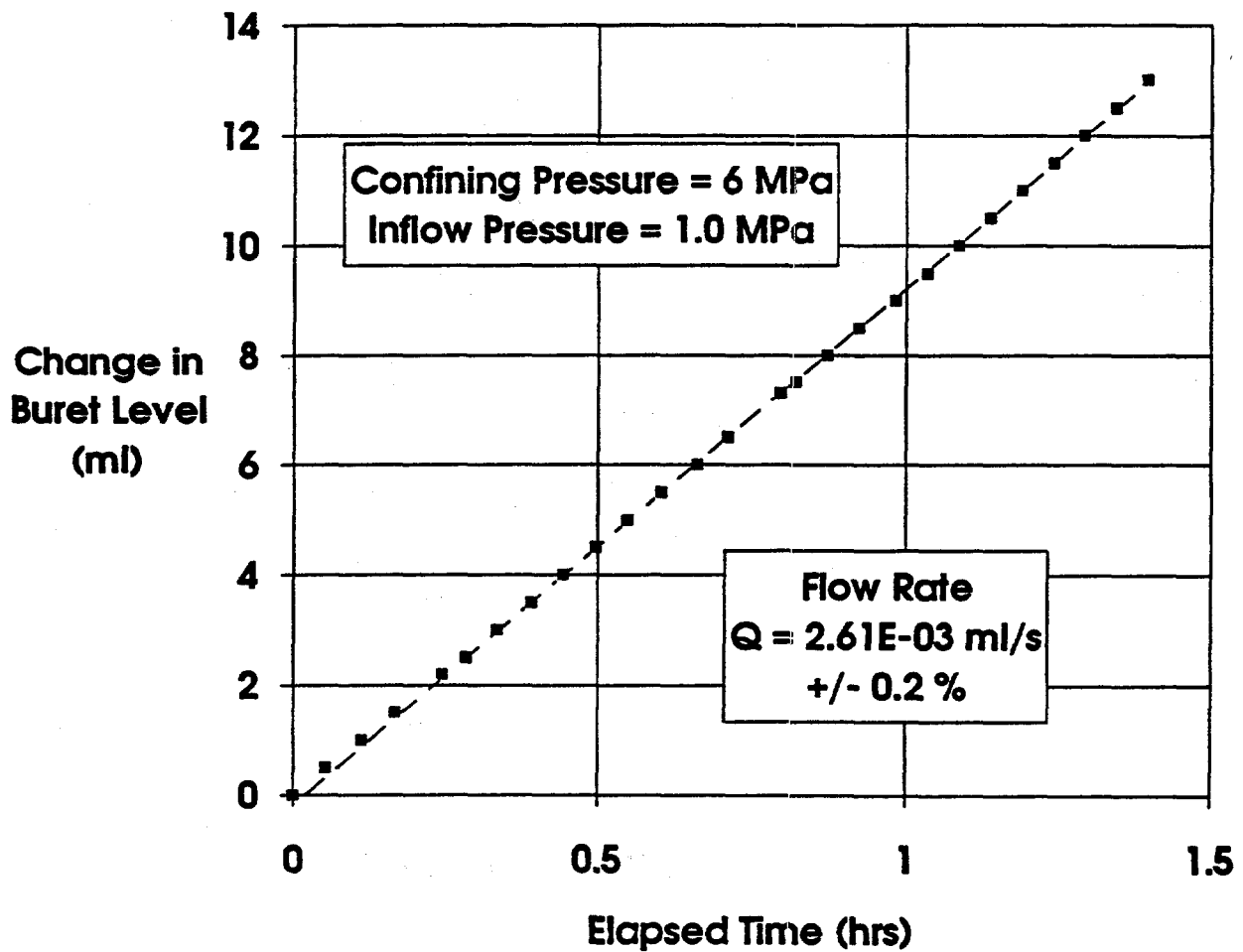
B-267

Figure I-12. Change in exit buret level (brine volume)-versus-time for tests on Specimen P3X10-6-SP2 at 10 MPa confining pressure and 0.4 MPa brine inlet pressure. Symbols are recorded data points; dashed lines are best fits to linear sections of data. Coefficient of variation for linear least square fits are given.
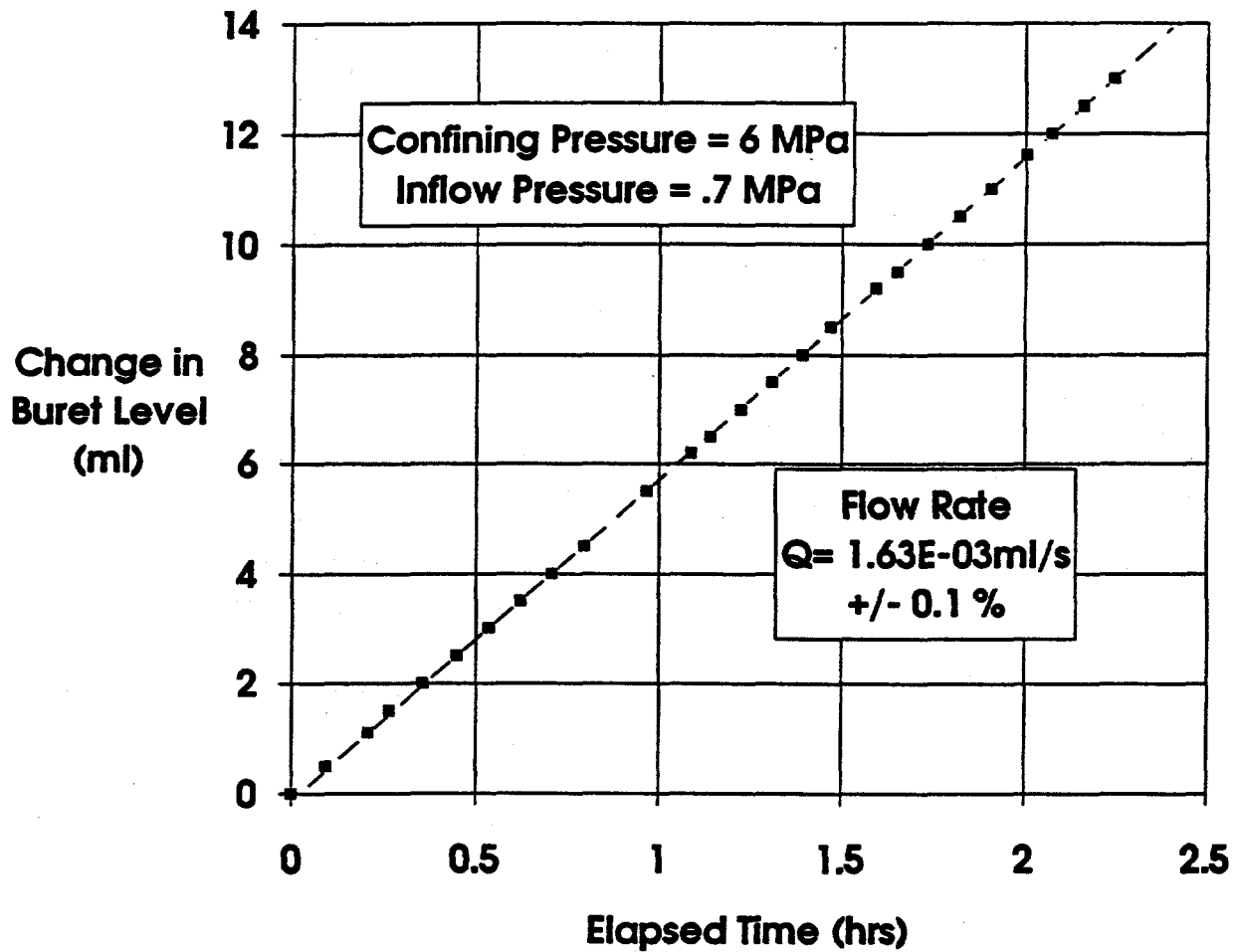
Figure I-13. Change in exit buret level (brine volume)-versus-time for tests on Specimen P3X11-5-3-SP3 at 2 MPa confining pressure and 1.0 MPa brine inlet pressure. Symbols are recorded data points; dashed lines are best fits to linear sections of data. Coefficient of variation for linear least square fits are given.
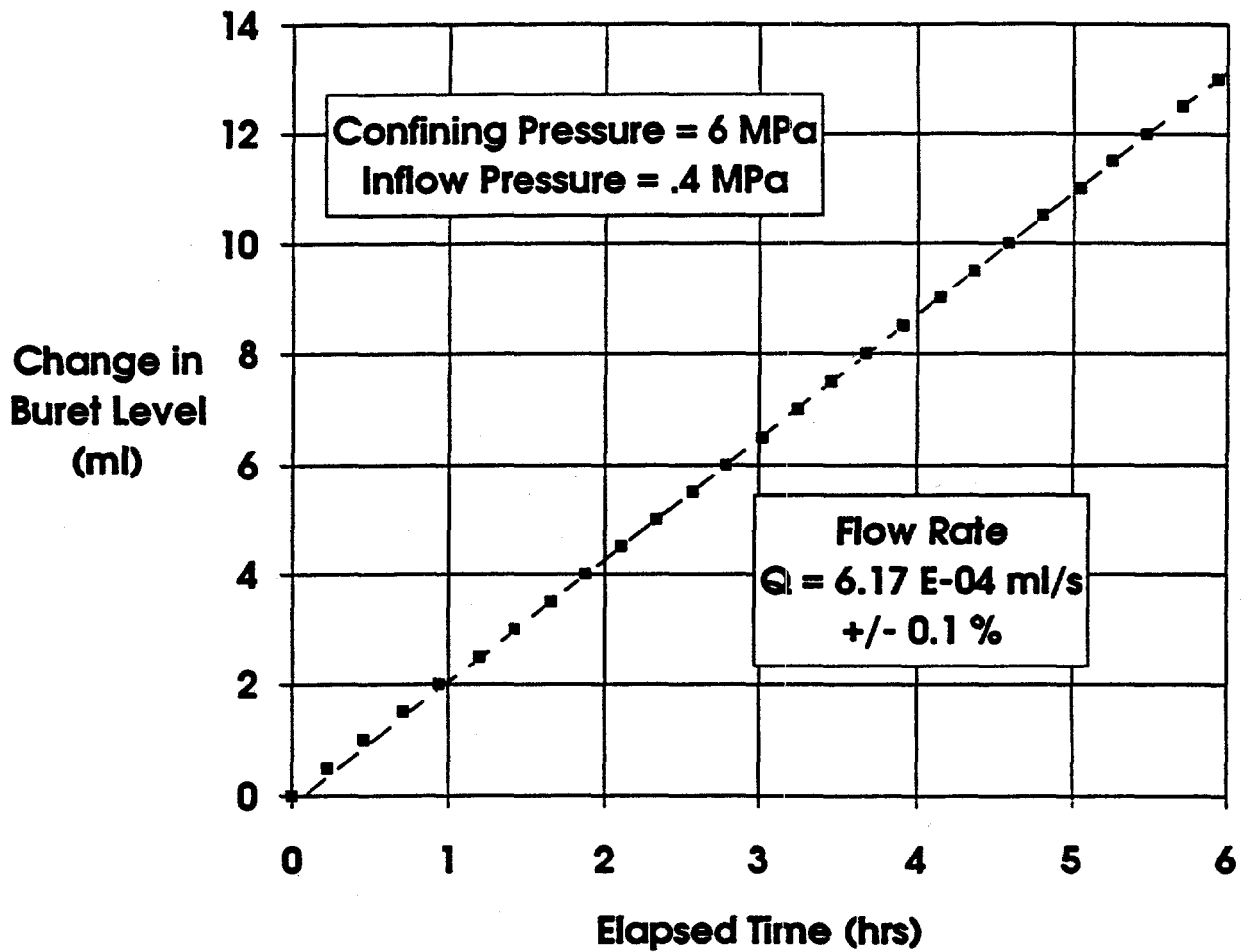
Figure I-14. Change in exit buret level (brine volume)-versus-time for tests on Specimen P3X11-5-3-SP3 at 2 MPa confining pressure and 0.7 MPa brine inlet pressure. Symbols are recorded data points; dashed lines are best fits to linear sections of data. Coefficient of variation for linear least square fits are given.

Figure I-15. Change in exit buret level (brine volume)-versus-time for tests on Specimen P3X11-5-3-SP3 at 2 MPa confining pressure and 0.4 MPa brine inlet pressure. Symbols are recorded data points; dashed lines are best fits to linear sections of data. Coefficient of variation for linear least square fits are given.
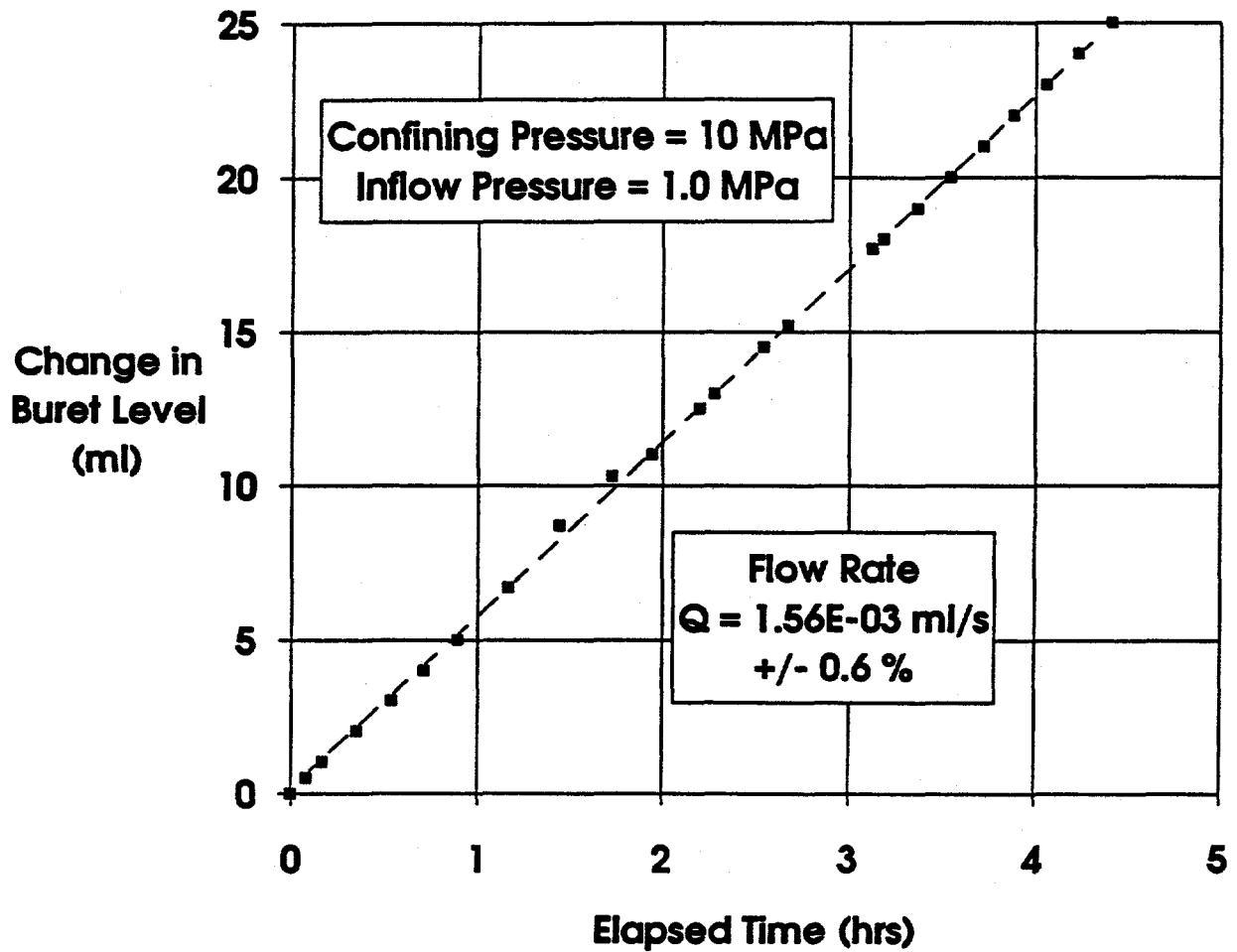
Figure I-16. Change in exit buret level (brine volume)-versus-time for tests on Specimen P3X11-5-3-SP3 at 6 MPa confining pressure and 1.0 MPa brine inlet pressure. Symbols are recorded data points; dashed lines are best fits to linear sections of data. Coefficient of variation for linear least square fits are given.
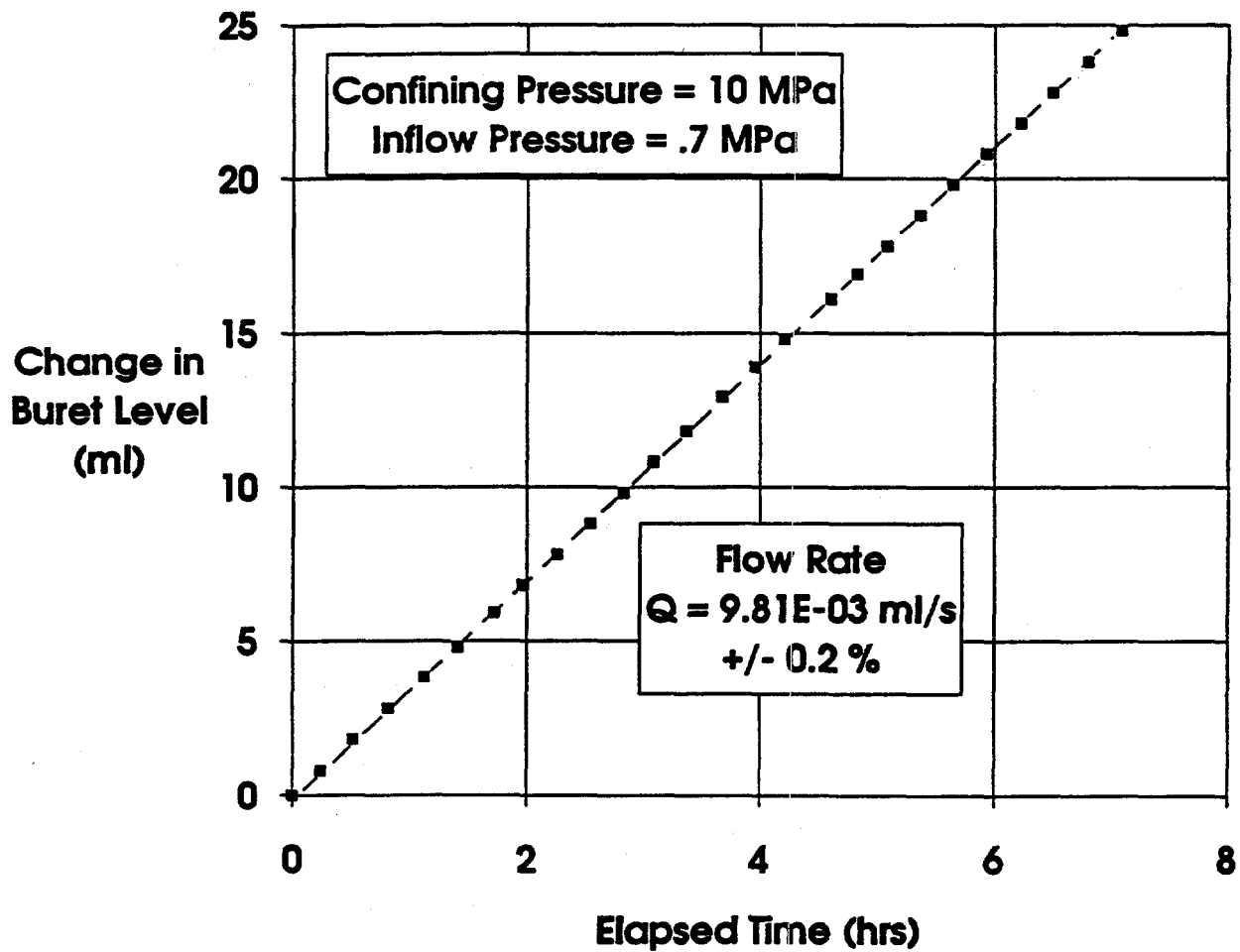
Confining Pressure = 6 MPa
Inflow Pressure = .7 MPa

Flow Rate
Q= 1.63E-03ml/s
+/- 0.1 %

RSI-248-94-017

Figure I-17. Change in exit buret level (brine volume)-versus-time for tests on Specimen P3X11-5-3-SP3 at 6 MPa confining pressure and 0.7 MPa brine inlet pressure. Symbols are recorded data points; dashed lines are best fits to linear sections of data. Coefficient of variation for linear least square fits are given.
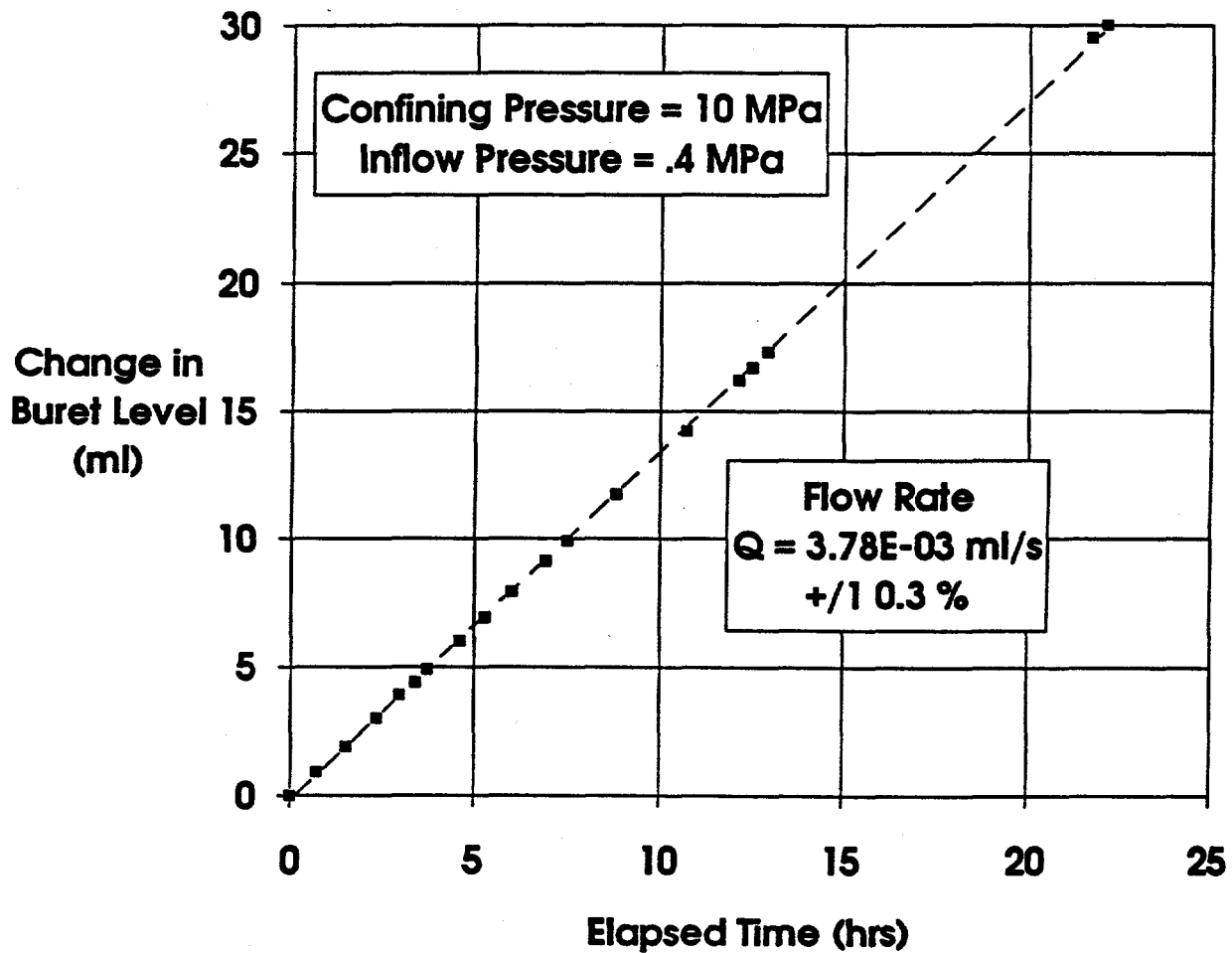
Figure I-18. Change in exit buret level (brine volume)-versus-time for tests on Specimen P3X11-5-3-SP3 at 6 MPa confining pressure and 0.4 MPa brine inlet pressure. Symbols are recorded data points; dashed lines are best fits to linear sections of data. Coefficient of variation for linear least square fits are given.

B-274

Figure I-19. Change in exit buret level (brine volume)-versus-time for tests on Specimen P3X11-5-3-SP3 at 10 MPa confining pressure and 1.0 MPa brine inlet pressure. Symbols are recorded data points; dashed lines are best fits to linear sections of data. Coefficient of variation for linear least square fits are given.

Figure I-20. Change in exit buret level (brine volume)-versus-time for tests on Specimen P3X11-5-3-SP3 at 10 MPa confining pressure and 0.7 MPa brine inlet pressure. Symbols are recorded data points; dashed lines are best fits to linear sections of data. Coefficient of variation for linear least square fits are given.
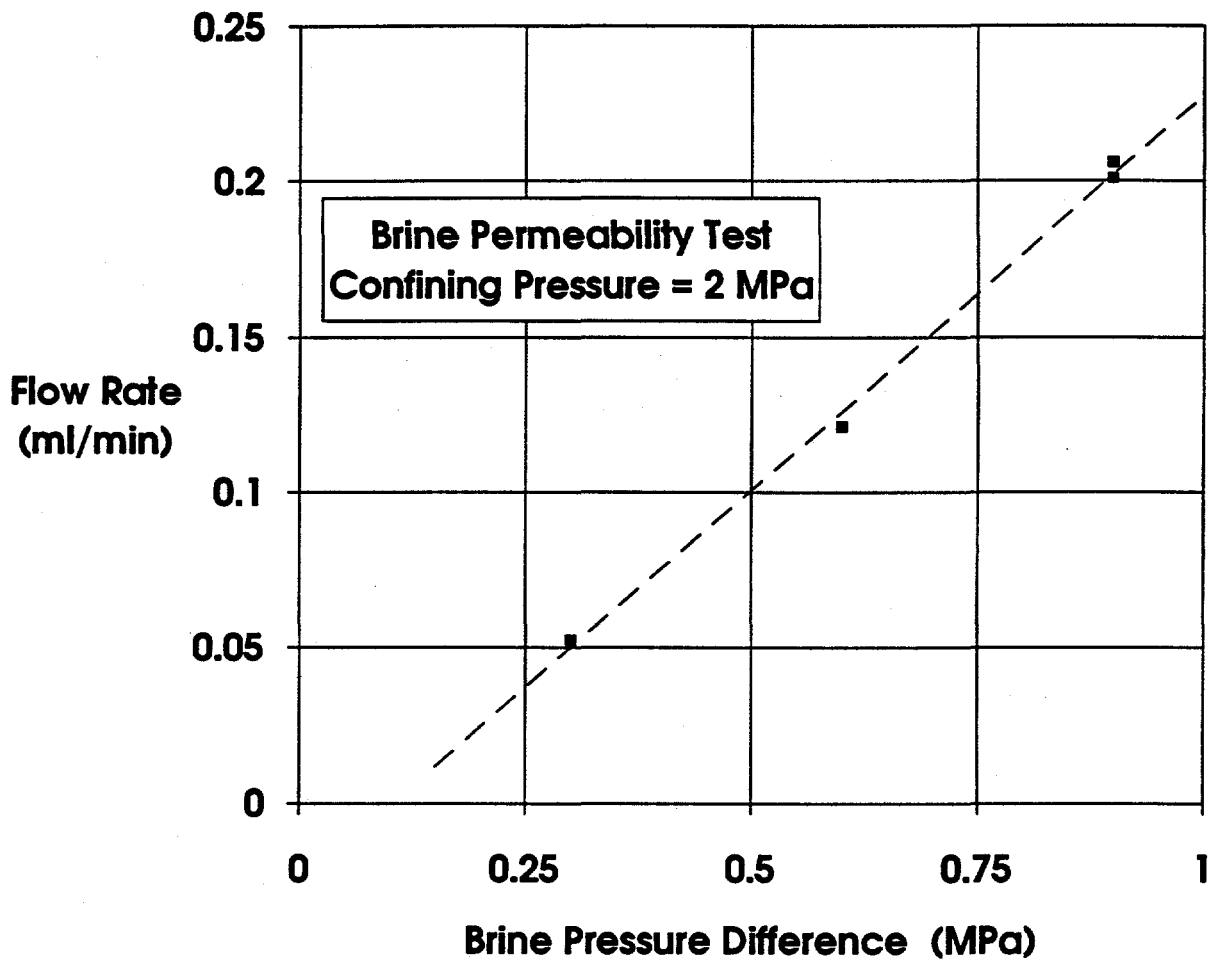
Figure I-21. Change in exit buret level (brine volume)-versus-time for tests on Specimen P3X11-5-3-SP3 at 10 MPa confining pressure and 0.4 MPa brine inlet pressure. Symbols are recorded data points; dashed lines are best fits to linear sections of data. Coefficient of variation for linear least square fits are given.

APPENDIX B.J
FLOW RATE-VERSUS-PORE PRESSURE DIFFERENCE
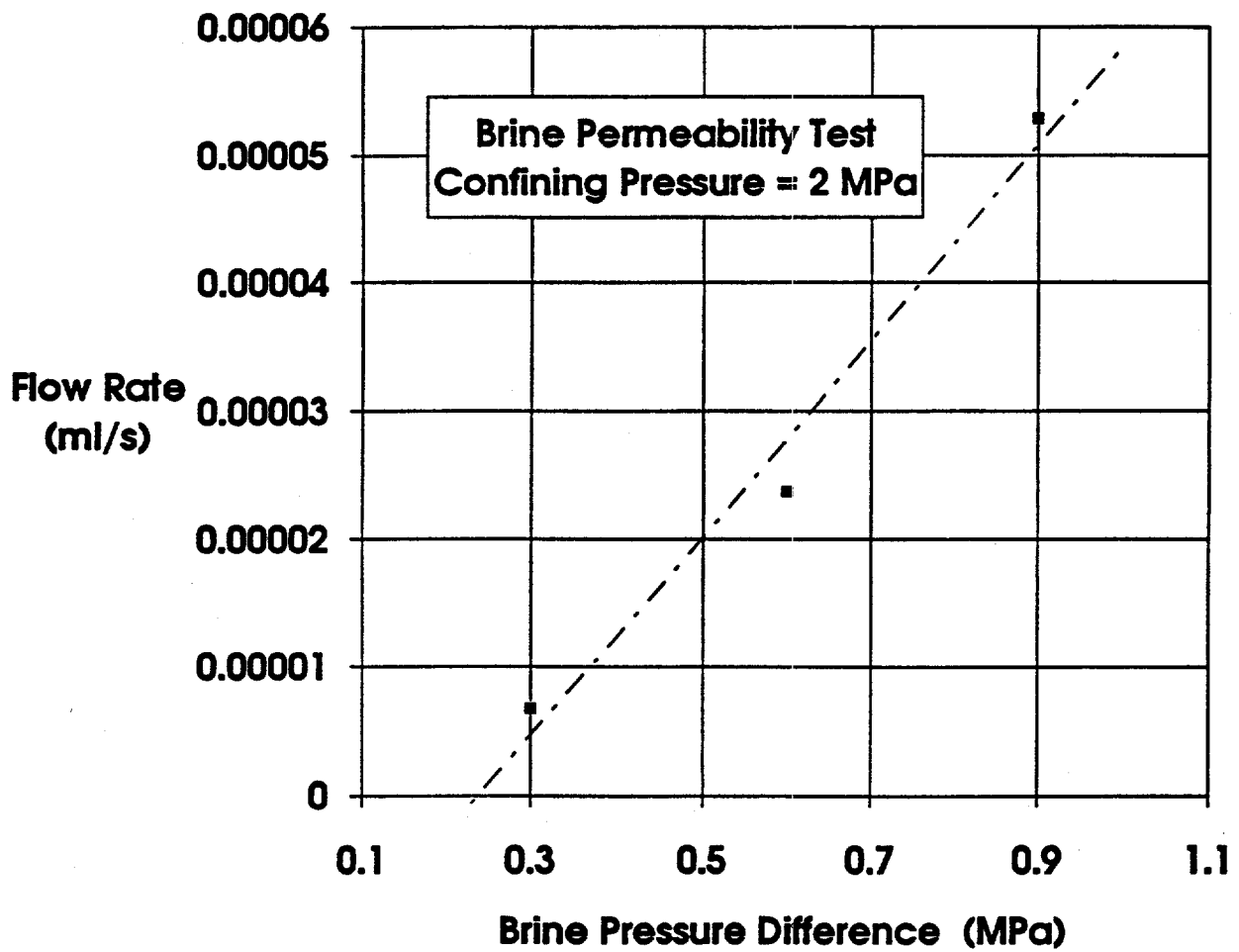# ACROSS SPECIMEN FOR ALL BRINE PERMEABILITY TESTS

Figures

Figure J-1. Flow rate-versus-brine pressure difference for Specimen P3X11-5-2-SP1 at 2 MPa confining pressure and all brine inlet pressures.

Figure J-2. Flow rate-versus-brine pressure difference for Specimen P3X10-6-SP2 at 2 MPa confining pressure and all brine inlet pressures.

Figure J-3. Flow rate-versus-brine pressure difference for Specimen P3X10-6-SP2 at 6 MPa confining pressure and all brine inlet pressures.
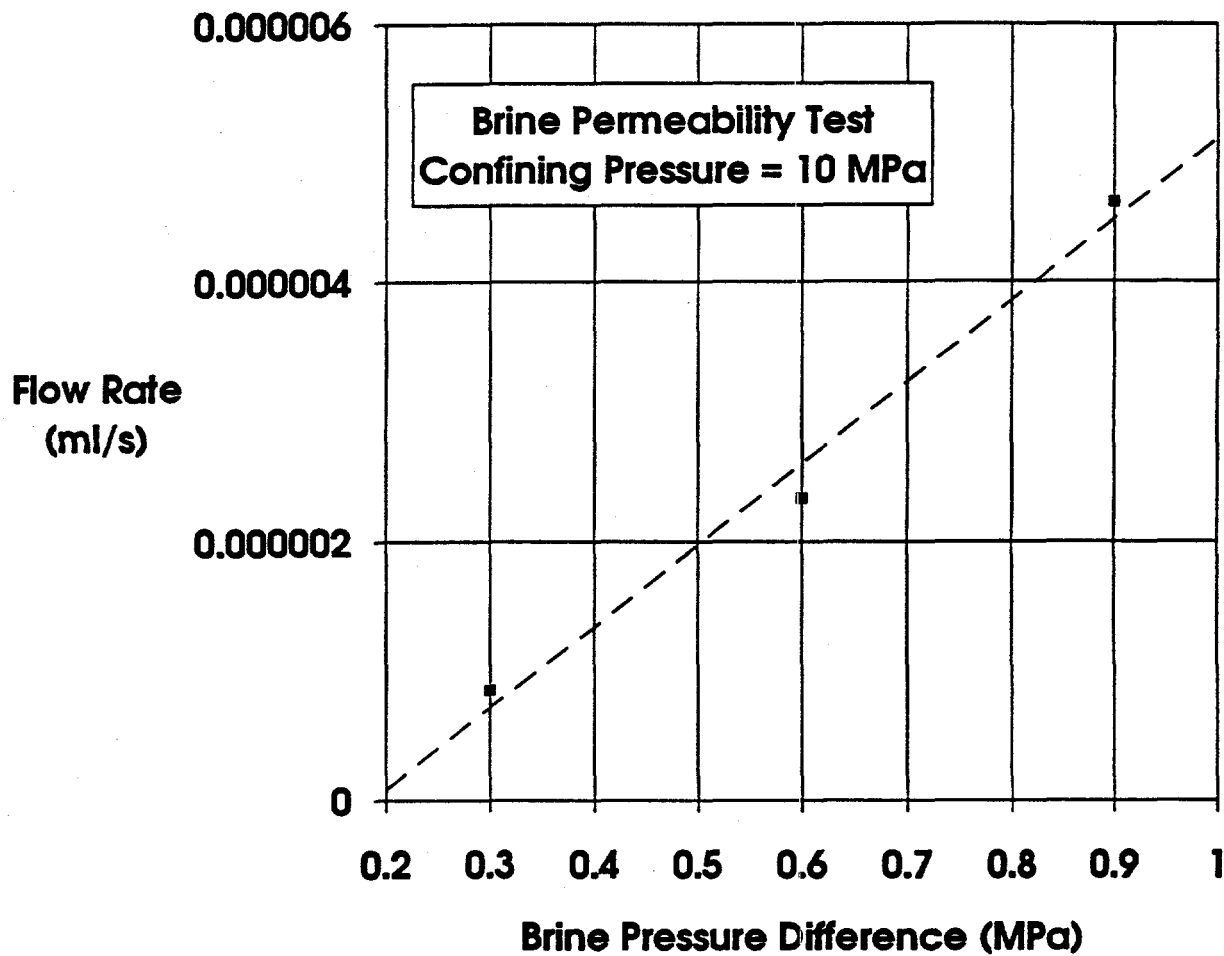
Figure J-4. Flow rate-versus-brine pressure difference for Specimen P3X10-6-SP2 at 10 MPa confining pressure and all brine inlet pressures.
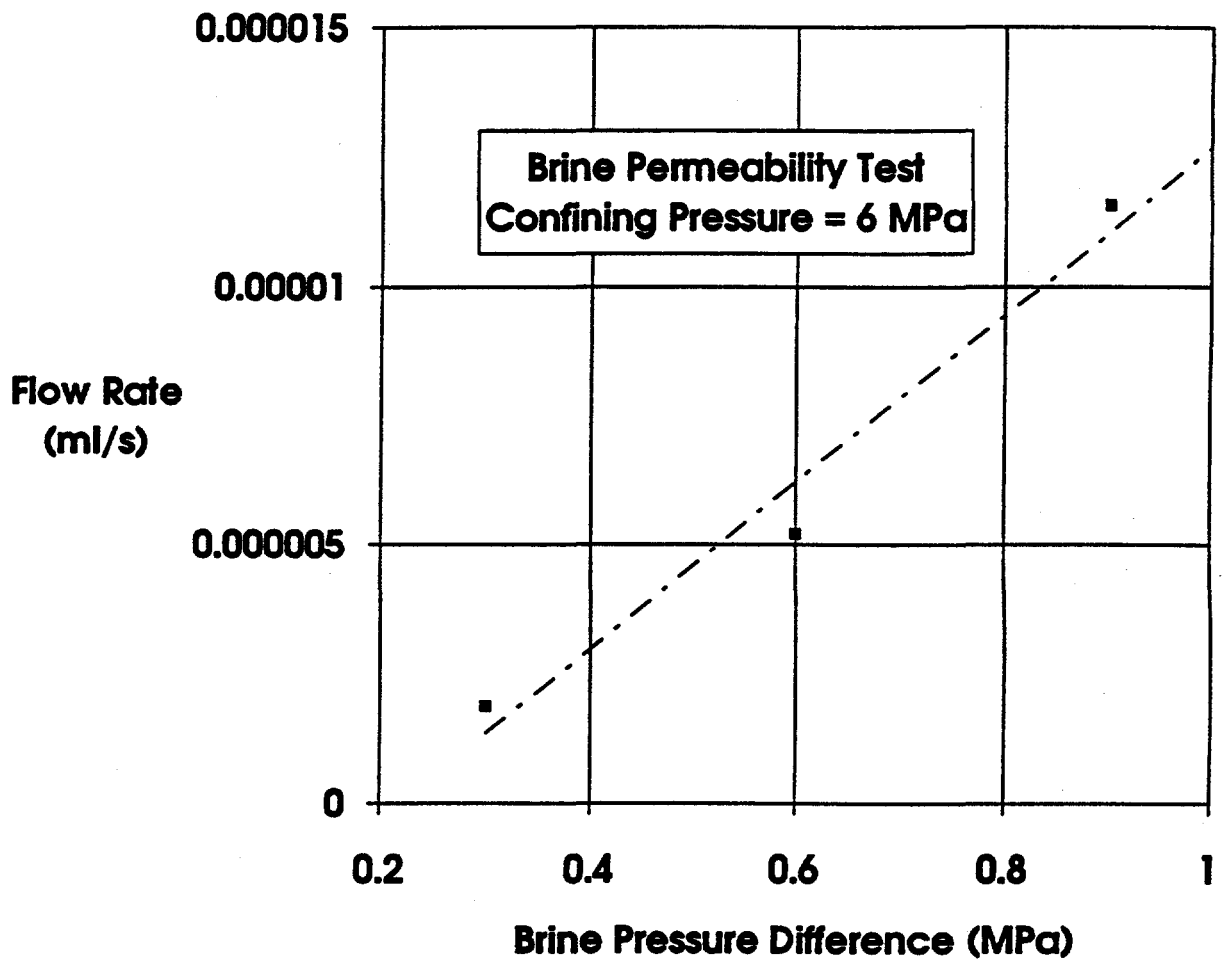
Figure J-5.   Flow rate-versus-brine pressure difference for Specimen P3X11-5-3-SP3 at 2 MPa
confining pressure and all brine inlet pressures.

Figure J-6. Flow rate-versus-brine pressure difference for Specimen P3X11-5-3-SP3 at 6 MPa confining pressure and all brine inlet pressures.

Figure J-7.   Flow rate-versus-brine pressure difference for Specimen P3X11-5-3-SP3 at 10 MPa confining pressure and all brine inlet pressures.

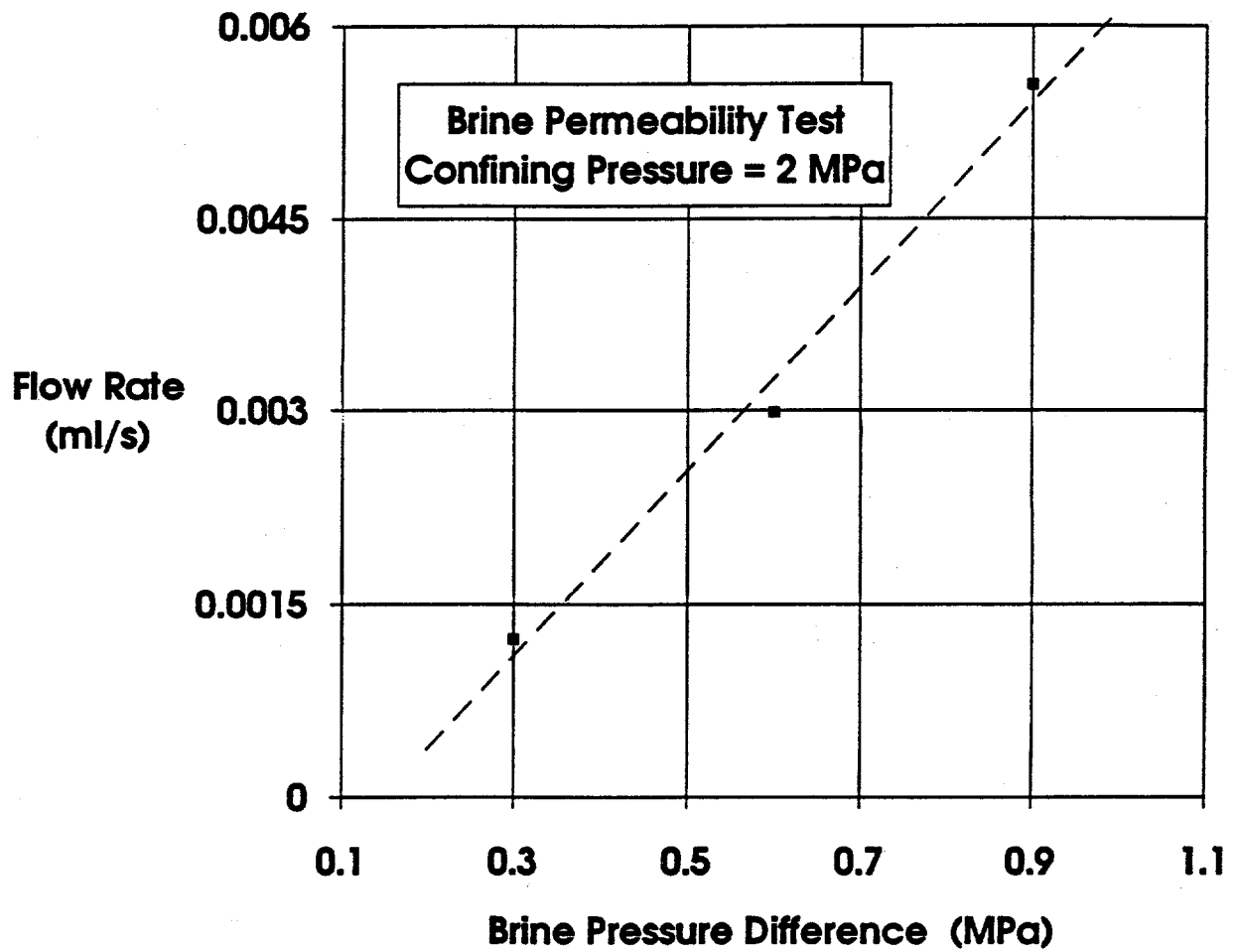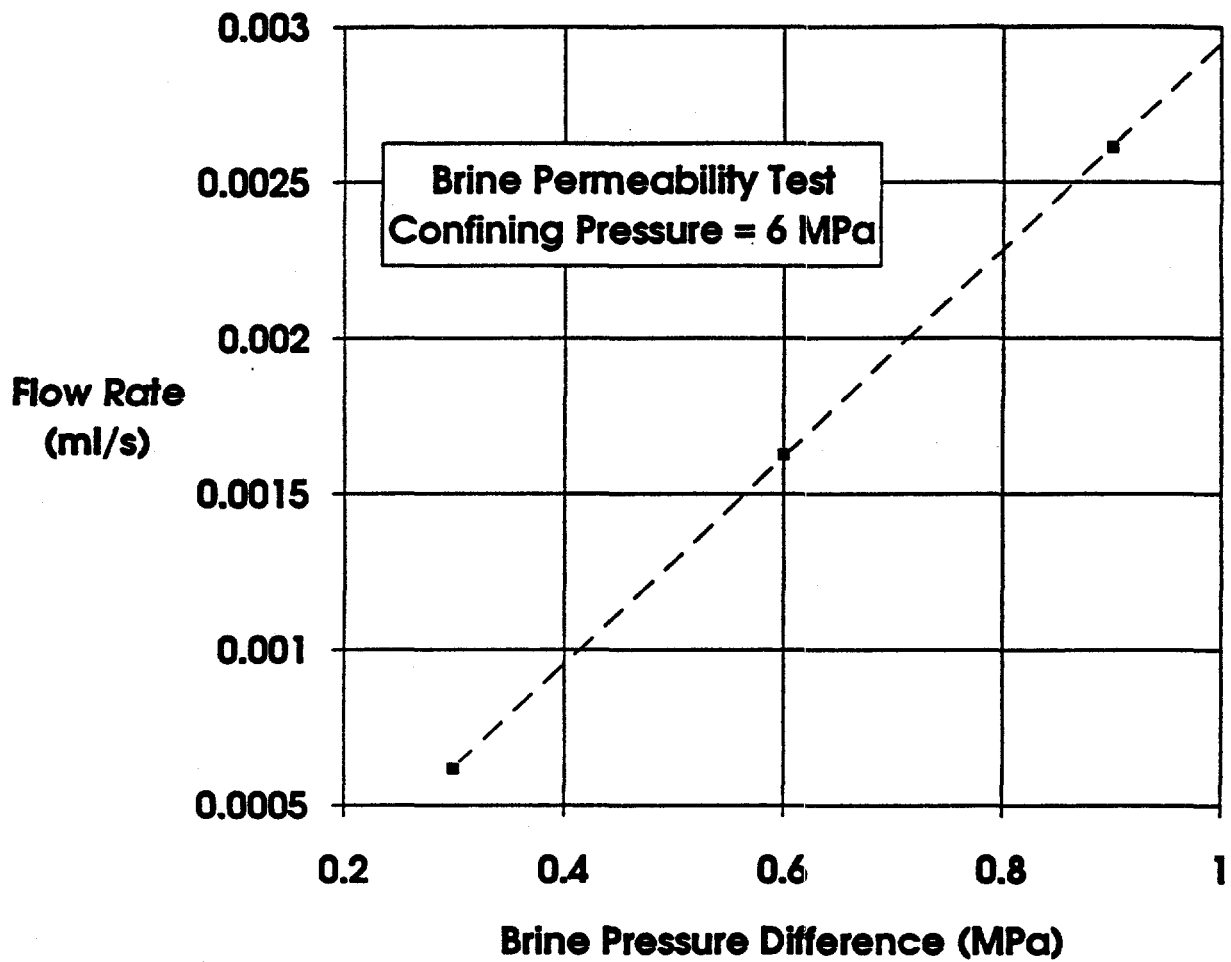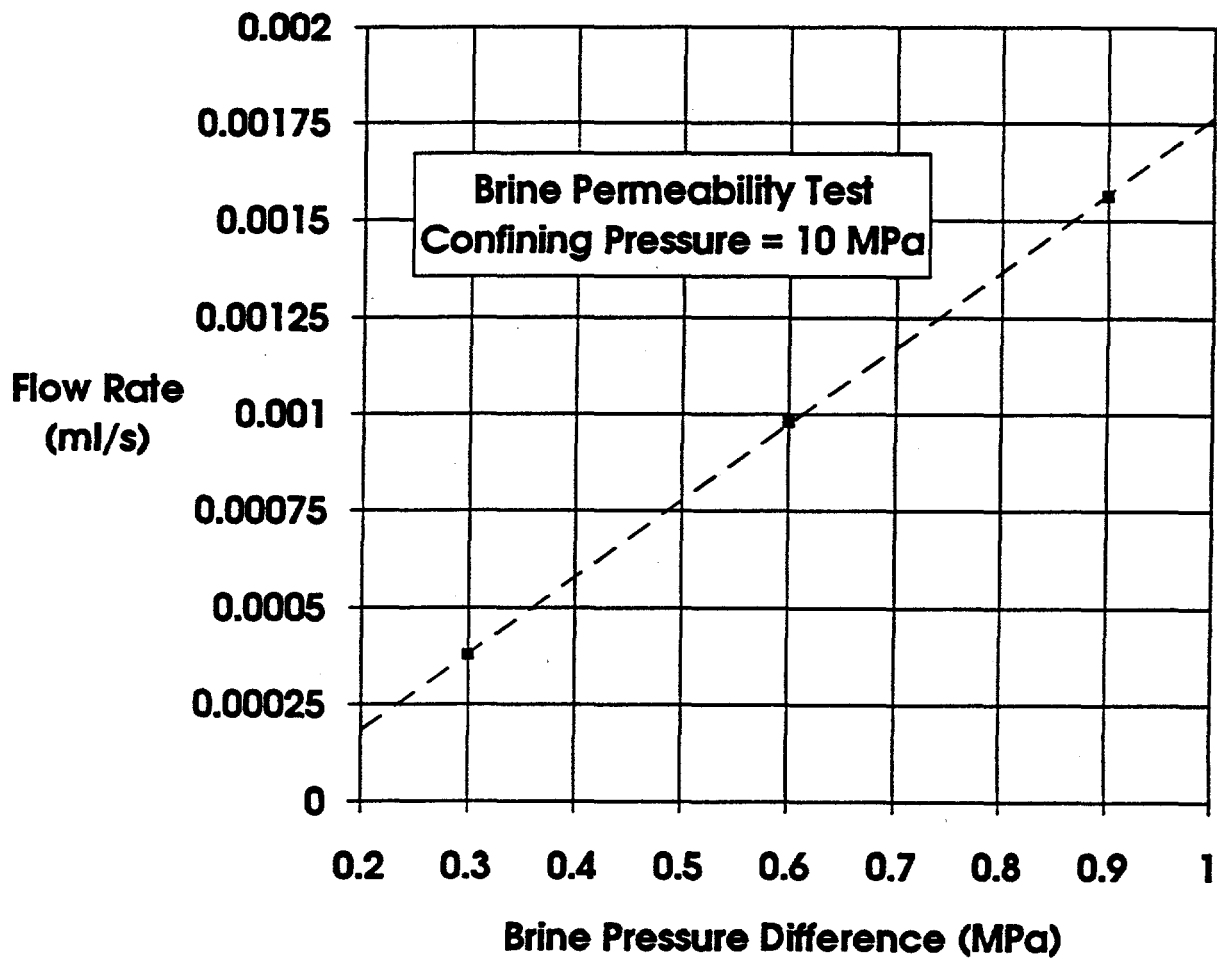# WIPP
UC721 - DISTRIBUTION LIST
SAND94-0472

Federal Agencies

US Department of Energy (4)
Office of Civilian Radioactive Waste Mgmt.
Attn: Deputy Director, RW-2
    Acting Director, RW-10
        Office of Human Resources & Admin.
    Director, RW-30
        Office of Program Mgmt. & Integ.
    Director, RW-40
        Office of Waste Accept., Stor., & Tran.
Forrestal Building
Washington, DC 20585

Attn: Project Director
Yucca Mountain Site Characterization Office
        Director, RW-3
        Office of Quality Assurance
P.O. Box 30307
Las Vegas, NV 89036-0307

US Department of Energy
Albuquerque Operations Office
Attn: National Atomic Museum Library
P.O. Box 5400
Albuquerque, NM 87185-5400

US Department of Energy
Research & Waste Management Division
Attn: Director
P.O. Box E
Oak Ridge, TN 37831

US Department of Energy (5)
Carlsbad Area Office
Attn: G. Dials
    D. Galbraith
    M. McFadden
    R. Lark
    J. A. Mewhinney
P.O. Box 3090
Carlsbad, NM 88221-3090

US Department of Energy
Office of Environmental Restoration and
    Waste Management
Attn: M Frei, EM-30
Forrestal Building
Washington, DC 20585-0002

US Department of Energy (3)
Office of Environmental Restoration and
    Waste Management
Attn: J. Juri, EM-34, Trevion II
Washington, DC 20585-0002

US Department of Energy
Office of Environmental Restoration and
    Waste Management
Attn: S. Schneider, EM-342, Trevion II
Washington, DC 20585-0002

US Department of Energy (2)
Office of Environment, Safety & Health
Attn: C. Borgstrom, EH-25
    R. Pelletier, EH-231
Washington, DC 20585

US Department of Energy (2)
Idaho Operations Office
Fuel Processing & Waste Mgmt. Division
785 DOE Place
Idaho Falls, ID 83402

US Environmental Protection Agency (2)
Radiation Protection Programs
Attn: M. Oge
ANR-460
Washington, DC 20460

Boards

Defense Nuclear Facilities Safety Board
Attn: D. Winters
625 Indiana Ave. NW, Suite 700
Washington, DC 20004

Nuclear Waste Technical Review Board (2)
Attn: Chairman
    J. L. Cohon
1100 Wilson Blvd., Suite 910
Arlington, VA 22209-2297

State Agencies

Attorney General of New Mexico
P.O. Drawer 1508
Santa Fe, NM 87504-1508

Environmental Evaluation Group (3)
Attn: Library
7007 Wyoming NE
Suite F-2
Albuquerque, NM 87109

NM Environment Department (3)
Secretary of the Environment
Attn: Mark Weidler
1190 St. Francis Drive
Santa Fe, NM 87503-0968

NM Bureau of Mines & Mineral Resources
Socorro, NM 87801

Laboratories/Corporations

Battelle Pacific Northwest Laboratories
Battelle Blvd.
Richland, WA 99352

INTERA, Inc.
Attn: G. A. Freeze
1650 University Blvd. NE, Suite 300
Albuquerque, NM 87102

INTERA, Inc.
Attn: J. F. Pickens
6850 Austin Center Blvd., Suite 300
Austin, TX 78731

Los Alamos National Laboratory
Attn: B. Erdal, INC-12
P.O. Box 1663
Los Alamos, NM 87544

RE/SPEC, Inc.
Attn: A. Robb
4775 Indian School NE, Suite 300
Albuquerque, NM 87110-3927

RE/SPEC, Inc.
Attn: J. L. Ratigan
P. O. Box 725
Rapid City. SD 57709

Tech Reps, Inc. (3)
Attn: J. Chapman (1)
        Loretta Robledo (2)
5000 Marble NE, Suite 222
Albuquerque, NM 87110

Westinghouse Electric Corporation (5)
Attn: Library
        J. Epstein
        J. Lee
        B. A. Howard
        R. Kehrman
P.O. Box 2078
Carlsbad, NM 88221

S. Cohen & Associates
Attn: Bill Thurber
1355 Beverly Road
McLean, VA 22101

Rock Physics Associates
Attn: J. Walls
4320 Steven Creek Blvd., Ste 282
San Jose, CA 95129

National Academy of Sciences, WIPP Panel

Howard Adler
Oxyrase, Incorporated
7327 Oak Ridge Highway
Knoxville, TN 37931

Tom Kiess
Board of Radioactive Waste Management
GF456
2101 Constitution Ave.
Washington, DC 20418

Rodney C. Ewing
Department of Geology
University of New Mexico
Albuquerque, NM 87131

Charles Fairhurst
Department of Civil and Mineral Engineering
University of Minnesota
500 Pillsbury Dr. SE
Minneapolis, MN 55455-0220

B. John Garrick
PLG Incorporated
4590 MacArthur Blvd., Suite 400
Newport Beach, CA 92660-2027

Leonard F. Konikow
US Geological Survey
431 National Center
Reston, VA 22092

Carl A. Anderson, Director
Board of Radioactive Waste Management
National Research Council
HA 456
2101 Constitution Ave. NW
Washington, DC 20418

Christopher G. Whipple
ICF Kaiser Engineers
1800 Harrison St., 7th Floor
Oakland, CA 94612-3430

John O. Blomeke
720 Clubhouse Way
Knoxville, TN 37909

Sue B. Clark
University of Georgia
Savannah River Ecology Lab
P.O. Drawer E
Aiken, SC 29802

Konrad B. Krauskopf
Department of Geology
Stanford University
Stanford, CA 94305-2115

Della Roy
Pennsylvania State University
217 Materials Research Lab
Hastings Road
University Park, PA 16802

David A. Waite
CH$_2$ M Hill
P.O. Box 91500
Bellevue, WA 98009-2050

Thomas A. Zordon
Zordan Associates, Inc.
3807 Edinburg Drive
Murrysville, PA 15668

Universities

University of New Mexico
Geology Department
Attn: Library
141 Northrop Hall
Albuquerque, NM 87131

Libraries

Thomas Brannigan Library
Attn: D. Dresp
106 W. Hadley St.
Las Cruces, NM 88001

Government Publications Department
Zimmerman Library
University of New Mexico
Albuquerque, NM 87131

New Mexico Junior College
Pannell Library
Attn: R. Hill
Lovington Highway
Hobbs, NM 88240

New Mexico State Library
Attn: N. McCallan
325 Don Gaspar
Santa Fe, NM 87503

New Mexico Tech
Martin Speere Memorial Library
Campus Street
Socorro, NM 87810

WIPP Public Reading Room
Carlsbad Public Library
101 S. Halagueno St.
Carlsbad, NM 88220

Foreign Addresses

Atomic Energy of Canada, Ltd.
Whiteshell Laboratories
Attn: B. Goodwin
Pinawa, Manitoba, CANADA R0E 1L0

Francois Chenevier (2)
ANDRA
Route de Panorama Robert Schumann
B. P. 38
92266 Fontenay-aux-Roses, Cedex
FRANCE

Claude Sombret
Centre d'Etudes Nucleaires de la Vallee Rhone
CEN/VALRHO
S.D.H.A. B.P. 171
30205 Bagnols-Sur-Ceze
 FRANCE

Commissariat a L'Energie Atomique
Attn: D. Alexandre
Centre d'Etudes de Cadarache
13108 Saint Paul Lez Durance Cedex
FRANCE

Bundesanstalt fur Geowissenschaften und
Rohstoffe
Attn: M. Langer
Postfach 510 153
D-30631 Hannover
 GERMANY

Bundesministerium fur Forschung und
Technologie
Postfach 200 706
5300 Bonn 2
 GERMANY

Institut fur Tieflagerung
Attn: K. Kuhn
Theodor-Heuss-Strasse 4
D-3300 Braunschweig
 GERMANY

Gesellschaft fur Anlagen und Reaktorsicherheit
(GRS)
Attn: B. Baltes
Schwertnergasse 1
D-50667 Cologne
GERMANY

Shingo Tashiro
Japan Atomic Energy Research Institute
Tokai-Mura, Ibaraki-Ken, 319-11
JAPAN

Netherlands Energy Research Foundation ECN
Attn: J. Prij
3 Westerduinweg
P.O. Box 1
1755 ZG Petten
THE NETHERLANDS

Svensk Karnbransleforsorjning AB
Attn: F. Karlsson
Project KBS (Karnbranslesakerhet)
Box 5864
S-102 48 Stockholm
SWEDEN

Nationale Genossenschaft fur die Lagerung
Radioaktiver Abfalle (2)
Attn: S. Vomvoris
      P. Zuidema
Hardstrasse 73
CH-5430 Wettingen
SWITZERLAND

AEA Technology
Attn: J. H. Rees
D5W/29 Culham Laboratory
Abington, Oxfordshire OX14 3DB
UNITED KINGDOM

AEA Technology
Attn: W. R. Rodwell
044/A31 Winfrith Technical Centre
Dorchester, Dorset DT2 8DH
UNITED KINGDOM

AEA Technology
Attn: J. E. Tinson
B4244 Harwell Laboratory
Didcot, Oxfordshire OX11 ORA
UNITED KINGDOM

Internal

MS	Org.	
1324	6115	P. B. Davies
1324	6115	T. L. Christian-Frear (5)
1324	6115	C. Boney
1324	6115	R. L. Beauheim
1324	6115	S. W. Webb
1320	6831	E. J. Nowak
1322	6121	J. R. Tillerson
1328	6849	D. R. Anderson
1328	6848	H. N. Jow
1335	6801	M. Chu
1335	6801	S. M. Howarth (15)
1341	6832	J. T. Holmes
1395	6800	L. Shephard
1395	6821	M. Marietta
0751	6117	L. S. Costin
0751	6117	N. S. Brodsky
0751	6117	J. T. Fredrich
0751	6117	D. J. Holcomb

0751	6117	D. H. Zeuch
0705	6116	D. J. Borns
1330	6811	K. Hart (2)
1330	4415	NWM Library (20)
9018	8940-2	Central Technical Files
0899	4414	Technical Library (5)
0619	12690	Review and Approval Desk (2), For DOE/OSTI